Searching for Autoimmune B Cells in Atherosclerosis

Chuankai Zhang

München 2022

Aus dem Institut für Prophylaxe und Epidemiologie der Kreislaufkrankheiten

Klinik der Universität München

Direktor: Univ.-Prof. Dr. med. Christian Weber

Searching for Autoimmune B Cells in Atherosclerosis

Dissertation

zum Erwerb des Doktorgrades der Humanbiologie

an der Medizinischen Fakultät der

Ludwig-Maximilians-Universität zu München

vorgelegt von

Chuankai Zhang

aus

Shandong, VR China

2022

Mit Genehmigung der Medizinischen Fakultät

der Universität München

Berichterstatter:	Univ.-Prof. Dr. rer. nat. Sabine Steffens
Mitberichterstatter:	Prof. Dr. Edgar Meinl
	Prof. Dr. Jürgen Bernhagen
	Prof. Dr. Klaus Parhofer
Mitbetreuung durch den promovierten Mitarbeiter:	
Dekan:	Prof. Dr. med. Thomas Gudermann
Tag der mündlichen Prüfung:	13.05.2022

Searching for Autoimmune B Cells in Atherosclerosis

Table of content

Table of content ..... *I*

Zusammenfassung ..... *V*

Abstract ..... *VII*

Abbreviations ..... *IX*

1. Introduction *1*

1.1. The immune system **1**

1.1.1 The innate immune system 1

1.1.2 The adaptive immune system 2

1.1.2.1 T cell-mediated immune response 2

1.1.2.2 B cell-mediated immune response 3

1.2 The B cell development pathways **4**

1.3 The GC B cell responses **6**

1.4 Immunoglobulins (Igs) **7**

1.4.1 Generation of Ig diversity 9

1.5 Central and peripheral B cell tolerance **10**

1.6 Tertiary lymphoid organs (TLOs) and autoimmune disease **12**

1.6.1 The distinction between autoimmune reactions and autoimmune diseases: Witebsky criteria 12

1.6.2 Mechanisms underlying autoimmune diseases 12

1.6.3 TLOs in systemic autoimmune diseases 13

1.7 Atherosclerosis **14**

1.7.1 Atherosclerosis is a chronic inflammatory disease of the arterial wall 14

1.7.2 Atherosclerosis and B lymphocytes 15

1.7.3 Atherosclerosis and autoimmune diseases 16

1.8 Murine and human Artery Tertiary Lymphoid Organs (ATLOs) **17**

1.9 Mouse models of atherosclerosis **18**

1.10 Hypothesis **19**

1.11 Aims of this project **20**

2 Materials and Methods ***22***

2.1 Materials 22

2.1.1 Animals 22

2.1.2 Standard solutions and buffers 22

2.1.3 Antibodies 23

2.1.4 Devices and reagents 25

2.1.5 Recombinant proteins and chimeric monoclonal antibodies 28

2.1.6 Primers 29

2.2 Methods 30

2.2.1 Mouse dissection and tissue collections 30

2.2.2 Complete blood count 30

2.2.3 Total cholesterol assay 31

2.2.4 Human samples 31

2.2.5 Isolation of single cells 31

2.2.5.1 Preparation of single cells from aorta, secondary lymphoid organs, liver, and lung 31

2.2.5.2 Cell counting 32

2.2.5.3 Staining with labeled antibody 32

2.2.5.4 Analysis of total leukocytes by flow cytometry 33

2.2.6 Polymerase chain reaction (PCR) 34

2.2.6.1 Complementary deoxyribonucleic acid (cDNA) synthesis 34

2.2.6.2 Nested PCR for amplification of mouse Ig transcripts 34

2.2.7.3 MinElute@PCR purification 36

2.2.7.4 Ig gene sequence analysis 36

2.2.7.5 Directional cloning into expression vectors 37

2.2.7.6 Recombinant antibody production and purification 37

2.2.8 Immunofluorescence staining 37

2.2.9 Quantification of $CD68^+$ macrophage and SMA^+ SMCs infiltration in the plaque areas 38

2.2.10 Protein analyses 38

2.2.10.1 Extract protein from aorta 38

2.2.10.2 Protein quantification (BCA protein assay kit) 39
2.2.10.3 Western blot 39
2.2.10.4 Antibody detection 39
2.2.11 Enzyme-linked immunosorbent assay (ELISA) for anti-histone H2b in the circulation 40
2.2.12 Immunoprecipitation (IP) and protein mass spectrometry (MS) 41
2.2.13 Surface plasmon resonance experiment 42
2.2.14 H2b vaccination on atherosclerosis development in ApoE$^{-/-}$ mice 42
2.2.14.1 Emulsion formation 42
2.2.14.2 H2b vaccination in ApoE$^{-/-}$ mice 43
2.2.14.3 Atherosclerosis quantification 43
2.2.15 Statistical analyses 44

3. Results ***45***

3.1 Cloning of paired heavy and light chains of BCRs from single B cells 45
3.2 Clonal expansion of ATLO GC B cells 50
3.3 Generation of recombinant chimeric monoclonal antibodies *in vitro* 57
3.4 ATLO-derived antibodies recognize plaque components 59
3.5 Screening the reactivity of ATLO GC-derived antibodies by tissue arrays 63
3.6 ATLO-derived A6 antibody reactivities in plaques 79
3.7 Reactivity of ATLO-derived A6 antibody in early stages of atherosclerosis 85
3.8 ATLO-derived antibody A6 recognizes human plaque constituents 86
3.9 ATLO-derived A6 antibody recognizes histones 88
3.10 ATLO-derived A6 antibody high-affinity binding to H2b 91
3.11 Serum anti-histone H2b antibodies titer increase in atherosclerosis 94
3.12 H2b vaccination promotes atherosclerosis progression in ApoE$^{-/-}$ mice on a chow diet 96
3.12.1 Experimental design for the immunization in ApoE$^{-/-}$ mice 96
3.12.2 Immunization increases histone H2b-specific antibody titers 97
3.12.3 H2b vaccination does not change body weight, blood parameters, and cholesterol levels

in 32 weeks ApoE$^{-/-}$ mice 98

3.12.4 H2b vaccination increases plaque size 100

3.14 ATLO-derived A7 antibodies in ApoE$^{-/-}$ mice 102

3.15 Searching for A7-related antigen(s) 105

4 Discussion 107

4.1 Using ATLOs to isolate autoimmune antibodies vs. LNs in atherosclerosis: Why is this effective and led to successful isolation of autoantigens? 108

4.1.1 Unbiased approach analysis of the GC B cells repertoire from ATLOs by single-cell PCR 109

4.1.2 The Ig gene repertoire of GC B cells from ATLOs and spleen 110

4.1.3 ATLOs generate self-reactive antibodies 110

4.2 Discovery of the pro-atherogenic roles of H2b autoimmunity 111

4.3 The atherosclerosis-related B cell response: harmful or beneficial? 112

4.4 Atherosclerosis vaccination strategies 113

4.5 Challenges ahead 114

References 116

Supplementary materials 137

Acknowledgments 153

Affidavit 154

Zusammenfassung

Atherosklerose ist eine chronisch-entzündliche Erkrankung der Arterienwand und die Haupttodesursache weltweit. Angeborene und adaptive Immunreaktionen sind an der Entwicklung der Atherosklerose während aller Stadien beteiligt. Eine fundamentale ungeklärte Frage hinsichtlich der Pathogenese der Erkrankung ist, ob die klinisch relevanten Spätstadien der Atherosklerose ausschließlich durch Zellen der angeborenen Immunantwort wie Makrophagen gekennzeichnet sind oder ob autoreaktive B2 Immunzellen gegen Autoantigene der Arterienwand gebildet werden. Eine Antwort auf diese Frage ist dringlich, um zukünftige Therapiestrategien der bisher nicht kausal therapierbaren Erkrankung zu entwickeln. Tertiäre Lymphorgane (TLOs) entwickeln sich bei zahllosen autoreaktiven und autoinflammatorischen Erkrankungen wie Krebs, Autoimmunerkrankungen und chronisch entzündlichen Darmerkrankungen. Mitglieder unserer Arbeitsgruppe charakterisierten Atherosklerose-assoziierte TLOs (ATLOs) in Apolipoprotein E-defizienten ($ApoE^{-/-}$) Mäusen und in erkrankten humanen Arterien. Fortgeschrittene Stadien dieser ATLOs sind durch separate T Zellregionen und aktivierte B Zellfollikel, die follikuläre dendritische Zellen (FDCs) enthalten, gekennzeichnet. Diese Daten deuteten an, dass autoreaktive B2 Zellimmunreaktionen in ATLOs stattfinden könnten. Die Methode der Nested Polymerase Chain Reaction wurde benutzt, um die schweren und leichten Ketten der B Zell Rezeptoren (membrangebundene Immunglobuline) in isolierten B2 Zellen aus den Keimzentren von ATLOs und von sekundären Lymphorganen zu klonieren und *in vitro* zu exprimieren. Die resultierenden rekombinanten monoklonalen Antikörper wurden in immunhistologischen Analysen verschiedener Organe eingesetzt, um in $ApoE^{-/-}$ Mäusen und erkrankten humanen Geweben deren Reaktivität zu untersuchen. Koimmunpräzipitation erkrankter muriner Arterien unter Benutzung der putativen Autoantikörper wurde benutzt, um potentielle Autoantigene erkrankter Arterien zu präzipitieren, die anschließend in massenspektrometrischen Analysen zur Identifikation der Autoantigene eingesetzt wurden. Western Blots und Enzyme Linked Immunosorbent Assays (ELISAs) wurden etabliert, um

die Serumkonzentration der klonierten Antikörper zu bestimmen. Die sogenannte Surface Plasmon Resonance Methode wurde eingesetzt, um die Affinität der klonierten Antikörper mit Autoantigenen direkt zu bestimmen. Acht Autoantikörper wurden aus 64 Kandidaten kloniert und *in vitro* exprimiert. Humane Gewebe wurden benutzt, um die Kreuzreaktivität dieser Antikörper gegen humane Antigene zu bestimmen. Diese Untersuchungen führten zur Identifikation des Histonproteins H2B als ein bona fide Autoantigen der murinen und humanen Atherosklerose (der Antikörper wurde als A6 Antikörper annotiert). Andere Antikörper reagierten gegen unterschiedliche Zellen der Arterienwand einschließlich gegen glatte Muskelzellen der Lamina Media. Weitere experimentelle und klinische Untersuchungen zeigten, dass der A6 Antikörper in atherosklerotischen Mäusen und im Serum erkrankter Patienten signifikant anstiegen. Schließlich wurde eine Impfstrategie mit H2B Autoantigen in Mäusen durchgeführt: ApoE$^{-/-}$ Mäuse entwickelten nach zwei Injektionen eine erhöhte Plaquebelastung ihrer Arterien. Diese Daten zeigen erstmals, dass die Atherosklerose eine Erkrankung ist, die mit einer polyklonalen B2 Autoimmunantwort assoziiert ist. Damit wurde der erste und entscheidende Schritt hinsichtlich der Charakterisierung der Atherosklerose als Autoimmunerkankung gemacht.

Abstract

Atherosclerosis is a chronic inflammatory disorder of arteries and the leading cause of mortality worldwide. Innate and adaptive immune responses are involved in all disease stages. It has been suggested that adaptive autoimmunity may play critical roles in the initiation and progression of atherosclerosis. However, this fundamental question remains unresolved. Indeed, whether human atherosclerosis is solely an auto-inflammatory disease, whether it is a *bona fide* B2-driven autoimmune disease or both is still unclear. A comprehensive answer to this question would provide unprecedented opportunities to develop next-generation therapeutic strategies to treat the root causes of atherosclerosis. Tertiary lymphoid organs (TLOs) emerge in tissues in response to non-resolving inflammation, including transplant rejection, most types of cancer, autoimmune diseases, and chronic infectious diseases. Artery TLOs (ATLOs) have also been identified in the aorta adventitia of aged apolipoprotein E-deficient ($ApoE^{-/-}$) mice and in human atherosclerotic tissues: ATLOs are organized into T cell areas and B cell follicles containing follicular dendritic cells (FDCs) in activated germinal centers (GCs). These data support the notion that atherosclerosis-specific B cell responses may be organized in ATLOs, which was the key question addressed in this thesis. The method of nested polymerase chain reaction (PCR) was used to clone paired heavy and light chains of B cell receptors (BCRs) in isolated B2 cells from germinal centers (GCs) of ATLOs and secondary lymphatic organs to express them *in vitro*. Using immunofluorescence (IF) staining, the reactivity of the recombinant antibodies in multiple murine tissues was confirmed. Co-immunoprecipitation and mass spectrometry (coIP-MS), Western blot, enzyme-linked immunosorbent assays (ELISA), and surface plasmon resonance analyses were used to determine antibody-cognate autoantigen binding characteristics. In translational studies, human atherosclerotic plaques were examined to test whether the potential autoantibodies reacted with their cognate antigen in the arterial wall. Histone H2b was thereby identified as the first common murine and human autoantigen. Importantly, H2b triggered autoimmunity responses *in vivo*, which was associated with

disease severity of both murine atherosclerosis and human patients with cardiovascular diseases (CVDs). Immunization against the H2b autoantigen promoted atherosclerosis in ApoE$^{-/-}$ mice, which demonstrated the pro-atherogenic role of H2b autoimmunity *in vivo*. In conclusion, these data lead us to propose that atherosclerosis is a disease that is associated with multiple autoreactive BCRs and that murine atherosclerosis and possibly human atherosclerosis may be a bona fide autoimmune disease.

Abbreviations

aa	Amino acid
ALDH4A1	Aldehyde dehydrogenase 4 family member A1
AICDA	Activation-induced cytidine deaminase
APCs	Antigen-presenting cells
ApoE	Apolipoprotein E
ATLOs	Artery tertiary lymphoid organ
BCR	B cell receptor
BM	Bone marrow
Breg	Regulatory B cell
BSA	Bovine serum albumin
C	Constant
CDRs	Complementarity-determining regions
CD40L	CD40 ligand
CVD	Cardiovascular disease
CXCL	C-X-C motif ligand
Cy3	Cyanine 3
DAPI	4’, 6-diamidino-2-phenylindole
DCs	Dendritic cells
dNTP	Deoxynucleoside triphosphate
DTT	Dithiothreitol
DZ	Dark zone
EDTA	Ethylenediaminetetraacetic acid
ELISA	Enzyme-linked immunosorbent assay
Fab	Fragment antigen-binding
FACS	Fluorescence-activated cell sorting

Fc	Fragment crystallizable
FDCs	Follicular dendritic cells
Fol-B	Follicular B cells
GC	Germinal center
GC B cell	Germinal center B cell
H&E	Hematoxylin- and eosin-stained
HEVs	High endothelial venules
HSC	Hematopoietic stem cell
HSP60	Heat shock protein 60
hr	Hour
HRP	Horseradish peroxidase
IF	Immunofluorescence
Ig	Immunoglobulin
IgA, D, E, G, M	Immunoglobulin A, D, E, G, M
IgH	Immunoglobulin heavy chains
Igk	Immunoglobulin kappa light chain
Igλ	Immunoglobulin lambda light chain
IHC	Immunohistochemistry
IL	Interleukin
IMGT	Immunogenetics information system
IP	Immunoprecipitation
KDa	Kilodaltons
LDL	Low density lipoprotein
LDLR	Low-density lipoprotein receptor
LN	Lymph node
LT	Lymphotoxin
LZ	Light zone

MOVAS	Mouse vascular aorta/smooth muscle cells
MS	Mass spectrometry
Min	Minute(s)
MZ	Marginal zone
NGS	Next-generation sequencing
NK	Natural killer
OD	Optical density
ORO	Oil-red-O
oxLDL	Oxidized low-density lipoprotein
PBS	Phosphate buffered saline
PC	Plasma cell
PCR	Polymerase chain reaction
PFA	Paraformaldehyde
PVDF	Polyvinylidene fluoride
RA	Rheumatoid arthritis
RAG	Recombination-activating gene
RF	Reading framework
RGS14	Regulator of G protein signaling 14
RIPA	Radioimmunoprecipitation assay buffer
RLN	Renal lymph node
RNase	Ribonuclease
RT	Room temperature
RT-PCR	Reverse transcription-polymerase chain reaction
scBCR-seq	Single-cell BCR receptor sequencing
SMA	α-smooth muscle actin
SMCs	Smooth muscle cells
SLE	Systemic lupus erythematosus

TCR	T cell receptor
TFA	Trifluoroacetic acid
TFH	T follicular helper cells
TGF-ß	Transforming growth factor ß
TNF	Tumour necrosis factor
T-SNE	t-distributed stochastic neighbor embedding
WT	Wild-type
β2GPI	β2 glycoprotein I
-/-	Deficient

1. Introduction

1.1. The immune system

The immune system can be divided into two principal arms, i.e., the innate and adaptive immune system. Both systems aim to identify and eliminate foreign antigens while preserving self [1-3]. Diverse innate and adaptive immune cell subsets are involved in this important task. The innate immune system contains basophils, eosinophils, natural killer (NK) cells, and phagocytic cells such as macrophages, neutrophils, and dendritic cells [4]. The adaptive immune system is composed of T- and B-lymphocytes, which recognize and respond to soluble or insoluble/particular antigens through their highly specialized antigen receptors located on the surface, i.e., T cell receptors (TCRs) and B cell receptors (BCRs), respectively. T- and B-lymphocytes differentiate into their respective memory cells after engaging with their cognate antigen providing lasting protection [5-7].

1.1.1 The innate immune system

The innate immune system is also known as the inborn immune system. When pathogens or other harmful agents encounter the host for the first time, innate immune responses provide immediate defense against the invader through the use of physical, cellular, and chemical barriers: (i) physical barriers such as the stratum corneum or mucus are pronounced in skin or gastrointestinal tract mucosal surfaces, respectively, just to name a few. The innate immune system, therefore, is viewed as the first line of defense. (ii) Phagocytic leukocytes (such as monocytes, macrophages, and dendritic cells) express receptors recognizing broad antigen patterns (such as CD36, CD14) on their surfaces. Phagocytes rapidly migrate to the infection site and kill the pathogens via a variety of different mechanisms [8]. As a class B scavenger receptor, CD36 forms part of non-specific receptors on macrophages and is involved in removing pathogens such as bacteria via phagocytosis. Innate immune cells also

contribute to the activation of the complement system, which is an essential component of innate immunity, via various molecular mechanisms, including the enhancement of phagocytosis and the direct killing of pathogens. (iii) NK cells are capable of killing those cells that had already been infected, i.e., by viruses or other pathogens, through a protein called perforin or the Fas-ligand pathway leading to apoptosis of the invader [9-13]. The innate immune system is immediately acting within seconds to minutes, whereas the emergence of the adaptive immune response takes days to weeks.

1.1.2 The adaptive immune system

The adaptive immune system has also been termed the acquired immune system. It is activated by pathogens or other harmful substances that escape or evade the innate immune system. Once the pathogen escaping from the innate immune system has been recognized, the adaptive immune system utilizes multiple networks of cells and pathways to provide a very specific and efficient immune response. The adaptive immune response contains two branches: T cell-mediated immunity and the humoral immune response provided by B cells [14,15].

1.1.2.1 T cell-mediated immune response

Lymphoid progenitor cells migrate from the bone marrow (BM) to the thymus, where they differentiate into naïve T cells through positive and negative selection [16]. In the adaptive immune system, a naïve T cell must encounter its specific pathogen, presented to it as a peptide, to become an effector T cell. Naïve T cells recognize peptide antigens presented by major histocompatibility complex (MHC) molecules on the surface of antigen-presenting cells (APCs). All effector T cells act on host cells, not the pathogen itself. CD8 T cells, also known as cytotoxic T lymphocytes, release a series of cytotoxins and cytokines (including tumor necrosis factor- alpha (TNF-α), TNF-β, and interferon-gamma (INF-γ)) and cytotoxic protein (including perforin and granzyme) to kill host cells harboring pathogens. CD8 T cells promote

differentiation of B cells and antibody isotype class switching by expressing B cell costimulatory proteins [17]. CD4 T cells recognize pathogen peptides presented by MHC class II molecules. MHC class II molecules carry peptide antigens from bacteria, toxins, or other foreign molecules to the cell surface and present them to $CD4^+$ T cells. These CD4 T cells will differentiate into T follicular helper (TFH) cells, Type 1 T helper (Th1) cells, Type 2 T helper (Th2) cells, and other cell types. Th1 cells can induce B cells to produce IgG antibodies to control extracellular pathogens effectively, and they can activate macrophages, which engulf and digest infected cells. Th2 cells secrete, among other, interleukin-4 (IL-4) to promote the development of B cells. TFH cells are named germinal center (GC) TFH cells because they play an important role in the formation and maintenance of GCs by upregulating the expression of CD40 ligand (CD40L) and secreting IL-21 and IL-4 [18-20].

1.1.2.2 B cell-mediated immune response

Humoral immunity is often called antibody-mediated immunity. Humoral immunity constitutes the second arm of adaptive immunity. Two types of antibody or immunoglobulin (Ig) molecules, i.e., surface Ig and secreted Ig, are expressed by B cells and plasma cells (PCs), respectively. The binding of antigen to cell surface Ig triggers intracellular signaling pathways initiating B cell development, activation, GC education, and differentiation into PCs. Secreted Ig can specifically bind to antigens to form Ig-antigen immune complexes to initiate multiple downstream effector functions, including complement activation and Fc-mediated macrophage phagocytosis. Therefore, understanding B cell development, activation, and differentiation pathways are crucial for experimental approaches to study humoral immunity. B cell development occurs in the BM, where hematopoietic stem cells (HSCs) differentiate into common lymphoid progenitor cells. Immature B cells differentiate into mature B cells before they emigrate into the blood and home to peripheral lymphoid organs. The functional rearrangement process of Ig during B cell development is the underlying mechanism leading to Ig diversification. The risk of Ig diversification may, however, lead to autoreactive BCR generation.

Central tolerance checkpoints control autoreactive BCRs in multiple ways. Mature naïve B cells encounter their cognate antigen with the help of T helper cells, then become activated. Some antigen-experienced naïve B cells enter the GC for somatic hypermutation (SHM), affinity maturation, and Ig class switching to differentiate into either memory B cells or PCs, thereby contributing to long-lasting humoral immunity. SHM occurs in GCs and to some extent outside of GCs [21]. Some of the activated B cells express activation-induced cytidine deaminase (AICDA) and begin to mutate their Ig dependent of GC reactions [22]. GC-dependent SHM is a major mechanism for Ig diversification. During these processes, peripheral tolerance mechanisms can prevent autoreactive B cells from being generated, which would lead to autoimmune tissue injury if unchecked.

1.2 The B cell development pathways

B cells are a category of white cells, which play essential roles in the innate and adaptive immune response by producing antibodies and secreting cytokines. The process of B cell development is strictly regulated by multiple factors. There are two main B cell subtypes, namely B-1 and B-2 cells (Fig.1).

B-1 B cells develop from HSCs in the fetal liver and adult BM. B-1 B cells are innate-like lymphocytes that proliferate in response to self-antigens, and self-renew to produce most of circulating natural antibodies and form short-lived PCs (Fig. 1A) [23]. B-1 B cells can be divided into two subtypes, i.e. the B-1a and B-1b cells. B1-a B cells are important for the productions of natural antibodies. B-1b B cells play an critical role in generating long-lasting protective against some specific pathogens such as *S. pneumoniae* and conferring T cell-independent long-lasting un-mutated IgM memory to pathogens [24,25].

B-2 cells develop from HSCs in the BM. Initially, B cell development from pro-B cells advances to pre-B cells and immature B cells. These developmental steps are termed central B cell development. It occurs along the functional rearrangement process of the Ig gene segment [26,27]. During these stages of development, B cells can express a mature BCR that is capable

of binding antigen. To prevent B cells from reacting to self-antigens during early development, central tolerance removes autoreactive B cells during development in the BM and generates the highly diverse BCR repertoire of mature naïve B cells in the periphery. For example, in the BM, self-reactive cells do not directly enter the periphery; instead, multivalent self-reactive B cells undergo receptor editing to modify them and - if that process fails – these BCRs will be removed by clonal deletion. Some BCRs, which recognize soluble self-molecules, become anergic by upregulating IgD on their surface. These mature naïve B cells leave the BM and enter the bloodstream, travel to secondary lymphoid organs (SLOs), where they respond to specific antigen challenges.

Mature naïve B2 cells are generated in the BM and circulate through the lymphatic and blood systems to enter the SLOs and differentiate into follicular B cells (Fol-B) and marginal zone (MZ) B cells. MZ B cells rapidly respond to antigens in the blood by secreting low-affinity antibodies [28]. Follicular B cells reside in the SLOs and participate in T cell-dependent humoral immune responses. When mature naïve B2 cells bind to their cognate antigen with T cell help, they can differentiate into short-lived PCs secreting low-affinity antibodies independent of the GC reaction or enter into a GC response where they undergo SHM and Ig class switching to generate long-lived PCs and memory B cells (Fig. 1B).

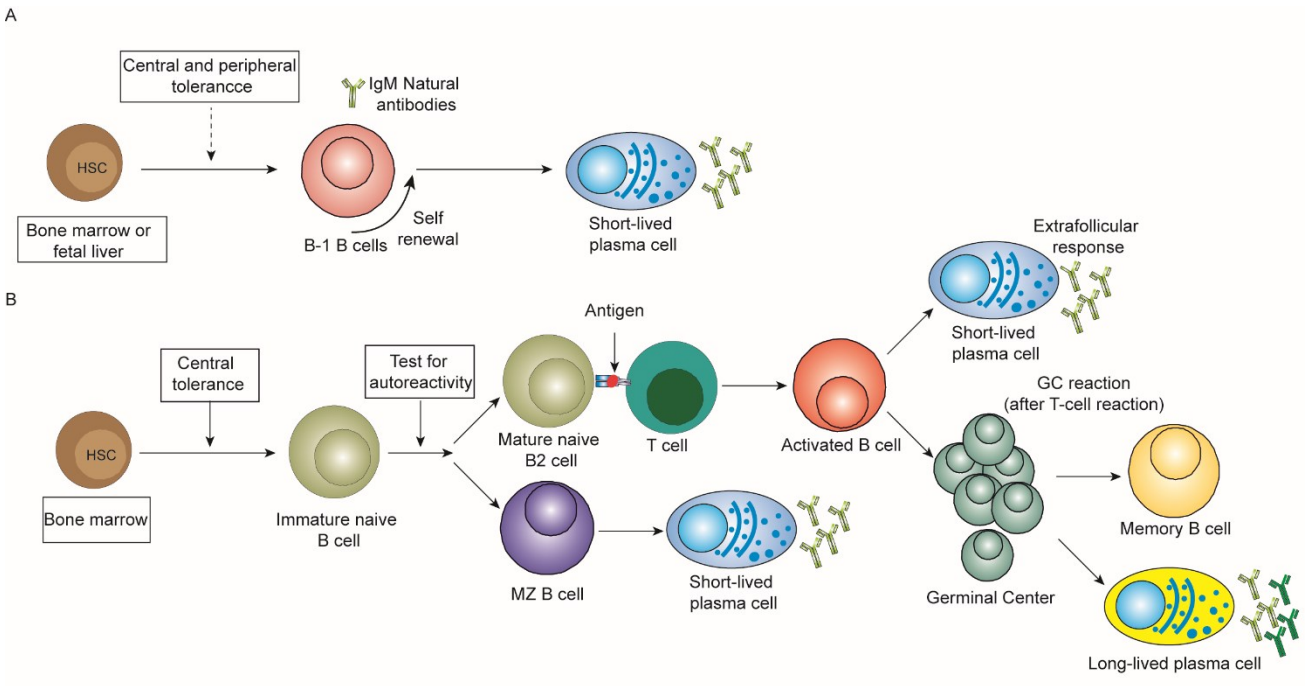

Figure 1. B cell development. (A) B1 cells may be produced in fetal liver and adult BM by HSCs. In the absence of specific antigens, they self-renew, secrete natural antibodies and differentiate into short-lived PCs. (B) HSCs in the BM are the major source of B2 cells. The development of B cells is typically considered as a linear process consisting of different stages of differentiation. The figure shows an outline of B cell lineage differentiation, with special focus on the developmental stage (adapted from Dörner T, et al. 2009) [29].

1.3 The GC B cell responses

There are two main types of B cell immune responses including T cell-independent and T cell-dependent immune responses. In the T cell-independent immune response, B cells can be activated directly by antigens. In the T cell-dependent immune response, B cells require help of T cells to respond to antigens. T cell-independent antigens contain two groups that stimulate B cells directly. The first group includes so-called mitogens, which can induce a polyclonal response in mature and immature B cells without T cell help and do not involve BCRs [28]. The second T cell-independent antigens have high molecular weight and repeating antigenic epitopes, such as bacterial capsular components and polysaccharides. T cell-dependent antigen elicits humoral immune response requires the help of T cells.

GCs, in the T cell-dependent humoral immune response against foreign pathogens, are the sites where antibodies are genetically tailored to attain high-affinity binding to their cognate antigen. The GC is divided into two different anatomical compartments, the dark zone (DZ) and the light zone (LZ). The DZ is the site of GC B cell proliferation and SHM, which contains the network of C-X-C motif ligand (CXCL) 12-producing stromal cells [30,31]. The LZ is the site of clonal selection, in which B cells capture the antigens presented on FDCs with the help of TFH to undergo selection [30]. The CD40-CD40L interaction is important for the generation of the GC reaction [32]. Human CD40L deficiency causes X-linked hyper IgM syndrome characterized by a high level of serum IgM and reduced levels of switched Ig [33].

During the GC response, when naïve B2 cells encounter cognate antigens and receive additional co-stimulatory signals in the SLO outside of the GC, they become activated. Some of the activated B cells may differentiate into short-lived PCs secreting low-affinity antibodies

independent of the GC reaction. The most likely scenario, however, is that activated B cells are recruited into the GC. In GCs, Tfh cells provide a survival signal, IL-21, which increases the affinity of B cells to antigen [34]. Meanwhile, the B cells produce lymphotoxin (LT) α and β, i.e. cytokines of the TNF family, to be involved in the generation and maintenance of FDC networks. The enzyme AICDA modifies the affinity of the BCR for the antigen by introducing SHMs. However, only a few B cells increase the BCR affinity through affinity maturation. These few B cells with higher affinity BCRs stay bound on the FDC for longer periods and are further activated to proliferate to undergo further rounds of affinity maturation. Some differentiate into long-lived antibody-secreting PCs, while others differentiate into high-affinity memory B cells. Most progeny of B cells that have undergone SHM but bind antigens with low or no affinity will be deleted through clonal selection and apoptosis, respectively. The selection of antigen-specific B cell death in GCs is usually regulated by cell death receptors and CD95 [35]. At the end of these cell cycles, various B2 cells having BCRs with distinct affinities are generated and released from the FDC surface depending on multiple factors [36]. Thus, the binding affinity of antibodies to FDC-bound antigens increases continuously during the GC response; the entire process is referred to as GC-dependent affinity maturation [32].

1.4 Immunoglobulins (Igs)

Igs are synthesized by B cells. The Igs expressed on the B cell surface are called BCRs, and those that are secreted by PCs are named antibodies.

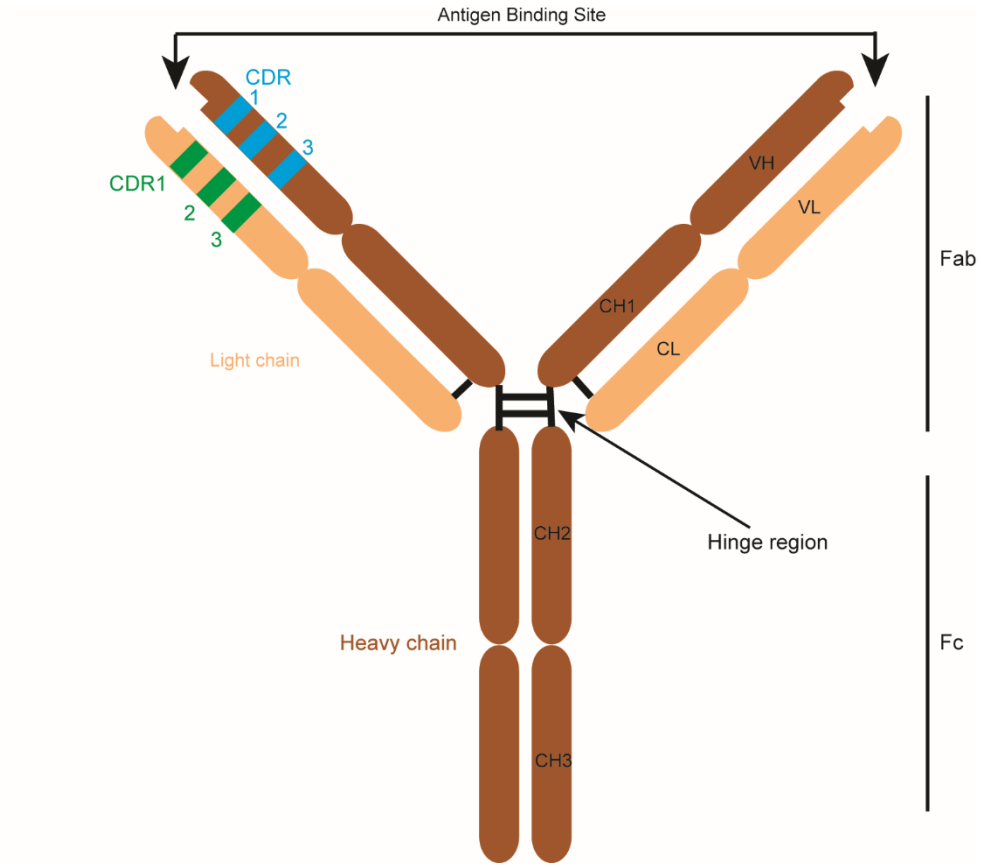

Figure 2. Schematic structure of Ig. Igs are glycoproteins. Two identical heavy chains and light chains form an Ig. The effector functions of the molecule are determined by the fragment crystallizable (Fc) region. The antigen-binding portion (Fab fragment) is joined to the Fc region through the hinge region. The complementarity-determining regions (CDRs) are part of the variable chains and serve as the antigen-binding sites (modified from Gudelj et al., 2018) [37].

Igs possess two identical heavy and light chains, which are linked by disulfide bonds. The heavy or light chain both possess a variable (V) region and a constant region (Fig.2). The V region determines antigen specificity. Three CDRs (CDR1, CDR2, and CDR3) form the critical part of the V region in Igs. These regions are sometimes called hypervariable regions, and CDR3 is the most variable region. The diversity of the CDR3 region of the V region is sufficient for most antibody specificities [38]. The structural backbone is provided by the framework regions, which make up about 85% of the V region. The constant region or Fc region can be divided into five categories (IgM, IgD, IgG, IgE, and IgA) by different heavy chains [39]. The Fc region can determine the molecular structure and modulate immune cell activity. Additionally to the five types of heavy chains, light chains can be classified into two types (kappa and

lambda light chains) based on minor differences in the polypeptide sequence of the light chain C region.

1.4.1 Generation of Ig diversity

The considerable diversity of pathogens and other foreign molecules requires an almost unlimited antibody repertoire to protect individuals from infection. There are more than 10^{12} different antibodies that a human can theoretically produce [40]. A complex multistep process generates this tremendous diversity of Igs. The process is initiated during early B cell development in the BM during somatic recombination, and then proceeds by further somatic recombination events to culminate in the GCs during affinity maturation. Thus, the B2 cell immune system can generate an almost unlimited number of different Igs highly efficiently by somatic recombination [41].

The assembly of Ig heavy chains (IgH) and Ig light chains (Ig kappa chain (IgK), Ig lambda chains (Igλ)) is slightly different. The heavy chain loci are composed of a V, joining (J), and diversity (D) gene segment, while the light chain is composed of a V and J gene segment. The enzymes RAG1 and RAG2 are encoded by recombination-activating gene (RAG), which regulate the assembly of the V, (D), and J gene segments resulting in Ig diversity [42]. The recombination process of the V region follows strict instructions. Firstly, the variable heavy chain recombines with the D-J segments. Then, the V gene is added to the DJ segment. Finally, RNA splicing of the primary RNA adds the constant region to the VDJ segment. The V region of the light chain begins with the recombination of the V and the J genes. Then, the C region is joined through RNA splicing of the primary RNA [39]. Fig.3 shows an outline of the respective V (D) J recombination processes for the assembly of the V region of the Ig. The SHM process of mature activated B cells further enhances the diversity of antibodies.

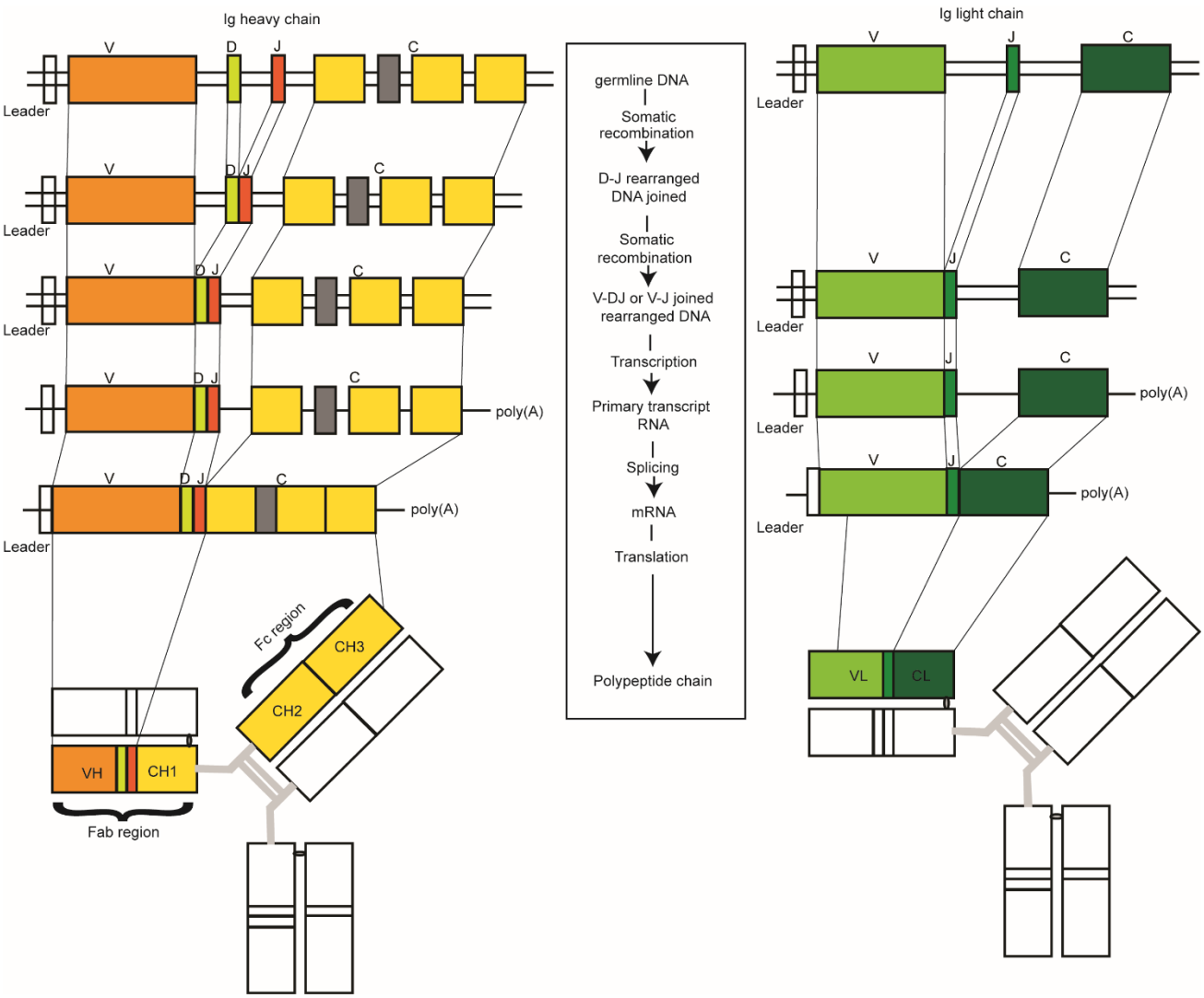

Figure 3. BCR gene recombination. The rearrangement of BCR heavy and light gene loci. The V regions of heavy chain are encoded by three gene segments (left panel). The V-region genes of light-chain are assembled by V and J segments (right panel). BCR heavy genes contain V, D, J, and constant gene segments. BCR light gene loci contain V, J, and constant gene segments. The rearrangement of V, D, and J gene segments yields a functional variable region transcribed and spliced to generate a constant gene segment. After mRNA translation, BCR heavy chains are generated. BCR light chains are rearranged in the same way. After that, synthetic BCR heavy and light chains are expressed on the surface of B cells (Modified from Janeway's Immunobiology, 8th edition, 2008) [39].

1.5 Central and peripheral B cell tolerance

Gene rearrangement and SHM of B lymphocytes are random, and therefore it is inevitable to produce some B lymphocytes or antibodies with high affinity to self-antigens. In healthy

individuals, these lymphocytes are normally removed by a variety of mechanisms. The mechanism of immune tolerance is a condition of the immune system that is mute to substances or tissues that may trigger an immune response. Immune tolerance to self-antigens must be established and strictly maintained by stringent control mechanisms to prevent autoimmunity [43]. During early B cell development, the heavy and light chains are rearranged and the B cells need to pass central tolerance checkpoints before leaving the BM (negative selection) [44]. Negative selection occurs in the BM, where immature B cells binding self-peptides are deleted. Only immature B cells with no weak or no affinity to self-antigens will survive and leave the BM to populate the periphery. On the contrary, all B cells with high-affinity binding to self-antigens will be deleted through clonal deletion, induced anergy, clonal ignorance, and more. However, negative selection cannot fully eliminate auto-reactive B cells, allowing some of the self-reactive B cells to migrate to the periphery. These B cells may cause an autoimmune attack unless they are inhibited by a series of peripheral tolerance checkpoints [45,46]. Peripheral B cell tolerance ensures that self-reactive B cells that have escaped from central tolerance do not trigger autoimmune reactions or even autoimmune disease. SHM occurs in GCs and to some extent outside of GCs [21]. SHM of BCRs in GCs or outside of GC may also lead to self-antigen responses [47]. Therefore, the mechanisms of examining self-reactive BCRs are indispensable for the establishment of peripheral tolerance. Peripheral B cell tolerance prevents the generation of autoantibodies in peripheral lymphoid organs through cytokine-driven mechanisms as well as the action of regulatory B cells (B_{reg}) and multiple further mechanisms including the action of T regulatory cells. However, the mechanism of peripheral tolerance remains an area of intense research which evolves rapidly, and many questions remain unanswered. In particular, the question of B cell tolerance in the context of atherosclerosis as a chronic inflammatory disease and the role of autoimmune B2 cells in particular remains challenging.

1.6 Tertiary lymphoid organs (TLOs) and autoimmune disease

1.6.1 The distinction between autoimmune reactions and autoimmune diseases: Witebsky criteria

Only a few autoimmune diseases meet the criteria according to the Witebsky's postulates to qualify as an autoimmune disease, such as Hashimoto thyroiditis [48], Graves disease [48], and myasthenia gravis [49,50]. These Witebsky criteria to define autoimmune disease are [51]: (i) autoantibodies can be detected in all cases of disease. (ii) The disease can be reproduced by antigen immunization. (iii) Experimental diseases must present immunopathological changes analogous to natural diseases. (iv) The disease can be transferred by serum (Igs) or lymphoid cells. It is essential to distinguish between autoimmune reactions and autoimmune diseases as autoimmune reactivity, which is commonly encountered in healthy individuals that do not develop disease pathology. Therefore, to define a disease as an autoimmune disease, the Witebsky criteria should first be tested in experimental animal models in vivo and then assessed in humans. If antibodies and T cells are directed against normal tissues, molecules, and other components, they are called "autoantibodies" and "autoreactive T cells". If we use autoantibodies and autoreactive T cells as indicators for autoimmune reactions, we will find numerous autoantibodies such as anti-nuclear antibodies anti-histone antibodies, and anti-dsDNA antibodies, and autoreactive T cells against different autoantigens in healthy and systemic autoimmune diseases [52]. In healthy individuals, the autoreactive T and B cells are kept under control and therefore do not trigger autoimmune disease [53,54]. The definition of autoimmune disease requires that the autoantibodies and/or autoreactive T cells cause a clinical symptom or damage organs [43].

1.6.2 Mechanisms underlying autoimmune diseases

The normal immune system has a highly specific and effective immune response to pathogens. A low level of a self-reactivity is physiological and essential to the normal immune response: low self-reactivity can trigger rogue cells and senescent cell apoptosis or

programmed death and therefore maintain a healthy state [55,56]. Low level of self-reactivity may also allow rapid immune responses in the early stage of infection. However, some autoreactive B cells bypass multiple tolerance checkpoints and attack self to develop autoimmune disease [57,58]. The autoimmune diseases are divided into two groups: systemic autoimmune diseases and organ-specific autoimmune diseases [59]. Autoimmunity alone may not lead to autoimmune disease. Like many complex disorders, it is believed that multiple factors cause autoimmune diseases [60]. One important phenomenon is epitope spreading, in which an increased number of autoantigens are increasingly recognized by B and T cells. Antigen spreading is often observed in autoimmune diseases from the early inflammatory stage to the chronic phase [61]. The above shows that defining disease as an autoimmune disease is very challenging since many criteria must be examined, and the disease must be triggered in experimental animals in vivo. Chronic inflammatory diseases constantly provide autoantigen epitopes to the immune system and thereby can induce polyclonal activation [62]. Genetically determined autoimmune diseases in humans are caused by polymorphisms in multiple genes involved in immune function, and there are few examples in which genetic changes in a single gene leads to autoimmunity [61]. Some environmental triggers also contribute to autoimmune diseases, such as infections, pathogenic microbiome alterations, and UV irradiation among others [63]. Thus, it is necessary to understand the mechanisms of autoimmune disease to allow pursuing therapeutic approaches as aimed in this thesis.

1.6.3 TLOs in systemic autoimmune diseases

TLOs are considered a hallmark of autoimmune diseases. They are usually present in many chronic inflammatory diseases and autoimmune diseases such as systemic lupus erythematosus (SLE) [64,65], rheumatoid arthritis (RA) [66], multiple sclerosis (MS), type 1 diabetes [67], chronic infection [68], and cancer [69-71]. Some TLOs share many features with SLOs, such as T cell areas and B cell follicles, APCs, FDCs, fibroblastic reticular cells, and high endothelial venules (HEVs) [72-76]. More than 50% of SLE patients have well-structured TLOs containing B cells, PCs, T cells, and GCs [64,65]. In half of the RA patients, TLOs ranging from

immune cell aggregates to GCs are discovered in the pathologically altered synovium and are associated with more severely affected joints and systemic inflammation [66,77-79]. TLOs are also found in Sjögren's syndrome [80-82], myasthenia gravis [50], and chronic inflammatory bowel disease [83,84]. However, the function of TLOs in autoimmune diseases is not clear. TLOs can maintain reactive CD8 memory T cells in influenza-infected mice and produce antivirus antibodies to provide effective host defense [68,85]. TLOs also maintain or stimulate lung innate lymphoid cells to limit lung cancer progression [86,87]. The infiltration of B cells and the presence of TLOs in tumors are related to the therapeutic response in patients [69-71]. After TLO formation with the help of IL-17-expressing cells, TLOs also help to support Th17 cell maintenance or acquisition of pro-inflammatory properties [88-90]. In addition, B cells in TLOs may be pathogenic, contributing to the inflammatory environment in lupus or RA [91,92]. It is tempting to speculate that TLOs in autoimmune diseases may be a source of potentially pathogenic lymphocytes, but there is no evidence for this conclusion at this point. The pathogenic or protective effect of TLOs in autoimmune diseases is still unclear, and further research is needed.

1.7 Atherosclerosis

1.7.1 Atherosclerosis is a chronic inflammatory disease of the arterial wall

Atherosclerosis is a chronic disease of the arterial wall and the major underlying cause of heart attacks and strokes, which are together the leading cause of death globally [93-95]. The disease pathology is characterized by the accumulation of lipids, monocyte-derived macrophages, T cells, rare B cells, dendritic cells (DCs), and T regulatory cells in the intima of all major arteries, including the aorta, coronary and cerebral arteries [96-98]. Epidemiological studies show that multiple risk factors, including tobacco use, unhealthy diet, hypertension, diabetes, sedentary lifestyle, obesity, gender, and age are associated with the development of atherosclerosis [99,100]. There is no treatment to target the root cause of atherosclerosis as its pathogenic mechanisms are multifactorial. Rudolf Virchow and Carl von Rokitansky were the first to describe inflammatory processes in arteries [101], which is still the focus of

atherosclerosis research today [101-104]. Both adaptive and innate immune cells, including B cells, T cells, DCs, macrophages, and neutrophils, have been identified in atherosclerotic lesions [105-107]. Under physiological conditions, the immune response is an effective mechanism to remove harmful substances and initiate healing. However, data suggest that inflammation also plays a role in injury. Immune cells can generate various cytokines that inhibit or promote atherosclerosis [108]. After decades of international research efforts, the treatment of atherosclerosis has made great progress, but atherosclerosis is still untreatable as the molecular mechanisms of the disease remain poorly understood. Several hypotheses have been proposed to explain the initiation of atherosclerosis: the “response to injury hypothesis”, the “altered lipoprotein” hypothesis, the “retention of modified low-density lipoprotein (LDL) hypothesis”, and the “autoimmune” hypothesis” [101].

1.7.2 Atherosclerosis and B lymphocytes

Innate and adaptive immune responses play crucial roles in atherosclerosis initiation and development. Different leukocyte subsets have been shown to affect the progression of atherosclerosis, including B cells. Atherosclerosis is associated with diverse B cell responses in humans and mice, although the specific functions are not fully understood[109-111]. Both atheroprotective and atherogenic B cell subtypes have been observed in atherosclerosis. Removal of the spleen in ApoE$^{-/}$ mice resulted in a more severe atherosclerotic plaque burden, while transferring splenic B cells to these mice reduced atherosclerosis, suggesting that B cells may have a protective effect on atherosclerosis [112]. However, depletion of B cells using anti-CD20 antisera in mice reduces atherosclerosis, suggesting B cells play an atherogenic role [113,114]. Therefore, the role of B cells in atherosclerosis remained controversial and provided the rationale for more in depth studies of B cell subset functions in atherosclerosis. Circumstantial evidence shows that GC B cells may promote the size and stability of atherosclerosis plaques [115]. B1a cells are atheroprotective by producing natural IgM and anti-inflammatory cytokine IL-10 [116]. However, the role of B-1b cells in atherosclerosis is not clear [117]. Recently, researchers have paid attention to B_{reg} cells due to their ability to secrete IL-10,

transforming growth factor beta (TGFß), and other presumably atheroprotective cytokines. B_{reg} cells mediate T cell immunity by IL-10, IL-12, TGF-ß, which may protect against or promote atherosclerosis [118]. The diverse roles of B cells in atherosclerosis, therefore, require more work as central questions remain unanswered.

1.7.3 Atherosclerosis and autoimmune diseases

Patients with systemic autoimmune diseases often develop severe atherosclerotic cardiovascular diseases (CVD), but the relationship between autoimmune diseases and atherosclerosis is unknown [119-121]. Atherosclerosis has been suggested to be an autoimmune disease, but proof of this notion has not been obtained. Potential autoantigens that have been proposed to play a role include low-density lipoproteins (oxidized or native), heat shock protein (HSP) 60/65, and β2 glycoprotein I (β2GPI) [122-124] . A few studies have recently shown the presence of professional APCs in atherosclerotic plaques, including classical DCs (cDCs) and monocyte-derived DCs, possibly contributing to antigen-specific immune responses in atherosclerosis[107, 123,125-128]. Oxidized low-density lipoprotein (OxLDL) is a critical pro-inflammatory mediator and may involve in the development of atherosclerosis [129]. OxLDL/C-reactive protein (CRP) complex may trigger an autoimmune response and accelerate the development of atherosclerosis [130]. Immunization with OxLDL results in the production of autoantibodies to play an atheroprotective role in atherosclerosis [131]. β2GPI, which is a natural anticoagulant, plays an important role in atherosclerosis development. OxLDL interacts with β2GPI forming pro-atherogenic oxLDL/β2GPI complexes [124]. OxLDL/β2GPI complexes trigger the production of autoantibodies, i.e., anti-β2GPI/oxLDL antibodies. The role of anti-β2GPI and anti-oxLDL antibodies in autoimmune-mediated atherosclerotic thrombosis was recognized in patients with antiphospholipid syndrome [132]. However, the autoimmune hypothesis of atherosclerosis remains on indirect evidence. Therefore, more work is required to determine which autoantigens, autoantibodies, or autoreactive cells play an essential role in the progression of atherosclerosis.

1.8 Murine and human Artery Tertiary Lymphoid Organs (ATLOs)

Lymphoid organs can be classified into primary lymphoid organs (PLOs) such as the BM and the thymus, SLOs include lymph nodes, spleen, and Peyer´s patches, and TLOs include ATLOs, which are located in the aorta adventitia of aged ApoE$^{-/-}$ mice and human patients with atherosclerosis. T- and B-lymphocytes together with other immune cells give rise to well-structured ATLOs (Fig.4) [133]. ATLOs can be divided into three stages [134]. Stage I is defined as a small number of mixed T cells and few B cells forming clusters, but they lack separate T cell vs. B cell areas. Stage II contains larger aggregates of immune cells, in which B and T cells are separated into distinct cellular compartments, but at this stage, there are no FDCs. Stage III, i.e., advanced ATLOs, show similar structures and cell compositions as SLOs, although the macrophage content in ATLOs is larger when compared to SLOs. Most strikingly, stage III ATLOs show activated GCs containing FDCs as its essential cell type. Unlike SLOs, ATLO neogenesis occurs in aged ApoE$^{-/-}$ mice, and ATLO size in mice correlates with the stages of atherosclerosis [134]., ATLO-like adventitial aggregates have also been observed in coronary arteries and abdominal aorta in human with atherosclerosis [135].

Potential mechanisms of ATLO neogenesis in aged ApoE$^{-/-}$ mice may involve T cell- and macrophage-triggered smooth muscle cell (SMC) lymphotoxin β receptor (LTβR) signaling to promote the expression of lymphorganogenic chemokines in SMCs, i.e., CXCL13 and CCL21 [136]. These SMC-derived chemokines may promote the formation of ATLOs by attracting immune cells to the adventitia. According to this notion, SMCs may function as lymphoid tissue organizer cells [137]. In support of this concept, deletion of the vascular smooth muscle cell (VSMC) LTβR in aged ApoE$^{-/-}$ mice disrupted ATLO structure and increased atherosclerosis. These data supported the hypothesis that ATLOs may protect arterial walls from atherosclerosis through VSMC-LTβR signaling [136]. More work is needed to fully understand the potential dichotomic nature of ATLOs in atherosclerosis progression.

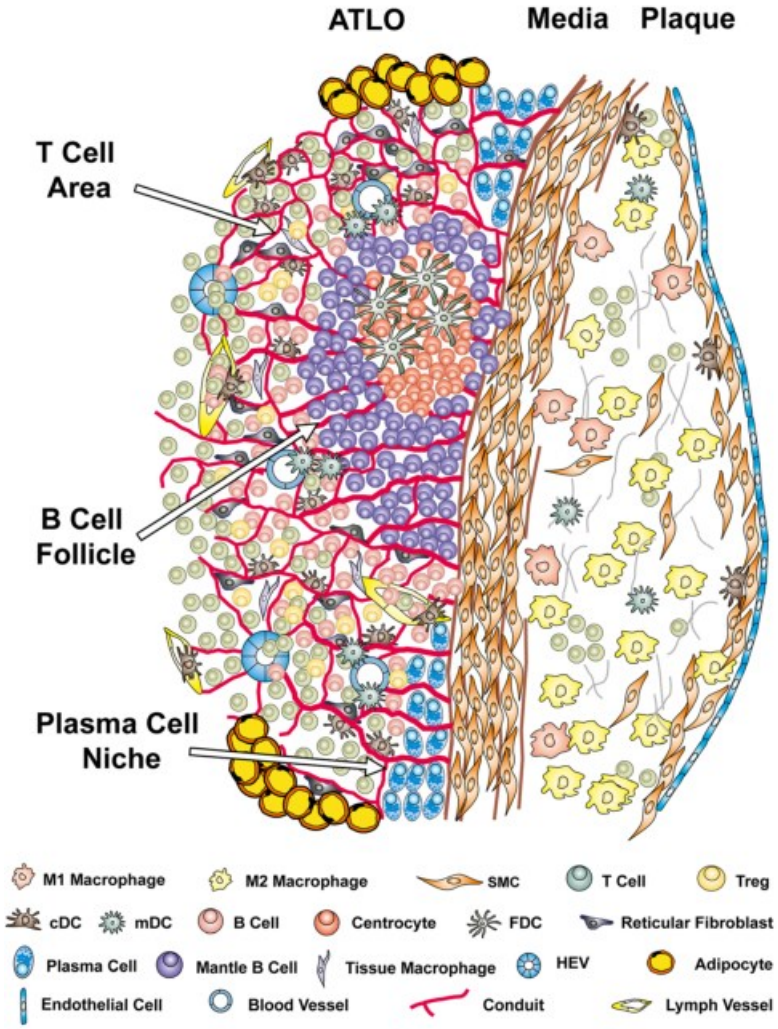

Figure 4. The structure and cellularity of ATLOs. This schematic graph shows an advanced ATLO stage in aged ApoE$^{-/-}$ mice. ATLOs show separate T cell areas and B cell follicle. The advanced ATLOs contain T cells, HEVs, aberrant lymph vessels, and B cell follicles, including activated GCs and FDCs. (Adopted from Mohanta, S.K. et al. 2014) [3].

1.9 Mouse models of atherosclerosis

Several genetically modified and transgenic animal models of atherosclerosis are available. Among them, ApoE$^{-/-}$ and low-density lipoprotein receptor (LDLR)-deficient (LDLR$^{-/-}$) mice have been widely used though each of them has limitations [138]. ApoE is a multifunctional protein, not only associated with lipid metabolism but also independently with the immune system. For example, ApoE can directly control the complement system [139]. The LDLR is a cell surface receptor that mediates ApoB-containing lipoprotein uptake in the liver. Mice that

are deficient in LDLR require a Western-type diet to develop atherosclerosis. LDLR$^{-/-}$ mice develop similar plaque pathologies when compared with ApoE$^{-/-}$ mice [140]. ApoE$^{-/-}$ mice on a normal diet and LDLR$^{-/-}$ mice on a Western-type diet have dramatically elevated cholesterol levels and atherosclerotic lesions throughout the arterial tree [141]. Although murine models of atherosclerosis have significantly contributed to our understanding of molecular mechanisms of atherogenesis, the translation of murine data to human disease remains a major challenge.

1.10 Hypothesis

Whether atherosclerosis is an autoimmune disease is one of the principal unresolved issues in atherosclerosis research. TLOs have been observed in four major groups of human diseases, including chronic microbe infection, most types of cancer, chronic transplant rejection, and autoimmune diseases. TLO formation appears to be linked to exogenous antigens: microbes, allogeneic transplantation antigens, autoantigens, and cancer antigens. The occurrence of ATLOs in atherosclerosis raises the question of whether the formation of ATLOs implies and requires one or more atherosclerosis-specific autoantigen(s). Several chronic inflammatory diseases, including atherosclerosis, show one or more components of auto-reactivity, such as auto-reactive antibodies (directed against oxidized LDL epitopes, aldehyde dehydrogenase 4 family member A1, or heat shock proteins) [122,142,143]. However, autoreactivity may be irrelevant for disease progression. We hypothesize that the presence of GCs and FDCs in ATLOs indicates the presence of one or more atherosclerosis-specific autoantigen(s) (Fig.5) [133]. If atherosclerosis indeed generates disease-specific autoantigens, ATLOs are likely to present these autoantigens in their GCs, thereby generating autoantigen-specific B cells during the GC reaction. To clarify this hypothesis, this thesis project focused on ATLO GC B cells as the source of identification of autoantigens specific for atherosclerosis. This approach is fundamentally different from previously used studies focusing on SLOs for autoantigen identification such as spleen GC B cells [142]. It is also important to note that the present approach does not seek to identify unspecific innate autoimmune B cells (for example, those generated against OxLDL) but aims to identify autoimmune B2 cells generated against

arterial wall-specific B cells from GCs.

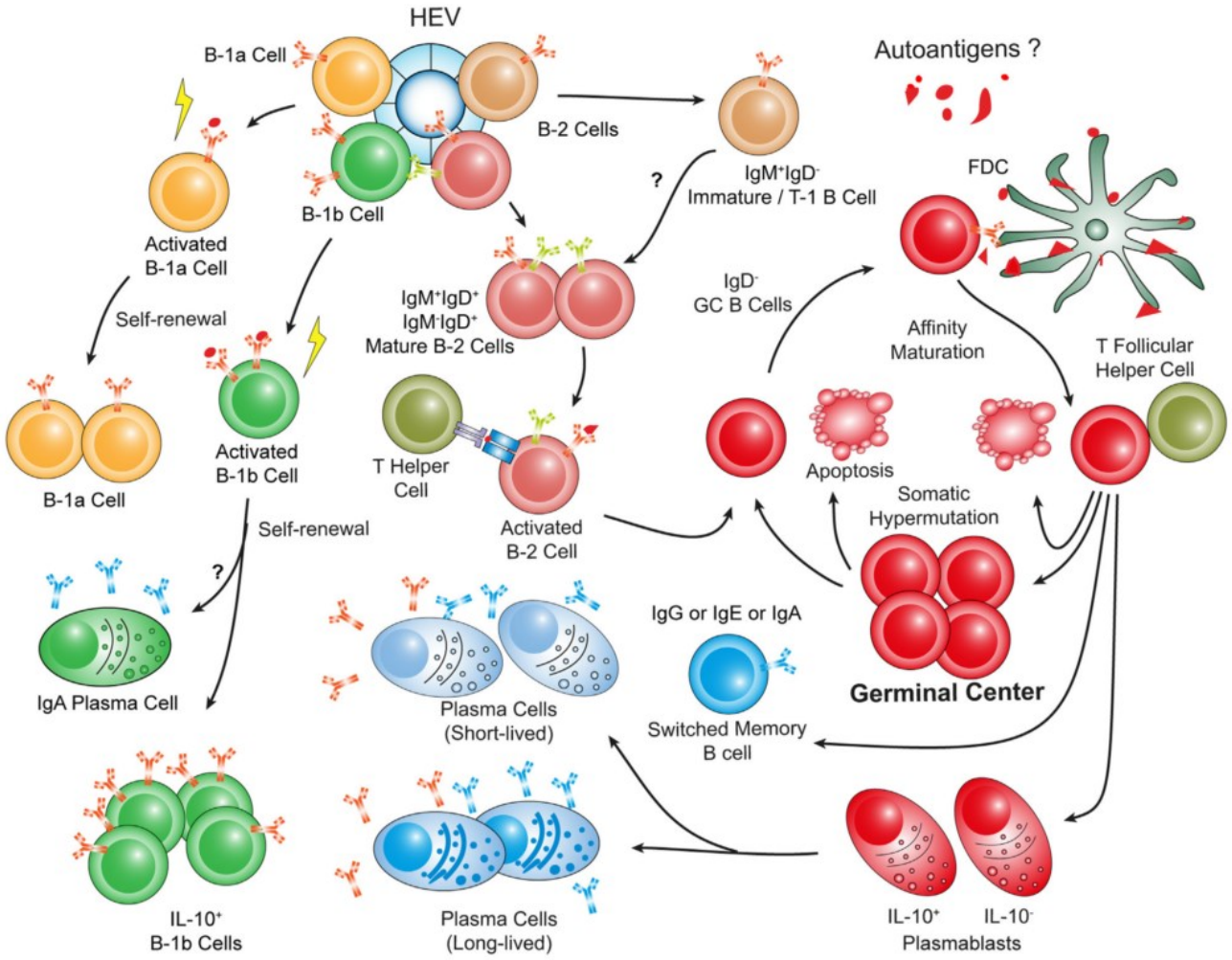

Figure 5. Hypothetical ATLO atherosclerosis-specific autoantigen-dependent B cell responses in mouse atherosclerosis. Naïve mature B cells enter ATLOs through newly formed HEVs [134,136]. There, they may bind autoantigen and are subsequently activated. Activated B1 B cells self-renew and undergo limited differentiation. Activated B2 cells enter the GC to undergo serial interactions with arterial wall-derived autoantigens presented on the surface of FDCs during multiple cell cycles resulting in affinity maturation of the mutated BCR. With the help of T helper cells, GC B cells differentiate into memory B cells with high-affinity BCRs or long-lived PCs (Adopted from Yin et al. 2016) [144].

1.11 Aims of this project

The objective of this thesis was to identify atherosclerosis-related autoantigen(s) and provide

preliminary evidence that atherosclerosis is a disease that is associated with the generation of autoimmune B2 cells capable of producing autoreactive Igs. In particular, the aim was to identify one or more atherosclerosis-related autoantigens via BCR cloning and isolation of the corresponding autoreactive B2 cells from ATLO GCs.

To identify atherosclerosis-related antigen(s) in ATLOs, the following specific aims were defined:

1) Identification of auto-reactive B cells via single-cell cloning of ATLO GC B2 cell BCRs from aged ApoE$^{-/-}$ mice.

2) *In vitro* expression of potential autoantibody candidates.

3) Examine whether these antibodies react to arterial wall constituents of aged ApoE-/- mice.

4) Examine candidate antibodies in other mouse tissues using a variety of techniques.

5) Identification of potential murine autoantigen targets of newly identified autoantibodies.

6) Translate murine findings to humans.

7) Verify the causal role of ATLO-derived autoantigen function as in atherosclerosis by vaccinating ApoE$^{-/-}$ mice.

The latter may ultimately serve as a proof of concept for the hypothesis that atherosclerosis can be considered as a bona fide autoimmune disease.

2 Materials and Methods

2.1 Materials

2.1.1 Animals

C57BL/6J mice and ApoE$^{-/-}$ mice on the C57BL/6J background were purchased from the Jackson Laboratories and maintained in a specific pathogen-free environment in the animal facility of our animal facility (ZVH - Chirurgische Klinik und Poliklinik Klinikum der Universität München). All mice were a fed standard rodent chow and on a 12 hr light/dark cycle environment. Eight weeks (young), 32 weeks (adult), and 78 weeks old (aged) male mice were used throughout this study.

2.1.2 Standard solutions and buffers

Table 2.1. Solutions and buffers

Solution	Composition	Storage
PBS (1x)	137 mM NaCl, 2.7 mM KCl, 10 mM Na2HPO4, 1.76 mM KH2PO4, pH: 7.4	RT
4 % PFA	40 g paraformaldehyde in PBS (1000 ml final), adjust pH to 7.2-7.4 with NaOH	4 °C
FACS buffer	PBS with 2 % fetal bovine serum (FBS)	4 °C
ACK lysis buffer	0.15 mM NH4Cl, 1 mM KHCO3, 0.1 mM Na2EDTA, pH 7.2-7.4	RT
MACS buffer	FACS buffer with 2 mM ethylenediaminetetraacetic acid (EDTA)	4 °C
Running buffer	35 mM SDS, 250 mM Tris, 1.92 M glycine	RT
Transfer buffer	25 mM Tris, 192 mM glycine, 20 % methanol	4 °C

TBST (1X)	20 mM Tris (pH=7.5). 150 mM Nacl, 0.1 % Tween20	RT
Blocking buffer	1x TBST with 2 % Bovine serum albumin (BSA)	4 °C
IP buffer	10 mM Hepes pH 7.6, 150 mM NaCl, 12.5 mM MgCl2, 0.1 mM EDTA, 0.5 mM EGTA, 10 % Glycerol	4 °C
ELISA coating buffer	50 mM carbonate buffer, pH 9.4	4 °C
Washing buffer	0.05 % Tween 20 in PBS	RT
Oil red O stock	0.5 % Oil red O in isopropanol	RT
Sudan IV stock	0.5 g Sudan IV in a mixture of 35 ml ethanol, 50 ml acetone, and 20 ml water	RT

2.1.3 Antibodies

Table 2.2. Antibodies for flow cytometry and immunofluorescence (IF) staining

Antibody	Clone	Format	Dilution	Company
Anti-CD16/32	93	purified	1:200	eBioscience
Anti-CD45	30-F11	PerCp-Cy5.5	1:200	eBioscience
Anti-CD19	eBio 1D3 (1D3)	APC	1:200	eBioscience
Anti-IgD	11-26c (11-26)	eFluor 450	1:200	eBioscience
PNA	--	FITC	1:200	Vector
GL-7	GL-7	Biotin	1:300	eBioscience
Streptavidin	--	APC eFluor 780	1:300	eBioscience
Anti-CD11B	M1/70	eFluor 450	1:200	eBioscience

Anti-CD11C	N418	FITC; PE	1:200	eBioscience
Anti-MHCII	M5/114.15.2	PE-cy7	1:200	eBioscience
Anti-TCRß	H57-597	Percp-cy5.5	1:200	eBioscience
Anti-CD4	GK1.5	PE-cy7	1:200	eBioscience
Anti-CD8a	53-6.7	V450	1:200	eBioscience
Fixable viability Dye	--	V500	1:1000	eBioscience
Fixable viability Dye	--	APC-cy7	1:1000	eBioscience
CD68	FA-11	Purified	1:300	serotec
SMA	1A4	FITC	1:300	SIGMA
CD11C	HL3	Purified	1:300	BD
EAH	--	Cy3	1:300	Dianova
EAR	--	Cy5	1:300	Dianova
EAK	--	Cy5	1:300	Dianova
ZAM IgG	--	AP	1:300	Santa Cruz
EAZ	--	Cy3	1:300	Dianova

Table 2.3. Digestion cocktail for murine aorta

Compound	**Final concentration**	**2.5 ml per mouse**	**company**
Collagenase I	450 units(U)/ml	9 mg	Sigma, 125 CDU/mg

Collagenase XI	125 U/ml	0.26 mg	Sigma, 1200 CDU/mg
Hyaluronidase	60 U/ml	0.34 mg	Sigma, 400 – 1000 U/mg
DNAse I	60 U/ml	0.075 mg	Sigma, 2000 U/mg
Hepes	20 mM	25 g	Sigma, MW 238.30
DPBS	1 X	2.5 ml	Invitrogen

2.1.4 Devices and reagents

Table 2.4. List of chemical kits and reagents

Name	Company	Catalogue No.	Storage
Random primers	Invitrogen	48190-011	-20 °C
SuperScript III Reverse Transcriptase	Invitrogen	18080085	-20 °C
HotStarTaq DNA polymerase	Qiagen	203203	-20 °C
RNasin Plus Ribonuclease (RNase) inhibitor	Promega	N2615	-20 °C
dNTP mix	Thermo Fisher	18427013	-20 °C
MinElute@PCR Purification kit	Qiagen	28004	RT
Corning Costar 96 Well Assay Plate	Corning	9018	RT
Substrate Reagent Pack	R&D Systems	DY999	4 °C
Novex® 4-20% Tris-Glycine Mini Gels	Invitrogen	XP04205BOX	4 °C
Bovine Serum Albumin	Sigma-Aldrich	A7030-100G	4 °C
TiterMax Gold Adjuvant	Sigma-Aldrich	T2684-1ML	4 °C
Cholesterol Quantitation Kit	Sigma-Aldrich	MAK043-1KT	-20 °C

Dynabeads™ Protein G	Thermo Fisher	10004D	4 °C
Protein A MagBeads	HöLZEL diagnostika	L00273	4 °C
PMSF Protease Inhibitor	Thermo Fisher	36978	RT
Halt™ Protease Inhibitor Cocktail (100X)	Thermo Fisher	87786	4 °C
Pierce™ BCA Protein Assay Kit	Thermo Fisher	23225	RT
RIPA Lysis and Extraction Buffer	Thermo Fisher	89900	4 °C
PageRuler™ Plus Prestained Protein Ladder, 10 to 250 kDa	Thermo Fisher	26619	-20 °C
SuperSignal™ West Femto Maximum Sensitivity Substrate	Thermo Fisher	34095	4 °C
Carbonate-Bicarbonate Buffer Capsules	Sigma-Aldrich	C3041-50CAP	RT
10% bovine serum albumin (BSA)	Aurion	70411/1	4 °C
Sudan IV	Sigma-Aldrich	198102-25G	RT
Oil red O	Romeis	S378	RT
Hematoxylin	Dako	S2020	RT
Acetone	Merck	K40718714	RT
Methanol	Roth	Sorte420	RT
Fluromount G	DAKO	S3023	4 °C
Faramount Aqueous Mounting Medium	DAKO	S3025	4 °C

Table 2.5. List of equipment

Name	Company	Application
LAS-3000 Imaging System	Fuji	Capture western blot imager
BD FACSAria™ III sorter	BD	Single-cell sorting
BD FACSCanto™ II	BD	FACS
Leica CM3050 S	Leica	Tissue section preparation
Eppendorf Master cycler PCR	Eppendorf	PCR
Leica TCS SP5 confocal microscope with four laser	Leica	Capture IF images
Infinite® 200 PRO	Tecan	ELISA
Qiaxcel Advanced	Qiagen	PCR products analysis
Biacore X 100	Cytiva	kinetics/affinity analysis, binding analysis
Sensor Chip C1	Cytiva	kinetics/affinity analysis, binding analysis
Mini Gel Tank	Thermo Fisher	Run western blot gel
Mini Trans-Blot® Cell	Bio-Rad	Western blot transfer
Centrifuge 5415 R	Eppendorf	Centrifuge
Complete blood cell counter	scil Vet abc	Blood parameter measurement
NanoDrop ND-2000	Thermo Scientific	Quantify DNA, RNA, and protein samples

2.1.5 Recombinant proteins and chimeric monoclonal antibodies

Table 2.6. List of recombinant proteins

Name	Company	Storage
Histone H2A Human, Recombinant	Biolabs	-20 °C
Histone H2B Human, Recombinant	Biolabs	-20 °C
Histone H2B Human, Recombinant	Active motif	-20 °C
Histone H4 Human, Recombinant	Biolabs	-20 °C
Histone H4 Human, Recombinant	Sigma-Aldrich	-80 °C

Table 2.7 List of recombinant chimeric monoclonal antibodies

Name	Isotype	Storage
ATLO-derived A1 antibody	Human IgG1 and mouse IgG2a	-80 °C
ATLO-derived A2 antibody	Human IgG1	-80 °C
ATLO-derived A3 antibody	Human IgG1	-80 °C
ATLO-derived A4 antibody	Human IgG1 and mouse IgG2a	-80 °C
ATLO-derived A5 antibody	Human IgG1	-80 °C
ATLO-derived A6 antibody	Human IgG1 and mouse IgG2a	-80 °C
ATLO-derived A7 antibody	Human IgG1 and mouse IgG2a	-80 °C
ATLO-derived A8 antibody	Human IgG1 and mouse IgG2a	-80 °C
Spleen-derived S1 antibody	Human IgG1 and mouse IgG2a	-80 °C
Spleen-derived S2 antibody	Human IgG1 and mouse IgG2a	-80 °C

2.1.6 Primers

All primers were synthesized and purified by Metabion international AG. The final concentration of all primers was 100 µM. The forward primers are located at the V region's beginning, and the reverse primers are in the constant region. The primers designed for the variable regions of the BCR heavy and light chains were according to the Hedda Wardemann and Michel C Nussenzweig as reported [145-147]. The primer designed “outer” or “inner” referred to the position of primers in nested PCR analyses. Primers were separated into small volume aliquots to avoid contaminations and stored at -80 °C.

Table 2.8 Primers used for amplification of BCRs from single B cell.

Forward primer	**Nucleotide sequence (5’-3’)**
Ig-Heavy	GAGGTGCAGCTGCAGGAGTCTGG
Ig-Kappa	GAYATTGTGMTSACMCARWCTMCA
Ig-Lambda 1/2	CAGGCTGTTGTGACTCAGGAATC
Ig-Lambda x	CAACTTGTGCTCACTCAGTCATC
Reverse primer	**Nucleotide sequence (5’-3’)**
IgA-outer	TGGGAAGTTTACGGTGGTTATATC
IgA-inner	TGCCGGAAGGGAAGTAATCGTGAAT
IgM-outer	TGGGAAGGTTCTGATACCCTGGATG
IgM-inner	TAGTTCCAGGTGAAGGAAATGGTGC
IgG-outer	AGAAGGTGTGCACACCGCTGGAC
IgG-inner	GCTCAGGGAARTAGCCCTTGAC
IgKappa-outer	ACTGAGGCACCTCCAGATGTT

IgKappa-inner	TGGGAAGATGGATACAGTT
Igλ-outer	GTACCATYTGCCTTCCAGKCCACT
Igλ -inner	CTCYTCAGRGGAAGGTGGRAACA

Red color code indicates degenerate primers. W = A or T, S = C or G, R = A or G, Y = C or T, K = G or T, M = A or C.

2.2 Methods

2.2.1 Mouse dissection and tissue collections

Each mouse was anesthetized intraperitoneally with a 500 µl solution containing 25µl ketamine (10 %) and 50 µl xylazine (20 mg). The mouse's arms were fixed on a cork platform. Blood was drawn from the heart by a 1 ml syringe and kept on a tube to obtain serum or plasma. The skin was opened from the abdomen to the thoracic part, and a small incision was made in the right atrium of the heart. Then, mice were perfused with 10 ml of 5 mM EDTA in PBS, 10 ml 1x PBS, and 10 ml FACS buffer to remove the blood from the blood vessels. Aorta, spleen, and LNs were collected and preserved in FACS buffer at ice-cold temperature to prepare single-cell suspensions. Other tissues such as the aortic root, liver, lung, kidney, spleen, and intestine were collected and embedded with Tissue Tec. Tissue blocks were kept at -80 °C.

2.2.2 Complete blood count

Blood was collected into an EDTA-precoated tube by using 1 ml syringes with a 23-gauge needle. Anticoagulated blood was used to analyze the blood parameters (such as lymphocytes, monocytes, and red blood cells) by using the complete blood cell counter (Scil Animal Care Company GmbH). The reports of blood parameters were automatically recorded.

2.2.3 Total cholesterol assay

Blood was collected into a EDTA-precoated tube by using 1 ml syringes with a 23-gauge needle. Anticoagulated blood samples from mice were centrifuged at 6000 rpm for 10 min, then the plasma was collected and used for the determination of total cholesterol according to the manufacturer's instructions using the cholesterol quantitation kit (Sigma).

2.2.4 Human samples

All human atherosclerosis plaque tissues were provided by the Bio-Bank Munich, TUM, Munich according to the guidelines, and the protocols were approved by the ethics committee of the Faculty of Medicine LMU. Atherosclerosis plaques were taken from patients who have high-grade carotid artery stenosis (>70 %) and underwent endarterectomy. Plasma samples were from 65 patients diagnosed with CVDs, of which 31 patients did not have neurological symptoms, and the remainder had undergone neurological symptoms. i,e, strokes. Plasma samples were stored at -80 °C, while human artery tissues were embedded with TissueTec and stored at -80 °C.

2.2.5 Isolation of single cells

2.2.5.1 Preparation of single cells from aorta, secondary lymphoid organs, liver, and lung

Aorta: The entire aorta was cut into small pieces and digested with enzyme cocktail (Table 2.3) at 37 °C for 50 min with shaking. After digestion, single cell suspensions were filtered through a 70-µm cell strainer. The collected single-cell suspensions were centrifuged at 400 x g for 5 min at 4 °C and re-suspended in 1 ml FACS buffer. **Spleen and LNs**: Mouse spleen and LNs were cut into small pieces, the tissues were softly smashed with syringe plunger and filtered through a 70 µm cell strainer. The collected cell suspensions were centrifuged at 400 x g for 5 min at 4 °C and re-suspended with 5 ml ACK lysis buffer and incubated for 5 min at RT to remove red cells (the step is unnecessary for LNs). Then, 5 ml FACS buffer was added to stop lysis and centrifuged at 400 x g for 5 min at 4 °C. The pellet was re-suspended

with 5 ml ice-cold FACS buffer and passed through a 70 µm cell strainer**. Liver and lung**: Mouse liver was collected, cut into small pieces, and mashed with a 70 µm cell strainer. A total of 15 ml ice-cold FACS buffer was added and centrifuged at 400 x g for 10 min at 4 °C. Percoll was diluted to 40 % and 60 % solutions with PBS. The pellet mixed with 4 ml of 40 % Percoll was slowly sliding along the 15 ml Falcon tube wall containing 5 ml 60 % Percoll solution and centrifuged at 900 x g for 25 min at 4 °C. The cells were carefully aspirated from the interface and collected in a 50 ml Falcon tube. The cell suspension was centrifuged at 300 x g for 10 min at 4 °C and re-suspended in 5 ml of ACK lysis buffer and incubated for 5 min at RT. An additional 5 ml FACS buffer was added to stop lysis and centrifuged at 400 x g for 5 min at 4 °C. The pellet was re-suspended with 5 ml ice-cold FACS buffer and passed through a 70 µm cell strainer. To prepare single-cell suspensions from lung, the lung was cut into small pieces and digested in 3 ml DPBS containing 0.2 mg/ml collagenase type IV and 0.1 mg/ml DNAseI at 37 °C for 45 min. The digested lung tissue was filtered through a 70 µm cell strainer, and the volume was adjusted to 10 ml with FACS buffer. The remaining procedures were similar to those described above.

2.2.5.2 Cell counting

Five µl cell suspension solution was mixed with 5 µl trypan blue. The pre-mix sample was loaded onto a slide (Bio-Rad), then the slide was inserted into TC20™ Automated Cell Counter (Bio-Rad) to obtain the total and live cell counts in 30 seconds.

2.2.5.3 Staining with labeled antibody

For flow cytometric analysis, 1.5 x 10^6 cells were added to 96 well v-shaped bottom plates, adjusted to 200 µl by adding FACS buffer, and centrifuged at 300 x g at 4 °C for 5 min. The supernatant was discarded, and FACS buffer with Fc Block (purified CD16/32) was added to incubate for 10 min and centrifuged at 300 x g at 4 °C for 5 min. Without washing, primary antibodies were added to the well and incubated for 25 min at 4 °C. Cells were washed twice

with FACS buffer and centrifuged at 300 x g at 4 °C for 5 min. For intracellular staining, the cell suspensions were incubated with 200 µl of freshly prepared fixation/permeabilization working solution according to the manufacturer's instruction for 1 hr at 4 °C. The sample was washed 2 times with 300 µl of 1 x permeabilization buffer and centrifuged at 300 x g at 4 °C for 5 min. After centrifugation, the antibody was added and incubated for 40 min at 4 °C. The sample was centrifuged and washed twice with 200 µl FACS buffer. Pellets were re-suspended with 200 µl FACS buffer and filtered through a 70 µm filter.

2.2.5.4 Analysis of total leukocytes by flow cytometry

BD FACS Canto™ II were used to perform Flow cytometry. FACS sorting were performed using BD FACSAria™ III sorter. Leukocytes from spleen, lung, and liver were stained with antibodies against FVD, CD45, CD19, TCRß, IgD, PNA, GL7, CD11b, CD11c, MHCII, and ATLO-derived antibodies. Leukocytes from aorta were stained with antibodies against FVD, CD45, CD19, IgD, PNA, GL7. Following gating for live cells, leukocyte subpopulations were defined as follows: B cells ($CD45^+TCRß^-CD19^+$), T cells ($CD45^+TCRß^+CD19^-$), GC B cells ($CD45^+CD19^+IgD^-$ $GL7^+PNA^+$), DCs ($CD45^+TCRb^-CD19^-CD11b^+CD11c^+$), CD11b+monocytes ($CD45^+TCRb^-CD19^-CD11b^+CD11c^-$), and $MHCII^+$ APCs ($CD45^+TCRb^-CD19^-MHCII^+$). Unless otherwise indicated, 500000 live cells were measured from spleen, liver, and lung. The single GC B cell ($CD45^+CD19^+IgD^-$ $GL7^+PNA^+$) was sorted with BD FACSAria™ III sorter. The monoclonal antibodies were purchased from eBiosciences and vector (see Table 2.2). Date were analyzed using FlowJo_v10.7.2 software (Tree Star).

The t-Distributed Stochastic Neighbor Embedding (t-SNE) is a method for visualizing multi-dimensional flow cytometry data in a two or three-dimensional distribution [148]. The t-SNE dimensionality reduction mapping was applied for total live $CD45^+$ leukocytes of spleen, liver, and lung analysis using FlowJo (version 10) [149]. Live leukocytes (5000 cells) were used for the t-SNE analysis.

2.2.6 Polymerase chain reaction (PCR)

2.2.6.1 Complementary deoxyribonucleic acid (cDNA) synthesis

Single cell was sorted into 96 well PCR plates containing 4-µl lysis buffer (final concentrations: 0.5 x DPBS without Ca/Mg, 3 U/µl RNasin Plus RNase inhibitor (Promega), 10 mM dithiothreitol (DTT). After sorting, plates were centrifuged at 400 x g for 30 s at 4 °C. Total RNA from a single GC B cell was reversely transcribed in RNA/DNA free water using 128 ng random primers (Invitrogen), 16.2 U RNasin Plus RNase inhibitor (Promega), 0.3 % IGEPAL CA-630 (Sigma-Aldrich), 100 mM DTT, 12.6 mM deoxynucleoside triphosphate (dNTP), and 50 U Superscript® III reverse transcriptase (Invitrogen). Analyses were performed under a hood to avoid spurious PCR product contamination. Plates were placed in a thermo cycler and ran using the following program:

Temperature (°C)	Duration (min)
42	10
25	10
50	60
94	5
4	Forever

2.2.6.2 Nested PCR for amplification of mouse Ig transcripts

Nested PCR was used to amplify mouse IgH and IgL chains independently. 4-µl cDNA was used as template to perform PCR reactions in 96-well plates in a total volume of 42 µl containing 0.3 µM/µl dNTP, 0.3 µM each primer or primer mix (Table 2.7), and 0.05 U/µl Hot Star Taq enzyme (Qiagen). Seq-PCR amplification of the IgH and IgL chains with gene-specific primers was performed with 4 µl of unpurified first PCR products. Each round of PCR was performed for 50 cycles to ensure sensitivity with a hot start reaction at 95 °C, which is

necessary to activate the enzyme (Table 2.8, Table 2.9, and Table 2.10).

Table 2.9. First PCR program

Cycle step	Number of cycles	Temperature	Duration
Initial denaturation	--	95 °C	15 min
Denaturation Annealing Extension	50 X	94 °C 55 °C 72 °C	0.5 min 0.5 min 1 min
Final extension	--	72 °C	10 min

Table 2.10. Seq-PCR amplification of the heavy chains

Cycle step	Number of cycles	Temperature	Duration
Initial denaturation	--	95 °C	15 min
Denaturation Annealing Extension	50 X	94 °C 60 °C 72 °C	0.5 min 0.5 min 1 min
Final extension	--	72 °C	10 min

Table 2.11. Seq-PCR amplification of the light chains

Cycle step	Number of cycles	Temperature	Duration
Initial denaturation	--	95 °C	15 min

Denaturation Annealing Extension	50 X	94 °C 58 °C 72 °C	0.5 min 0.5 min 1 min
Final extension	--	72 °C	10 min

The QIAxcel advanced system (Qiagen) was used to identify amplification products of appropriate size.

2.2.7.3 MinElute@PCR purification

PCR purification was performed to remove plethora primers, nucleotides, and DNA polymerase from PCR reactions, which is a necessary procedure for DNA construction. MinElute@PCR Purification kit (Qiagen) was used to purify PCR products according to the manufacturer's instructions. Five volumes of Buffer PB were added to 1 volume of the PCR reactions and mixed well. The mixture was transferred into spin columns and centrifuged at 13000 rpm for 1 min. The liquid was discarded and 750 µl PE buffer was added to wash spin column. The sample was centrifuged at 13000 rpm for 2 min to remove PE buffer, and 10 µl EB was added to elute DNA products. As a result, purified DNA was ready for sequencing.

2.2.7.4 Ig gene sequence analysis

All samples were sequenced by Sanger sequencing at the Faculty of Biology, LMU (*http://www.gi.bio.lmu.de/sequencing*), Munich. Sample requirements for 'cycle clean and run 3.0'. Purified PCR products were sequenced in a final volume of 7 µl. Respective reverse primers for sequencing were provided at 1:30 (original concentration 100 µM) according to the instructions of the Faculty of Biology, LMU. Obtained Ig gene sequences were analyzed by Immunogenetics information system (IMGT) (*http://www.imgt.org/IMGT_vquest/vquest?livret=0&Option=mouseIg*).

2.2.7.5 Directional cloning into expression vectors

After obtaining detailed amino acid sequences of Ig genes, two or more sequences that shared >70% identical CDR3 amino acid sequences were grouped into one cluster [150]. Paired heavy and light chains from these clusters were selected to generate monoclonal antibodies *in vitro*. The selected paired V regions of IgH and IgL gene segments were synthesized and cloned into modified pcDNA 3.4 vectors at GenScript company (*https://www.genscript.com/)*. The pcDNA 3.4 vectors contained the nuclei sequences of C regions of human IgG1 or sequences of C regions of mouse IgG2a.

2.2.7.6 Recombinant antibody production and purification

The recombinant antibodies were produced and purified at GenScript company. (*https://www.genscript.com/)*.

2.2.8 Immunofluorescence staining

Immunofluorescence staining was performed using ATLOs-derived antibodies, spleen-derived antibodies, CD68, alpha-smooth muscle actin (SMA), and CD11c.10 µm fresh-frozen sections from mice tissues and humans carotid plaques were prepared by a cryostat and stored at -80 °C. Tissue sections were heated on the hotplate at 37 °C for 1 min and air dried at RT for 30 min. Sections were fixed with 4 % paraformaldehyde (PFA) for 3 min at 4 °C, followed by rinsing with PBS. After diving in acetone for 2 min at RT, the sections were rinsed in PBS for 10 min. Primary antibodies (diluted in PBS / 0.25 % BSA) were incubated overnight at 4 °C in a humid chamber. Sections were incubated with fluorescently labeled secondary antibodies (diluted in PBS with 0.25 % BSA) and 4', 6-diamidino-2-phenylindole (DAPI) (1: 500, 0.1 g/ml) in a humid chamber for 60 min in the dark after washing three times with PBS. After washing with PBS, slides were mounted with Fluoromount G (DAKO).

Human sections were heated on the hotplate at 37 °C for 1 min and air dried at RT for 30 min. Sections were fixed with 4 % PFA for 3 min at 4 °C, followed by rinsing with PBS. After fixation,

specimens were blocked with blocking buffer (1 X PBS / 5 % normal serum / 0.3 % Triton X-100) for 30 min at RT and incubated with diluted ATLOs derived antibodies overnight at 4 °C, and then rinsed with PBS for 3 X 5 min. Specimens were incubated with an antibody without a fluorescent label (purified goat anti mouse IgG) for 1 hour at RT. After that, specimens were incubated with secondary antibodies (donkey anti goat) with fluorescently and DAPI (1: 500, 0.1 g/ml) for 1 hr at RT, then sections were washed with PBS in the dark and mounted with Fluoromount G. The primary antibody was omitted as a negative control, and the rest of the procedure was carried out as described.

2.2.9 Quantification of $CD68^+$ macrophage and SMA^+ SMCs infiltration in the plaque areas

10 μm mouse aortic root sections were stained with CD68 (macrophage/DCs), SMA (SMCs) by immunofluorescence staining as described above. 6-8 aortic root sections per mouse were used for quantification. Confocal laser scanning microscope TCS SP8 (Leica, Germany) was used to take digital pictures. 20x objective and 10x ocular lens were used. The ImageJ software was used to quantify the $CD68^+$ macrophage areas and SMA^+ areas within plaques. The calibration was done in TIFF format, the ‘polygon selections’ tool was used to delineate the intimal layer manually. The size of CD68 positive areas were measured by ImageJ software.

2.2.10 Protein analyses

2.2.10.1 Extract protein from aorta

Aorta was washed with ice-cold PBS twice to remove the blood, and then weighted.The aorta was cut into small pieces while keeping it on ice. 300 μl ice-cold RIPA buffer (for 5 mg tissues) was added, and then, homogenized with an electric homogenizer on ice. Samples were centrifuged at 13000rpm for 10 min at 4 ℃.Supernatant was collected into a fresh tube and was kept on ice. Lysates were aliquoted and stored at -80 °C and remained stable for several

months.

2.2.10.2 Protein quantification (BCA protein assay kit)

The BSA standard was diluted stepwise to 2 mg/ml, 1 mg/ml, 0.5 mg/ml, and 0.25 mg/ml in radioimmunoprecipitation assay (RIPA) buffer. The BCA working reagent was prepared by mixing 50 parts of BCA Reagent A with 1 part of BCA Reagent B (50: 1, Reagent A: B). A blank, the standards, and mouse aortic lysates were mixed with the BCA working reagent (sample to BCA ratio 1: 20) respectively and incubated at 37 °C for 30 min in the dark. The absorbance was measured with a spectrophotometer set to 562 nm. The corrected OD was plotted against the standard protein concentrations. The protein concentrations were calculated by using the following formula: Concentration (mg/ml) = [(OD of the test sample) / (OD of the standard sample)] X concentration of the standard sample.

2.2.10.3 Western blot

Equal amounts of protein lysates (20 – 30 µg of total tissue homogenate) were mixed with the corresponding volume of 2 X SDS sample buffer (ThermoFisher) and heated at 85 °C for 5 min. Subsequently, samples were loaded onto a 4 - 20 % Tris-Glycine gel (ThermoFisher), along with molecular weight marker. The proteins were separated on the gel for 1 – 2 hr at 120 voltage, and transferred from the gel to the membrane at 300 mA for 1.5 hr on ice.

2.2.10.4 Antibody detection

Membranes were subsequently blocked for 2 hr at RT in 5 % BSA blocking buffer. After that, the membrane was incubated with ATLO-derived antibodies overnight in a shaker at 4 °C. Membrane was washed with TBST and incubated with the horseradish peroxidase (HRP) conjugated secondary antibody in blocking buffer at RT for 1 hr. The last step was to wash the membrane three times with TBST for 10 min. The HRP chemiluminescent substrate (Thermo Fisher) working solution was prepared by mixture of equal parts stable peroxide

solution and enhanced substrate solution in a clear tube (600 µl per membrane) and added to the membrane. CCD camera imaging devices were used to detect chemiluminescence.

2.2.11 Enzyme-linked immunosorbent assay (ELISA) for anti-histone H2b in the circulation

In order to determine the titer of anti-histone H2b in the circulation of humans and mice, 100 µl purified recombinant histone H2b proteins at 2µg/ml concentration in the carbonate-bicarbonate buffer (Sigma) were immobilized on high binding capacity microliter plates (Costar) overnight at 4 °C. Then, the microliter plates were blocked with 300 µl per well of 2 % BSA for at least 2 hr at RT. Subsequently, H2b-coated plates were incubated for 1hr at RT with 100 µl recombinant anti-histone H2b antibody as standard (recombinant anti-histone H2b antibody was diluted stepwise to 500 ng/ml, 250 ng/ml, 100 ng/ml, 50 ng/ml, 25 ng/ml, 10 ng/ml, and 5 ng/ml in antibody dilution buffer) or serum from 8, 32, 78 weeks WT and ApoE$^{-/-}$ mice (at 1: 250 dilution) and humans with atherosclerosis (at 1: 200 dilution). The plates were incubated with HRP-conjugated secondary antibodies (1: 2000, Southern Biotech) for 1 hr at RT in the dark. In the end, 100 µl per well of TMB (Kementec Diagnostics) was used to incubate plates for 5-15 min at RT. The 2 N sulfuric acid (100 µl per well) was used to stop the ELISA reaction at an OD value between 1-2. The absorbance was measured at 450 nm using a multi-well plate reader (SpectraFluor Plus, Tecan). 250 µl per well washing buffer was used to wash plates five times between incubations.

The standard curve was drawn based on known recombinant anti-histone H2b antibody concentrations plotted against the absorbance values after subtracting the OD value from the background value (no antibody background). Sigmoidal 4-parameter was used to fit the standard curve in GraphPad Prism 6. The serum samples background-subtracted OD values were inputted into Prism and the concentration of serum samples were reported as ng/ml.

2.2.12 Immunoprecipitation (IP) and protein mass spectrometry (MS)

IP-MS was used to examine whether an antibody interacts with target proteins. Firstly, Protein A and Protein G were used to capture ATLO derived antibodies through binding the Fc regions of Igs to protein A/G. Fifty µl of total protein A/G beads were taken (i.e., 25 µl of protein A + 25 µl of protein G) into a clean tube and washed three times with 500 µl IP buffer for 5 min at RT. The tube was placed on the magnet and the supernatant was removed in each wash. After that, 8 µg antibodies (500 µl IP buffer+ antibodies) were added to couple to the 50 µl beads and incubated on a rotating wheel overnight at 4 °C in a 1.5 ml clean tube. The next day, after washing 3 times with IP buffer, protein extract was added to the IP solution. The samples were incubated for 2 - 4 hrs on a rotating wheel at 4 °C, depending on the quality/concentration of the antibody and the abundance of the input material. Then, samples were washed 3 times with IP buffer but this time with 5 - 10 min incubations on a rotating wheel at 4 °C. The tube was added 50 mM NH_4HCO_3 to invert 10 times, and placed on the magnet to remove the supernatant. After the second NH_4HCO_3 wash, 1 ml NH_4HCO_3 was added to re-suspend the beads and moved them to a fresh tube. The tube was placed on the magnet to remove as much supernatant as possible with 200 µl pipette tips. The samples were digested 30 minutes at 25 °C at 800 rpm with 100 µl (or enough to cover the beads) of 10 ng/µl trypsin in 1 M urea in 50 mM NH_4CO_3. The supernatant was collected into a fresh tube. After that, the beads were washed twice with 50 µl of 50 mM NH_4HCO_3 and pooled the supernatants into the corresponding tube. These tubes were added DTT to a final concentration of 1 mM DTT (2 µl for 200 µl) and digested overnight at 25 °C at 800 rpm. The next day, samples were added 10 µl of iodoacetamide (5 mg/ml) and incubated for 30 min in the dark at 25 °C. Then, 1 µl of 1 M DTT was added to incubate for 10 min at 25 °C. During incubation, the following buffer was prepared: (I) Methanol; (II) 80 % acetonitrile, 0.1 % trifluoroacetic acid (TFA); (III) 0.1 % TFA; (IV) 80 % acetonitrile, 0.25 % TFA, and washed 2 X C18 stagetips by 20 µl buffer I, 20 µl buffer II, and 20 µl buffer III. After incubation, 2.5 µl TFA was added to desalt the samples. Samples were loaded to C18 tips and centrifuged at 300 g for 3min. In the following, C18 tips were washed 3 times with 20 µl buffer III and a fast

stir of dry at 11000 g for 5 min. 3 X 15 µl buffer IV was used for eluting samples and samples were dried with freeze dryer. Then, 15 µl buffer III was used to dilute and ultrasound samples. The final step was to load the sample to the sample tube (avoid bubbles) and run MS with the help of Dr. Shibojyoti Lahiri, at Biomedical Center Munich Molecular Biology, LMU.

2.2.13 Surface plasmon resonance experiment

The surface plasmon resonance experiments were performed by Dr. Xavier BLANCHET IPEK, LMU using a BIAcore X 100 (Cytiva, Freiburg, Germany) equipped with a research-grade C1 sensor chip. The ligand was immobilized using amine-coupling chemistry at a density of 492 resonance U on flow cell 2; flow cell 1 was left empty to be used as a reference surface. Analytes in running buffer (PBST: 0.1 % tween 20 with 0.05 % BSA in PBS, pH 7.4) were injected at a flow rate of 90 µl/min. The complex was allowed to associate and dissociate for 60 and 240 s, respectively. The surfaces were regenerated with 2 pulses (60 s) of 30 mM NaOH, 2 M NaCl, 0.3 % TritonX - 100. Responses from analyte injections (colored curves) were overlaid with the fit of the 1: 1 interaction model (shown as red curve) determined using BIACORE X 100 evaluation 2.0 software.

2.2.14 H2b vaccination on atherosclerosis development in ApoE$^{-/-}$ mice

2.2.14.1 Emulsion formation

Five hundred µl TiterMax@Gold Adjuvant (Sigma) was loaded in one syringe and 500 µl H2b protein (containing 125 µg H2b proteins) in PBS was loaded in the second syringe. Then, two syringes were connected with a 3-way stopcock. Firstly, the H2b protein was pushed into the adjuvant syringe to mix the adjuvant and the H2b protein. The emulsion was formed by pushing the adjuvant and H2b mixture back and forth through the stopcock for few mins. By dropping the adjuvant - H2b emulsion on the surface of water, the adjuvant - H2b emulsion should look similar to whipped cream and should be kept together.

2.2.14.2 H2b vaccination in ApoE$^{-/-}$ mice

After preparing the adjuvant – H2b emulsion, each 8 week-old ApoE$^{-/-}$ mouse either received 200 µl PBS alone, adjuvant, or H2b (25 µg) + adjuvant by intraperitoneal injection. Four weeks after the primary injection, 25 µg H2b in 200 µl PBS was used as the booster injection. The control group received the same volume of PBS. Every 1 or 2 weeks, the body weight was measured. The blood was collected through the tail vein at 0, 20, and 32 weeks to measure the titer of antibodies and cholesterol levels. Animals were sacrificed at 32 weeks of age. The whole aorta and aortic root were collected to analyze the atherosclerosis development.

2.2.14.3 Atherosclerosis quantification

En-face Sudan IV staining was used to analyze the total plaque burden load in the aortic arch, thoracic and abdominal aorta. For en-face Sudan IV staining, the whole aorta was fixed with 4 % PFA at 4 °C overnight. Then, the adventitial adipose tissues were carefully removed. The aortas were pinned on a black plate after the whole aorta was cut open longitudinally. Aorta was washed three times with PBS for 10 min; a working solution of Sudan IV was used to immerse the aorta for 10 min. Aortas were washed twice with 70 % ethanol and stored at 4 °C after covering with PBS.

To assess the percentages of lipid in the whole aorta, arch, thoracic, and abdominal parts, a digital camera (Leica) was used to capture images with a standard bar. Image J was used to measure the percentages of lipid deposition in the whole aorta, arch, thoracic, and abdominal parts as previously [139,151].

Oil-red-O (ORO) staining was used to analyze atherosclerotic plaque areas. The frozen aortic root (10 µm) sections were heated at 37 °C for 1 min, and air-dried for 30 min in RT. These aortic root sections were immersed in 60% isopropanol for 5 min and then were stained in ORO work solution for 10 min. After that, these aortic root sections were immersed in 60 % isopropanol for several seconds and washed with tap water. Hematoxylin was used to stain sections for 6 min, followed by tap water washings for 10 min. Faramount Mounting Medium was used to mount the cover slides on tissue sections.

Thunder imaging system (Leica) was used to capture ORO staining images. Atherosclerotic lesion areas were quantified by Image J. After image calibration as described above, the measurement toolbar ‘polygon selections’ icon was chosen to delineate the intimal layer aortic root. The size was measured by ImageJ.

2.2.15 Statistical analyses

GraphPad-Prism 6 was used to perform statistical analysis. The measured values were expressed as means of n samples ± SEM. Two-tailed unpaired Student’s t-test was used to compare two groups; one-way analysis of variance (ANOVA) was used to compare multiple independent groups, and two-way ANOVA was used to compare multiple groups of two factors. P-value <0.05 was considered statistically significant.

3. Results

3.1 Cloning of paired heavy and light chains of BCRs from single B cells

Each B cell carries a unique BCR or antibody sequence on the cell surface, which contains the paired IgH and IgL chains. It was hypothesized that atherosclerosis-relevant B2 cell responses may be organized in GCs of ATLOs in aged ApoE$^{-/-}$ mice. In order to experimentally approach this hypothesis, an experimental strategy as shown in Fig. 6 was designed. In order to sort ATLO GC B cells, the following principal markers were used: CD45, CD19, IgD, GL7, and PNA. GC B cells do not express IgD; GL7 is a marker of GC B cells because activated B cells express GL7 whereas mature B cells do not [152], indicating that activated B cells undergoing a GC reaction are detected by GL7 [153]; furthermore, PNA^{+}, IgD^{-} GC B cells in ATLOs in the diseased abdominal aorta of aged ApoE$^{-/-}$ mice were identified previously by members of our group by IF [134]. To obtain single GC B cells from ATLOs, the whole aorta was digested with appropriate enzyme cocktails into single cell suspensions and then sorted GC B cells were defined by a combination of surface markers FVD^{-} CD45^{+}CD19^{+}IgD^{-}GL7^{+}PNA^{+} [152,154] into 96 well plates. The same GC B cell population was detectable in the spleen and sorted into 96 well plates as shown in the representative gating strategy shown (Fig. 7). GC B cells in RLNs (26,393 $\pm$ 12,200) and ATLOs (192 $\pm$ 54) of aged ApoE$^{-/-}$ mice were previously quantified by our group using FACS. In the thoracic aorta of aged ApoE$^{-/-}$ mice, GC B cells were not detectable [133]. Table 3.1 shows total GC B cell numbers sorted from ATLOs per mouse. This data indicate that GC B cells were sorted from ATLOs but not from paraaortic LNs.

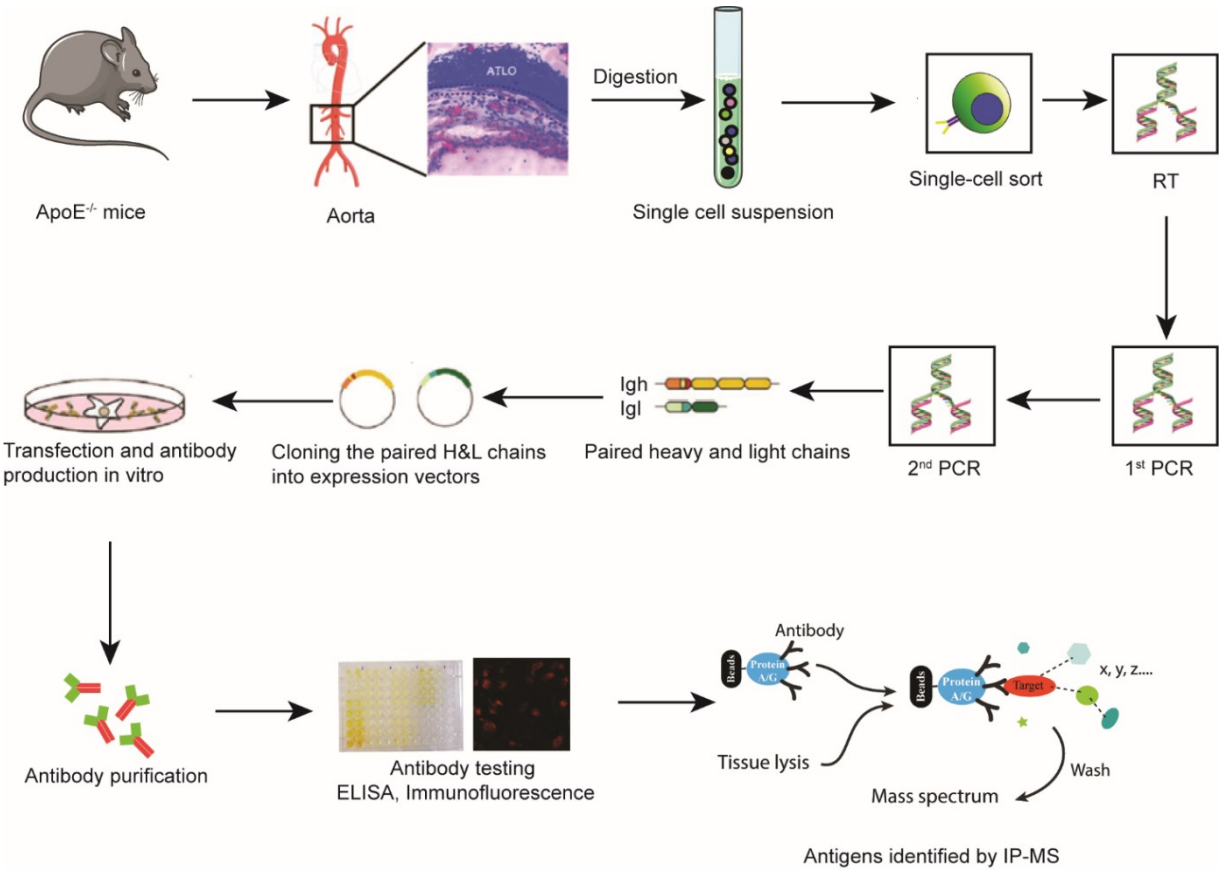

Figure 6. Experimental strategy. Single GC B cells are sorted according to a GC B2 cell surface marker cocktail ($FVD^{-}CD45^{+}CD19^{+}IgD^{-}GL7^{+}PNA^{+}$) [152,154] into 96 well plates by FACS from aged $ApoE^{-/-}$ mice aorta bearing ATLOs. For each single GC B cell, the variable region genes of Ig heavy (IgH) and Ig light (IgL) chain were amplified by nested RT-PCR with primer mixes and sequenced by Sanger sequencing. Cloning the paired heavy- and light- chains (Igk) into expression vectors. The paired heavy- and light-chains (Igk) were co-transfected into cells to produce monoclonal antibodies *in vitro*. ELISA and IF experiments were used to test recombinant antibodies. Co-IP/MS experiments were used to search for cognate antigens.

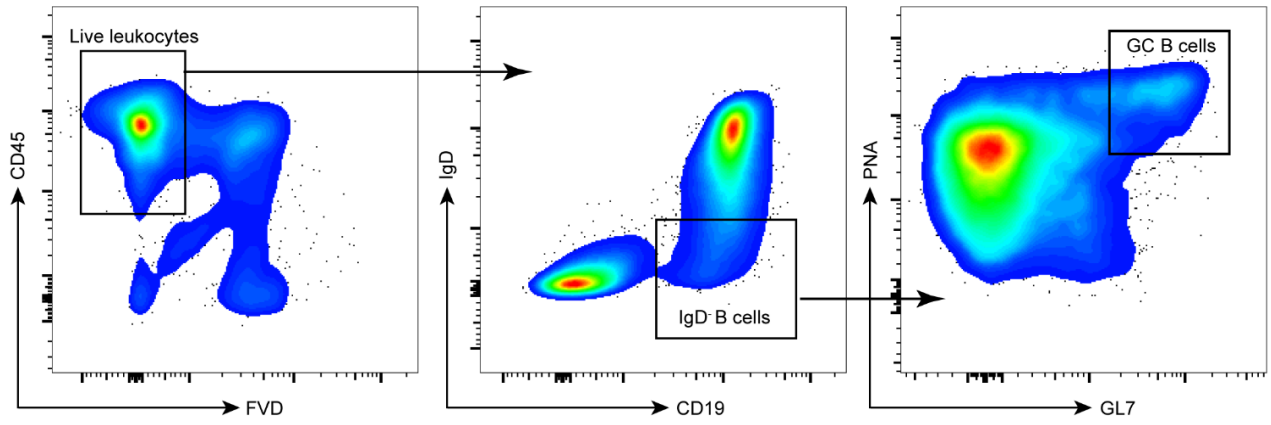

Figure 7. Strategy for sorting GC B cells from spleen of ApoE$^{-/-}$ mice. FACS plots show representative sorting gates for the isolation of FVD^{-} CD45^{+} CD19^{+} IgD^{-} GL7^{+} PNA^{+} single live GC B cells from aged ApoE$^{-/-}$ mice of the spleen. CD19^{+} B cells were gated from CD45^{+} FVD^{-} total live leukocytes. Due to lack of IgD expression in GC B cells, IgD^{-} B cells were separated from total live CD19^{+} B cells first, and then GC B cells were separated from IgD^{-} B cells by PNA^{+} and GL7^{+} markers.

Mouse No.	Number of GC B cells sorted from ATLOs
1	124
2	47
3	66

Table 3.1. GC B cell numbers in ATLOs. GC B cells in ATLOs were sorted from 3 individual aged ApoE$^{-/-}$ mice.

As our PCR analyses are based on extremely low amount of RNA from a single cell, the method of nested PCR approach is used to reliably amplified the IgH and IgL genes while avoiding PCR-induced errors (Fig. 8A). Spleen GC B cells from the same mouse were isolated (Fig. 8A). PCR products were purified and sequenced by Sanger sequencing to obtain their entire length of variable (V) gene sequences of IgH and IgL. Some features of the BCR repertoire (such as the CDR3 length, positive charges of amino acid) have been proven by others to be associated with auto-reactivity [155-159]. Thus, the features of Ig sequencing were examined to provide an initial understanding of the antibody repertoire in each tissue. In order to identify the BCRs of each IgH and IgL sequence, the IMGT (*http://www.imgt.org/*) databank was used, which contains all published unmutated germine line BCR sequences of mice as controls to be compared with the BCRs in our experimental models.

The sub-families of the IgH V region (*IgH V*), J region (*IgH J*), D region (*IgH DH*), IgL V region (*IgK V*), J region (*IgK J*), reading frame (RF) 1, 2, and 3, and the CDR3 length, SHMs of IgH and IgL chains were compared between ATLO-GC B cells and spleen-GC B cells in aged ApoE$^{-/-}$ mice (Table S1-S2). These parameters are critical to define the molecular features of the experimental BCRs in our approach, as we are the first to isolate the BCRs from GC B cells from ATLOs. Our data reveal that ATLO GC B cells and spleen GC B cells show similar

usage frequency in IgH V, IgH J, RF, and IgH DH sub-families (Fig. 8B-D). There is no difference in the length of CDR3 and the number of positively charged residues in IgH CDR3 between ATLO GC B cells and spleen GC B cells (Fig. 8E, G). Next, the class switch recombination and gene mutations were examined in GC B cells, which may indicate antigen-mediated selection in GCs [47,160-162]. Strikingly, significant higher somatic mutations of IgH were observed in ATLO GC B cells when compared to spleen GC B cells (Fig. 8F), while there are no differences in somatic mutation of IgK between ATLO GC B cells and spleen GC B cells (Fig. 8I). Previous studies showed that the mediator of SHM, AICDA, is controlled by distinct inflammatory cytokines, such as IL-10 and IL-4 [163,164]. It can be speculated that the inflammatory environment of ATLOs might contribute to higher mutations observed in ATLO GC IgH chains. ATLO GC B cells showed higher VK3 family usage of IgK chain and lower VK1 family usages of IgK chain when compared to spleen GC B cells (Fig. 8H); there is no difference on J family usages of IgK chain (Fig. 8H). These data indicate that the VK3 family might be oligoclonal and recognize the same antigen(s). Furthermore, they confirm that the established protocol to obtain the paired IgH and IgL chains of BCR sequences from a single isolated GC B cell is working. ATLO GC B cells showed major similarities in IgH/IgL subfamily usages, CDR3 lengths, and the number of positively charged residues compared to spleen GCs. As spleen GCs is a well-recognized structure to organize antigen-dependent affinity maturation [142], the major similarities on BCR repertoire between two GCs support the notion that antigen-dependent affinity maturation can also be organized in ATLO GCs.

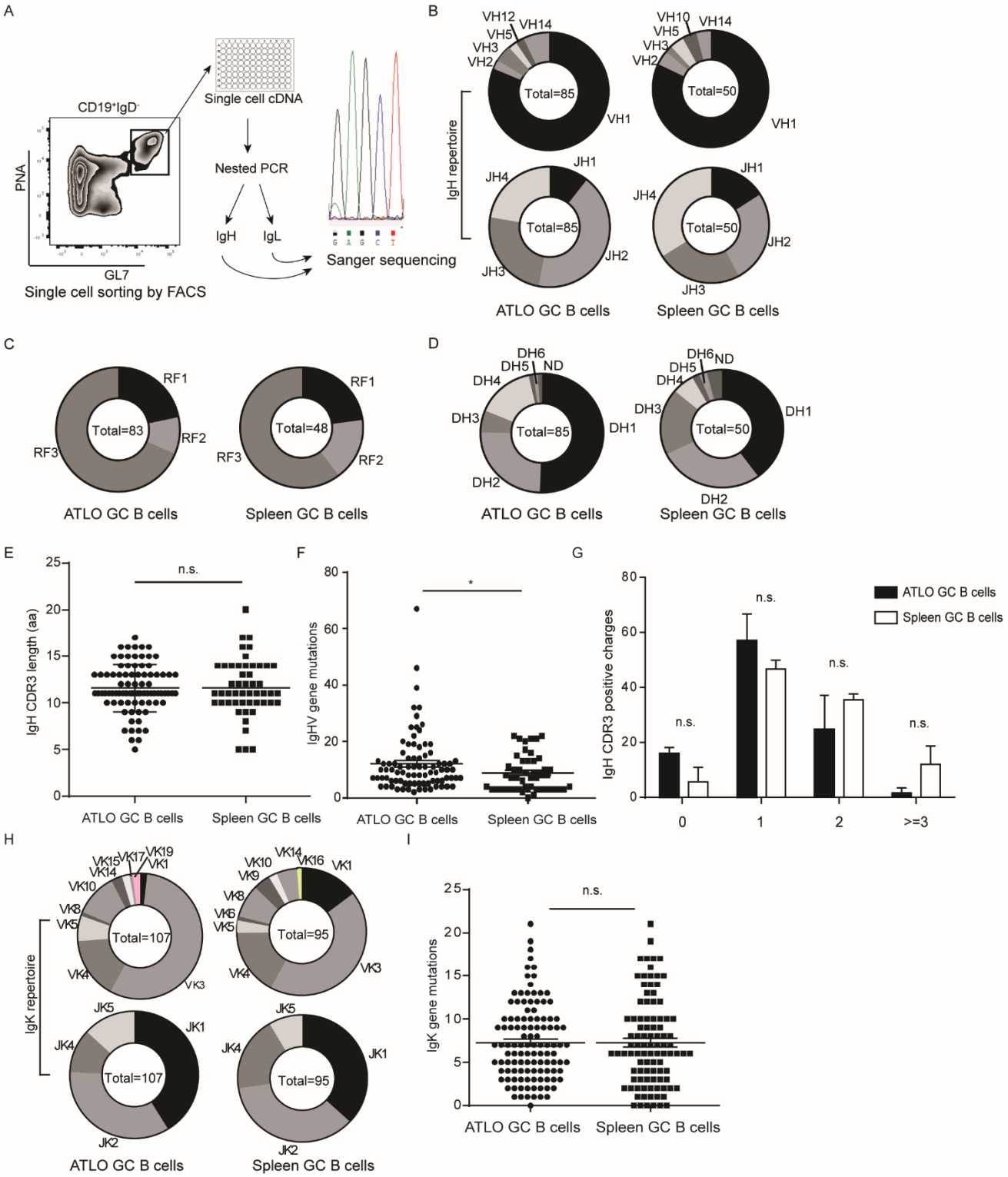

Figure 8. Ig gene features of GC B cells from ATLOs and spleen. (A) Strategy to clone the paired heavy and light chains from isolated single GC B cells. (B-D) IgH chain variable (V), reading frame1, 2, and 3, D, and joint (J) family usage of ATLO GCs and spleen GCs. The total number of GC B cells for each group was documented in the inner circle; the size of each sub-family was labeled in the outer circle, whereby the outer circle represents 100%. The same family from different groups was labeled with identical color. i.e., IgH V1 family is the largest family used by ATLO GCs and spleen GCs; RF3 and DH1 are the

largest families used by ATLOs and spleen; JH2 is the largest family used by ATLOs and JH4 is the largest families used by spleen; (E) The CDR3 lengths of ATLO GCs and spleen GCs. (F) The number of mutations in ATLO GCs or spleen GCs. Dots represent the absolute number of somatic mutations. Unpaired two-tailed Student t-test was applied for E, F; n = 85 from ATLO GC B cells, n = 50 from spleen GC B cells. * $P < 0.05$. (G) The number of positively charged residues in IgH CDR3 of ATLO GCs, and spleen GCs. (H) IgL chain variable (V) and joint (J) family usage of ATLO GCs, and spleen GCs. The number in the circles indicates the total BCR sequences obtained from 3 aged $ApoE^{-/-}$ mice. (I) The number of mutations in ATLO GCs, and spleen GCs of light chains. Unpaired two-tailed Student T-test was applied for P value, n = 107 from ATLO GC B cells, n = 95 from spleen GC B cells. * $P < 0.05$.

3.2 Clonal expansion of ATLO GC B cells

As the clonal expansion of B2 cells indicates engagement of BCRs with their cognate (auto) antigen, a major aim of the current work is to examine if there was clonal expansion of B2 cells in $ApoE^{-/-}$ mice and where such potential clonal expansion may occur. To approach this, the amino acid sequences of ATLOs and spleen GC-derived antibodies were compared (Fig. 9 and 10). The IgH chains´ nucleic acid sequences were submitted to the IMGT databank to translate them into amino acid sequences, which can be further aligned for Ig families, FR3 regions, CDR3 region, FR4 region, and constant regions. Mutations of amino acid sequences compared to germline line BCR sequence were identified. Amino acid sequences of IgHs were clustered using ClustalW (*https://www.genome.jp/tools-bin/ clustalw*), which is a widely used program for aligning any number of homologous nucleotide or protein sequences, according to their sequence similarity. A cluster of expanded BCRs is defined if more than two IgH sequences share identical CDR3 regions as a bona fide measure to indicate antigen-dependent BCR clonal expansion. In the process of antigen-dependent B cell clonal expansion, many copies of B cells arise from a parent cell. These copies are referred to as “preponderance clusters” that have affinities and specificities for the same antigen. Here, several expanded BCR clusters were identified, indicating that more than one autoantigen may be involved in ATLO GC responses. More than three IgH sequences that shared the identical CDR3 region is defined as a preponderance cluster. Of note, preponderance clusters, i.e., VH1-42, VH1-26, VH1-75, and VH14-4, were observed in ATLO GCs (Fig. 8). Although no preponderance clusters were found, two IgH sequences that shared the identical

CDR3 region were observed in spleen GCs, i.e., VH1-42, VH1-53, and VH1-72 (Fig. 9). Here, four preponderance clusters were determined that have the same amino acid sequence in CDR3 were encoded by different nucleotides in ATLOs. This indicates that particular autoantigens triggered GC B cell clonal expansion. These data are consistent with our hypothesis that there are atherosclerosis-related autoantigens in ATLOs that are presented by FDCs. Meanwhile, the spleen clusters provide evidence that immunogenicity triggering atherosclerosis-related immunity also occurs in the spleen. When taken together, the preponderance clusters found in ATLOs raise the strong possibility that B2 autoimmune responses are organized against unknown autoantigens in ATLOs.

Family No.	***FR3***	***CDR3***	***FR4***	***COS***
IGHV1-82*01	…NYNGKFKGKATLTADKSSSTAYMQLSSLTSEDSAVYFC	ARFFYYYGG---------	DYWGQGTTLTVSSESQ	*
IGHV1-82*01	…NYNGKFKGKATLTADKSSSTAYMQLSSLTSEDSAVYFC	ARFFYYYGG---------	DYWGQGTTLTVSSESQ	*
IGHV1-82*01	…NYHGKLKGKATLTAYKSSSPAYMQLCNLTSEDSAAYFC	ASFFYYYIG---------	NYWAQGTTLPLSSAKT	
IGHV1-80*01	…KYNGKFKGKATLTTDKSSSTAYMQLSSLTSEDSAVYFC	VRFYYGRG---------	FDYWGQGSTLTVSSESQ	
IGHV1-80*01	…KYNGKFKGKATLTADKSSSTAYMQLSSLTSEDSAVYFC	ARFYYGRG---------	FDYWGQGTTLTVSSAKT	
IGHV1-80*01	…NYNGKFKGKATLTADKSSSTAYMQLSSLTSEDSAVYFC	AKGYYYGSSS----YWYFDV	WGTGTTVTVSSAKT	
IGHV1-80*01	…NYSGKFKGTATLTADKSSSTAYMHLRSLTSEDSAVYFC	AISRGYYGSP-------	FDYWGPGTTLTVSSESQ	
IGHV1-82*01	…NYNGNFKDKASLTADKSSNTAYMQLSSLTSEDSAVYFC	ARWAGTFY---------	FDYWGQGTTLTVSSAKT	
IGHV1-82*01	…NYNGKFKGKATLTTDKSSTTAYMQLSSLTSEDSAVYFC	ARFSLWLRRG----DWYFDV	WGTGTTVTVSSESQ	
IGHV1-82*01	…NYNGKFKGKATLTADKSSSTAYMQLSSLTSEDSAVYFC	ARRANWDEY------WYFDV	WGTGTTVTVSSAKT	
IGHV1-47*01	…KYNEKFKGKATLTVEKSSSTVYLELSRLTSDDPAVYYC	AR----------	GGFAYWGQGTLVTVSAESQ	
IGHV1-47*01	…KYNEKFKGKATMTVEKSSSTVYLELSRLTSDDSAVYYC	VRGS---------	WDGYFDV	WGTGTTVTVSSAKT
IGHV1-42*01	…SYNQNFKAKATLTVDKSSSTAFMQLKSLTSEDSAVYYC	ARRELTG---------	SWDYWGQGTSVTVSSESQ	**
IGHV1-42*01	…SYNQNFKAKATLTVDKSSSTAFMQLKSLTSEDSAVYYC	ARRELTG---------	SWDYWGQGTSVTVSSESQ	**
IGHV1-42*01	…TYNQNFKAKATLTVDKSSSTAFMQLKSLTSEDSAVYYC	ARRELTG---------	SWDYWGQGTSVTVSSESQ	**
IGHV1-42*01	…TDNQNFKAKATLTVDKSSSTAFMQLKSLTSEDSAVYYC	ARRELTG---------	SWDYWGQGTSVTVSSESQ	**
IGHV1-42*01	…TYNQNFKAKATLTVDKSSSTAFMQLRSLTSEDSAVYYC	ARRELTG---------	SWDFWGQGTSVTVSSESQ	**
IGHV1-42*01	…TYNQHFKAKATLTVDKSSSTAYMQFKSLTSEDSAVYYC	ARRELTG---------	SWDYWGQGTSVTVSSESQ	**
IGHV1-42*01	…TYNQKFKAKATLTVDKSSRTAYMQFKSLTSEDSAVYYC	ARRELTG---------	SWDYWGQGTSVTVSSESQ	**
IGHV1-26*01	…NYHQKFKDKATLTVDKSSSTAYMELRSLTSEDSAVYYC	ARRLVY----------	YFDYWGQGTTLTVSSESQ	
IGHV1-26*01	…NYHQKFKDKATLTVDKSSSTAYMELRSLTSEDSAVYYC	ARRLVY----------	YFDCWGQGTTLTVSSESQ	
IGHV1-26*01	…SYNQKFKGKATLTVDKSSSTAYMEFRSLTSEDSAVYYC	AR---WGD--DGYYDWYFDV	WGTGTTVTVSSAKT	
IGHV1-18*01	…ICNQKFKGEATLTVDKSSSTAYMELRSLTSEDTAVYYC	AR---RGLGYGSSYVWYFDV	WGTGTTVTVSSAKT	
IGHV1-26*01	…NYNQTFKGKATLTVDKSSITAYMELRSLTSEDSAVYYC	VR---LGRG-------	YFDVWGTGTTVTVSSESQ	
IGHV1-26*01	…SYNQKFKGKATLTVDRSSSTAYMELRSLTSEDSAVYYC	ARGG-----VYYGSNSWFAY	WGQGTLVTVSAESQ	***
IGHV1-26*01	…SYNQKFKGKATLTVDRSSSTAYMELRSLTSEDSAVYYC	ARGG-----VYYGSNSWFAY	WGQGTLVTVFAESQ	***
IGHV1-26*01	…SYNQKFKGKATLTVDRSSSTAYMELRSLTSEDSAVYYC	ARGG-----VYYGSNSWFAY	WGQGTLVTVSAESQ	***

```
IGHV1-26*01 …SYNQKFKGKATLTVDRSSSTAYMELRSLTSEDSAVYYCARGG-----VYYGSNSWFAYWGQGTLVTVSAESQ ***
IGHV1-26*01 …TYNQKFKGKATLIVDKSSSTAYMELRSLTSEDSAVYFCARPSYQGGP--------MDYWGQGTSVTVSSESQ
IGHV1-26*01 …DYAQKFKGKATVTIDKSSSTADMELRSLTSEDSAVYYCARG-------YYGYDRWFAYWGQGTLVTVSAAKT
IGHV1-20*01 …FYNQKFKGKATLTVDKSSSTAHMELRSLTSEDSAVYYCARGR-----GGSSYG--FAYWGQGTLVTVSAESQ
IGHV1-53*01 …NYNEKFKSKATLTVDKSSSTAYLQLSSLTSEDSAVYYCARH-----------YLFMDYWGQGTSVTVSSESQ
IGHV1-53*01 …NYNEEFKSKATLTVDKSSSTAYMQLSSLTSEDSAVYYCARYGDYYG----SSPYAMDYWGQGTSVTVSSESQ
IGHV1-53*01 …NYNEKFKSKATLTVDKSSSTAYMQLSSLTSEDSAVYYCAPITAG----------YFDVWGTGTTVTVSSESQ
IGHV1-53*01 …SYNEKFKSKATLTVDKSSSTAYMQLSSLTSEDSAVYYCTRSETG----------HFDYWGQGTTLTVSSESQ
IGHV1-53*01 …NYNEKFKNKATLTVDKSSSTAYMQLSSLTSEDSAVYYCARPNYGS---------SLDYWGQGSTLTVSSESQ ****
IGHV1-53*01 …NYNEKFKNKATLTVDKSSNTAYMQLSSLTSDDSAVYYCARPNYGS---------SLDYWGQGSALTVSSESQ ****
IGHV1-53*01 …NYNEKFKSKATLTVDKSSSTAYMQLSSLTSEDSAVYYCARQDYYG---------CNYYWGQGTTLTVSSESQ
IGHV1-53*01 …NYNEKFKSKATLTVDKSSSTAYMQLSSLTFEDSAVYYCARQDYYG---------SSYYWGQGTTLTVSSESQ
IGHV1-53*01 …NYNEKFKTKATLTVDKSSSTAYMQLTSLTSVDSAVYYCARLDYYG---------STFYWGQGTTLTVSSESQ
IGHV1-53*01 …NYNEKFKSKATLTVDKSSTTAYMQLSSLTSEDSAVYYCARSPYS----------DSYYWGQGTTLTVSSAKT
IGHV1-53*01 …NYNERFRTKATLTVDKSSSTAYMQLSSLTSEDSAVYSCASRVTRG----------QRGQGTLVPVSEESQ
IGHV1-53*01 …RYNQKFKGKATLTVDQSSSTAYMQLNRLTSEDSAVYYCARDYGSSYVW-------FDYWGQGTLVTVSAAKT
IGHV1-53*01 …NYNEKFKSKATLTVDKSSRTAYMQVSSLTFEDVAVYYCASGGL----------FDYWGQGTTVTVSSAKT
IGHV1-72*01 …ENNGKFKSKASLTVDKPSSTVYMQLSSLTSEDSAVYYCSREEMGA----------MDYWGQGTSVTVSSESQ
IGHV1-72*01 …KYNEKFKSKATLTVDKPSSTAYMQLSSLTSEDSAVYYCARYYYGSY---------FDYWGQGTTLTVSSESQ
IGHV1-64*01 …NYNEKFKSKATLTVDKSSSTAYMQLSSLTSEDSAVYYCARSYDSW----------FAYWGQGTLVTVSAAKT
IGHV1-50*01 …NYNQKFKGKATLTVDTSSSTAYMQLSSLTSEDSAVYYCARS-------------EFAYWGQGTLVTVSAESQ
IGHV1-50*01 …NYNQKFKGKATLTVDTSSSTAYMQLSSLTSEDSAVYYCARWRYYYG----SSEVYFDYWGQGTTLTVSSAKT
IGHV1-50*01 …NNNQKFKGKATLIVDTSSSTAYNQLSSLTSEECEVYCCTRH-------------DYDYWGQGTTLTVSSESQ
IGHV1-4*01  …KYNQKFKDKATLTADKSSSTAYMQLNSLTSEDSAVYYCAR----LP----LLSYAMDYWGQGTSVTVSSESQ *****
IGHV1-4*01  …RYSQKFKDKATLTADKSSSTAYMQLNSLTSEDSAVYYCAR----LP----LLSYPMDYWGQGTSVTVSSESQ *****
IGHV1-78*01 …KYNEKFKGKATLTADKSSSTAYMQLNSLTSEDSAVYFCATPIYDGY----YVTWFAYWGQGTLVTVSAESQ
IGHV1-75*01 …YYNEKFKGKATLTVDKSSSTGYLLLSSLTSEDSAVYFCARGDYYGS----S--FHFDYWGQGTTLTVSSESQ ******
IGHV1-75*01 …YYNEKFKGKATLTVDKSSSTGYMLLSGLTSEDSAVYFCARGDYYGS----S--FHFDYWGQGTTLTVSSESQ ******
IGHV1-75*01 …YYNEKFKGRATPTADKSSSTGYMLLSSLTSEDSAVYFCARGDYYGN----S--FHFDYWGQGTTLTVSSESQ
IGHV1-75*01 …YYNEKFKGKATLTVDKSSSTGYMLLSSLTSEDSAVYFCARGDYYGS----S--FHFDYWGQGTILTVSSAKT ******
IGHV1-76*01 …YYNEKFKGKATLTAEKSSSTAYMQLSSLTSEDSAVYFCARGSSS---------FGFDYWGQGTTLTVSSESQ
IGHV1-76*01 …YYNEKFKGKATLTAEKSSSTAYMQLSSLTSEDSAVYFCARELTG---------AWFAYWGQGTLVTVSVAKT
IGHV1-77*01 …YYNEKFKGKATLTADKSSSTAYMQLSSLTSEDSAVYFCARENYY---------GSLAYWGQGTLVTVSAESQ
IGHV1-81*01 …YYNEKFKGKATLTADKSSSTAYMELRSLTSEDSAVYFCARSDFEGQ----LRPYYFDYWGQGTTLTVSSESQ
IGHV1-81*01 …YYNEKFKGKATLAADKSSSTAYMELRSLTSEDSAVYFCARGGPD-YDG----YWYFDVWGTGTTVTVSSESQ
IGHV14-4*01 …EYASKFQGKATITADTSSNTAYLQLSSLTSEDTAVYYCTFYYYGSS-------YAMDYWGQGTSVTVSSESQ *******
IGHV14-4*01 …EYASKFQGKATITADTSSNTAYLQLSSLTSEDTAVYYCTFYYYGSS-------YAMDYWGQGTSVTVSSESQ *******
IGHV14-4*01 …KYASKFLGKATITADTSSNTAYLQLTRLTSEDTAVYYCTRI---------------WNWGQGTTLTVSSESO
IGHV14-4*01 …EYASKFQGKATITADTSSNTAYLQLSSLTSEDTAVYYCTFYYYGSS-------YAMDYWGQGTSVTVSSAKT *******
IGHV14-2*01 …KYAPKFQGKATITADTSSNTAYLQLSSLTSEDTAVYYCASN--------------FDYWGQGTTLTVSSESQ
IGHV5-4*01  …YYPDNVKGRFTISRDNAKNNLYLQMSHLKSEDTAMYYCAR----ASDSS-----FFDYWGQGTTLTVSSESQ
IGHV5-17*01 …YYADTVKGRFTISRDNAKNTLFLQMTSLRSEDTAMYYCARPPPTEAAQA-----PFAYWGQGTLVTVSAAKT
IGHV10-1*01 …YYADSVKDRFTISRDESESRLYLQMNNLNTEDTAMYYCVR-DYYDYDGY-----AMDYWGQGTSVTVSSAKT
```

```
IGHV2-3*01  …TYHSALISRLSISKDNSKSQVFLKLNSLQTDDTATYYCAG--------------AFAYWGQGTLVTVSAESQ
IGHV2-2*01  …DYNAAFISRLSISKDNSKSQVFFKMNSLQADDTAIYYCASDYYGSR--------AMDYWGQGTSVTVSSESQ
IGHV3-6*01  …NYNPSLKNRISITRDTSKNQFFLKLNSVTTEDTATYYCARG-HYYG--------TFDYWGQGTTLTVSSESQ
IGHV12-3*01 …FYNPSLQSPISITRETSKNQFFLQLNSVTTEDTAMYYCAGDSSGYW--------YFDVWGTGTTVTVSSESQ
IGHV3-3*01  …YYNPSLESRTFITRDTSKNQFSLKLSSVTTEDTATYYCARSTMVTTSW-------FAYWGQGTLVTVSAESQ
IGHV1-84*01 …KYNAKFKGKATLTVDTSSSTAYMQLSSLTSEDSAVYFCARLHYYGSNA-------MDHWGQGTSVTVSSAKT
```

Figure 9. BCR amino acid sequences alignment of GC B cells of ATLOs. Amino acid sequences translated from ATLO GC BCR nucleic acid sequences. The germline V families and alleles of the chains are shown in the first column. The amino acid sequences of IgH-FR3 are listed in the second column. The amino acid sequences of CDR3s are listed in the third column. The CDR3 regions are shown in red letter. The amino acid sequences of the IgH-FR4 are listed in the fourth column. The amino acid sequences of part of the constant region are listed in the fifth column. Mutations of the variable region (red) are identified using the IMGT databank. Clones marked with the same star (with identical CDR3 sequences and from the same V family) are considered expanded clones. Grey backgrounds represent the conserved cysteine (C) residues in the V region, the tryptophan glycine (WG) residues in the J and C region.

```
Family No.                FR3                                CDR3                  FR4      COS

IGHV14-4*01   …KYASKFLGKATITADTSSNTAYLQLTRLTSEDTAVYYCT----------------TIWNWGQGTTLTVSSESQ
IGHV14-2*01   …KYAPKFQGKATITADTSSNTAYLQLSSLTSEDTAVYYCARQPIY------YGNPYYAMDYWGQGTSVTVSSESQ
IGHV1-67*01   …TYNRKFSDKATMTVDKSSSIAYMELARLTSEDSAVSYCG---------------SPFFDYWGQGTTLTVSSAKT
IGHV1-67*01   …SYNQKFKDKATMTVDKSSSTAYMELARLTSEDSAVYYCAR--------AGVMVTTGGFAYWGQGTLVTVSAESQ
IGHV1-36*01   …SYNQKFKGKATLTVDTSSSTAYMELNSLTSEDSAVYYCAK-------GYYY-----AMDYWGQGTSVTVSSESQ
IGHV1-36*01   …NYSQKFRGKATLTVYPSSSTAYMEMRSRTSEDSAVYYCAR-------GNYYGGSDWGFDVWGQGTLVTVSAAKT
IGHV1-19*01   …SYNQKFKGKATLTVDKSSSTAYMELNSLTSEDSAVYYCARGYYA-------------FDYWGQGTTLTVSSESQ
IGHV1-31*01   …AYNQKFKGKATLTGDKSSSTAYMELRSLTSDDSAVYYCAR-----------YTTSVVADYWGQGTTLTVSSAKT
IGHV1-20*01   …LYNQKFKGKATLTVDKFSSTAHMELRSLTSEDSAVYYCAR------------SGGFYAMDYWTGTTVTVSSESQ
IGHV1-42*01   …TYNQKFKAKATLTVDKSSSTAYMQLKSLTSEDSAVYYCAR------------KEGRYFDVWGQGTSVTVSSESQ*
IGHV1-42*01   …TYNQKFKAKATLTVDKSSSTAYMQLKSLTSEDSAVYYCAR------------KEGRYFDVWGTGTTVTVSSAKT*
IGHV1-42*01   …TYNQKFKAKATLTVDKSSSTAYMQLKSLTSEDSAVYYCARS-----------LLLRYLDVWGTGTTVTVSSESQ
IGHV1-42*01   …SYNQNFKAKATLTVDKSSSTAFMQLKSLTSEDSAVYYCARR-----------ELTGSWDYWGQGTSVTVSSESQ
IGHV1-42*01   …SYNQNFKAKATLTVDKSSSTAFMQLKSLTSEDSAVYYCARR-----------ELTGSWDYWGQGTSVTVSSESQ
IGHV1-42*01   …TYNQNFKARATLTVDKSSSTAYMQLDNLTSEDSAVYYCSR------------RGGFSLDYWGQGTTLTVSSESQ
IGHV1-42*01   …TYNQKFKSKATLIVDKSSSTAYMQLKSLTSEDFAVYYCARKG----------SFSGAMDYWGQGTSVTVSSESQ
IGHV1-53*01   …DYDEKFKSKATLTVDKSSSTAYMQLSRLTSEDSAVYHCARGSG-----------YYPFDYWGQGTTLTVSSAKT**
IGHV1-53*01   …NYDEKFKSKATLTVDKSSSTAYMQLSRLTSEDAAVYYCARGSG-----------YYPFDYWGQGTTLTVSSESQ**
IGHV1-72*01   …NYNEKFKAEATLTVDKPSSTAFMQLTSLTSEVSAVYYCTRGAY-----------SGALDYWGPGISVTVSSESQ***
IGHV1-72*01   …DYNEKFKAEATLTVDKSSSTAFMQLSSLTSEVSAVYYCTRGAY-----------SGALDYWGPGISVTVSSESQ***
IGHV1-55*01   …NYNEKFKSKAIVTVDTSSSTAYMQLSSLTFEDFAVYYCARSLR------------GGGDYWGQGTSVTVSSESQ
IGHV1-55*01   …NYNEKFKSKATLTVDTSSSTAYMQLSSLTSEDSAVYYCAR--------------SHAMDYWGQGTSVTVSSESQ
IGHV1-50*01   …NYNQKFKGKAILTVDTSSSTAYMQLSSLTSEDSAVYYCARSGSSGYFS--------WFAYWGQGTLVTVSAESQ
IGHV1-5*01    …SYNQKFKGKAKLTAVTSASTAYMELSSLTNEDSAVYYCTRR--TYYGN--------WFAYWGQGTLVTVSAESQ
IGHV1-9*01    …NYNEKFKGKVTFTADPSSNTAYMQLSGLTTEDSAIYYCARDYYGSSYG--------GFTYWGQGTLVTVSAESQ
```

IGHV1-81*01	…YYNEKFKGKATLTADKSSSTAYMELRSLTSEDSAVYFC	ARRGY--------	GSSSYAMDYWGQGTSVTVSSESQ
IGHV1-81*01	…YYNEKFKGKATLTADKSSSTAYMELRSLTSEDSAVYFC	ANG----------	YYAMDYWGQGTAVSS--ESQ
IGHV1-81*01	…YYNEKFKGKATLTADKSSSTAYMELRSLTSEDSAVYFC	AKGP----------	LRLNFDVWGTGTTVTVSSESQ
IGHV1-81*01	…YYNEKFKGKATLTADKSSSTAYMELRSLTSEDSAVYFC	ARNPPYY-----GSSYRRYFDV	WGTGTTVTVSSESQ
IGHV1-81*01	…YYNEKFKGKATLTADKSSSTTYMELRSLTSEDSAVYFC	ASPWD----------	EKVDYWGQGTTLTVSSESQ
IGHV1-81*01	…YYNEKFKGKATLTADKSSSTAYMELRSLTSEDSAVYFC	AREGD--------	SSGYGGVGYWSQGTSVTVSSAKT
IGHV1-71*01	…KYNEKFKDKATLTADKSSSTVYMELSRLTSEDSAVYFC	ARHEDAYYYG-----SSWYFDV	WGTGTTVTVSSESQ
IGHV1-71*01	…KYNEKFKDKATLTADKSSSTVYMELSRLTSEDSAVYFC	ARHEERFYYYG--SSYGAWFAY	WGQGTLVTVSAESQ
IGHV1-75*01	…YYNEKFKGKATLTVDKSSSTAYMLLNSLTSEDSAVYFC	ARDED---------	DYDPWFAYWGQGTLVTVSAESQ
IGHV1-82*01	…NYNGKFKGKATLTADKSSSTAYMQLSSLTSEDSAVYFC	AR----------	FSPAWFAYWGQGTLVTVSAESQ
IGHV1-82*01	…NYNGKFKGKATLTADKSSSTAYMQLSSLTSEDSAVYFC	ARG--------	GTAQATKSMDYWGQGTSVTVSSESQ
IGHV1-82*01	…KYNGKFKDRATLTADKSSSTACMQLSSLTSEDSAVYFC	AREG----------	LGPFDSWGQGTTLTVSSAKT
IGHV1-80*01	…NYNGKFKGKATLTADKSSSTAYMQLSSLTSEDSAVYFC	ALIR-------	DGSSYVDYFDYWGQGTTLTVSSESQ
IGHV1-80*01	…NYNGNFKGKATLTADTSSSTAYMQLSSLTSEDSAVYFC	ARG----------	AYWGQGTTLTVSSESQ
IGHV1-80*01	…NYNGKFKDKATLTVDRSSNTAYMQLISLTSEDSAVYFC	ATYD----------	FGFIFWGQGTLVTVSSESQ
IGHV10-1*01	…YYADSVKDRFTISRDDSESMLYLQMNNLKTEDTAMYYC	VRHTYG----------	AMDYWGQGTSVTVSSESQ
IGHV10-3*01	…YYADSVKDRFTISRDDSQSMLYLQMNNLKTEDTAMYYC	VREPYY--------	GS--SYDYWGQGTTLTVSSESQ
IGHV5-4*01	…YYPDTVKGRFTISRDNVKNNLYLQMSHLKSEDTAMYNC	VRDGGE--------	RWSLCMDYWGQGTSVTVSSAKT
IGHV5-6*01	…YYPDSVKGRFTISRDNAKNTLYLQMSSLKSEDTAMYYC	GRQGYY--------	GSSGYFDVWGTGTTVTVSSESQ
IGHV2-9-1*01	…NYNSTLKSRLSISKDNSQSQVFSKMNSLQTDDTARYYC	ASPLLL--------	RSLYYFDYWGQGTTLTVSSESQ
IGHV2-9-1*01	…HYNSALKSRLSISKDTSRSQVFLKMNSLQTDDTARYYC	AR----------	SYDDAMDYWGQGTSVTVSSESQ
IGHV3-8*01	…YYNPSLKSRISITRDTSKNQYYLQLNSVTTEDTATYYC	AR--YM--------	DWVHYFDVWGTGTTVTVSSAKT

Figure 10. BCR amino acid sequences alignment of GC B cells of spleen. Amino acid sequences were deduced from spleen GC BCR nucleic acid sequences. The germline V families and alleles of the heavy chains are shown in the first column. The amino acid sequences of IgH-FR3 are listed in the second column. The amino acid sequences of CDR3s are listed in the third column. The CDR3 regions are shown in red letter. The amino acid sequences of the IgH-FR4 are listed in the fourth column. The amino acid sequences of part of the constant region are listed in the fifth column. Mutations of the variable region (red) are identified using the IMGT databank. Clones marked with the same star (with identical CDR3 sequences and from the same V family) are considered expanded clones. Grey backgrounds represent the conserved cysteine (C) residues in the V region, the tryptophan glycine (WG) residues in the J and C region.

Each GC is considered to be arising from a small number of independent ‘founder clones’, many of which are lost because the competition during affinity maturation has gradually focused on the most successful progeny with the highest affinities to their cognate antigen and those become preponderance clusters (which is termed as “ homogeneous selection”) [150,165]. Homogeneous GC B cells may derive from the pool of highly diverse early GC B cells by the phenomenon referred to as ‘clonal bursts’ [150]. Tas et al. reported that efficient affinity maturation in GCs could lead antibodies to lose diversity [150]. Losing diversity and gain of

somatic mutation are essential mechanisms to generate higher affinity antibodies during GC responses. During GC responses, B cells undergo somatic mutations in the genes encoding the BCRs. Because this mutation process is random, it is necessary to select mutant B cells to ensure that only BCR-carrying B cells with higher affinity for antigen can survive and generate antibodies. This process can lead to the appearance of B cell clones that have high-affinity binding to antigen. Combining imaging methods and single-cell sequencing to analyze the data of GCs from 15 days after immunization showed that varying degrees of clonal dominance among individual GCs with dominance >70 %. This high-dominance GC is mainly monoclonal, which seems to be caused by clonal expansion, resulting in a widespread loss of clonal diversity. Thus, in this thesis functional V(D)J sharing identical length and more than 70 % amino acids in the CDR3 were grouped into clones [150]. In order to investigate the underlying clonal composition of ATLO-derived GC B cells and spleen GC B cells, IgH and IgL chains were grouped respectively according to the similarity of CDR3 amino acid sequences. Two or more sequences shared >70 % identical CDR3 amino acid sequences were grouped into one cluster (Fig. 11A-D). 11 IgH clusters and 10 IgL clusters were identified from ATLOs from 3 individual mice (Fig. 11A, B). 4 IgH clusters and 16 IgL clusters were identified from spleen from these identical mice (Fig. 11C, D). Of major interest was the observation that some IgH or IgL chains from different ATLOs from different mice shared identical ancestor sequences raising the in our view extremely important possibility that different ATLOs from different mice may present the same antigen to FDCs in ATLO GC reactions. These data support our hypothesis that, indeed, antigen-dependent affinity maturation of B cells is organized in ATLOs, and indicated that atherosclerosis-relevant autoimmune B cells and antigens could be isolated using ATLO GCs as the target.

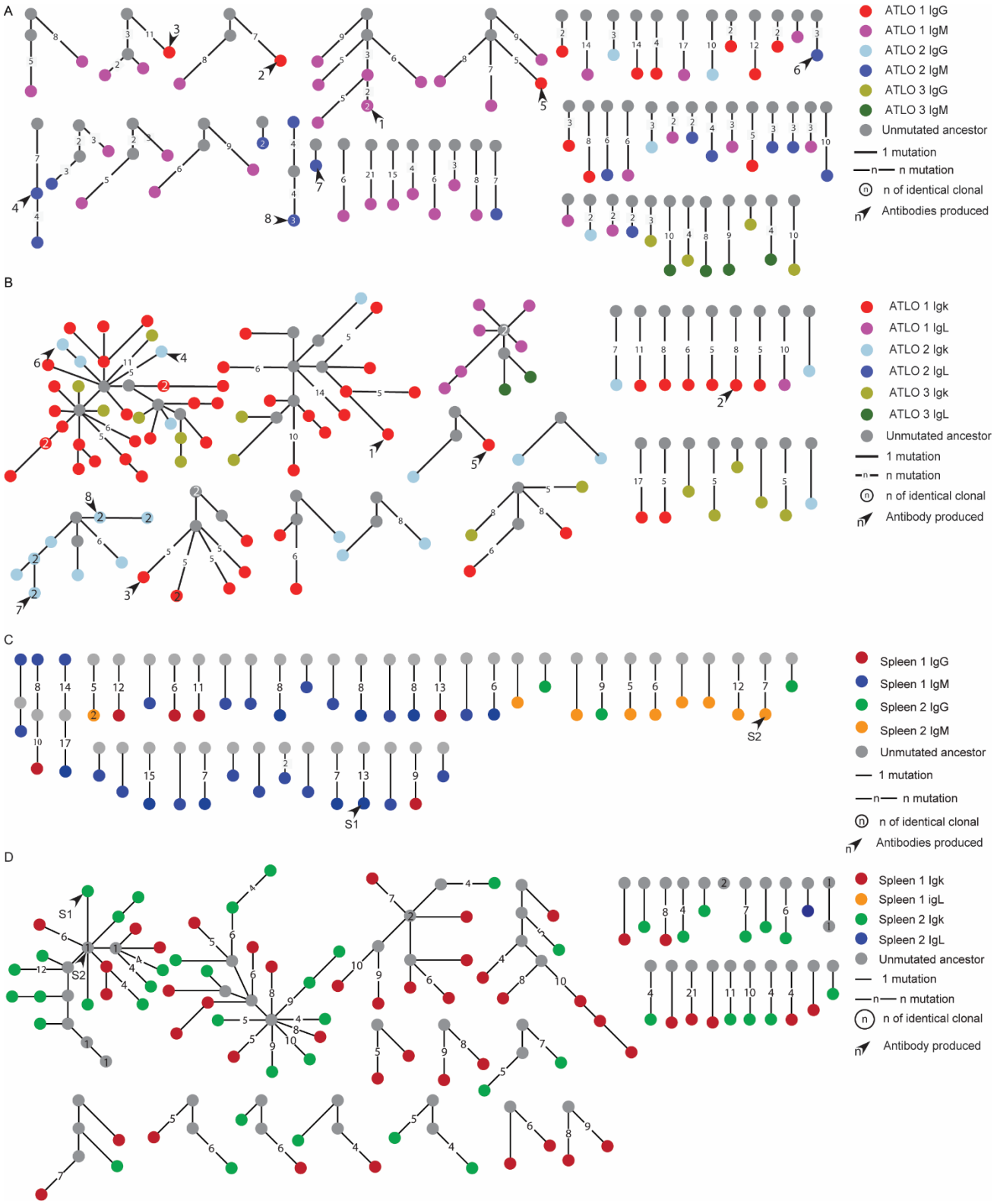

Figure 11. Clonal relationships among ATLO and spleen GC B cells. Clonal relationships of ATLO and spleen GC B cells based on the sequences of BCR H chains from ATLOs and spleens (A and C) and light chains (B and D). BCR clones that shared >70 % identical CDR3 amino acids were grouped in one cluster. The unmutated ancestors obtained from IMGT were marked as grey. The number of somatic

mutations and the number of identical clonotypes are included. Arrows indicate paired heavy and light chains selected to produce the recombination antibodies *in vitro*.

3.3 Generation of recombinant chimeric monoclonal antibodies *in vitro*

Recombinant chimeric monoclonal antibodies were generated *in vitro*. The BCR repertoire of ATLO and spleen GC B cells showed distinct features regarding clonal expansion. However, the function of BCRs cannot be concluded from the BCR repertoire. In order to test the functions of BCRs from ATLO and spleen GC B cells, the paired full mouse V region of IgH and IgL chains were cloned into expression plasmids (pcDNA 3.4) containing the constant (C) region of human IgG1 and Igκ. The expression plasmids produced chimeric antibodies, containing the sequences of the mouse V regions and the corresponding human constant regions. Mouse V regions of the chimeric antibodies will allow to examine the antigen-binding capacity, while the human C regions of the antibodies will allow to separate the recombination antibodies from endogenous mouse antibodies using IF staining and other *in vitro* experiments (see below). In order to examine whether the recombinant antibodies can recognize human plaque antigens, a second type of recombinant antibody was generated that carries the identical mouse V regions and mouse C regions of IgG2 and mouse C regions of Igκ. In this research, eight monoclonal antibodies from ATLOs and two randomly selected monoclonal antibodies from spleens were generated *in vitro* (Fig. 11 and Fig 12A). WB and sodium dodecyl sulphate–polyacrylamide gel electrophoresis (SDS-PAGE) were used to check the antibody quality. Two examples of antibodies (ATLO-derive A4 and A8) obtained are shown by WB and SDS-PAGE (Fig.12B). These data reveal that the recombinant antibodies were successfully produced *in vitro*. For each antibody, both mouse-human chimeric antibodies and full mouse antibodies were generated. Next, the question was addressed whether these antibodies from ATLOs can be found in SLOs and blood in the same mouse. To clarify this, BCR sequences from total $CD19^+$ B cells of spleen, RLN, and blood of the same mouse were sorted and analyzed by next-generation sequencing (NGS) [98]. The eight ATLO GC-derived BCRs used to generate monoclonal antibodies *in vitro* were

compared with the systemic total CD19⁺ BCR repertoire from the same mouse. The resulting data show that some ATLO-derived BCRs share the same CDR3 amino acid with spleen BCRs (A4 and A8 antibody), RLNs BCRs (A8 antibody), or blood B cell-derived BCRs (A1 and A7 antibody). Some ATLO-derived BCRs recognize ATLO-specific antigens as they remained undetectable in spleen, RLN, and blood (such as A2, A3, A5, and A6 antibody) (Fig. 12A). These data indicate two possibilities: i) most likely, ATLO GC-derived memory B cells are released from their FDC binding sites and then migrate to other tissues and organs, or ii) less likely, the identical antigen was presented in ATLO GCs and SLOs GCs, triggered antigen-dependent GC-affinity maturation, which in turn, generated two GC B cells with the identical BCR. More experimental evidence is required to address the question of whether these ATLO-derived specific antibodies recognize atherosclerosis-specific antigens.

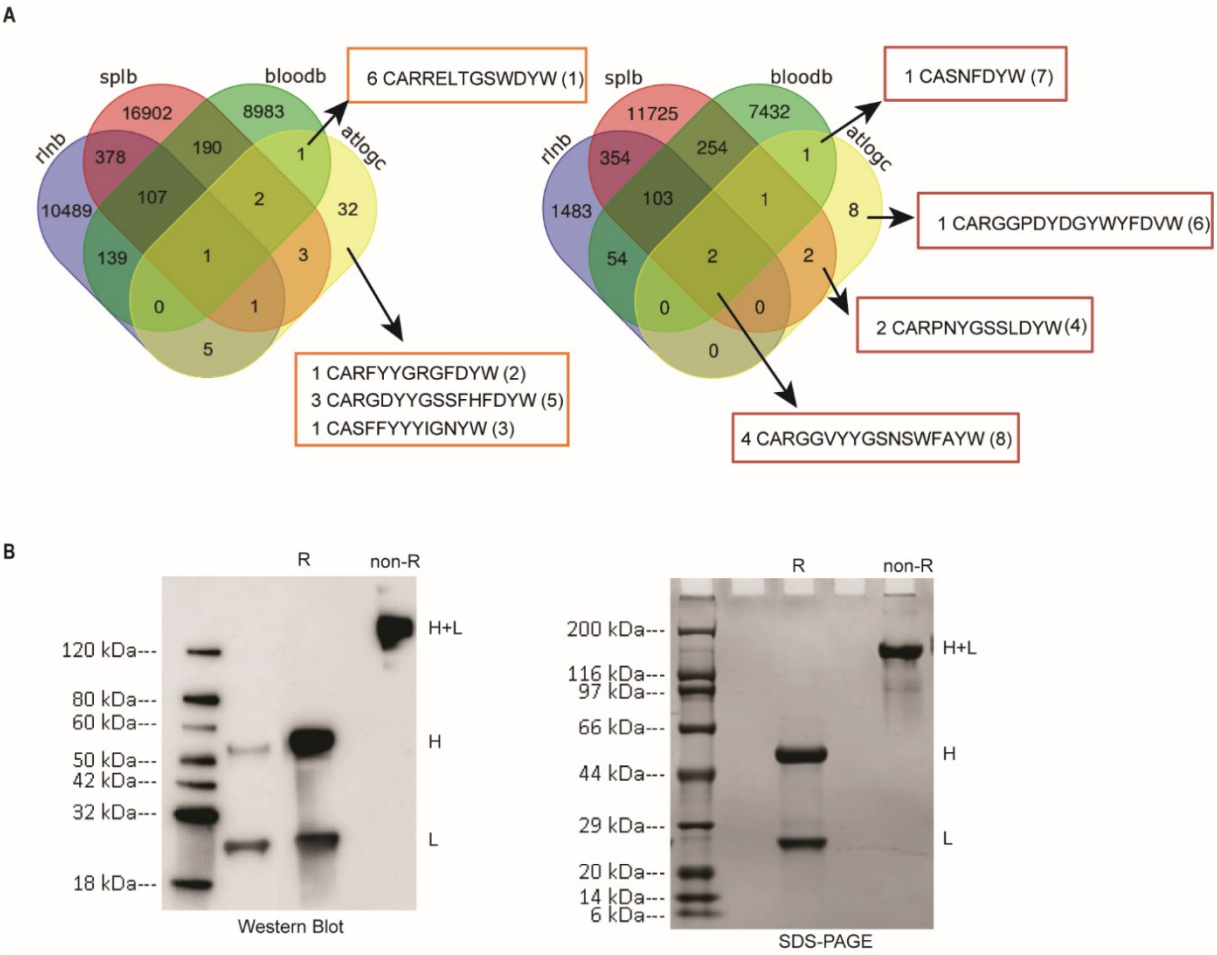

Figure 12. Generation of recombinant chimeric monoclonal antibodies *in vitro*. (A) Venn diagram shows the number of BCRs from ATLOs (yellow), blood (green), spleen (red), and RLNs (purple). Numbers

in overlapping sets show the same CDR3 amino acid sequences of BCRs in four tissue comparisons. The eight recombinant chimeric monoclonal antibodies' CDR3 amino acid sequences from ATLOs were showed in the Venn diagram. Before CDR3 amino acid, the number of BCRs shared the same CDR3 in ATLOs from the same mouse. The number after CDR3 amino acid is our nomenclature for the eight recombinant chimeric antibodies (from 1 to 8). These BCRs from the spleen, blood, and RLN were compared with the four recombination monoclonal antibodies that were produced from the first mouse (top left). Three BCRs are ATLO-specific; 1 BCR shared the same CDR3 amino acid sequence with blood BCRs. Next, these BCRs from the spleen, blood, and RLN were compared with the four recombination monoclonal antibodies that were produced from the second mouse (top right). One BCR is ATLO-specific; 1 BCR shared the same CDR3 with blood BCRs; 1 BCR shared the same CDR3 with the spleen; 1 BCR was found in all tissues (spleen, RLN, and blood). (B) Reducing Western blots (R) show separated H chains (around 50 kilodaltons (kDa)) and L chains (around 25 kDa), non-reducing WB (non-R) shows the combination antibody (around 150 kDa). Shown are 2 examples of antibodies obtained from ATLOs. ATLOs-derived A8 (left) and A4 (right) were used to stain the bands.

3.4 ATLO-derived antibodies recognize plaque components

Next, the reactivities of the eight recombinant chimeric monoclonal antibodies from ATLOs and the two recombinant monoclonal antibodies from the spleen were examined in the ApoE$^{-/-}$ mouse model of atherosclerosis. Eight ATLO and two spleen recombinant antibodies were used to stain atherosclerotic plaques in the aorta of aged ApoE$^{-/-}$ mice by IF staining. In order to test the sensitivities of our recombinant antibodies, serially diluted recombinant antibodies (0 µg/ml, 1 µg/ml, 5 µg/ml, 10 µg/ml, 25 µg/ml, 50 µg/ml) were used as primary antibodies, and fluorescent-labeled anti-human C region secondary antibodies were subsequently used to detect the recombinant antibodies in mouse tissues (avoiding reactivity with endogenous mouse Igs). Leica TCS SP8 confocal microscopy was used to detect the fluorescent signals (Fig. 13). The findings reveal that the concentration of 25 µg/ml ATLO-derived antibodies resulted in an appropriate signal-to-noise ratio for A1, A4, A7, and S1. 10 µg/ml and 25 µg/ml was also suitable for A6 to react with plaques. The other antibodies were not or weakly reactive with plaque components, even as high as 50 µg/ml. To compare the plaque reactivity of all the antibodies under the same concentration, 25 µg/ml was subsequently used for all follow-up IF experiments.

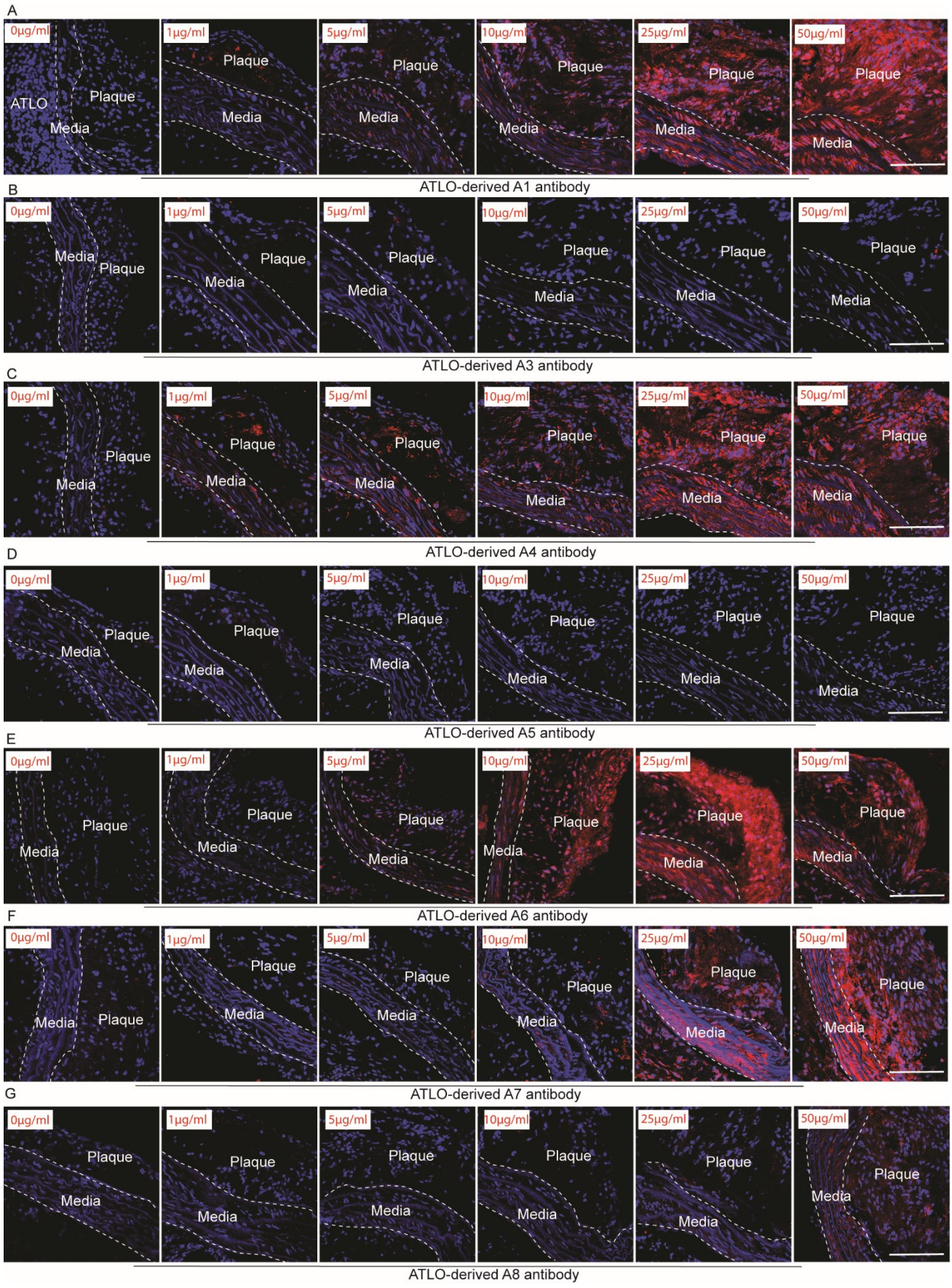
A
0µg/ml
ATLO
Plaque
Media
1µg/ml
Plaque
Media
5µg/ml
Plaque
Media
10µg/ml
Plaque
Media
25µg/ml
Plaque
Media
50µg/ml
Plaque
Media
ATLO-derived A1 antibody
B
0µg/ml
Media
Plaque
1µg/ml
Plaque
Media
5µg/ml
Plaque
Media
10µg/ml
Plaque
Media
25µg/ml
Plaque
Media
50µg/ml
Plaque
Media
ATLO-derived A3 antibody
C
0µg/ml
Plaque
Media
1µg/ml
Plaque
Media
5µg/ml
Plaque
Media
10µg/ml
Plaque
Media
25µg/ml
Plaque
Media
50µg/ml
Plaque
Media
ATLO-derived A4 antibody
D
0µg/ml
Plaque
Media
1µg/ml
Plaque
Media
5µg/ml
Plaque
Media
10µg/ml
Plaque
Media
25µg/ml
Plaque
Media
50µg/ml
Plaque
Media
ATLO-derived A5 antibody
E
0µg/ml
Plaque
Media
1µg/ml
Plaque
Media
5µg/ml
Plaque
Media
10µg/ml
Plaque
Media
25µg/ml
Plaque
Media
50µg/ml
Plaque
Media
ATLO-derived A6 antibody
F
0µg/ml
Media
Plaque
1µg/ml
Plaque
Media
5µg/ml
Plaque
Media
10µg/ml
Plaque
Media
25µg/ml
Plaque
Media
50µg/ml
Plaque
Media
ATLO-derived A7 antibody
G
0µg/ml
Plaque
Media
1µg/ml
Plaque
Media
5µg/ml
Plaque
Media
10µg/ml
Plaque
Media
25µg/ml
Plaque
Media
50µg/ml
Plaque
Media
ATLO-derived A8 antibody

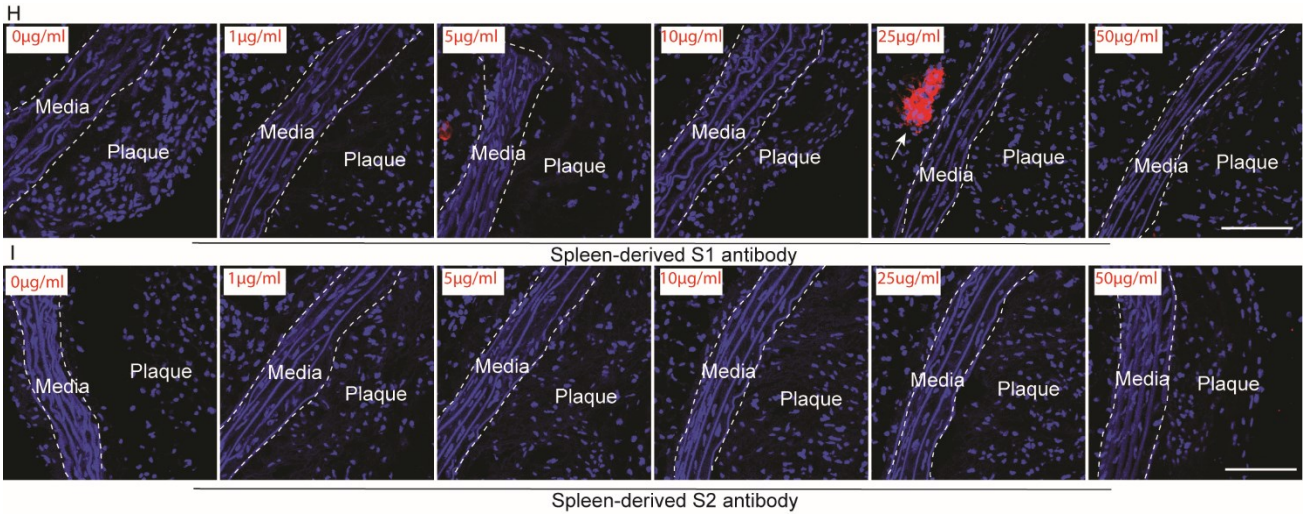

Figure 13. Serial dilution of recombination antibodies used in aorta segments with atherosclerosis. Fresh frozen abdominal aorta sections (10 μm) were collected from 78 weeks ApoE$^{-/-}$ mice. Serially dilutions of recombination antibodies (A1 to A8, S1, and S2 antibodies, from 0 μg/ml to 50 μg/ml) were used as primary antibodies, fluorescent-labeled anti human C region secondary antibody was used to detect the reactivity of these recombination antibodies in 78 weeks ApoE$^{-/-}$ mice aorta plaques. ATLO-derived antibodies were stained red; DAPI was stained blue. Scale bar: 100 μm.

ATLO-derived antibodies (25 μg/ml) were used to screen diseased aortas from aged ApoE$^{-/-}$ mice. ATLO-A1, ATLO-A2, ATLO-A4, ATLO-A6, and ATLO-A7 antibody recognized atherosclerotic plaque constituents and constituents presented in the adventitia while ATLO-A3, ATLO-A5, and ATLO-A8 antibody did not or weakly react with atherosclerotic plaque constituents (Fig. 14A). ATLO-A1 antibody mainly recognizes atherosclerotic plaque and media constituents, while ATLO-A2 antibody mainly recognizes constituents presented in the plaques and the adventitia. ATLO-A4 and ATLO-A6 antibody mainly recognize atherosclerotic plaque constituents. ATLO-A7 antibody mainly recognizes constituents presented in the media. Although two spleen GC-derived antibodies did not recognize atherosclerotic plaque constituents, spleen-derived S1 antibody reacted with adventitia (Fig. 14B). These data show that 5 out of 8 ATLO GC-derived antibodies recognize atherosclerotic plaque constituents supporting the concept that atherosclerosis plaque-relevant autoantigens may trigger autoimmune B cell responses in ATLOs in aged ApoE$^{-/-}$ mice. One out of 2 spleen-derived antibodies reacted with adventitia indicating that GC B2 cells outside of the arterial wall may also be an important source of autoimmune antibody production in

atherosclerosis. The adventitia contains immune cells, blood vessels, nerves, and other components, which play essential roles in atherosclerosis [144]. Spleen-derived S1 antibody might react with one or several specific tissue(s) or cell(s) in the adventitia. To clarify this in more detail, the S1 antibody was costained with cell type-specific markers to verify this preliminary assumption, including CD68 for macrophages, smooth muscle cell actin (SMA) for smooth muscle cells, CD11c, and CD11b for APCs, and neurofilament 200 for nerves.

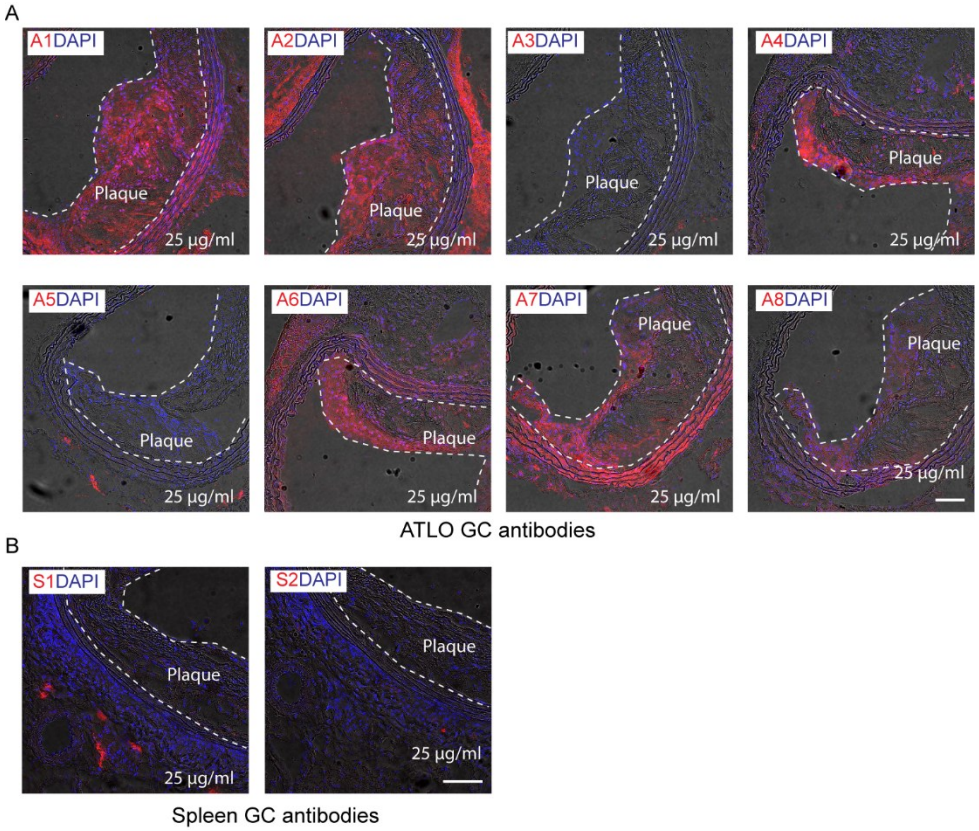

Figure 14. ATLO-derived antibodies recognize atherosclerotic plaque constituents. Aorta sections of 78 week old ApoE$^{-/-}$ mice on a chow diet were incubated with ATLO-derived primary antibodies (A1-A8 antibody) or spleen-derived primary antibodies (S1 and S2 antibody) at the concentration of 25 µg/ml; anti-human Ig antibody was used as the secondary antibody. A1, A2, A4, A6, and A7 antibodies react with plaque constituents. A5 and S1 antibodies react with antigen(s) present in the adventitia. A3, A5, A8, S1, and S2 antibodies show no or weak reaction with plaque constituents. ATLO- and spleen-derived antibodies were stained red; DAPI was stained blue. Scale bar: 100 µm.

3.5 Screening the reactivity of ATLO GC-derived antibodies by tissue arrays

Some autoantibodies in autoimmune diseases are associated with systemic autoimmune injury in multiple organs, such as ANAs for systemic rheumatic diseases [166], anti-centromere antibodies for autoimmune hepatitis [167], and anti-histone antibodies for SLE [168]. In order to examine whether ATLO GC-derived autoantibodies recognize multiple tissues, IF staining was performed by using tissue arrays: multiple tissues (spleen, lung, liver, pancreas, intestine, colon, kidney, muscle, and spinal cord) were collected and placed on a single slide (Fig. 15) allowing efficient screening of antibody reactivities with multiple specimens. With this technology, tissue samples were treated in an identical manner, such as incubation times, antibody concentration, and washing procedures.

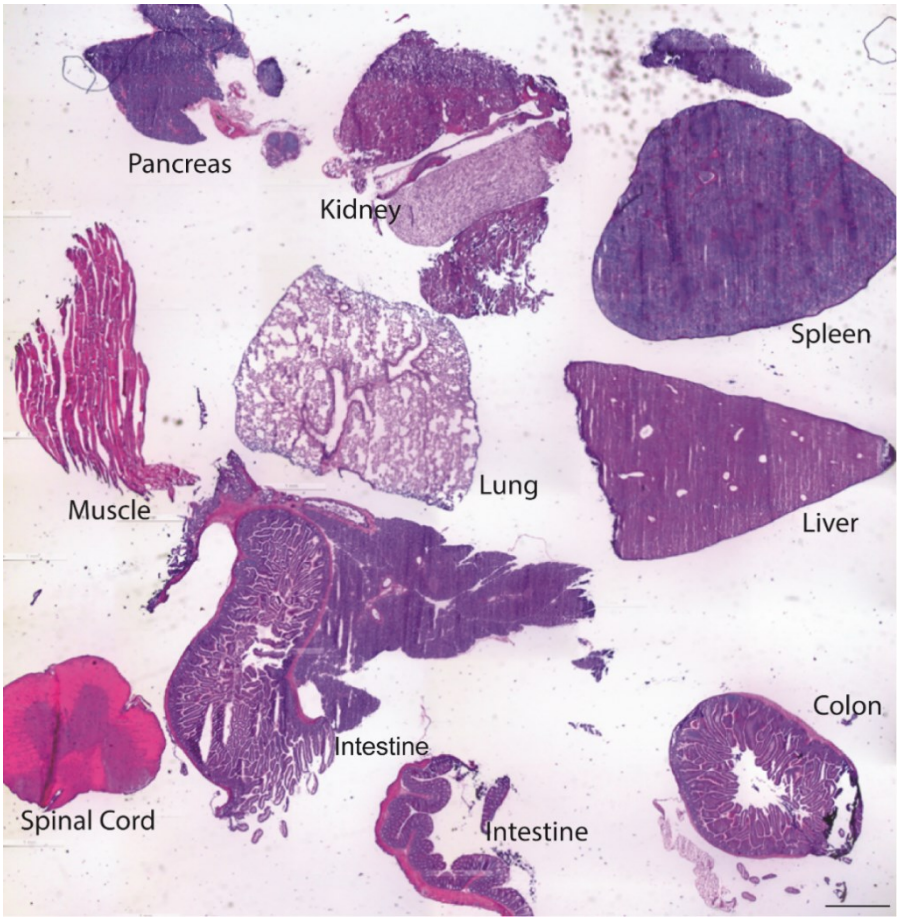

Figure 15. Hematoxylin and eosin (H&E) staining images of tissue array. Pancreas, kidney, spleen, muscle from abdominal, lung, liver, spinal cord, small intestine, colon from 78 weeks old ApoE$^{-/-}$ mice and WT mice were prepared for histological staining. Representative images of hematoxylin- and eosin-stained (H&E) staining of tissue array from aged ApoE$^{-/-}$ mice. Scale bar: 1 mm.

ATLO GC-derived antibody reactivities were examined by IF staining in tissue arrays from WT and ApoE$^{-/-}$ mice. The 25 µg/ml concentration of primary antibodies, followed by donkey anti-human secondary antibody, was used to detect the recombinant antibodies in mouse tissue sections to avoid the contamination of endogenous mouse Igs. ATLO-derived A1 antibody recognizes antigens presented in multiple organs, including liver, colon, muscle, intestine, kidney, lung, spleen, and spinal cord (Fig. 16). However, the positive signals of the A1 antibody shows distinct patterns in different tissues: (1) liver, colon, kidney, and pancreas were stained weakly with A1 antibody (Fig. 16A, B, E, H); few A1 positive extracellular components were observed in liver, colon, and pancreas, and A1 positive signals located mainly in the glomerulus in the kidney (Fig. 16E); (2) muscle fibers were stained positively by A1 antibody (Fig. 16C); (3) villi of intestine stained strongly with A1 antibody (Fig. 16D); (4) in lung and spinal cord tissue sections, A1 antibody stained intracellular components (Fig. 16F, I); (5) A1 positive signals located in the spleen surrounding the white pulp (Fig. 16G). These data support the conclusion that the A1 antibody recognizes multiple tissues, including atherosclerotic plaques, in aged ApoE$^{-/-}$ and WT mice. The following two possibilities are considered: 1) A1 antibody recognizes a single antigen, and this A1 antigen is present on multiple tissues; 2) A1 recognizes multiple antigens in multiple tissues. In order to address this question, Western blots in multiple tissues of WT and ApoE$^{-/-}$ mice should be performed to identify the molecular weight of A1 antigen(s). The functional roles of A1 antibody and A1 antigen(s) during atherosclerosis development of mice also need to be addressed in the future.

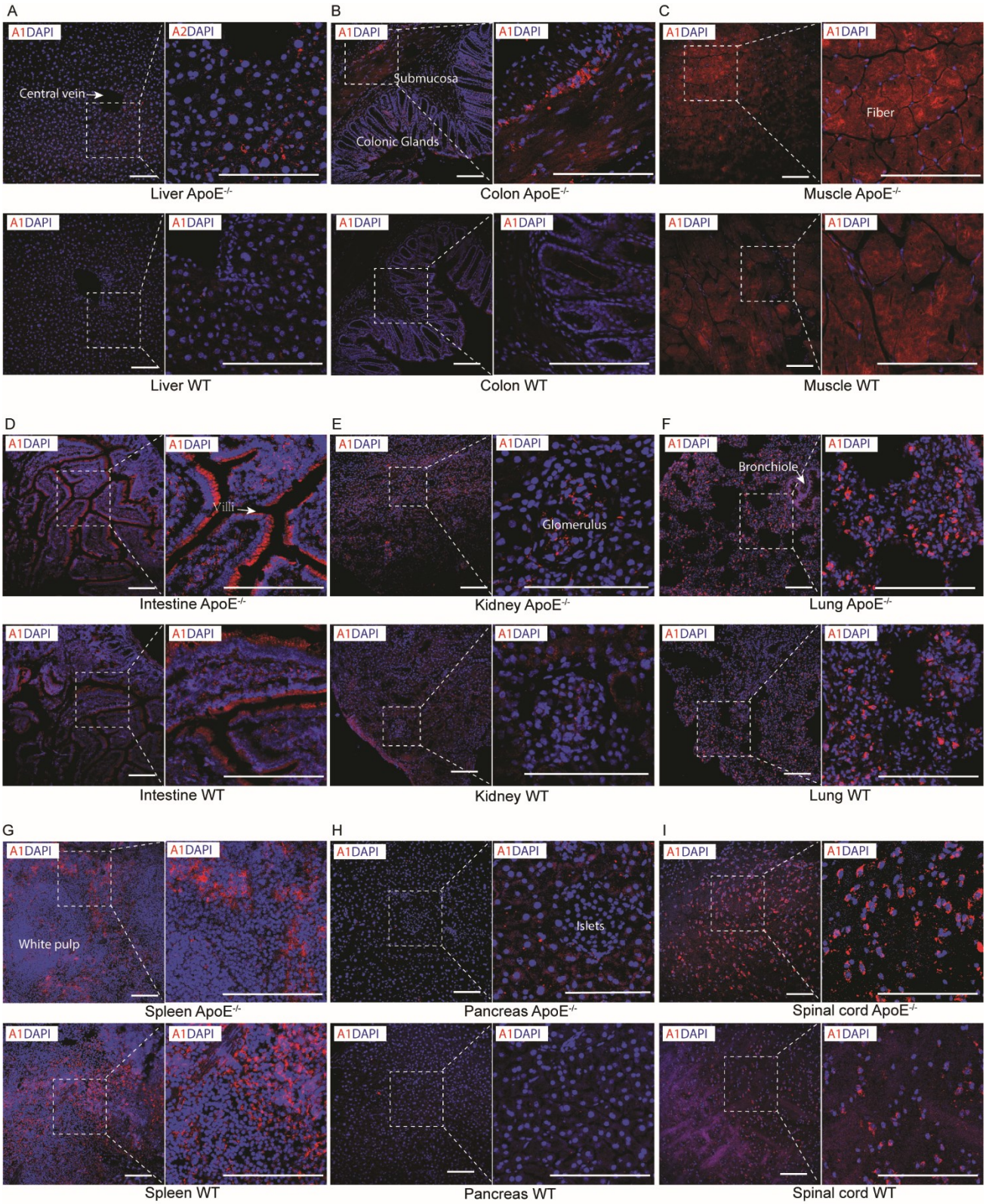

Figure 16. Detection of A1 positive signals by tissue array. IF staining of A1 antibody in tissue arrays. Liver, colon, muscle, intestine, kidney, lung, spleen, pancreas, and spinal cord tissues were collected from aged WT and ApoE$^{-/-}$ mice. All tissues were prepared on one slide, and tissues were stained under identical conditions. Data are representative for 3 aged ApoE$^{-/-}$ and WT mice. A1 antibody was stained red, nuclei

was stained with DAPI (blue). Scale bars: 100 μm.

ATLO GC-derived A2 antibody mainly recognizes constituents presented in the adventitia of aorta from aged ApoE$^{-/-}$ mice (Fig. 14A). The adventitia is the artery's outer layer composed of fibroblasts, nerves, blood vessels, irregular connective tissue, and other components[144]. The A2 antibody was also examined by tissue array IF staining in aged WT and ApoE$^{-/-}$ mice (n=3). It was found that A2 antibody recognizes constituents present in the outer layer of the arteries in the liver, lung, and spleen (Fig. 17A, F, G), and extracellular constituents of liver, colon, muscle, intestine, kidney, pancreas (Fig. 17A, B, C, D, E, H), and a portion of cells in the spleen and spinal cord (Fig. 17G, I). These data indicate that the A2 antibody recognizes antigen(s) of extracellular matrix components in multiple tissues in WT and ApoE$^{-/-}$ mice. Similar to the situation of the A1 antibody, the A2 antigen(s) still needs to be identified and characterized, and their roles in atherosclerosis development needs to be addressed in the future.

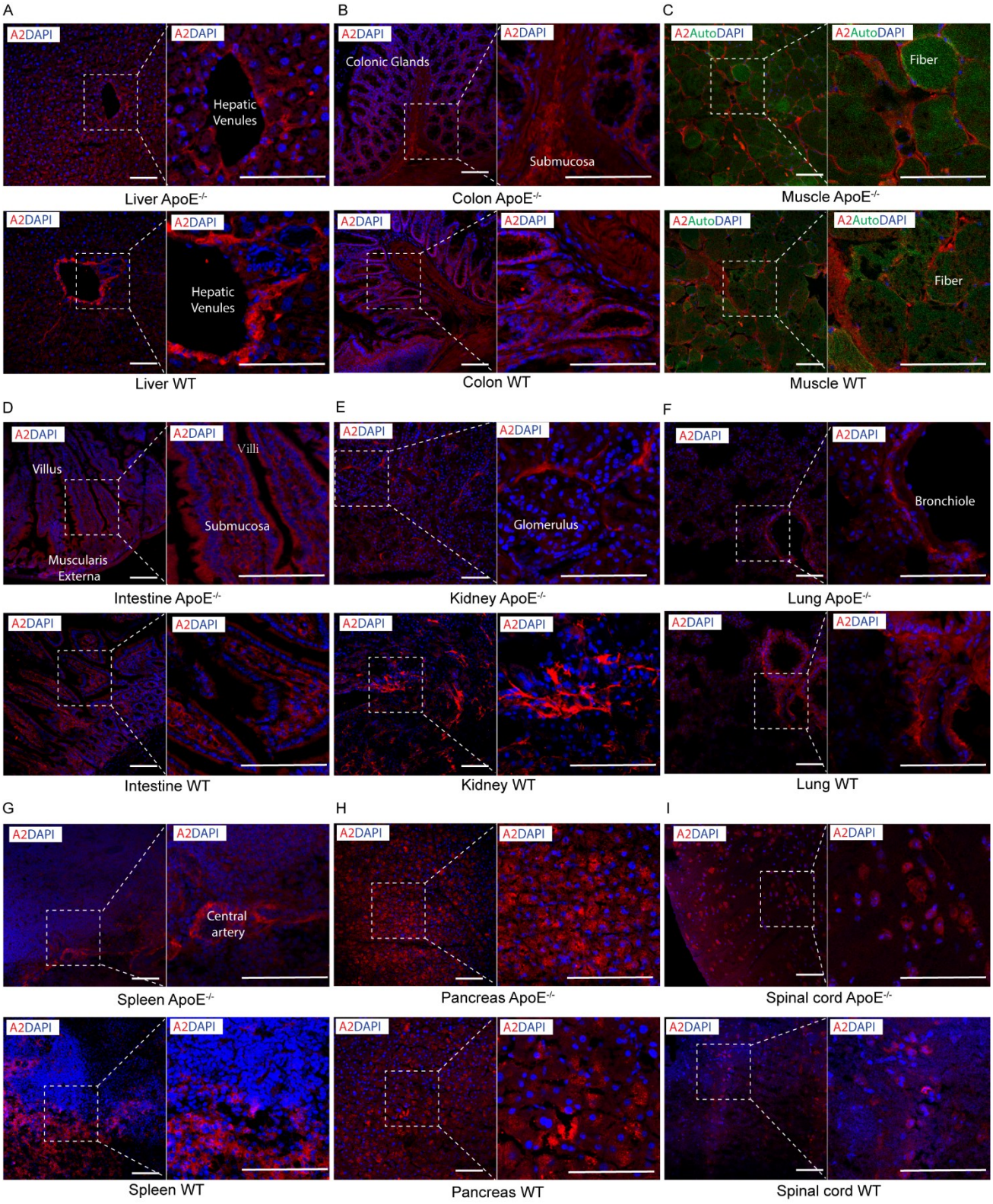

Figure 17. Detection of A2 positive signals in tissue arrays. IF staining of A2 antibody in tissue array. Liver, colon, muscle, intestine, kidney, lung, spleen, pancreas, and spinal cord tissues were collected from aged WT and ApoE$^{-/-}$ mice. All tissues were prepared on one slide, and tissues were stained under identical conditions. A2 antibody was stained red; nuclei was stained with DAPI (blue). Scale bars: 100 μm.

Next, the A4 antibody was studied by IF staining in tissue arrays from aged WT and ApoE$^{-/-}$ mice. Multiple tissues are stained by A4 antibody, including liver, colon, intestine, kidney, lung, spleen, pancreas, and spinal cord (Fig. 18). However, no/rare A4 positive signals were observed in the muscle (Fig. 18C). A4 positive signals were observed in the cytoplasm of the liver, lung, spleen, and spinal cord cells (Fig. 18A, F, G, I), indicating A4 antibody recognizes cytosolic antigens of these tissues. Extracellular signals were observed in the colon, kidney, and pancreas (Fig. 18B, E, H), which indicated A4 antibody recognized extracellular antigens of these tissues. Interestingly, the single epithelial layer of the intestine is stained positively by the A4 antibody (Fig. 18D), raising the possibility that the antigen that presented in epithelial cells was also recognized by the A4 antibody. Strong A4 positive signals were observed in the liver (Fig. 18A). Strikingly, the IF staining showed that different subcellular locations were recognized by A4 antibody in the liver of WT and ApoE$^{-/-}$ mice. In ApoE$^{-/-}$ mice, the A4-related antigen(s) was observed in the cytoplasm. In the WT mice, the different staining locations were observed, both in the extracellular and cytoplasm. Taken together, these data indicate two possibilities: 1) A4 antibody recognizes the same antigen present in multiple tissues; the subcellular location of A4 related antigen is cytoplasm and can be released into extracellular milieu. 2) A4 antibody recognizes different antigens in different tissues. Again, more experiments are needed to identify A4-related antigen(s) and the function of the A4 antibody and A4 antigen(s) in atherosclerosis in the future.

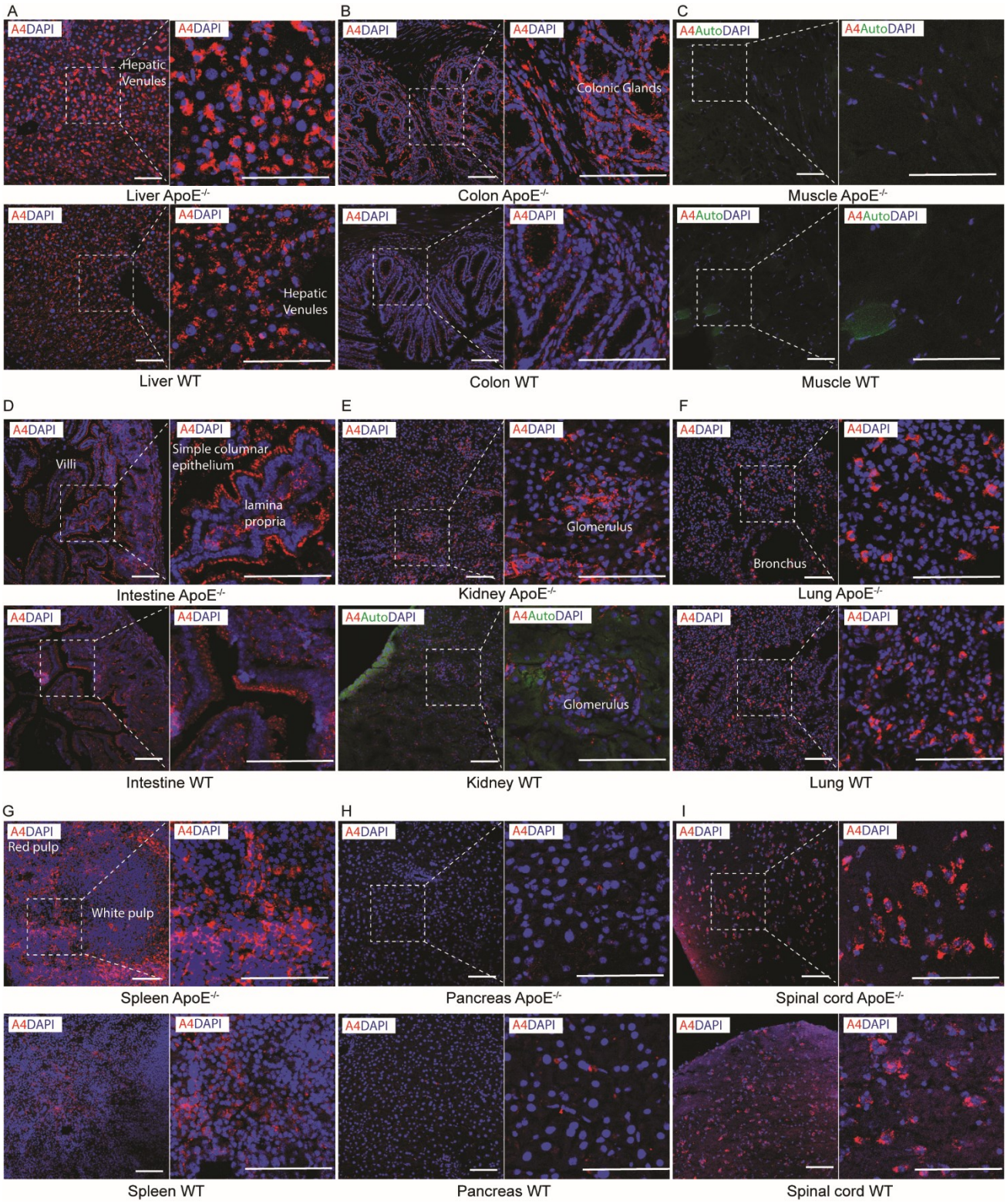

Figure 18. Detection of A4 positive signals in tissue arrays. Representative images of IF staining of A4 antibody in tissue arrays from aged ApoE$^{-/-}$ and WT mice. Liver, colon, muscle, intestine, kidney, lung, spleen, pancreas, and spinal cord tissues were collected from aged WT and ApoE$^{-/-}$ mice (n=3). All tissues were prepared on one slide, and tissues were stained under identical conditions. A4 antibody was stained red; nuclei was stained with DAPI (blue). Scale bars: 100 µm.

Next, the A6 antibody was studied by using tissue arrays from aged WT and ApoE$^{-/-}$ mice. Unlike the strong A6 positive signals were observed in atherosclerotic plaques (Fig. 14A), the A6 antibody stained a small portion of cells in the liver, colon, muscle, lung, spleen, and pancreas (Fig. 19A, B, C, F, G, H). Importantly, similar to atherosclerotic plaques, the A6 antibody signals co-localized with DAPI in these tissues indicating that the A6 antibody may recognize the same nuclear antigen(s) in multiple tissues. Weak extracellular A6 signals were also detected in the intestine and kidney (Fig. 19D, E). These data suggest two possibilities: 1) The A6 antibody recognizes a single antigen, which is released from the nuclei of dead cells into the extracellular milieu; 2) A6 antibody recognizes multiple antigens, including nuclear antigens and extracellular antigens. In the follow-up experiments, the A6 antibody was selected to identify its cognate antigen by IP-MS as a proof of concept experiment.

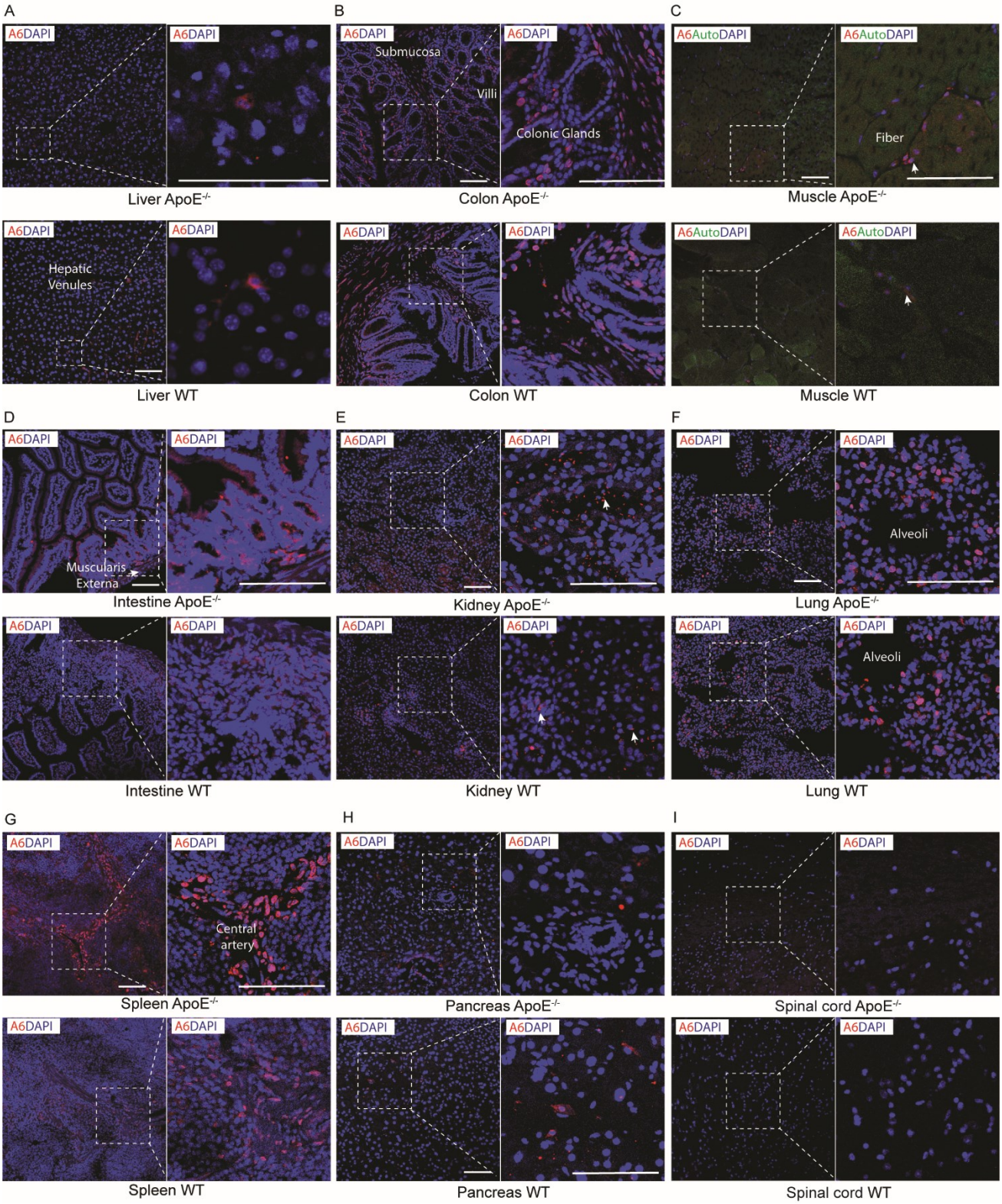

Figure 19. Detection A6 positive signal in tissue array. Representative images of IF staining of A6 antibody in tissue array from aged ApoE$^{-/-}$ and WT mice. Liver, colon, muscle, intestine, kidney, lung, spleen, pancreas, and spinal cord tissues were collected from aged ApoE$^{-/-}$ and WT mice (n=3). All tissues were

prepared on one slide, and tissues were stained with identical conditions. A6 antibody was stained red; nuclei was stained with DAPI (blue). Scale bars: 100 µm.

Firstly, spleen, liver, and lung were analyzed by FACS. In order to examine whether the A6 antibody recognizes cell surface antigens or intracellular antigens, surface and intracellular staining methods were performed. Consistent with the IF staining (see above Fig. 19), flow cytometry data showed that the A6 antibody stains intracellular antigen but not cell surface antigen (Fig. 20A). In order to examine which cell subsets were stained by the A6 antibody in the spleen, liver, and lung, CD45 was used for total leukocytes. A6 positive signals were compared between $CD45^-$ cells (non-leukocytes) and $CD45^+$ cells (leukocytes) in these tissues. The A6 positive population was mainly CD45 positive, indicating that A6 essentially stains leukocytes (Fig. 20B).

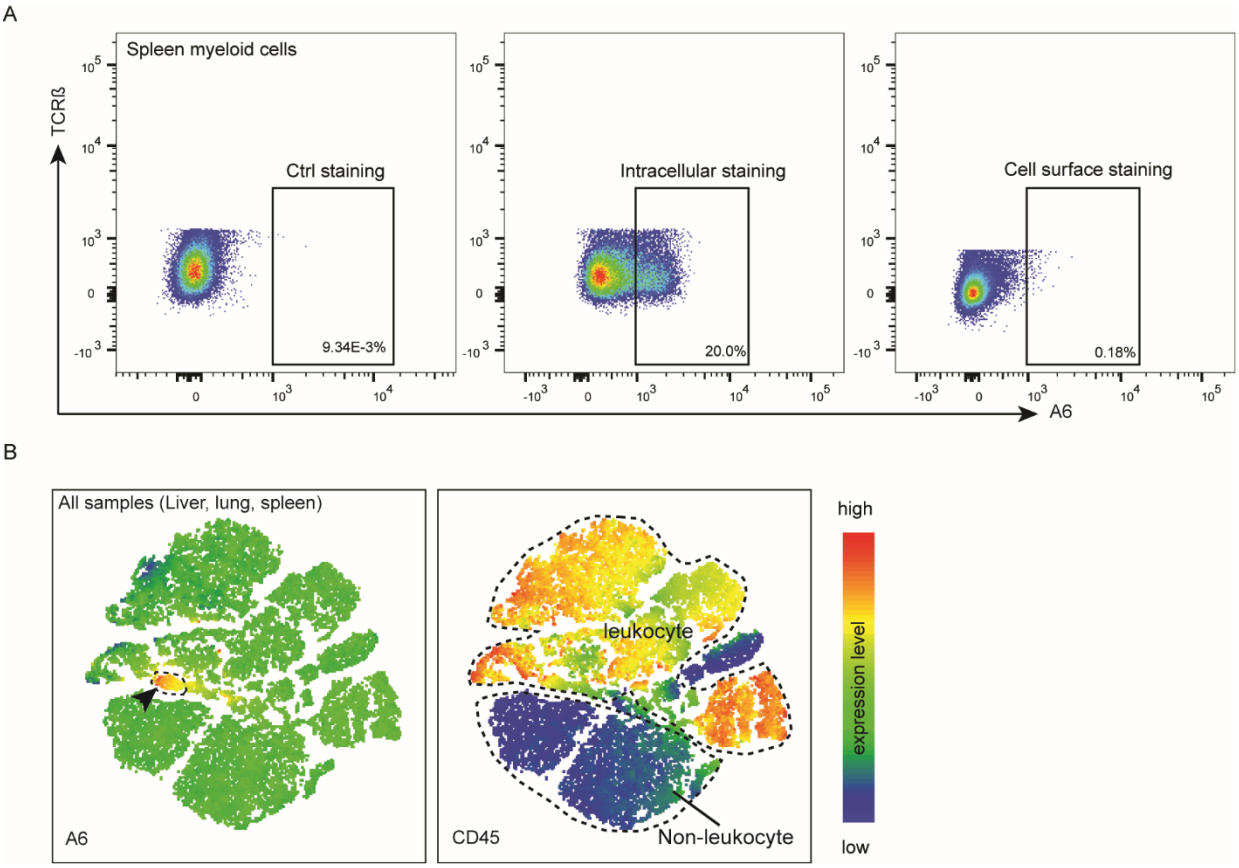

Figure 20. Flow cytometry analyses of $A6^+$ cell populations. (A) Flow cytometry analysis of $A6^+$ cells to stain the plasma membrane or intracellularly. To stain intracellular A6-related antigens, lung, liver, and spleen cells must be fixed in suspension and then permeabilized before the A6 antibody was added. Spleen myeloid cells were gated from FVD^-CD45^+ total live leukocytes; $A6^+$ cells were gated from

$CD45^+CD19^-$ $TCR\beta^-$ cells. Approximately 20% of $A6^+$ cells of the total $CD45^+CD19^-TCR\beta^-$ myeloid cells were positive using the intracellular staining protocol. No or rare $A6^+$ cells of the total $CD45^+CD19^-TCR\beta^-$ myeloid cells stained using cell surface staining protocols (B) T-SNE defines the population of A6 positive cells in total live cells in the spleen, liver, and lung. 5000 total live cells for each tissue were used for t-SNE analysis. The tSNE was run by using the FlowJo software. The different cell populations are visualized by the tSNE heat map.

In order to address which leukocyte subsets contribute to A6 positive cells in the spleen, the following markers were used in combination with A6 staining: CD45 for total leukocytes, TCR β for T cells, CD19 for B cells, CD11b, CD11c, and MHCII for professional APCs such as DCs or macrophages in the spleen. Most A6 positive cells were found in $CD45^+TCR^-CD19^-CD11b^+CD11c^+MHCII^+$ myeloid cells in the spleen (Fig. 21A). These data indicate that $A6^+$ cells are mainly APCs. In the future, more defined markers are needed to better address the question which APC subtypes are $A6^+$ cells. Next, the percentage of B cells, T cells, and myeloid cells were compared between WT and $ApoE^{-/-}$ spleen; no significant differences were found (Fig. 21B). The percentage of A6 positive cells per total $CD45^+CD19^-TCR\beta^-$ myeloid cells was significantly higher in $ApoE^{-/-}$ mice when compared to WT mice (Fig. 21C).

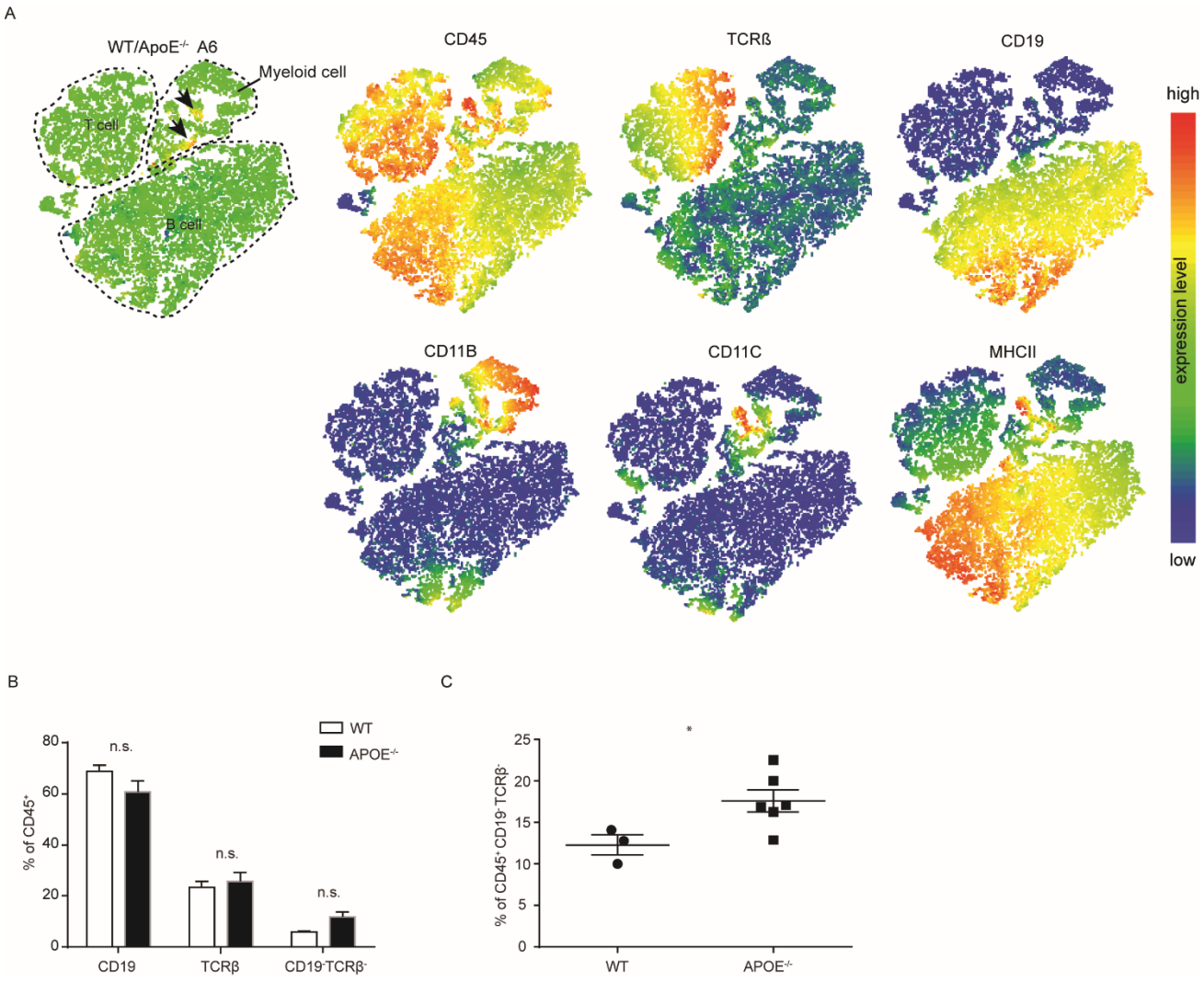

Figure 21. Flow cytometry analyses of A6⁺ cell populations in spleen. (A) T-SNE defines the population of A6 positive cells in total CD45⁺ cells. 5000 total live leukocytes were used for t-SNE analysis. The different cell populations are visualized by the tSNE heat map. (B) Flow cytometry analysis of leukocytes in WT and ApoE$^{-/-}$ mice. CD19 for B cells, TCRβ for T cells, and CD19^{-} TCRβ^{-} for myeloid cells were gated from total live leukocytes, i.e., CD45⁺ cells. (C) The percentage of A6⁺ populations in myeloid cells of WT and ApoE$^{-/-}$ mice. A6⁺ cells were gated from CD45⁺ CD19^{-} TCRß$^{-}$ myeloid cells. Data represent means of percentage ± SEM; two-tailed unpaired Student´s t-test, n.s.: not significant; *: p<0.05.

Next, the A7 antibody was examined by tissue array from aged WT and ApoE$^{-/-}$ mice. Similar to A7 staining results in the diseased artery, specific structures were recognized by A7 antibody in the liver, colon, muscle, kidney, lung, spleen, pancreas, which might be blood vessels. (Fig. 22A, B, C, E, F, G, H). These data support the interpretation that the A7 antibody recognizes artery components of multiple tissues in WT and ApoE$^{-/-}$ mice. The

lamina propria of the intestine was stained by A7 antibody, which is composed of collagen, blood vessels, lymphatic vessels, and numerous immunologically competent cells and nerve endings (Fig. 22D), and neuron-like cells in the spinal cord were also stained by the A7 antibody (Fig. 23I). To determine which cell types contribute to A7 positive cells in the spinal cord, NeuN, a marker for neurons should be co-stained with A7 in the future.

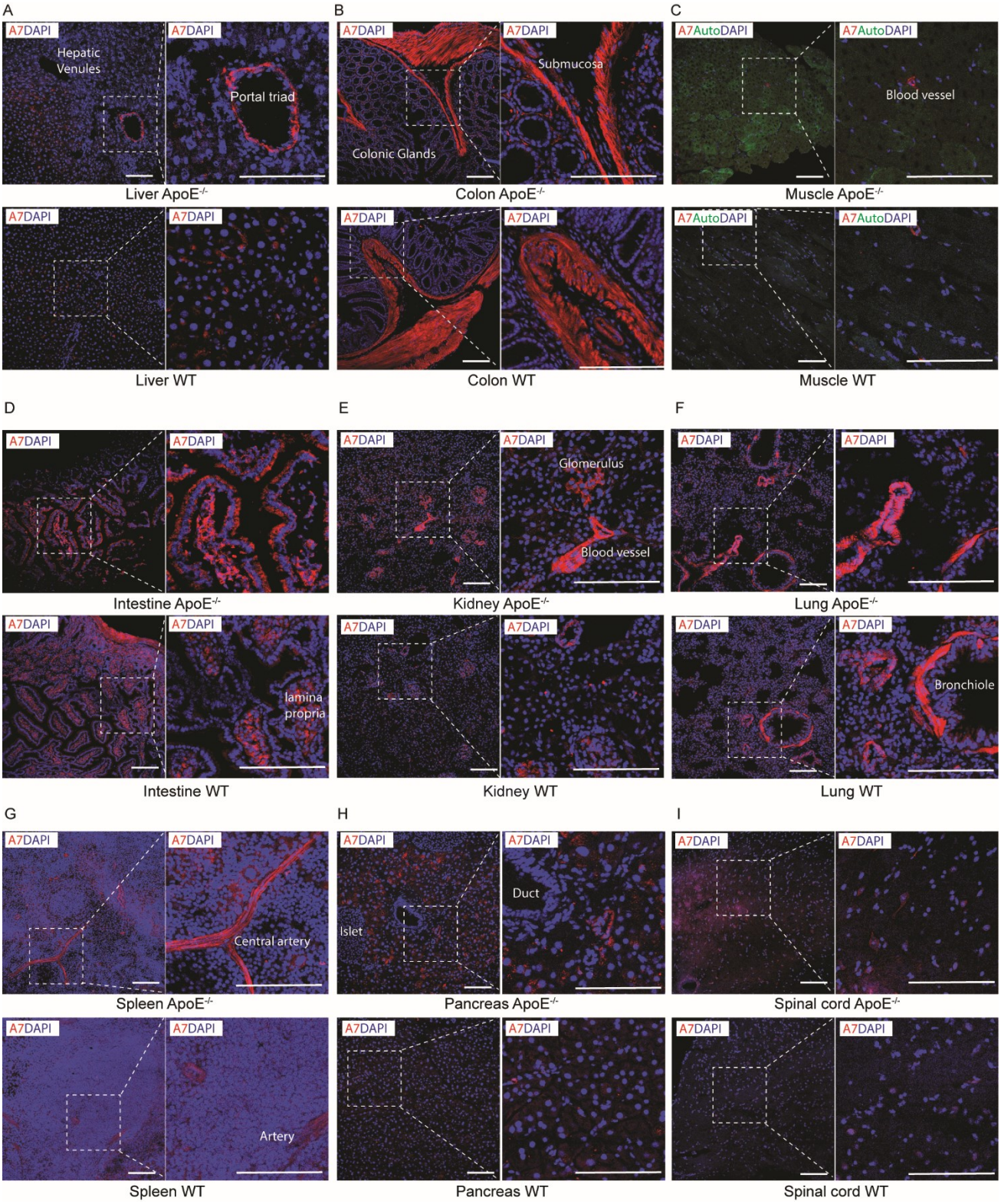

Figure 22. Detection of A7 positive signals in tissue array analyses. Representative images of IF staining of A7 antibody in tissue array. Liver, colon, muscle, intestine, kidney, lung, spleen, pancreas, and spinal cord were collected from aged ApoE$^{-/-}$ and WT mice. All tissues were prepared on one slide, and tissues were stained with identical conditions. A7 antibody was stained red; nuclei was stained with DAPI (blue). Scale bars: 100 µm.

The A8 antibody was studied by using tissue array. Similar to A8 antibody staining results in the aorta, no A8 antibody positive signals were observed in the liver, colon, muscle, intestine, spinal cord, and pancreas (Fig. 23A, B, C, D, F, H). Conversely, the spleen of WT and ApoE$^{-/-}$ mice (Fig. 23G), few cells in the lung (Fig. 23F) and a specific cell type in the kidney were stained with A8 antibody. The kidney is composed of three main areas: the outer cortex, the middle medulla, and the renal pelvis. Only a small portion of kidney tissue was included in the tissue array, which was not sufficient to detail the structural staining of A8 in the kidney. Therefore, whole kidney sections were subsequently used to stain with A8 antibody (Fig. 24A). This revealed that the A8 antibody did not or weakly stain kidney capsular structures, cortex structures, or collecting ducts (Fig. 24B). Interestingly, the cells located on the surface of the medulla distal to collecting tubules were strongly stained with the A8 antibody (Fig. 24B). However, identifying the A8 target antigens within the kidney was out of the scope of this thesis and remain to be identified in future experiments.

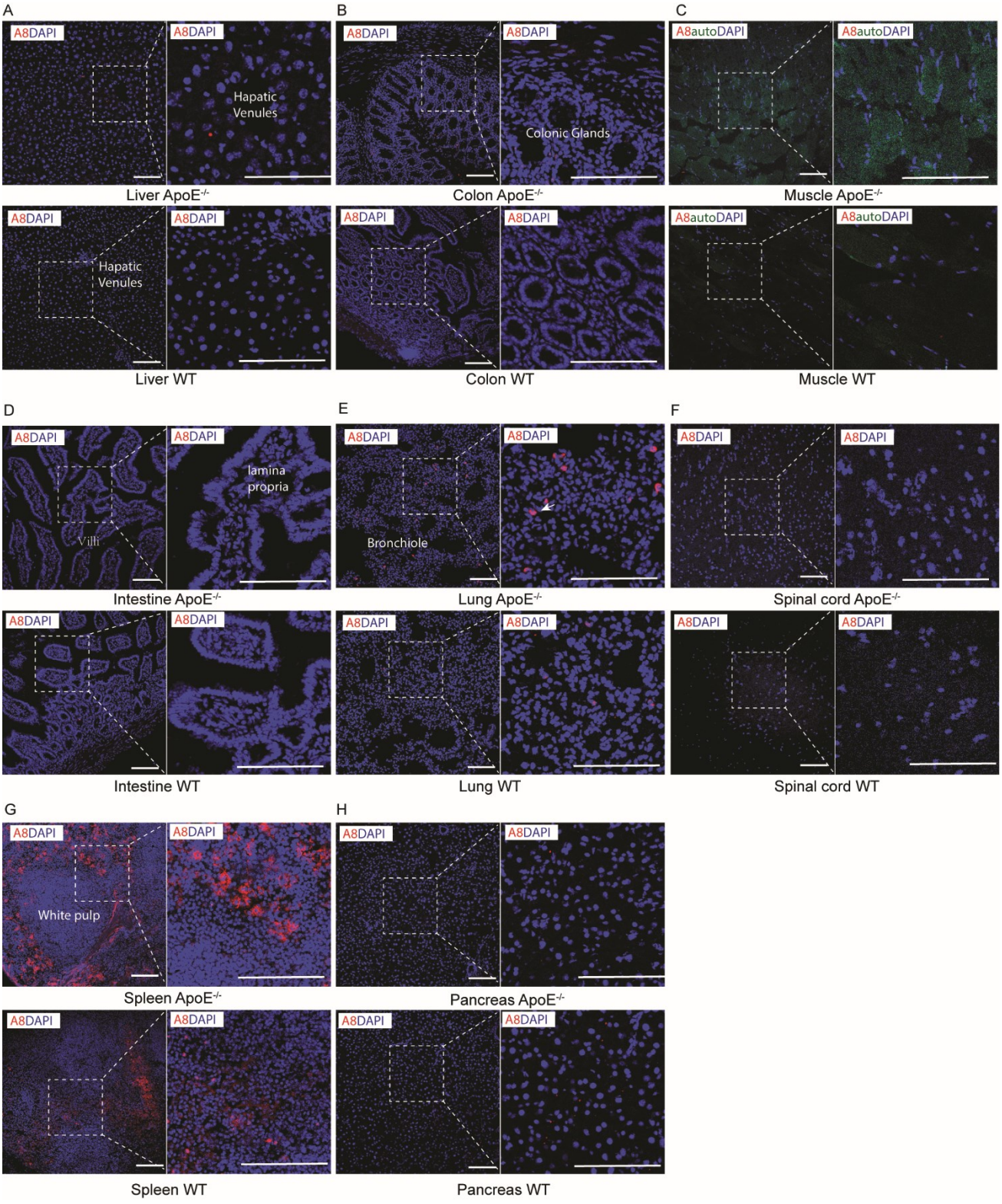

Figure 23. Detection of A8 positive signals in tissue array. Representative images of IF staining of A8 antibody in tissue array from aged WT and ApoE$^{-/-}$ mice. Liver, colon, muscle, intestine, kidney, lung, spleen, pancreas, and spinal cord were collected from aged WT and ApoE$^{-/-}$ mice. All tissues were prepared on one slide, and tissues were stained under identical conditions. A8 antibody was stained red; nuclei was stained with DAPI (blue). Scale bars: 100 μm.

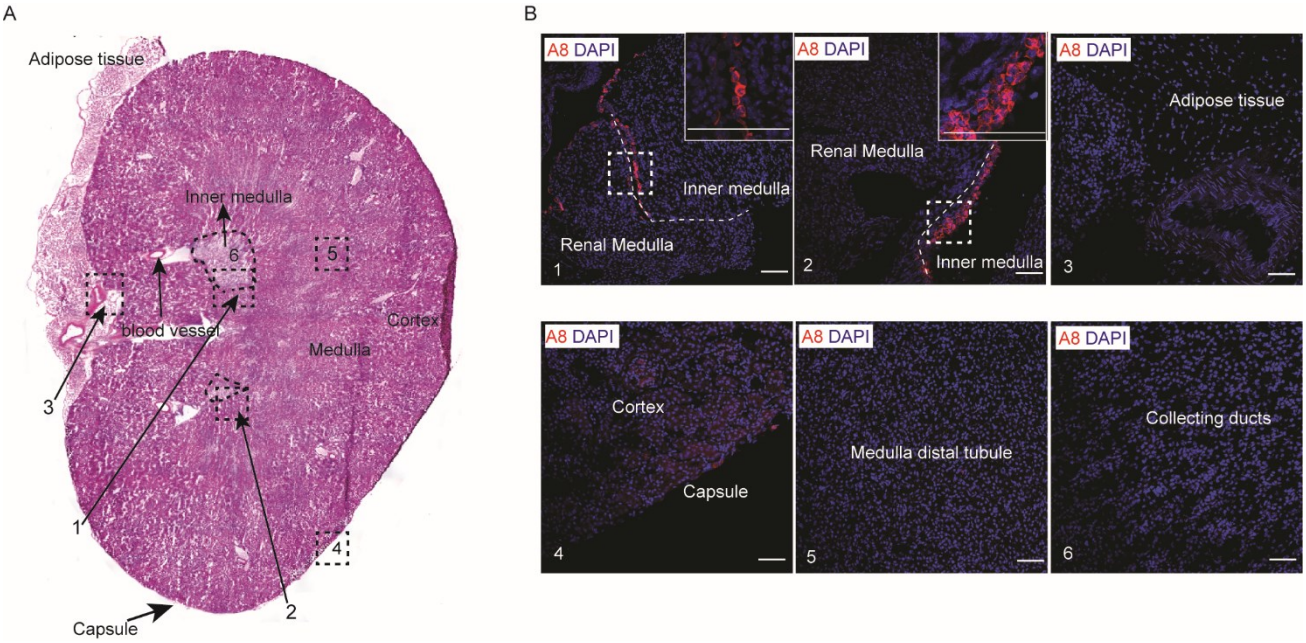

Figure 24. Detection of A8 positive signal in kidney. (A) Histology section of mouse kidney from aged ApoE$^{-/-}$ mice. 10 µm fresh-frozen mouse kidney sections were stained with H&E staining. The kidney is composed of three regions, including the cortex, medulla, and renal pelvis. The medulla contains medullary collecting ducts, loops of Henle, and tubules. (B) Representative images of IF staining of A8 antibody in the kidney. A8 antibody was stained red; nuclei was stained with DAPI (blue). Scale bars: 100 µm.

3.6 ATLO-derived A6 antibody reactivities in plaques

The data obtained so far support the hypothesis that ATLO GC-derived antibodies recognize arterial wall-specific or/and atherosclerosis-specific antigens. To understand which antigens can be recognized, ATLO-derived antibodies were characterized in more detail. ATLO-derived A6 antibody, which showed strong plaque reactivity in ApoE$^{-/-}$ mice, was used as an example. Different concentrations of A6 antibody (ranging from 0 µg/ml to 50 µg/ml) were used to stain aortas of aged WT and ApoE$^{-/-}$ mice. A6 antibody-positive signals co-staining with DAPI (arrow) were observed in plaques (Fig. 25A). The IF results confirmed the flow cytometry and tissue array results that the A6 antibody recognizes nuclear antigen(s). A6 antibody signals were further quantified in the aorta by determining the areas of A6 positive signals in aortas of aged WT and ApoE$^{-/-}$ mice (Fig. 25B). Strong A6 signals were detected in

the plaques and ATLOs of aged ApoE$^{-/-}$ mice (Fig. 25C). Plaques and ATLOs are inflammatory tissues. The high A6 positive signal intensity in ATLOs and plaques provide evidence for the possibility that A6-related antigen(s) are associated with inflammation. Whether the increase of the A6 signal is related to the degree of inflammation needs to be resolved. Weak A6 signals were detected in the media and adventitia of aged WT and ApoE$^{-/-}$ mice; The A6 signal detected in the perivascular adipose tissue of aged ApoE$^{-/-}$ mice was higher than that of aged WT mice (Fig. 25C). Immune cell infiltration in perivascular adipose tissue plays an important role in the pathogenesis of atherosclerosis [169]. The higher A6 signal may be caused by the accumulation of immune cells in perivascular adipose tissue of aged ApoE$^{-/-}$ mice. These data indicate that the A6 antibody recognizes nucleus-derived antigens. The A6 antigen increased in plaques, ATLOs, and perivascular adipose tissue areas may be associated with inflammation.

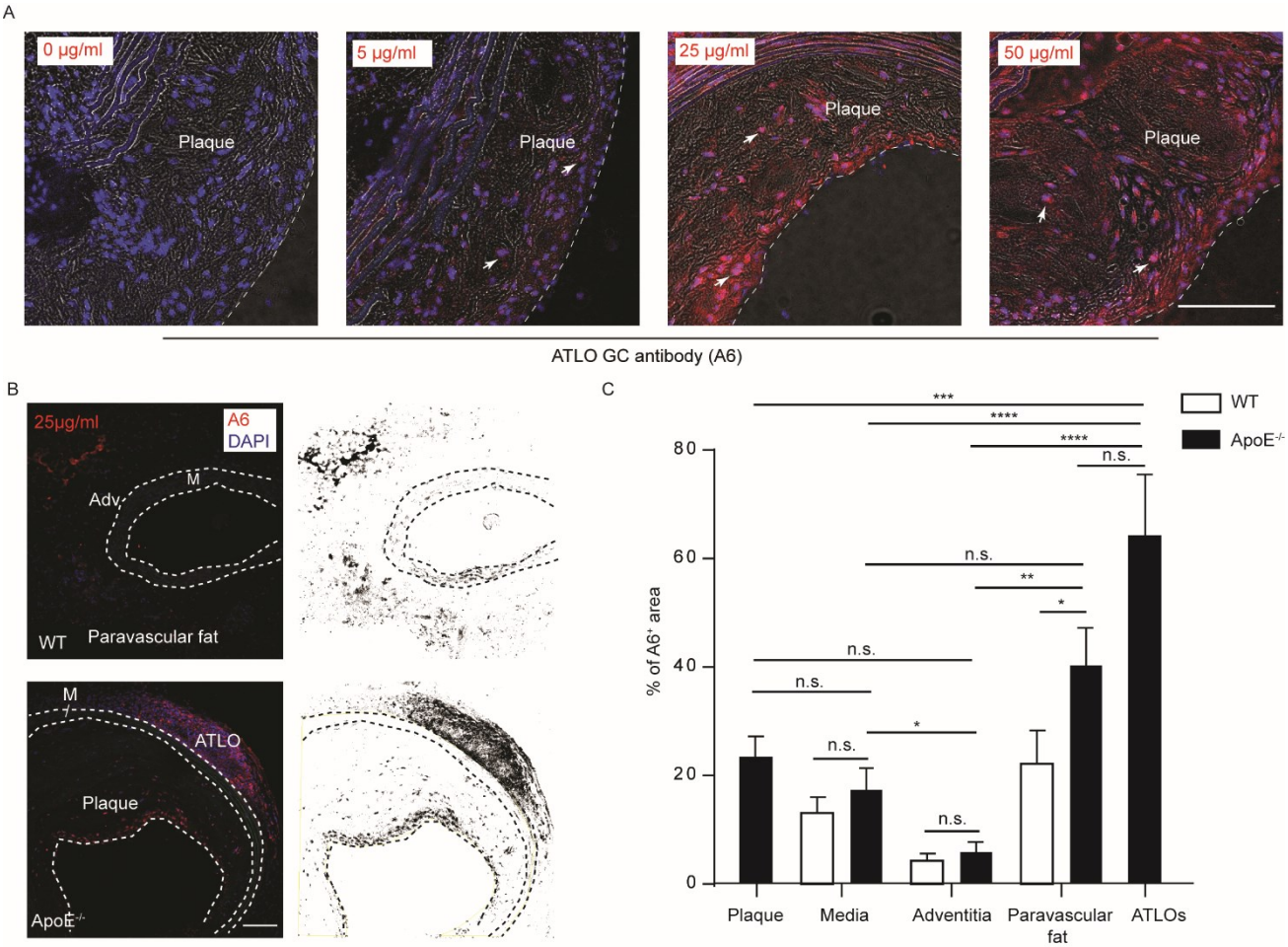

Figure 25. ATLO-derived A6 antibody stains plaque components. (A) ApoE$^{-/-}$ and WT mouse aorta sections of 78 week old mice were incubated with different concentrations of ATLO-derived A6 antibody. Anti-human Ig secondary antibody was used to detect the recombinant antibody (A6^{+}, red). DNA was stained blue. (B) Quantification analysis of A6 staining signals in WT and ApoE$^{-/-}$ mice (n = 3 WT, 3 ApoE$^{-/-}$ mice). (C) Higher staining signals in ATLOs are observed when compared to media and adventitia of ApoE$^{-/-}$ and WT mice. (Data represent means of area ± SEM, 4 sections per mouse, n = 3 WT and 3 ApoE$^{-/-}$ mice; two way ANOVA was applied for P, n.s.: not significant; *: p<0.05, **: p<0.01, ***: p<0.001, ****: p<0.0001). Scale bar: 100 µm.

Macrophages/monocytes and SMCs are major cell components of atherosclerotic plaques [170,171]. Next, A6 antibody was co-stained with macrophages and SMCs in plaques of aged ApoE$^{-/-}$ mice, i.e., CD68 for macrophages/DCs, SMA for SMCs, and CD11c for dendritic cells or macrophages. A6 antibody signals are mainly located intracellularly and colocalized with DAPI. A few extracellular A6 positive signals were observed (Fig. 26), which may raise the possibility that damaged cells may release A6 antigens into plaque environments.

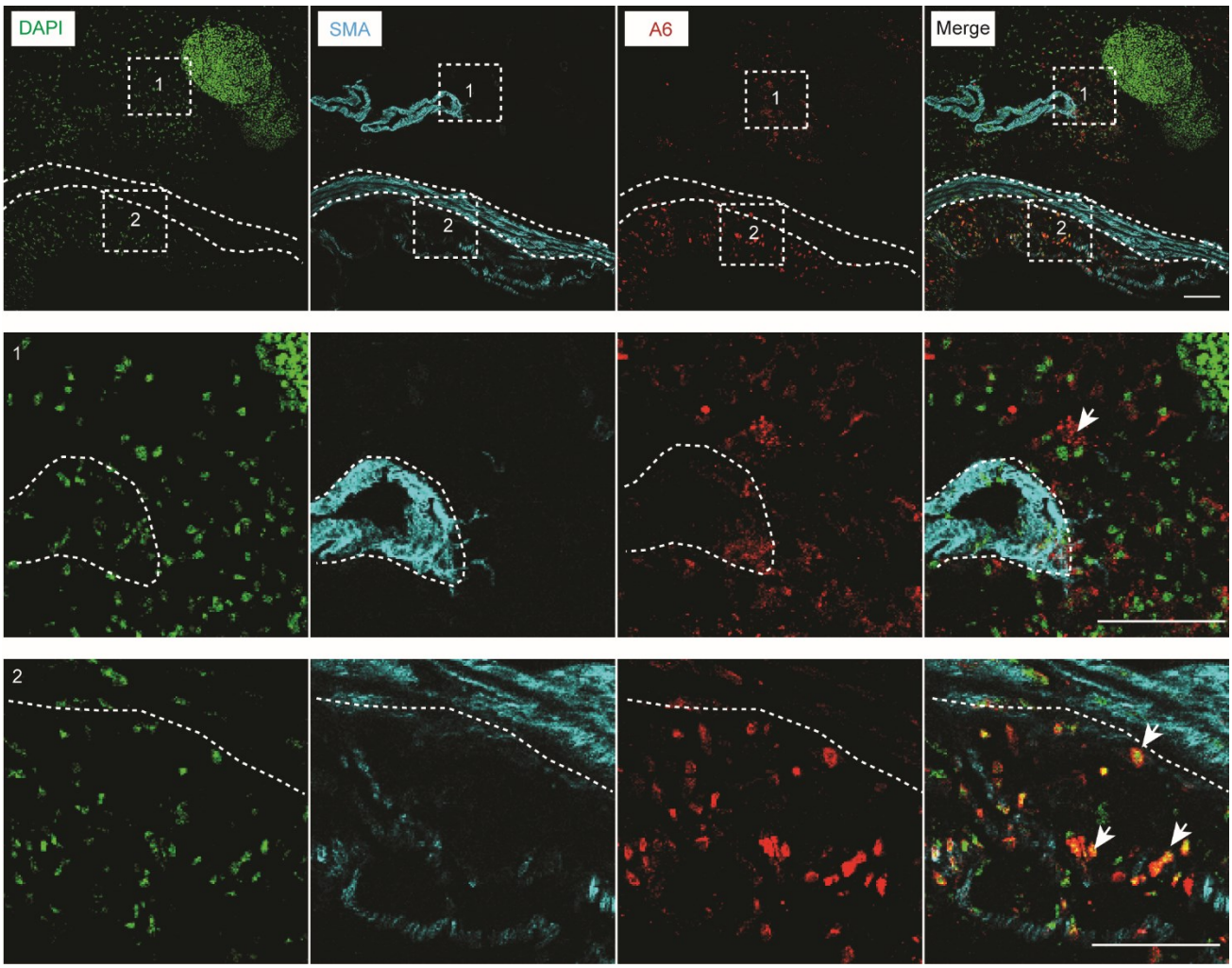

Figure 26. Co-localization staining of A6 antibodies in aged ApoE$^{-/-}$ mice. Representative images of A6 antibody, DAPI, and SMA co-localization in abdominal aorta sections of 78 weeks old ApoE$^{-/-}$ mice. 10 µm fresh-frozen abdominal aorta sections of aged ApoE$^{-/-}$ mice were stained with SMA and A6 antibodies. SMA was stained cyan; A6 was stained red; DNA was stained green. Few extracellular A6 positive signals have also been observed. Co-localization staining shows that the A6 antibody recognizes nuclear-related proteins (arrows). Scale bar: 100 µm.

That A6 antibody co-stained with CD11c supports that A6 positive signals are mainly located within the plaques of the diseased aorta. Interestingly, adventitial areas that were positively stained with CD11c (indicative for inflammation) were also intensely stained with A6^{+} signals compared to other areas without staining CD11c (Fig. 27). This result indicates that inflammation is associated with higher A6 antigen staining. Extracellular A6 positive signals in perivascular LNs were also observed (Fig. 27).

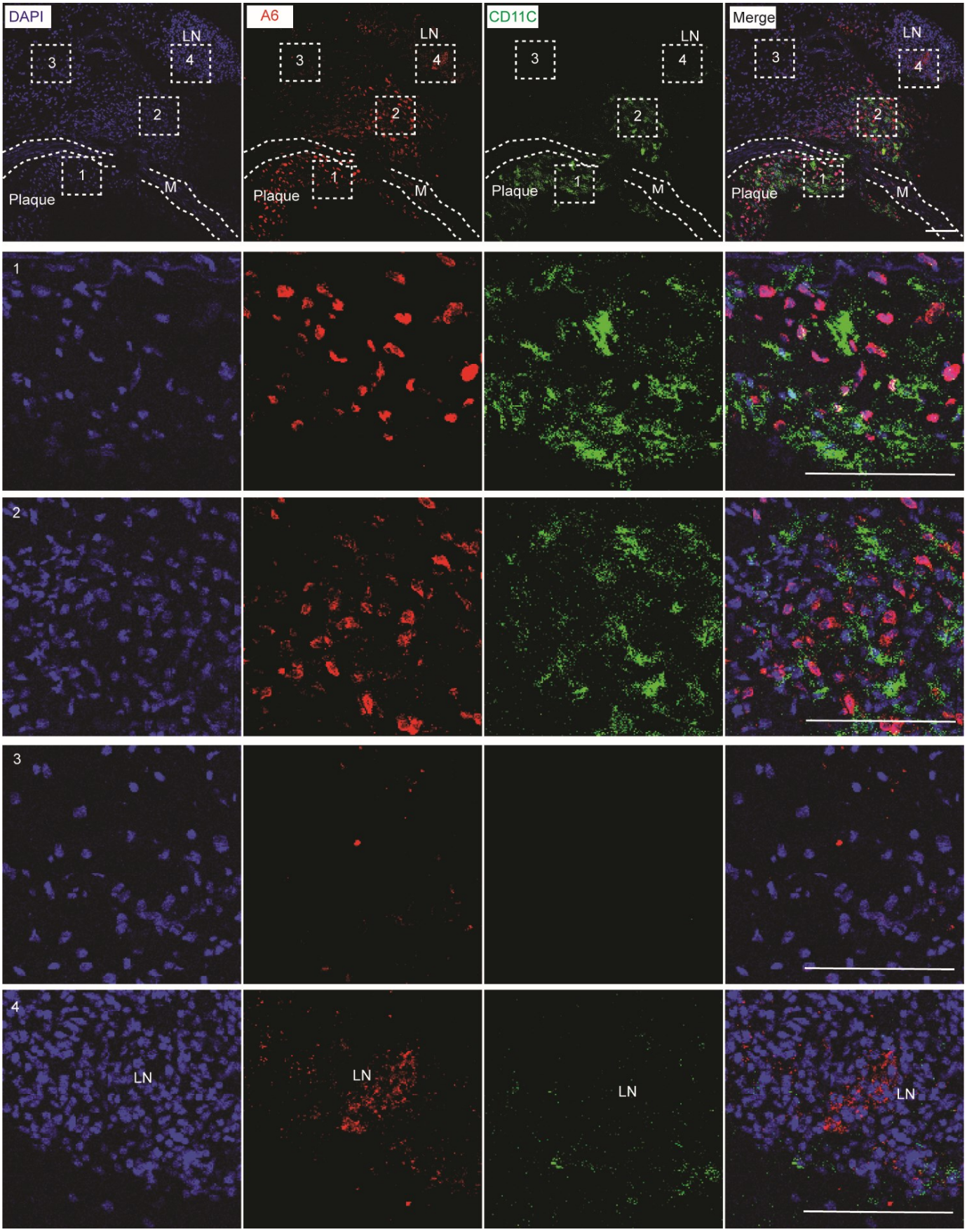

Figure 27. A6 antibody is closely associated with inflammatory responses in aged ApoE$^{-/-}$ mice.

Representative images of A6 antibody and CD11C co-localization in abdominal aorta sections of 78 weeks old ApoE$^{-/-}$ mice. 10 µm fresh frozen abdominal aorta sections of aged ApoE$^{-/-}$ mice were stained with CD11C and A6 antibodies. CD11C was stained green; A6 was stained red; DNA was stained blue. A6 signals are located in plaques (A6^{+}, red, zoom 1). Adventitial areas with inflammatory cells show significantly more A6^{+} areas than those without inflammation (A6^{+}, red, zoom 2, 3). The extracellular A6 positive signals in the perivascular LN indicated that A6 antigens may be released from nuclei (A6^{+}, red, zoom 4). Scale bar: 100 µm.

Macrophages and SMCs play essential roles in the pathogenesis of atherosclerosis [170,172]. Both pro-inflammatory macrophage subsets and anti-inflammatory macrophage subsets participate in the initiation, progression, and stabilization of plaque [171,172]. Whether the A6 signal can be found in macrophages and/or SMCs as a question was raised. CD68 is a marker for macrophages, activated microglia cells, and some DCs. CD68 is highly expressed on macrophages and DCs in plaques. During atherosclerosis, some SMCs loose classic SMC markers and transdifferentiate into macrophage-like cells [173]. Therefore, some neointimal cells express macrophage markers [174]. SMA is a marker for smooth muscle cells. Some studies showed that smooth muscle-like cells in plaques might be BM-derived. Therefore, some SMA-expressing cells may be of hematopoietic origin in plaques. Here, CD68 was used for CD68^{+} macrophage/DCs, SMA for SMCs in plaques. Our data show that A6 signals colocalize with macrophages/DCs (CD68) and with a few SMA-expressing cells (Fig. 28). When taken together, our data indicate that the A6 antibody recognizes nuclear antigens, and the A6 antibody recognized epitopes increase in areas associated with inflammation.

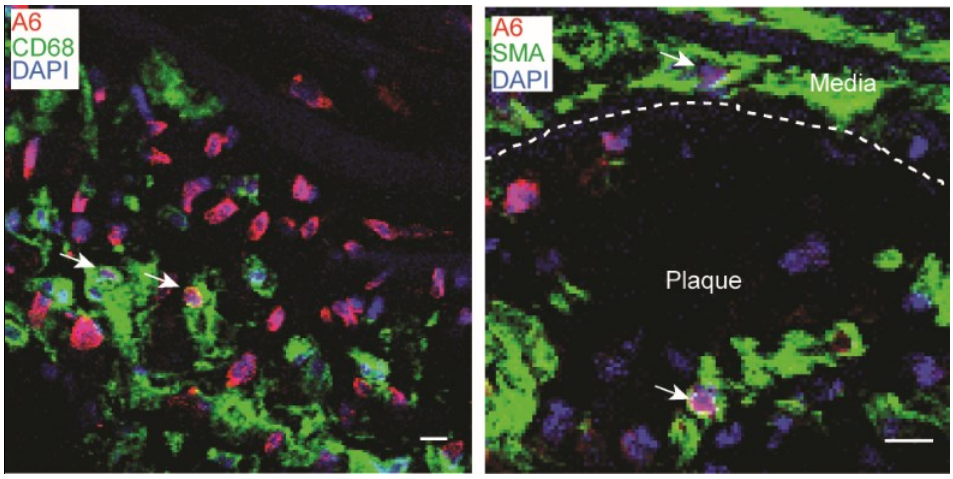

Figure 28. Co-localization of A6 antibodies with macrophage and SMA^{+} cells in advanced plaques in aged ApoE$^{-/-}$ mice.

Representative images of co-localization of A6 antibody, macrophages/DCs (CD68), and SMA positive cells in plaques of 78 weeks of ApoE$^{-/-}$ mice. 10 µm fresh-frozen sections of aged ApoE$^{-/-}$ mice plaques were stained with CD68 and SMA antibodies. A6 was stained red; CD68 and SMA were stained green; DNA was stained blue. A6 positive signals are co-expression and colocalized with CD68 but not all macrophages. A6 positive signals are colocalized with few SMA positive cells. Scale bar: 10 µm.

3.7 Reactivity of ATLO-derived A6 antibody in early stages of atherosclerosis

Atherosclerosis is a chronic inflammatory disease of arteries. Macrophage infiltration occurs during early atherosclerosis and may promote or reduce inflammation or be involved in tissue repair [172]. To investigate whether the A6 antigen is involved in the early stages of atherosclerosis, A6 antibody was stained in the aorta of 32 weeks ApoE$^{-/-}$ mice fed with chow diet, which develop early stages of plaques. A6 positive signals were observed in nuclei of infiltrated macrophages in plaques (Fig. 29). These data suggest that the A6 antigen is present in atherosclerotic plaques associated with macrophages during the early developmental stages of the disease.

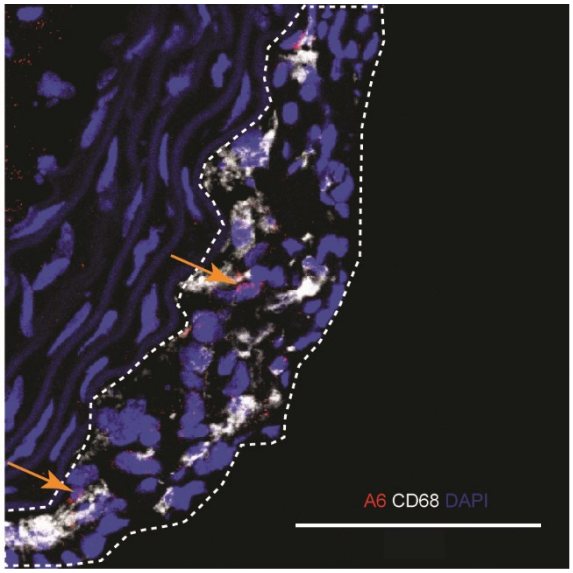

Figure 29. Co-localization of A6 antibodies in early stage of atherosclerosis. Representative images of co-localization of A6 antibody and macrophage/DCs marker (CD68) in early atherosclerotic plaques, i.e., fatty streak. 10 µm fresh-frozen sections of plaques were obtained from 32 weeks old ApoE$^{-/-}$ mice fed with chow diet. These sections were stained with CD68 and A6 antibody. A6 was stained red; CD68 was stained white; DAPI was stained blue. Scale bar: 100 µm.

3.8 ATLO-derived antibody A6 recognizes human plaque constituents

Another important question is whether A6 antibody-related antigens can be observed in human plaques. The recombinant antibody that carries the A6 variable and mouse constant regions was produced to address this issue. Human atherosclerotic plaques were obtained from patients with more than 70% carotid artery stenosis. Indeed, plaque constituents were recognized by the A6 antibody in human carotid plaques by immunofluorescence staining (Fig. 30). Moreover, A6 positive signals were also located in the nuclei in human plaques (Fig. 30).

Likewise, immunohistochemistry (IHC) analyses confirmed the A6 antibody reactivity in human plaques (Fig. 31). Thus, the A6 antibody recognizes nuclear antigens that are expressed in human atherosclerosis plaques.

In conclusion, plaque constituents in humans and mice were recognized by the ATLO-derived A6 antibody, i.e. an ATLO-derived antibody from ATLO GCs. In particular, nuclear antigens in

multiple tissues were recognized by the A6 antibody, and the A6 immunoreactivity increases in areas associated with inflammation. A6-related antigens were observed in early atherosclerosis plaques, indicating that A6-related antigen(s) may play essential roles in the initiation of atherosclerosis. Moreover, the observation of A6 extracellular staining raises the possibility that A6-related antigen is released from dead cells within plaques and/or the ATLOs. Further work will be needed to determine the A6-related antigen and its function in atherosclerosis in ApoE$^{-/-}$ mice.

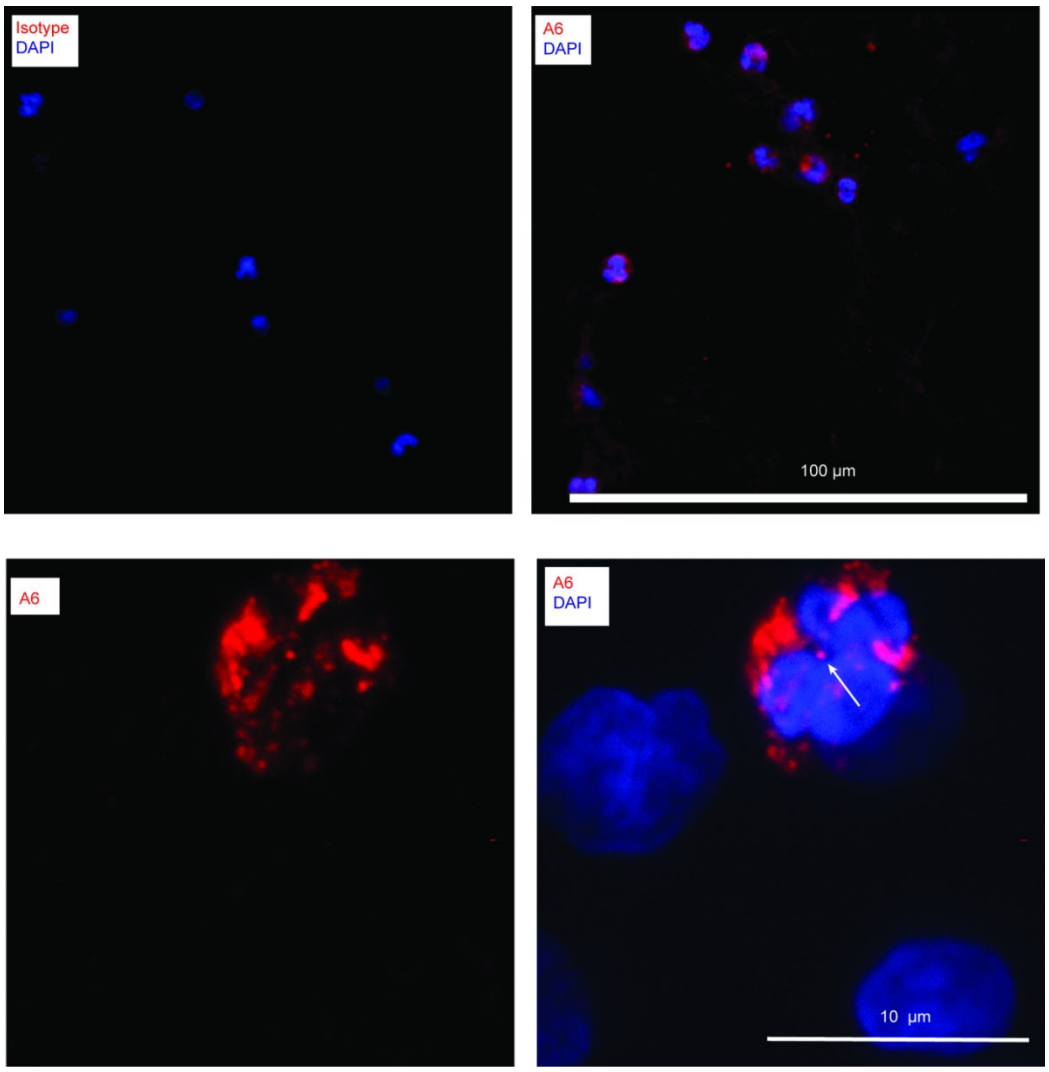

Figure 30. Immunofluorescence staining of A6 antibody in human plaques. All human atherosclerosis plaque tissues were obtained from carotid endarterectomy of patients with more than 70% carotid artery stenosis. 10 µm fresh-frozen human atherosclerotic plaques sections were fixed with 1% paraformaldehyde (PFA). A6 recombinant antibody labeled with the mouse C region as the primary

antibody. The goat anti mouse IgG conjugated to cy3 was used to detect A6 positive signals. A6 was stained red; nuclei was stained with DAPI (blue). Human plaque samples: n = 4.

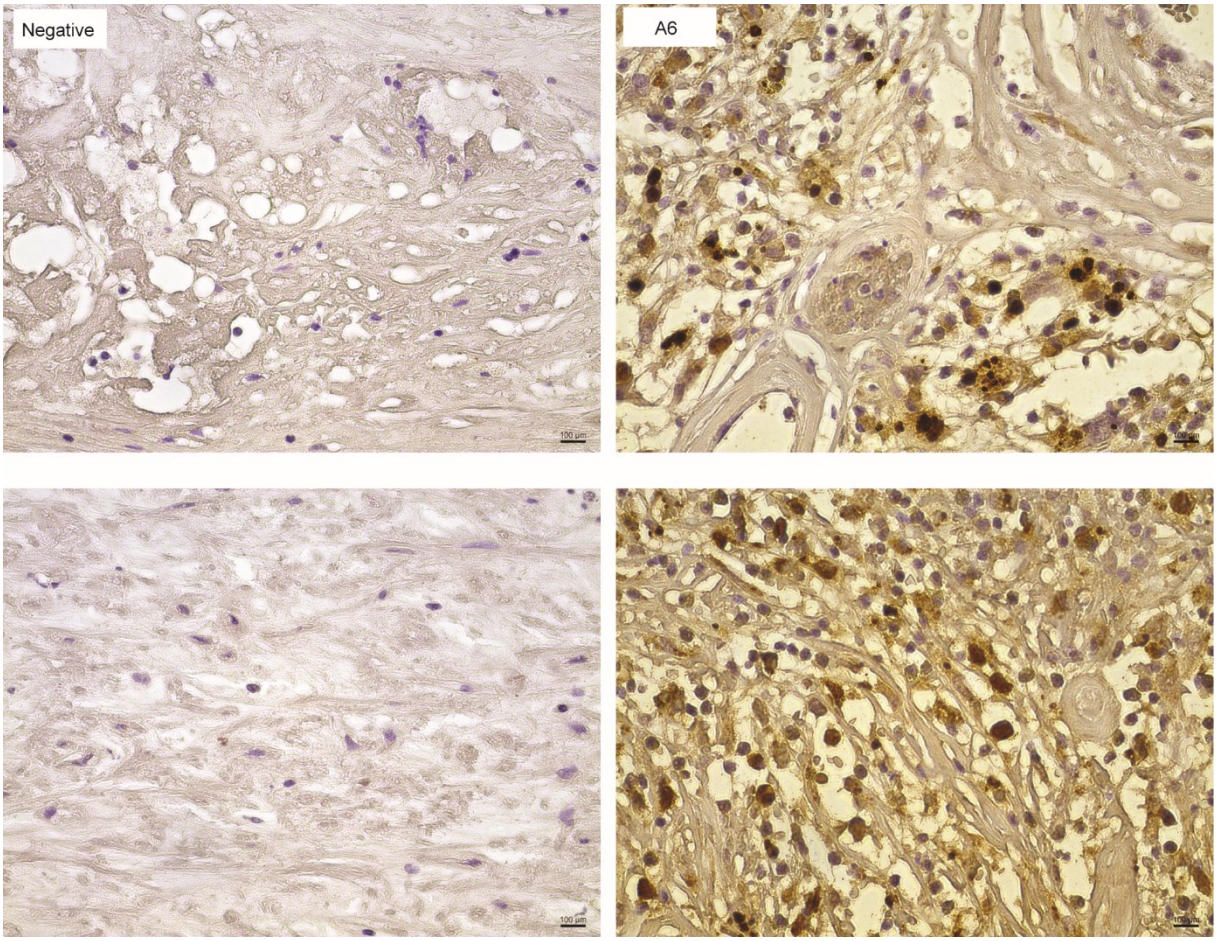

Figure 31. Immunohistochemistry staining analysis of A6 antibody in human carotid plaques. Representative images of IHC analysis of A6 recombinant antibody in human plaque tissues. These human atherosclerosis plaques were fixed with 10% formalin. Human atherosclerosis plaques were stained for A6 by 3,3' - Diaminobenzidine (DAB) and hematoxylin. Scale bar: 100 μm

3.9 ATLO-derived A6 antibody recognizes histones

Next, immunoprecipitation and mass spectrometry (IP/MS) were applied to search for A6-related autoantigens. IP is a technique to identify protein-protein interactions by using target protein-specific antibodies to capture candidate protein antigens and antigen-binding partners from a tissue extract. As shown in Fig. 32A, protein A/G beads were used to bind

antibodies through binding Fc regions of Igs. Then, the whole aorta extracts from aged ApoE$^{-/-}$ mice were immunoprecipitated with A6 antibodies. High-throughput MS was carried out to determine the amino acid sequences of the protein complexes that were pulled down by A6 antibodies. A shortlist of candidate proteins for A6 antigen and antigen-binding proteins were generated by analyzing immunoprecipitates (Fig. 32B). From this shortlist, some candidate proteins are located in the cytoplasm while others are in the nucleus were observed (Fig. 32B). Based on the IF staining results indicating that the A6 antibody recognizes nuclear proteins, the nuclear proteins in the shortlist were chosen for further consideration.

For this purpose, the A6 antibody was used as a primary antibody to perform Western blot analyses to determine the size of candidate A6 antigens. A major A6 positive band was detected between the protein sizes 10kd to 15kd (Fig. 32C). Thus, histone H2b (13.7kd) and histone H4 (11.2kd) were considered as possible A6 antigens. To examine this hypothesis, Western blot experiments were carried out with diseased aorta tissue lysates from aged ApoE$^{-/-}$ mice and a commercially available histone protein mixture (H1/5, H2, H3, H4) derived from calf thymus (Fig. 32D). As expected, the A6 antibody recognizes a similar band in aorta tissue lysates and the histone mixture (Fig. 32D). These results were validated by ELISA with diseased aorta tissue lysates and the histone protein mixture. Indeed, A6 specifically recognizes antigens in the aorta tissue lysates and histone protein mixture (Fig. 32E). Notably, the binding of the A6 antibody and histone mixture showed concentration-dependent characteristics in the ELISA (Fig. 32F). These data strongly support that the A6 antibody recognizes histone proteins. Next, the surface plasmon resonance technology was used to validate the A6 antibody-histone mixture interaction. Human serum albumin was used as negative control. The surface plasmon resonance results confirmed that the A6 antibody shows high-affinity binding to the histone mixture (Fig. 32G), confirming that one or more histone proteins were recognized by the A6 antibody. In conclusion, these data suggest that histones are the cognate antigens of the ATLO-derived A6 antibody.

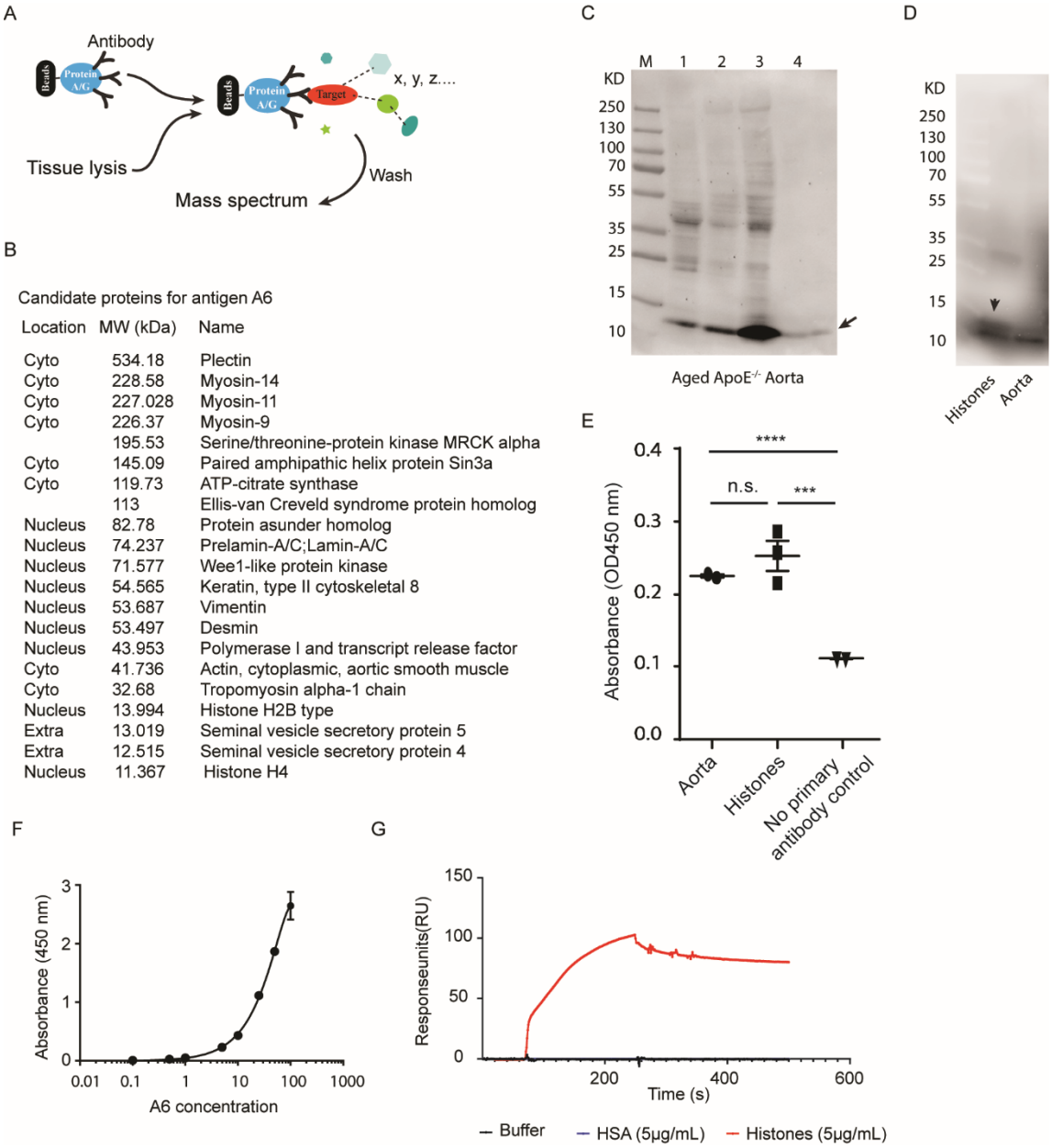

Figure 32. Histones are the cognate antigens for the A6 antibody. (A) Workflow of IP/MS. Monoclonal A6 antibody against a specific target protein forms an immune complex with that target in aorta lysates from aged ApoE$^{-/-}$ mice. The immune complex was captured on bead support-immobilized protein A and G. The antigen was eluted from the beads and analyzed by MS. (B) List of A6 antigen candidates are revealed by MS. (C) Western blot of aorta tissue lysates of 4 aged ApoE$^{-/-}$ mice; M, marker; 1-4, 4 individual aorta lysates from aged ApoE$^{-/-}$ mice; (D-E) Western blot and ELISA of aorta tissue lysates and histone protein mixture from calf thymus; (F) A6 antibody binds to a recombinant mixture of human histones in a dose-dependent manner. 100 ng human histone protein mixture was transferred to the 96-well plates, 0.1 μg/ml, 0.5 μg/ml, 1 μg/ml, 5 μg/ml, 10 μg/ml, 25 μg/ml, 50 μg/ml, 100 μg/ml of A6 antibody were used as primary antibody; (G) A6 antibody binds to histone protein mixture isolated from calf thymus by surface plasmon resonance analyses. Human serum albumin was used as a control.

3.10 ATLO-derived A6 antibody high-affinity binding to H2b

Histones are basic and highly conserved proteins across species, including H1 (21.1kd), H2A (13.9kd), H2B (13.7kd), H3 (15.2kd), and H4 (11.2kd) (Table 3.2) [175]. Therefore, the following question remained: which histone is recognized by the A6 antibody: histone H2a, H2b, or H4? To address this issue, the surface plasmon resonance experiment was performed to analyze A6 antibody interactions with human recombination histone H2a (13.9kd), histone H2b (13.7kd), and histone H4 (11.2kd). Under native conditions, both H2a and H2b bind to ATLOs-derived A6 antibodies. The binding of A6 to H2b presents a 6.5-fold (31.5 vs. 205 nM) higher affinity when compared to the binding of A6 antibody to H2a (Fig. 33A, B). Histone H4 does not show any binding to the A6 antibody under native conditions (Fig. 33C). These data show that the ATLOs-derived A6 antibody has high-affinity binding to histone H2b (31.5nM).

Types and properties of the common Histones

Histone	Number of amino acid residues	Molecular Weight
H2A	129	13.960
H2B	125	13.774
H3	135	15.273
H4	102	11.236
H1(H5)	223	21.130

Table 3.2. Types and molecular weights of the common histones. Histones are highly basic proteins. There are five major families in eukaryotic cells: H1/5, H2a, H2b, H3, and H4. Histones H2a, H2b, H3, and H4 are called core histones, and histones H1/5 are named linker histones.

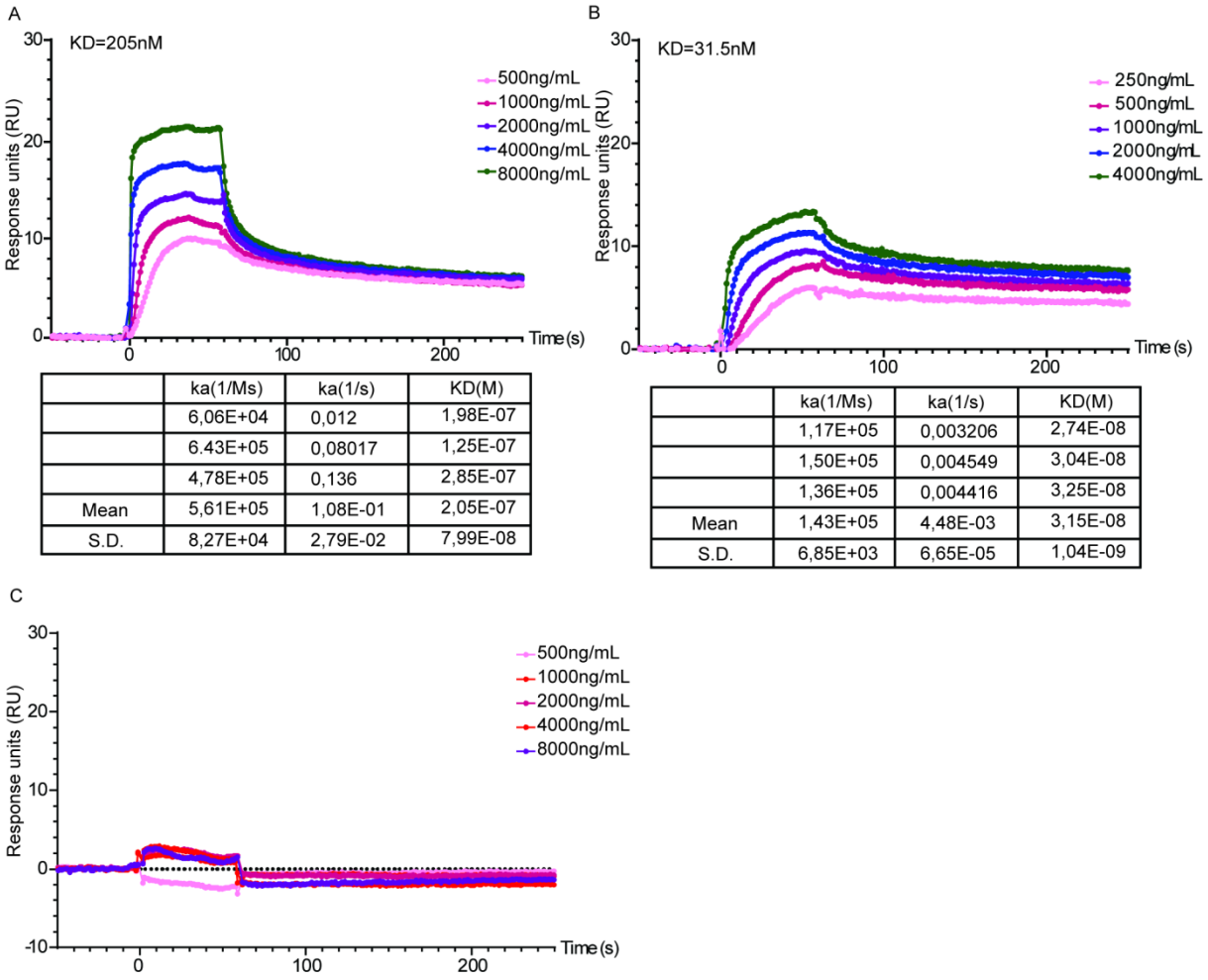

	ka(1/Ms)	ka(1/s)	KD(M)
	6,06E+04	0,012	1,98E-07
	6.43E+05	0,08017	1,25E-07
	4,78E+05	0,136	2,85E-07
Mean	5,61E+05	1,08E-01	2,05E-07
S.D.	8,27E+04	2,79E-02	7,99E-08

	ka(1/Ms)	ka(1/s)	KD(M)
	1,17E+05	0,003206	2,74E-08
	1,50E+05	0,004549	3,04E-08
	1,36E+05	0,004416	3,25E-08
Mean	1,43E+05	4,48E-03	3,15E-08
S.D.	6,85E+03	6,65E-05	1,04E-09

Figure 33. Physical interaction of histone H2a, H2b, H4, and A6 antibody. The surface plasmon resonance experiments were performed using a BIAcore X100 equipped with a research-grade C1 sensor chip. The complex is allowed to associate and dissociate for 60 and 240 seconds, respectively. (A) Binding measurements of histone H2A on A6 antibody-C1 sensor chip. The concentrations of histone H2A proteins are 500 ng/ml, 1000 ng/ml, 2000 ng/ml, 4000 ng/ml, and 8000 ng/ml. (B) Binding measurements of histone H2b on A6 antibody-C1 sensor chip. The concentrations of histone H2b proteins are 250 ng/ml, 500 ng/ml, 1000 ng/ml, 2000 ng/ml, 4000 ng/ml. (C) Binding measurements of histone H4 on A6 antibody-C1 sensor chip. The concentrations of histone H4 proteins are 500 ng/ml, 1000 ng/ml, 2000 ng/ml, 4000 ng/ml, 8000 ng/ml. Data represent means of five independent experiments ± S.E.M.

ELISA was performed to validate the reactivities between the A6 antibody and histone H2a and H2b. High binding plates were coated with identical purified recombination histone H2a and histone H2b proteins. The different concentrations of A6 antibody (mouse FC) was used as primary antibody, anti-mouse IgG (HRP) as the secondary antibody to measure absorbance at 450 nM. The ELISA results show that the A6 antibody can recognize H2a and

H2b. Notably, ELISA binding the A6 antibody with histone H2a and H2b is concentration-dependent (Fig. 34A, B). Thus, both the ELISA and surface plasmon resonance experiment confirm that the ATLO-derived A6 antibody binds to H2a and H2b under native conditions.

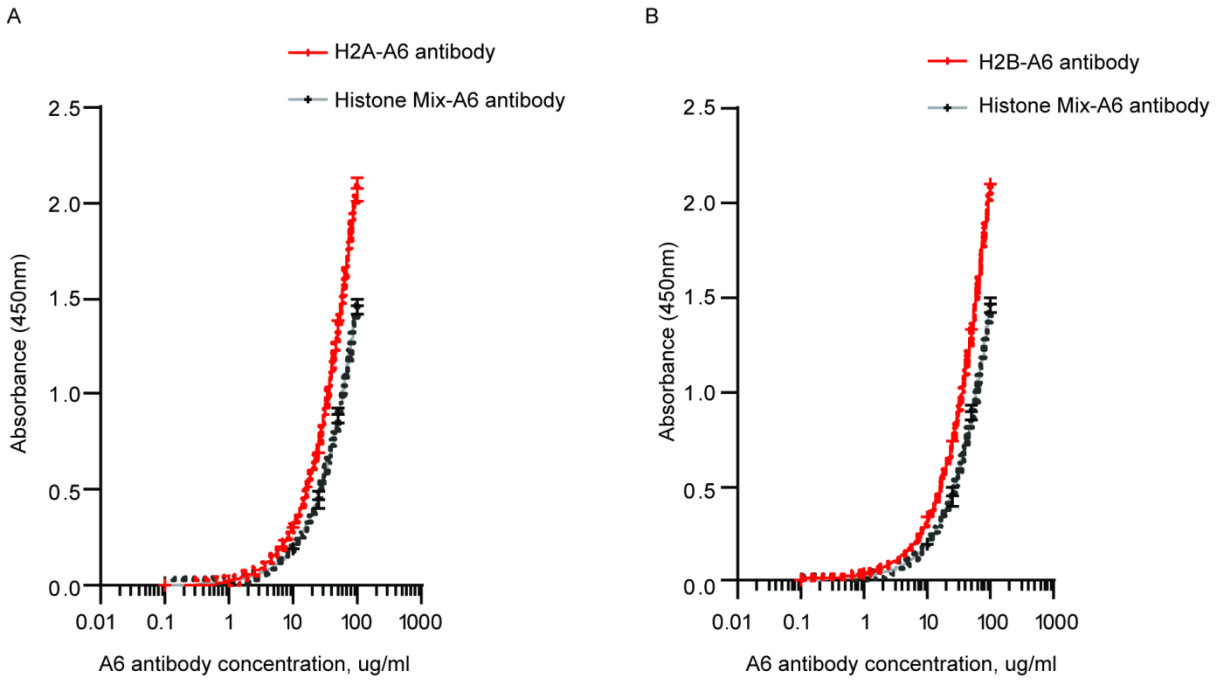

Figure 34. Detection of the reactivity of A6 antibody with histone H2a and H2b by ELISA. A6 antibody binds to recombinant human histone H2a and H2b proteins in a dose-dependent manner. 100 ng human histone protein mixture or histone H2A or histone H2b separately were incubated in high binding 96-well plates, 0.1 µg/ml, 0.5 µg/ml, 1 µg/ml, 5 µg/ml, 10 µg/ml, 25 µg/ml, 50 µg/ml, 100 µg/ml of A6 antibody were used as primary antibody. The line graph shows group means of absorbance ± SEM.

To validate the reactivities of ATLO-derived A6 antibody with histone H2a, H2b, and H4 under denaturating conditions, Western blot analyses were performed using the same purified recombinant histone H2a, H2b, and H4 proteins as used above. A6 was used as primary antibody, combined with anti-human IgH&L conjugated with HRP as the secondary antibody for detection. The Western blot data showed that A6 antibody recognizes histone H2b (Fig. 35), supporting the notion that histone H2b is indeed the cognate antigen for the A6 antibody.

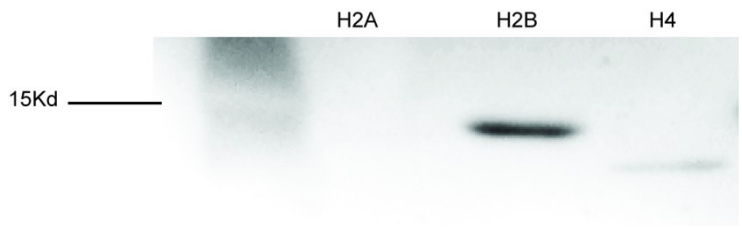

Figure 35. Western blot analysis of the reactivities of A6 antibody with histone H2a, H2b, and H4 proteins. Identical concentrations of denatured purified recombinant histone H2A, H2B, and H4 proteins were loaded on 4%-20% Tris-glycine gel (Thermo Fisher) and transferred to polyvinylidene fluoride (PVDF) membranes. A6 antibody as primary antibody, anti-human IgH&L HRP as the secondary antibody was incubated with the PVDF membrane. Western blotting detection reagent was added to the membrane, and LAS-3000 was used for capturing the image.

3.11 Serum anti-histone H2b antibodies titer increase in atherosclerosis

Current studies showed that higher levels of anti-citrullinated-histone H2b antibodies are associated with more elevated coronary artery calcium scores when compared to lower antibody levels [176]. Coronary artery calcium is a marker of advanced atherosclerosis [177]. Citrullination is a histone modification that converts arginine into citrulline to reduce hydrogen bonds and lose chromatin structure. In this research, histone H2b was identified as the cognate antigen of the A6 antibody. To examine whether the H2b antigen triggers autoimmune responses during atherosclerosis development, the titer of anti-histone H2b antibodies was quantified in mice and human serum by ELISA. The titer of anti-histone H2b antibodies in aged ApoE$^{-/-}$ mice with severe atherosclerosis significantly increased compared to aged WT mice (Fig. 36A). However, no considerable difference between WT and ApoE$^{-/-}$ mice in young and adult mice was observed (Fig. 36A). Next, the titer of anti-histone H2b antibodies was compared by using ELISA between asymptomatic patients sera and symptomatic patients sera, both of which are afflicted with carotid artery disease (CAD): asymptomatic patients are defined with carotid artery atherosclerosis but without neurological symptoms whereas the symptomatic patients had suffered a stroke due to carotid artery atherosclerosis. Therefore, these two cohorts represent patients with atherosclerosis, but they may differ in the severity of atherosclerotic plaque sizes, as shown by carotid artery

atherosclerosis evaluated by ultrasound [178]. Sera of symptomatic/stroke patients had higher levels of anti-histone H2b antibodies when compared to sera of asymptomatic patients without neurological symptoms (Fig. 36B). This suggests that high levels of anti-H2b antibodies may be associated with a higher burden of atherosclerosis. This striking observation shows that H2b protein triggered H2b autoimmune responses in vivo in humans, indicating that the tolerance mechanisms to prevent autoimmune injury may be compromised in patients with CVDs.

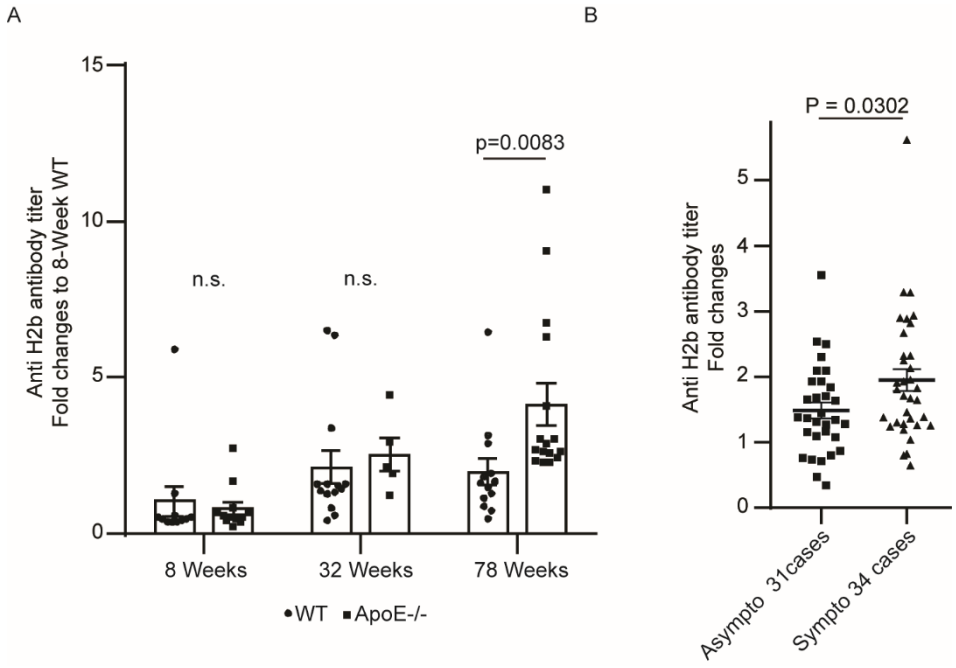

Figure 36. The titer of anti-histone H2b serum antibodies in murine atherosclerosis during aging and in human patients afflicted with atherosclerosis. (A) ELISA was used to examine anti-histone H2b antibody titers in the serum of WT and ApoE$^{-/-}$ mice. High binding plates were coated with recombinant H2b proteins and serum from mice or humans as the primary antibody. Anti-mouse or human secondary antibody labeled with HRP was used for detection. Each dot represents one mouse: (n = 5 - 14 mice per group), one-way ANOVA test, P <0.05 is statistically significant. (B) anti-histone H2b antibody titers in human patients with carotid artery disease. ELISA was used to examine anti-histone H2b antibody titers in age- and sex-matched asymptomatic patients sera (n = 31) and symptomatic patients (n = 34) with carotid artery disease. Data represent means of fold changes ± SEM; two-tailed Student t-test. P <0.05 is statistically significant.

3.12 H2b vaccination promotes atherosclerosis progression in ApoE$^{-/-}$ mice on a chow diet

3.12.1 Experimental design for the immunization in ApoE$^{-/-}$ mice

A6 antibody reacts with H2b and anti-histone H2b antibodies are increased in mice serum with atherosclerosis were observed in this research. These data raise an important new question: are H2b autoimmune responses promoting or attenuating disease, or are they irrelevant for disease progression? To address the function of H2b autoimmune responses in atherosclerosis in vivo, a vaccination strategy was performed in hyperlipidemic mice. For this purpose, 8 week old ApoE$^{-/-}$ mice (there is no atherosclerotic plaques formation in the aorta at this age) were treated with histone H2b (25 µg) + TiterMax® Gold-adjuvant (sigma), adjuvant or PBS alone. Mice were maintained under normal mouse chow and were sacrificed at 32 weeks. The immunization schedules and workflow is shown in Fig. 37. Spleen, blood, liver, kidney, lung, skin, root, and aorta were harvested for further analyses.

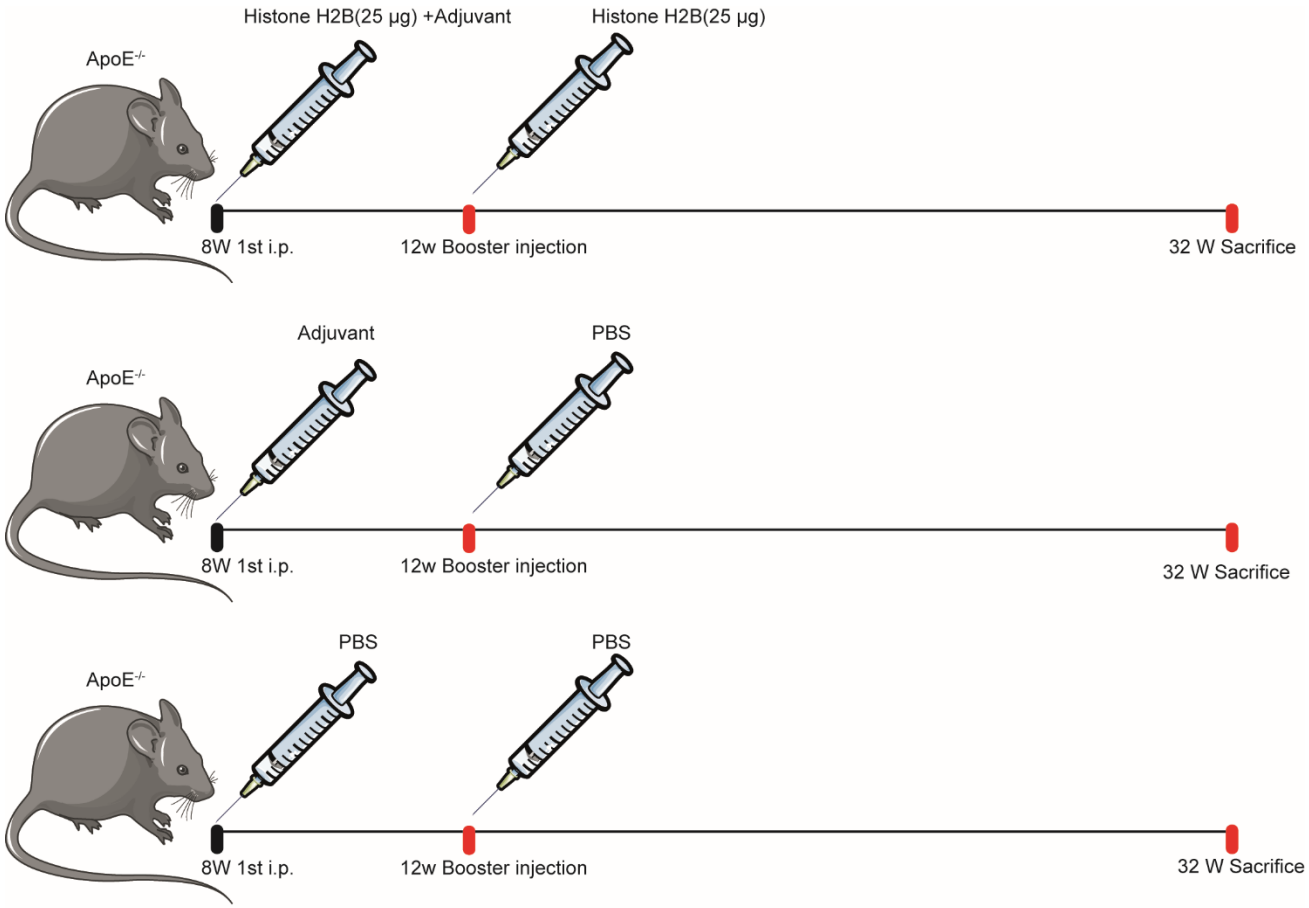

Figure 37. Mouse immunization experiment. 8 weeks old ApoE$^{-/-}$ mice were immunized by intraperitoneal injection using 25 µg histone H2b protein per injection with adjuvant (n = 10). The control group received the same volume of adjuvant (n = 7) or PBS (n = 7) without histone H2b proteins. Booster vaccinations were administered, i.p., using a total of 25 µg histone H2b proteins without adjuvant after 4 weeks of the primary immunization. The control group received the same amount of adjuvant or PBS alone. Mice were fed with normal mouse chow and sacrificed at 32 weeks.

3.12.2 Immunization increases histone H2b-specific antibody titers

ELISA was used to quantify the concentration of anti histone H2b antibodies in serum. The levels of anti-histone H2b antibodies were determined before injection, at 20 weeks, and 32 weeks after injection. A high concentration of anti-histone H2b antibodies was elicited by histone H2b + adjuvant (Fig. 38), whereas the levels of anti-histone H2b antibodies remained low in control groups, i.e., the PBS group or adjuvant group. These data demonstrate that a high concentration of anti histone H2b antibodies was successfully elicited in ApoE$^{-/-}$ mice on

a chow diet during adolescence and young age.

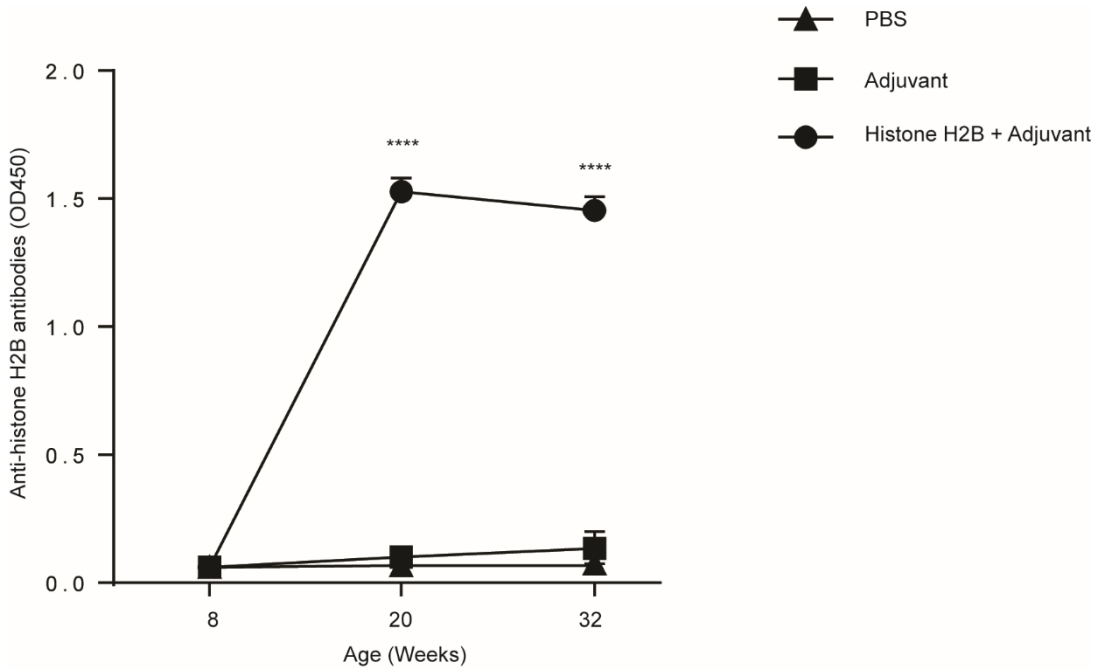

Figure 38. Histone H2b + adjuvant immunization elicits a high titer of anti-histone H2b antibodies of ApoE$^{-/-}$ mice on a chow diet. Blood was collected before primary immunization, 20 weeks, and 32 weeks after immunization. Anti-histone H2b antibody levels were determined by ELISA. The line graph shows group of means of absorbance ± SEM; one-way ANOVA was applied to determine P values. ****P < 0.0001; H2b vaccine group: n = 8; PBS group: n = 7; Adjuvant group: n = 7.

3.12.3 H2b vaccination does not change body weight, blood parameters, and cholesterol levels in 32 weeks ApoE$^{-/-}$ mice

Body weight and plasma cholesterol concentration were measured to monitor the effects of the H2b + adjuvant, adjuvant, and PBS alone treatment in ApoE$^{-/-}$ mice. The body weight was determined every 1 or 2 weeks after injection. The body weight of mice with a high level of anti-histone H2b antibodies showed no statistical difference with the control group (Fig. 39A), showing that the vaccination protocol had not an effect on the body weight in ApoE$^{-/-}$ mice on a chow diet. Next, the cholesterol level was studied by using cholesterol quantitation Kit (Sigma). No statistically discernible alteration between the three groups was noted (Fig. 39B). This demonstrates that the H2b vaccination protocol had no effect on the total serum cholesterol levels. To assess whether vaccination has an effect on other blood parameters in

ApoE$^{-/-}$ mice on a chow diet, the blood cell count was determined after 32 weeks in all 3 experimental groups, without revealing any differences. Our data show that there were no significant changes in the blood parameters (Fig. 39C, D). These data indicate that the vaccination protocol has no effect on major blood parameters in ApoE$^{-/-}$ mice on a chow diet.

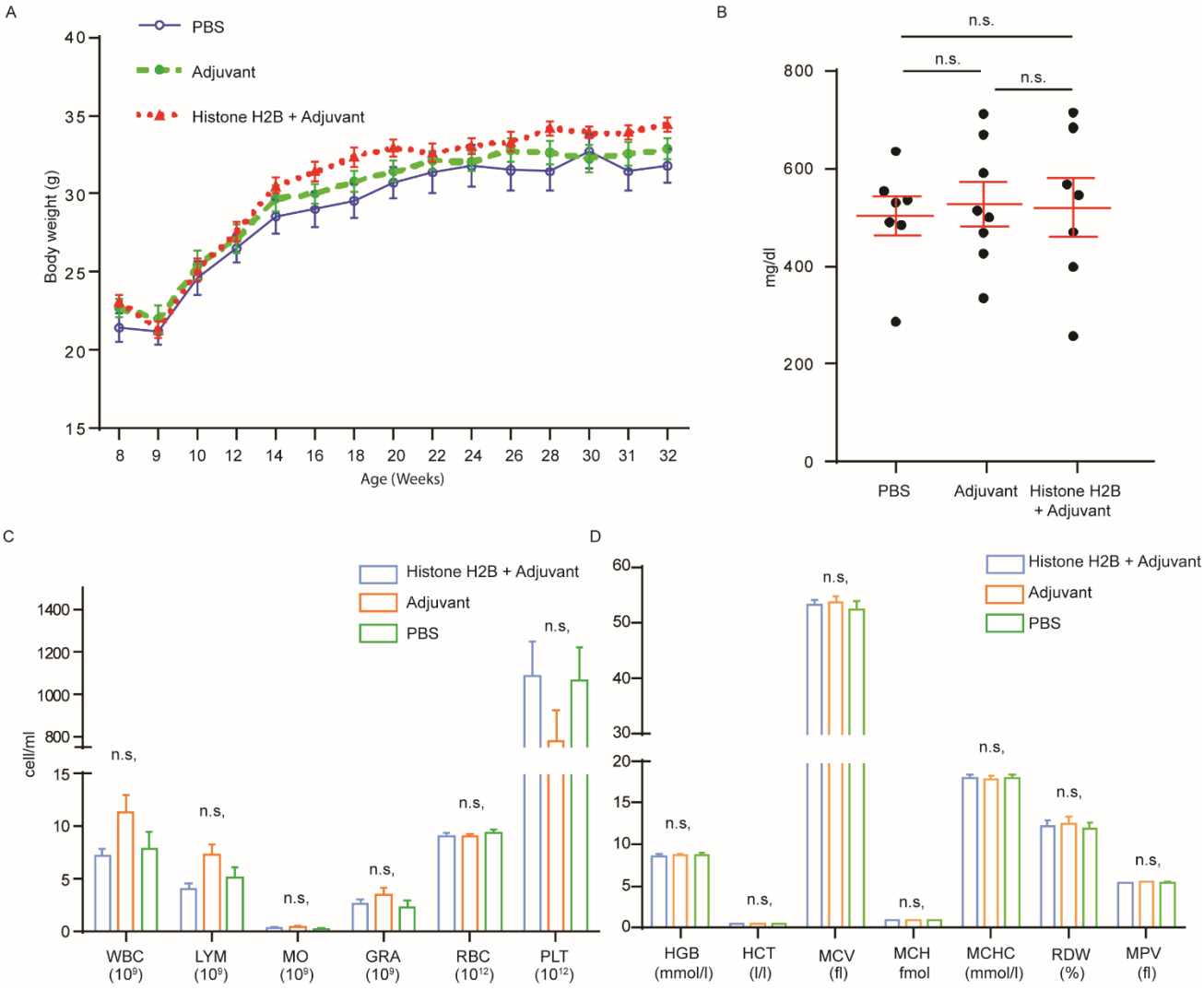

Figure 39. Vaccination using H2b does not impact body weight, total cholesterol levels, and blood parameters in ApoE$^{-/-}$ mice on a chow diet. (A) Body weight was measured every 1 or 2 weeks after treatment**.** (B) The concentration of total cholesterol in 32 weeks Apoe$^{-/-}$ mice treated with PBS (n = 7), adjuvant (n = 7), or H2b with adjuvant (n = 8). (C-D) Blood was collected from 32 weeks of ApoE$^{-/-}$ mice into EDTA tubes. A complete blood cell counter analyzed the parameters of the blood. Data represent means ± SEM of independent samples: PBS (n = 7), adjuvant (n = 7), or H2b with adjuvant (n = 8); one-way ANOVA was applied to determine P values, n.s.: no significant difference. The parameters of blood included: WBC, white blood cell; MO, monocytes; LYM, lymphocytes; RBC, red blood cell; GRA, granulocytes; PLT, platelets; HGB, hemoglobin; HCT, hematocrit; MCV, mean corpuscular volume; MCH,

mean corpuscular hemoglobin; MCHC, mean corpuscular hemoglobin concentration; RDW, red blood cell distribution width, and MPV, mean platelet volume.

3.12.4 H2b vaccination increases plaque size

To determine the influence of the H2b vaccination on plaque size, the whole aorta was collected and analyzed with *en-face* Sudan IV staining. The entire aorta was collected from 32 weeks old ApoE$^{-/-}$ mice treated with PBS, adjuvant, or H2b + adjuvant. After 24 weeks after the initial vaccination, mice vaccinated with H2b + adjuvant had larger plaques in the total aorta or the thoracic arch vs. mice treated with PBS or adjuvant (Fig. 40). The size of plaques in the abdominal aorta showed no significant difference in the H2b + adjuvant group versus the PBS or adjuvant group. These data indicates that H2b is an autoantigen that triggers pro-atherogenic autoimmune responses in ApoE$^{-/-}$ mice under chow diet condition.

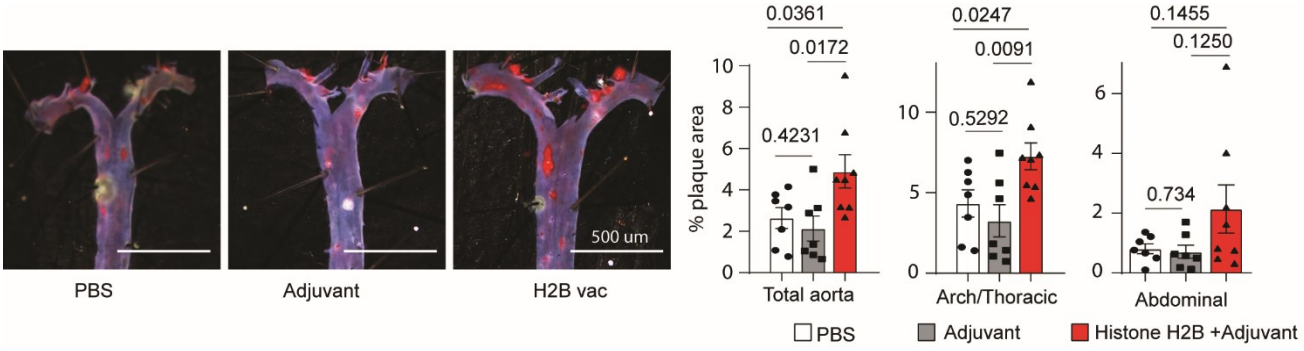

Figure 40. H2b vaccination increased atherosclerosis lesion sizes in aorta of 32 weeks ApoE$^{-/-}$ mice on a chow diet. Representative en-face Sudan IV staining in the whole aorta from 32 weeks ApoE$^{-/-}$ mice treated with PBS, adjuvant, or H2b with adjuvant. Quantification of the plaque sizes in the total aorta, arch with thoracic segments, and abdominal aorta segments. Quantification was performed by image J. Date represent mean of lesion size ± SEM: PBS (n = 7), adjuvant (n = 7), or H2b with adjuvant (n = 8); one-way ANOVA with Welch's t-test was applied to determine P values. H2b vaccine group: n = 8; PBS group: n = 7; adjuvant group: n = 7.

The aortic root was sectioned and quantified to analyze the effect of histone H2b + adjuvant，adjuvant or PBS treatment on plaque sizes. Representative images of the aortic root plaques stained ORO/ hematoxylin are shown in Fig. 41. The aortic root lesions were quantified in 6 sections, located at a distance of 100, 200, 300, 400, 500, and 600 μm from the proximal

inferior end. The lesion area was markedly increased in H2b + adjuvant-treated ApoE$^{-/-}$ mice on a chow diet compared to the control group, i.e., PBS or adjuvant-treated group. The origin of histone H2b immunogenicity and the mechanism how H2b + adjuvant treatment affects plaque progression remain unknown. The effect of H2b + adjuvant, adjuvant, or PBS treatment on the stability of atherosclerotic plaques in ApoE$^{-/-}$ mice on a chow diet remains to be further studied. The main structural determinants of vulnerability should be examined in the future, including the necrotic core size and thickness of the fibrous cap.

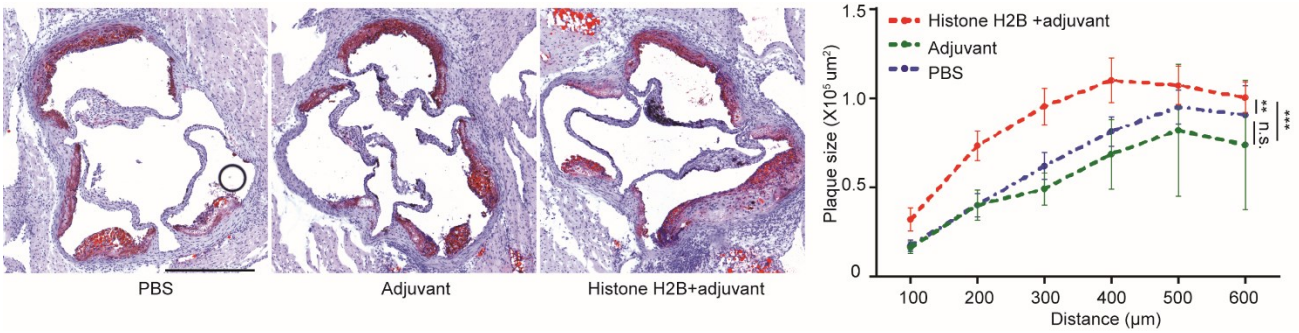

Figure 41. H2b vaccination increased atherosclerosis lesion sizes in aortic roots of 32 weeks ApoE$^{-/-}$ mice on a chow diet. 10 μm fresh-frozen aortic root sections were collected from 32 weeks ApoE$^{-/-}$ mice, which were treated with H2b + adjuvant, adjuvant, or PBS alone. The sections of the aortic root were stained with Oil-Red-O/ hematoxylin. Quantitative analysis of the plaque sizes in the aortic root. The means of plaque sizes of each cross-section of the aortic roots of H2b + adjuvant (n = 8), PBS (n = 7), or adjuvant (n = 7) treated ApoE$^{-/-}$ mice on a chow diet. Data represent means of plaque area ± SEM, two-way ANOVA, * *p<0.01; *** p<0.001; n.s.: no significant difference.

3.12.5 Evaluation of plaque cell composition after H2b + adjuvant treatment

To assess the effect of H2b + adjuvant on plaque composition, CD68+ macrophage/DC- and SMA$^+$ SMC- areas of the aortic root plaque were analyzed. The aortic root sections from 32 weeks old ApoE$^{-/-}$ mice treated with PBS (n = 7), adjuvant (n = 7), or H2b + adjuvant (n = 8), were stained with CD68 for macrophage/DCs and SMA for SMCs (Fig. 42 and 43). In the H2b + adjuvant treated mice, the content of macrophage and SMCs showed no significant differences compared to PBS or adjuvant-treated mice.

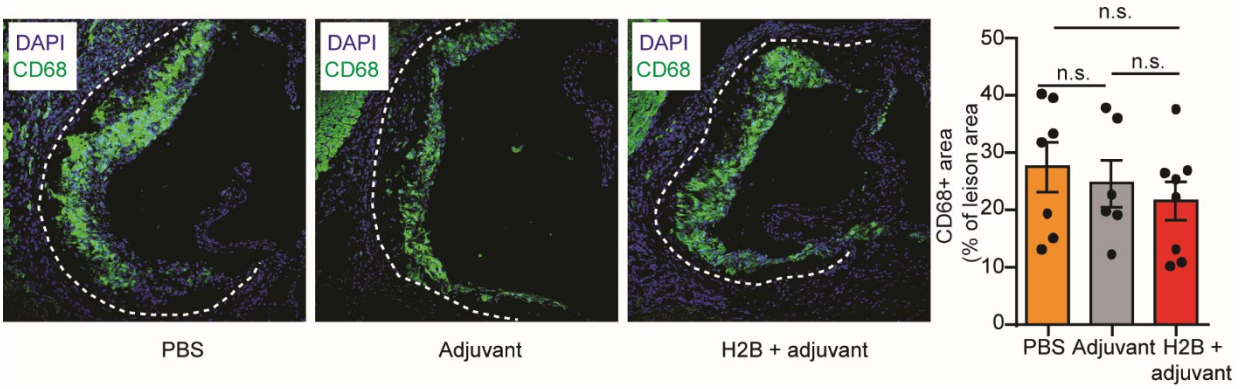

Figure 42. H2b vaccination has no effect on CD68⁺ macrophage infiltration in the plaques of 32-week-old ApoE$^{-/-}$ mice. Representative staining of CD68⁺ macrophage (CD68, green) in the aortic root from 32 weeks ApoE$^{-/-}$ mice treated with PBS (n = 7), adjuvant (n = 6), or H2b + adjuvant (n = 8). The area of macrophages in aortic root plaques was quantified by ImageJ. Data represent the means of area ± SEM; one-way ANOVA with Welch's t-test was applied to determine P values. Scale bars: 100 μm. n.s.: not significant difference.

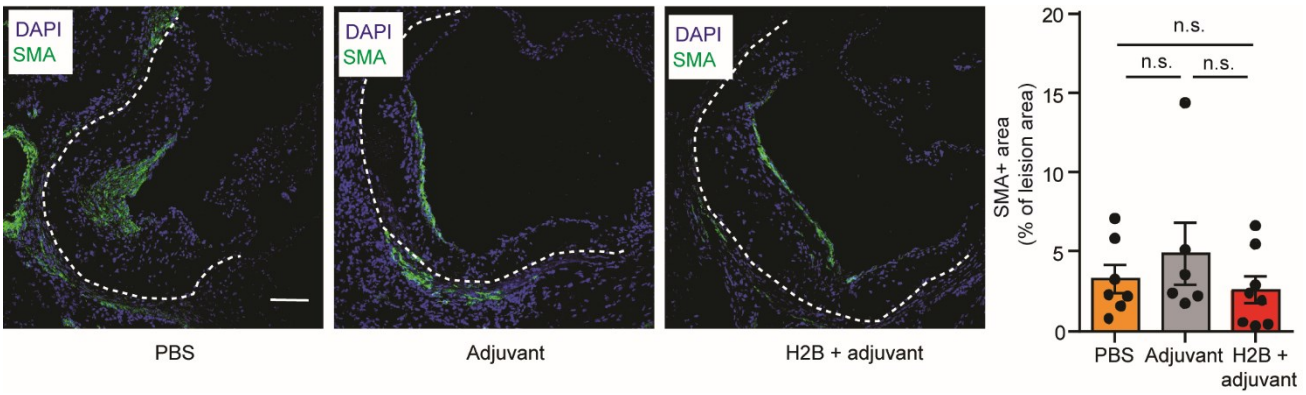

Figure 43. H2b vaccination did not affect SMC content in plaque from 32 weeks ApoE$^{-/-}$ mice on a chow diet. Representative staining of SMA⁺ SMCs (SMA, green) in aortic root (10 μm frozen sections) from 32 weeks ApoE$^{-/-}$ mice treated with PBS (n = 7), adjuvant (n = 6), or H2b + adjuvant (n = 8). The area of SMA⁺ SMCs in aortic root plaques was quantified by ImageJ. Data represent the means of area ± SEM; one-way ANOVA with Welch's t-test was applied to determine P values. Scale bars: 100 μm. n.s.: not significant difference.

3.14 ATLO-derived A7 antibodies in ApoE$^{-/-}$ mice

As another interesting candidate autoantibody, GC B cell-derived antibody A7 was further characterized. In particular, A7 elicited signals were quantified in the aorta in WT and ApoE$^{-/-}$ mice. A7 staining data showed that the A7 antibody largely recognizes the media in both WT

and ApoE$^{-/-}$ mice (Fig. 44). However, from these results, we cannot know the subcellular structure of the A7 staining. SMCs are the main cellular component of the artery media. To detect the subcellular location of A7-related antigen(s), A7 antibody was used to stain mouse vascular aorta/smooth muscle cells *in vitro* (MOVAS) (ATCC, CRL-2797). As shown in Fig. 45, A7 weakly stains cytosol and strongly stains nuclei but which subcellular structure in the nucleus was by A7 stained remains to be determined. These data indicate that the A7 antibody recognizes artery components in multiple tissues and might be used as a novel marker to stain arteries.

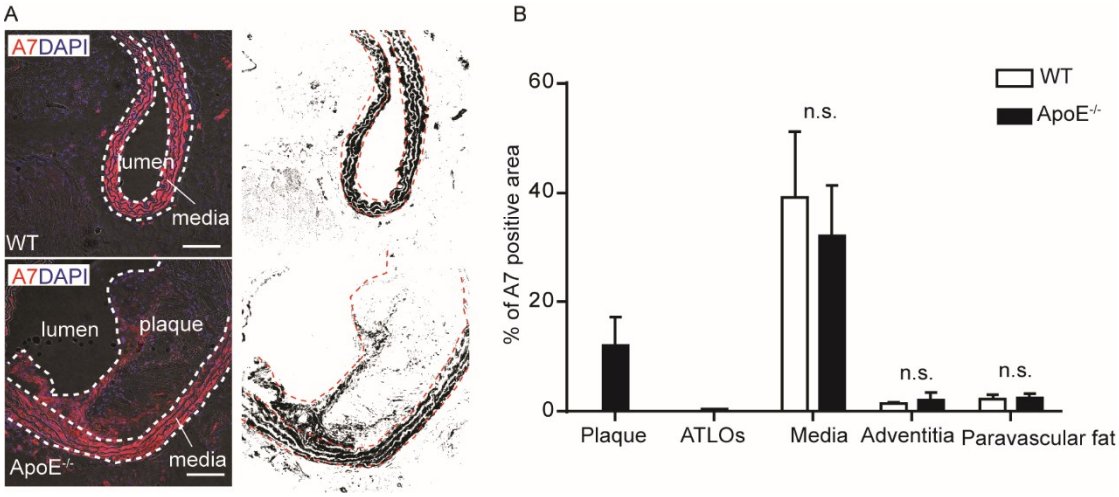

Figure 44. ATLO-derived A7 antibody stain components of media. (A) Representative images of A7 staining signals in WT and ApoE$^{-/-}$ mice (3 WT vs 3 ApoE$^{-/-}$ mice). 10 μm fresh-frozen abdominal aorta sections were stained with A7. A7 was stained red; DAPI was stained blue. Scale bar: 100 μm. (B) Quantitative analysis of A7 positive areas. 4 aorta sections per mouse were analyzed in 3 mice. The area of A7 in the aorta was quantified by image J. Data show ApoE $^{-/-}$ mice have higher staining signals in media and plaque. Data represent means of area ± SEM; n.s.: not significant.

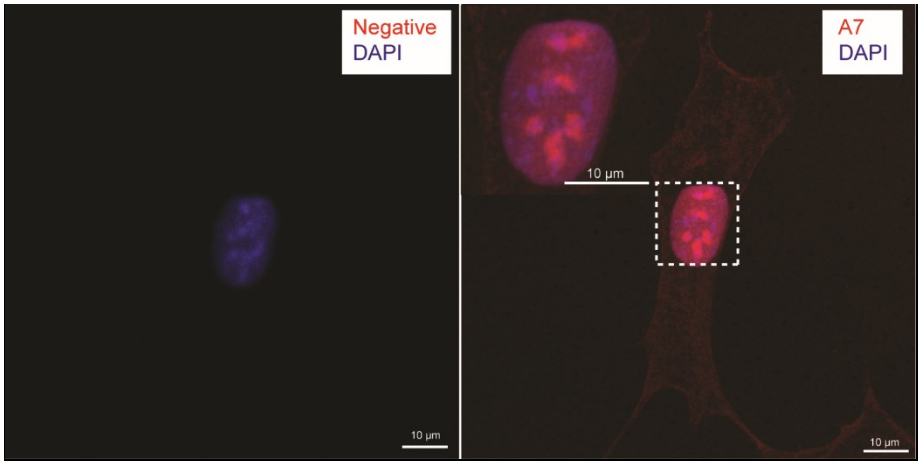

Figure 45. ATLO-derived A7 antibody stain mouse vascular aorta/SMCs. Representative images of A7 staining signals in mouse vascular aorta/SMCs (MOVAS): negative staining (left), A7 staining (right). Cells were seeded on a slide at an appropriate density. After fixation with 4 % PFA, A7 was stained red; DAPI was stained blue.

SMCs are a major cell type in the artery wall media and play an important role in all stages of atherosclerotic plaque development [179]. To examine the possibility that the A7-related antigen reacts with SMCs and macrophages, co-localization staining of A7 antibodies with CD68 and SMA were performed in aged ApoE$^{-/-}$ mice. Strikingly, our results show that A7 positive signals co-localized with SMCs in the artery and some macrophages in plaque and adventitia (Fig. 46).

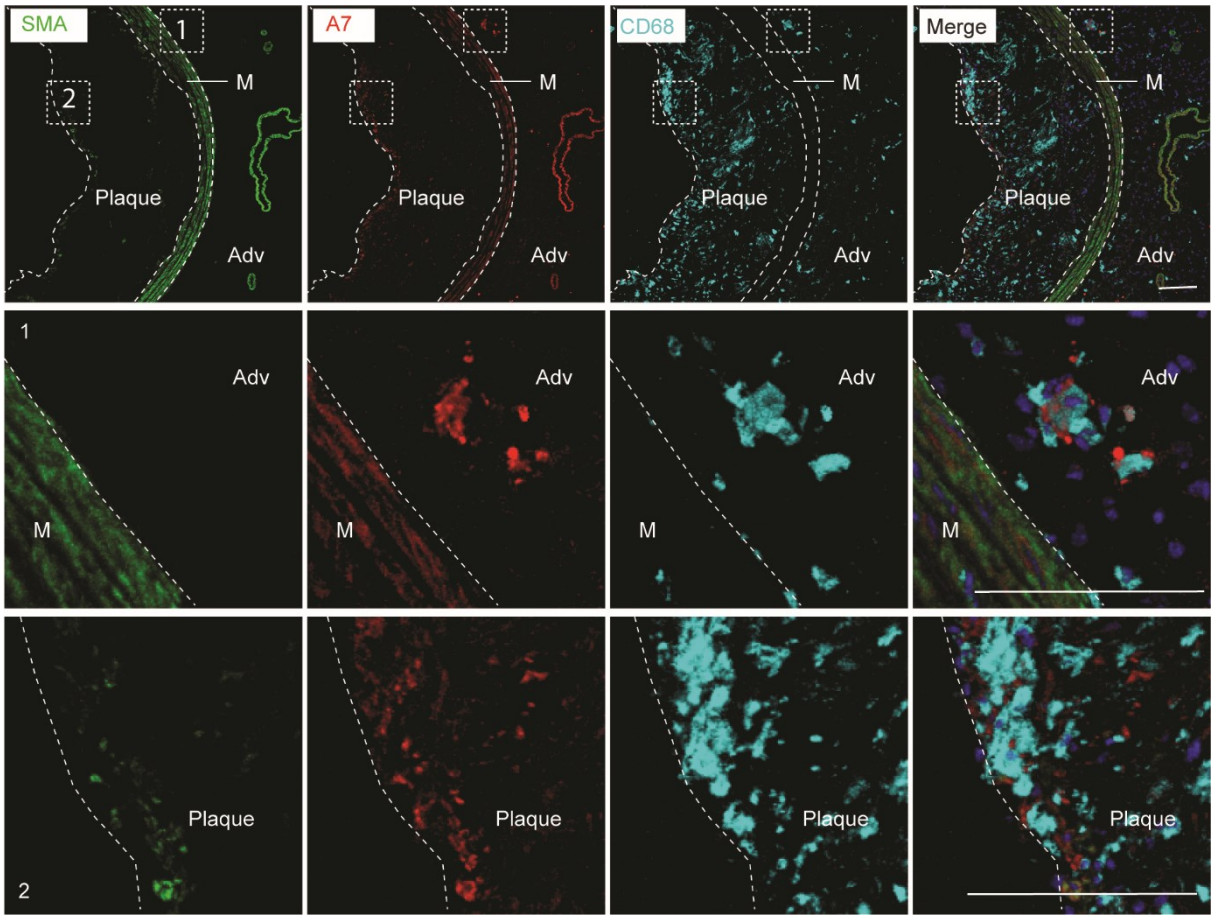

Figure 46. Co-localization staining of A7 antibody in aged ApoE$^{-/-}$ mice. Representative images of co-localization staining of A7 antibodies, macrophages (CD68), and SMCs (SMA) in aged ApoE$^{-/-}$ mice. A7 was stained red; SMA was stained green; CD68 was stained cyan; DAPI was stained blue. Co-localization staining shows that the A7 antibody recognizes SMCs and some macrophages in plaque and adventitia. Scale bar: 100 μm.

3.15 Searching for A7-related antigen(s)

Similar to A6, IP-MS studies were performed by using aorta tissue lysates. Through the coIP-MS experiment, a shortlist of candidate proteins were obtained that may bind to antibody A7 (Fig. 47A). From this shortlist, it is not yet possible to determine which protein is the cognate A7-related antigen. To determine the size of the A7-related protein, the A7 antibody was used as the primary antibody to perform Western blots using SMC tissue lysates. Western blots showed that the bands reacting with A7 were detected between 55 kDa and 70 kDa (Fig. 47B). Compared with Western blot, the shortlist of candidate proteins for A7 as determined

by MS is in the range of 55 kDa and 70 kDa, which are the regulator of G protein signaling 14 (RGS14) and protein lin-9 homolog. Further work will be needed to determine the A7-related antigen(s) by using recombinant protein.

A

Protein names	Mol.weight
Myosin-6	223.56
THO complex subunit 2	182.77
Ellis-van Creveld syndrome protein homolog	113
Sodium/potassium-transporting ATPase subunit alpha-2/3	111.69
Rho GTPase-activating protein 6	108.84
Vomeronasal type-2 receptor 26	96.199
Arginine/serine-rich protein PNISR	92.144
Fibrinogen alpha chain	87.428
Wee1-like protein kinase	71.577
Protein lin-9 homolog	61.758
Regulator of G-protein signaling 14	59.846
Serine/arginine-rich spline rich splicing factor 4	55.979
Vimentin	53.687
Tubulin alpha-4A chain	49.924
Heterogeneous nuclear ribonucleoprotein A3	39.652
Loricrin	38.2
Adaptin ear-binding coat-associated protein2	28.598
Histone H1,3	22.099
Histone H1.4	21.977
Histone H1.2	21.266
Histone H1.0	20.861
Alpha-crystallin B chain	20.069

B

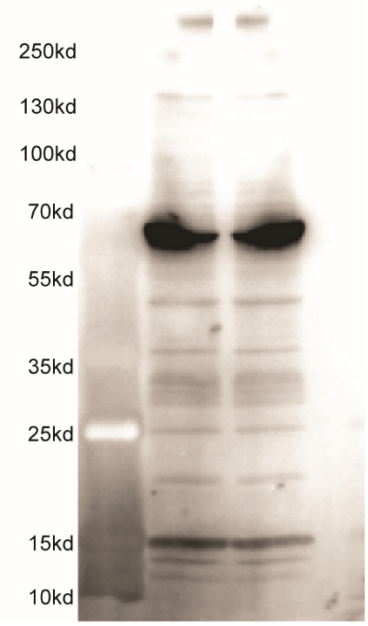

Figure 47. Searching for A7-related cognate antigen(s). Validation of specificity of A7 binding to cognate antigen(s) by coIP-MS combined with Western blot analysis. (A) Monoclonal A7 antibody was incubated with aged ApoE$^{-/-}$ aorta lysates. Immune complexes were captured by protein A and protein G. List of A7 antigen candidates revealed by coIP-MS. (B) Western blot analysis of A7 positive bands via using SMCs lysates. Identical protein was loaded on a 4-20 % tris glycine gel. A7 antibody as primary antibody, anti-human IgH&L HRP as the secondary antibody were incubated with the PVDF membrane. Western blotting detection reagent was added to the membrane, and LAS-3000 was used to detect the HRP chemiluminescent signals. Our data shows that the main band has a size between 55kd and 70kd.

4 Discussion

This study supports the following conclusions: (1) Atherosclerosis in mice and humans is associated with B2-mediated humoral autoimmune reactions resulting in the generation of multiple autoimmune antibodies. (2) A proof of concept experiment identifies the histone protein H2b as one of the first known autoantigens in murine and human atherosclerosis. (3) Some of the identified autoimmune antibodies isolated here are directed against arterial wall constituents and/or immune cells that infiltrate the arterial wall during atherosclerosis progression. (4) A6 autoantibodies increase in the circulation of atherosclerosis during aging in hyperlipidemic mice. (5) H2b may be a relevant autoantigen driving atherosclerosis progression, as shown by accelerated atherosclerosis following vaccination with H2b as an exogenous antigen. When taken together, the here provided data revealed that murine atherosclerosis and - most likely human atherosclerosis - qualifies as an autoimmune disease, meeting several but not all Witebsky criteria. In humans, only a small group of *bona fide* autoimmune diseases meet all Witebsky criteria, including Myasthenia, Hashimoto Thyroiditis, and Graves Disease Gravis [51]. Further work is required to substantiate the association between autoantibody generation and atherosclerosis in larger cohorts of human patients.

These data were made possible by the implementation of a unique approach to study and target ATLO GC B2 cells in a murine model of advanced atherosclerosis. It is tempting to speculate that other chronic inflammatory diseases associated with TLO formation might be similarly and successfully targeted to isolate disease-promoting and/or disease-attenuating autoantibodies, including cancer and numerous chronic inflammatory diseases.

4.1 Using ATLOs to isolate autoimmune antibodies vs. LNs in atherosclerosis: Why is this effective and led to successful isolation of autoantigens?

TLOs emerge in tissues in response to non-resolving inflammation, including atherosclerosis. TLO formation is linked to conditions associated with exogenous antigens, such as microbes, allogeneic transplantation antigens, endogenous autoantigens, and cancer antigens [76,144,180]. However, information on atherosclerosis-specific antigen(s) is very limited. It has been reported that ATLOs contain distinct B-2 B cell subtypes (naïve B2 B cells, mantle zone B cells, and GC B cells) [133]. These B cells are organized in specific zones within the B cell compartment of ATLOs. Similar to SLOs, advanced ATLOs have activated GCs and separate T cell areas. The discovery of FDCs in activating the GC B cell area had previously indicated that adaptive B2 cell immune responses are organized in ATLOs. These fundamental observations was the starting point for this project to engage in a wide-ranging research exploration that addressed the unresolved issue in atherosclerosis: Is atherosclerosis a disease with a significant humoral B2 autoimmune response, which could lead to disease-controlling generation of endogenous autoantigens? These basic questions were addressed in a murine model of atherosclerosis using aged ApoE$^{-/-}$ mice and translated at least partially to a human patient cohort afflicted with atherosclerosis.

What, then, is the advantage of using TLOs as the target organ to isolate autoimmune antibodies vs. isolating them from SLOs? First, chronic inflammation tissues may release autoantigens, and these autoantigens may be diluted if they were to be transported to the distant SLOs. Such dilution may not occur if the autoantigen is close to the inflammatory tissue, i.e., the TLO. The principle advantage why the immune system generates TLOs has never been explored. The present study focused on the hypothesis that a TLO might represent a powerful tool of the immune system to generate autoimmune B2 cells as self-antigens near the place where they are generated, thereby lowering the antigen threshold to trigger the disease-related adaptive immune response. The inflammatory environment of

TLOs can stimulate cDCs that reside in the tissues, including atherosclerotic plaques, and recruit blood monocytes and generate monocyte-derived DCs [127,181,182]. When compared with the FDCs in the more distant GC of the SLOs, disease-related antigens may enter the TLOs and bind to FDCs in the GC at a higher concentration [3,183-187]. After activation, proliferation, affinity maturation, and selection, the antigen-specific T and B cells produced in TLOs can home to the target tissue that initially contained the antigen during the primary immune response [188,189]. After successfully eradicating the disease-related antigens, TLOs neogenesis may be reversible. These features increase the possibility of isolating high-affinity autoimmune antibodies ATLOs in ApoE$^{-/-}$ mice.

4.1.1 Unbiased approach analysis of the GC B cells repertoire from ATLOs by single-cell PCR

In this thesis, an unbiased and efficient method was established, which combines Ig gene repertoire analysis and Ig reactivity at the single-cell level. The single-cell PCR strategy only requires small cell numbers and can isolate any stage of B cells dependent on the marker combination. This method can be used to exploit positive selection in the GC under normal immune conditions in human and mouse models [190-192]. In addition to single-cell PCR, the single-cell BCR receptor sequencing (scBCR-seq) approach is widely used to define the BCR repertoire. scBCR-seq can be used to rapidly discover large numbers of diverse BCRs by using commercially available instruments and reagents, i.e., the 10 X Genomics platform [193]. The scBCR-seq method needs a large amount of cells [194]. However, the number of GC B cells in ATLOs is 192 ± 54 [133]. Compared with SLOs, the GC B cells number in ATLOs is too small to obtain their BCR sequences with NGS, i.e., scBCR-seq. Thus, single-cell cloning, i.e., single-cell PCR, provided us with the possibility to analyze the GC B cells repertoire from ATLOs. This concept proved highly efficient, as shown here.

4.1.2 The Ig gene repertoire of GC B cells from ATLOs and spleen

In recent years, the field of adaptive immunity was rapidly transformed by sequencing the antibody repertoire. The ig gene repertoire was analyzed in GC B cells from ATLOs and spleen in order to address the following aspects: 1) How do the GC B cell Ig genes differ between ATLOs and SLOs? 2) The basic understanding of Ig gene features that can be extrapolated to ATLO antibodies.

The existence of oligoclonal Ig bands in most patients with multiple sclerosis indicates that B-cell clonal expansion is a characteristic of autoimmune disease [195,196]. Somatic hypermutations are a mechanism to increase specificity and affinity of B cells to the antigen, usually several orders of magnitude [197,198]. Some autoimmune diseases like RA showed the change of usage of the variable gene. BCRs with long IgKappa CDR3 regions (≥ 11 amino acids) were discovered to be autoreactive or polyreactive [195]. These reports showed that ig gene features (of V, J, D region, CDRs, and somatic mutations) are associated with specificity for self-antigen. In this thesis, ig gene sequence analysis of GC B cell populations from ATLOs and spleen allows us to understand the antibody repertoire. Sequence analysis of different V H regions (ATLOs n=83; Spleen n=50) and VL regions (ATLOs VL n=107; Spleen VL n=95) demonstrated that the V H /V L gene repertoire of the GC B cells was similar when compared to spleen GC B cells. Moreover, the here presented data showed that VH from ATLOs GC B cells has a higher number of somatic mutations than spleen GC B cells. Point mutations were introduced into the DNA coding for the BCR in GC B cell responses. The affinity and specificity of BCRs were altered by these higher mutations [199]. The elevation of VH gene somatic mutations was displayed in ATLOs, suggesting that in ATLOs Ig gene recombination occurred after antigen-mediated activation.

4.1.3 ATLOs generate self-reactive antibodies

Autoantibodies are antibodies against at least one self-antigen epitope. These antibodies may be reactive with all cell types or highly specific for a specific cell type. Autoantibodies

found in atherosclerotic plaques indicate a link between atherosclerosis and autoimmunity [200,201] and indicate that atherosclerosis may be an autoimmune disease.

In this thesis, single-cell PCR was used to clone paired heavy and light chains of B2 GC cells from ATLOs to produce monoclonal antibodies *in vitro* to solve the new question that ATLOs are the site where the immune system carries out atherosclerosis autoimmune reactions. The monoclonal antibodies obtained from ATLOs provided the opportunity to identify atherosclerosis-specific antigens. By isolating GC B cells from ATLOs, high-affinity antibodies were produced against endogenous autoantigens. These ATLO-derived antibodies could recognize plaque constitutes, and/or SMCs, and adventitia (Fig. 13 and 14). In autoimmune diseases, nuclear components are prominent targets in the autoantibody reaction [202]. Some autoimmune diseases are caused by systemic autoantibodies, which affect multiple organs or tissue systems. The fact that the ATLO-derived A6 antibody recognizes a nucleoprotein raised the important possibility that atherosclerosis autoimmune lymphocytes are generated in ATLOs. These results support the conclusion that ATLOs generate self-reactive antibodies supporting the hypothesis that ATLOs organize atherosclerosis-specific adaptive immune responses target a variety of antigens in atherosclerosis plaques.

4.2 Discovery of the pro-atherogenic roles of H2b autoimmunity

The main finding of this thesis is that ATLO-derived A6 antibody reacts with histone H2b protein (Figs. 32, 33, 34, and 35). Using A6 antibody as a novel tool, anti-histone H2b antibodies were found to be increased during atherosclerosis progression in ApoE$^{-/-}$ mice, which suggests that H2b triggered autoimmune responses occur in mice. Moreover, anti-histone H2b antibodies were detected in cardiovascular patients at a higher antibody titer when compared to patients with less atherosclerosis (Fig. 36), suggesting that H2b autoimmune responses are also organized *in vivo* in patients with atherosclerosis. It remains to be clarified whether H2b autoimmune responses may serve as a diagnostic marker to distinguish CVD patients with or without clinically significant disease. In order to address the

causal role for anti-H2b autoimmunity in atherosclerosis in *vivo*, H2b vaccination was performed in ApoE$^{-/-}$ mice (from 8 weeks to 32 weeks) on a chow diet that covers the critical periods during the initiation and progression of atherosclerosis. One of the main findings of our research is that the lesion of aortic atherosclerosis, determined by enface Sudan IV and ORO staining, was significantly increased in the aorta and aortic root of 32 weeks old ApoE$^{-/-}$ mice following H2b vaccination compared to PBS alone and adjuvant alone (Fig. 40 and 41). Our data demonstrates a pro-atherogenic role of H2b autoimmunity in atherosclerosis development in *vivo,* and H2b autoimmunity impacts atherosclerosis development independent blood lipid lowing effects and independent of changing blood leukocyte percentages.

The discovery of atherosclerotic autoimmunity provides new important insight into the possibilities of future immunoprevention or immunotherapy [203]. Our data indicate that ATLOs organize atherosclerosis autoimmunity and the pro-atherogenic roles of H2b autoimmunity. These data provided the principal possibility for the development of vaccination strategies to treat atherosclerosis. However, a multitude of questions remains to be addressed: 1) The origin of histone H2b immunogenicity and the mechanism of the pro-atherogenic roles of H2b autoimmunity in ApoE$^{-/-}$ mice remain unknown; 2) whether anti-histone H2b antibodies directly bind human and murine plaques *in vivo* is currently unknown; 3) the disease-specific impact of A6 antibody remains to be studied in further antibody *in vivo* treatment experiments. When taken together, many unexpected opportunities were provided by our data for developing new strategies for the treatment of atherosclerosis.

4.3 The atherosclerosis-related B cell response: harmful or beneficial?

Recently, Ramiro and colleagues discovered that SLO GC-derived antibody A12 recognized aldehyde dehydrogenase 4 family member A1 (ALDH4A1) and ocLDL antigens in young/adult LDLR$^{-/-}$ mice fed with a high-fat diet [142]. Serum ALDH4A1 antigen levels increased in human and murine atherosclerosis. A12 antibody significantly reduced blood

lipid levels and atherosclerosis plaque burden in LDLR$^{-/-}$ mice fed with a high-fat diet, indicating protective roles of A12 antibody may be achieved via its lipid-regulation roles or other means [142]. As no data in this work was provided on serum ALDH4A1 antibody levels, it is still unclear whether ALDH4A1 antigen can trigger autoimmune B responses in human. These data broadens our understanding of B cell immune response during atherosclerosis and highlights the potential of A12 as a therapeutic agent for atherosclerosis. However, ALDH4A1 is a 359aa length protein, most likely, can trigger a range of autoantibodies against different epitopes of ALDH4A1 *in vivo* (A12 antibody is one of these many antibodies). Thus, it will be necessary to determine whether anti-ALDH4A1 autoimmunity is pro- or anti-atherosclerotic using animal models of atherosclerosis.

In this thesis, the roles of anti-H2b autoimmunity in atherosclerosis were addressed rather than focusing on the functions of the A6 antibody. The H2b vaccination data discovered the pro-atherogenic roles of H2b autoimmunity. However, the specific roles of the A6 antibody in atherosclerosis (if protective or proatherogenic) will be examined by injection of recombinant A6 antibody in *vivo*. Overall, our study is part of growing evidence that supports further research in cardiovascular immunology and inflammation.

4.4 Atherosclerosis vaccination strategies

Vaccination is one of the most effective medical strategies to prevent infectious diseases [204] [205] and some cancers [206,207]. The idea that vaccines can prevent or reduce atherosclerosis was born because of two experiments' in the mid-1990s [208]. Some atherosclerosis-related antigens have been studied in mice, including Ox-LDL, apoB100, and heat shock protein 60 (HSP60). Compared with the control group, mice immunized with MDA-LDL significantly reduced atherosclerosis [209]. Another study showed that rabbits immunized with LDL and OxLDL can reduce atherosclerotic lesions [210]. Circulating anti-HSP antibodies have been identified in patients with atherosclerosis, and HSP-60-specific T cells have been detected in plaques of atherosclerosis [211]. Anti HSP 60 autoantibodies are involved in the development

of atherosclerosis and increase atherosclerotic lesions in ApoE$^{-/-}$ mice [212-215].

However, none of these earlier studies was able to address the issue of *bona fide* arterial wall-derived autoantigens in atherosclerosis because such autoantigens have not yet been identified as disease-specific autoantigens or because the autoimmune antibodies were innate low antigen-binding antibodies with broad specificities binding to many antigens. We hypothesized that further work on a multitude of autoimmune B2-triggered immune responses need to be conducted to identify both pro-atherogenic and anti-atherogenic autoimmune antibodies to better understand atherosclerosis autoimmunity and to identify initial autoantigens that promote atherosclerosis autoimmunity the disease.

Autoantibodies are usually not correlated with clinically significant diseases and can be detected in a large percentage of healthy people. For the vaccination against atherosclerosis, an extremely challenging task is to isolate pathogenic autoantibodies of atherosclerosis. Chronic inflammatory diseases, including atherosclerosis, is associated with multiple autoantigens; thus, identifying the autoantigens that cause atherosclerosis to design atherosclerosis vaccination strategies will become a major task of the scientific community in the future.

4.5 Challenges ahead

The impact of ATLOs on atherosclerosis progression is still not understood until now. In this research, it was identified that ATLOs organize atherosclerosis-related B2 cell response and found one of 64 ATLO-derived antibodies recognizes histone H2b and immunizing mice with H2b increases the size of plaques in ApoE$^{-/-}$ mice. This thesis clearly demonstrated that ATLOs organize autoimmune responses in atherosclerosis. Further work needs to be performed to address the following popen questions: which of the autoimmune B2 cells are pro- and which are anti-atherogenic; to identify additional autoantigens based on our B2 GC cloning strategy and examine their impact on disease development; develop strategies to distinguish between initial and secondary B2 GC cells derived from unspecific autoantigen

spreading events; examine human cohorts to translate the data obtained in murine models to human disease.

References

1 Tomar, N. & De, R. K. A brief outline of the immune system. *Methods Mol Biol* **1184**, 3-12, doi:10.1007/978-1-4939-1115-8_1 (2014).

2 Aloisi, F. & Pujol-Borrell, R. Lymphoid neogenesis in chronic inflammatory diseases. *Nat Rev Immunol* **6**, 205-217, doi:10.1038/nri1786 (2006).

3 Mohanta, S. K. *et al.* Artery tertiary lymphoid organs contribute to innate and adaptive immune responses in advanced mouse atherosclerosis. *Circulation research* **114**, 1772-1787, doi:10.1161/CIRCRESAHA.114.301137 (2014).

4 Medzhitov, R. & Janeway, C. A., Jr. Decoding the patterns of self and nonself by the innate immune system. *Science* **296**, 298-300, doi:10.1126/science.1068883 (2002).

5 Dranoff, G. Cytokines in cancer pathogenesis and cancer therapy. *Nature reviews. Cancer* **4**, 11-22, doi:10.1038/nrc1252 (2004).

6 Maynard, C. L., Elson, C. O., Hatton, R. D. & Weaver, C. T. Reciprocal interactions of the intestinal microbiota and immune system. *Nature* **489**, 231-241, doi:10.1038/nature11551 (2012).

7 Janeway CA Jr, T. P., Walport M, et al. Immunobiology: The Immune System in Health and Disease. 5th edition. *New York: Garland Science Chapter 9, The Humoral Immune Response* (2001).

8 Dyer, D. P. *et al.* Chemokine Receptor Redundancy and Specificity Are Context Dependent. *Immunity* **50**, 378-389 e375, doi:10.1016/j.immuni.2019.01.009 (2019).

9 Heim, M. H. & Thimme, R. Innate and adaptive immune responses in HCV infections. *Journal of hepatology* **61**, S14-25, doi:10.1016/j.jhep.2014.06.035 (2014).

10 Iannello, A., Debbeche, O., Samarani, S. & Ahmad, A. Antiviral NK cell responses in HIV infection: I. NK cell receptor genes as determinants of HIV resistance and progression to AIDS. *Journal of leukocyte biology* **84**, 1-26, doi:10.1189/jlb.0907650 (2008).

11 Jakasa, I., Thyssen, J. P. & Kezic, S. The role of skin barrier in occupational contact

dermatitis. *Exp Dermatol* **27**, 909-914, doi:10.1111/exd.13704 (2018).

12 Schifferli, J. A., Ng, Y. C. & Peters, D. K. The role of complement and its receptor in the elimination of immune complexes. *The New England journal of medicine* **315**, 488-495, doi:10.1056/NEJM198608213150805 (1986).

13 Sun, J. C., Beilke, J. N. & Lanier, L. L. Adaptive immune features of natural killer cells. *Nature* **457**, 557-561, doi:10.1038/nature07665 (2009).

14 Krumbholz, M., Derfuss, T., Hohlfeld, R. & Meinl, E. B cells and antibodies in multiple sclerosis pathogenesis and therapy. *Nat Rev Neurol* **8**, 613-623, doi:10.1038/nrneurol.2012.203 (2012).

15 Hisamatsu, T., Erben, U. & Kuhl, A. A. The Role of T-Cell Subsets in Chronic Inflammation in Celiac Disease and Inflammatory Bowel Disease Patients: More Common Mechanisms or More Differences? *Inflammatory intestinal diseases* **1**, 52-62, doi:10.1159/000445133 (2016).

16 Kumar, B. V., Connors, T. J. & Farber, D. L. Human T Cell Development, Localization, and Function throughout Life. *Immunity* **48**, 202-213, doi:10.1016/j.immuni.2018.01.007 (2018).

17 Valentine, K. M. *et al.* CD8 Follicular T Cells Promote B Cell Antibody Class Switch in Autoimmune Disease. *Journal of immunology* **201**, 31-40, doi:10.4049/jimmunol.1701079 (2018).

18 Seo, G. Y., Youn, J. & Kim, P. H. IL-21 ensures TGF-beta 1-induced IgA isotype expression in mouse Peyer's patches. *Journal of leukocyte biology* **85**, 744-750, doi:10.1189/jlb.0708450 (2009).

19 Glatman Zaretsky, A. *et al.* T follicular helper cells differentiate from Th2 cells in response to helminth antigens. *The Journal of experimental medicine* **206**, 991-999, doi:10.1084/jem.20090303 (2009).

20 Moens, L. & Tangye, S. G. Cytokine-Mediated Regulation of Plasma Cell Generation: IL-21 Takes Center Stage. *Frontiers in immunology* **5**, 65, doi:10.3389/fimmu.2014.00065 (2014).

21 William, J., Euler, C., Christensen, S. & Shlomchik, M. J. Evolution of autoantibody

responses via somatic hypermutation outside of germinal centers. *Science* **297**, 2066-2070, doi:10.1126/science.1073924 (2002).

22 Viant, C. *et al.* Germinal center-dependent and -independent memory B cells produced throughout the immune response. *The Journal of experimental medicine* **218**, doi:10.1084/jem.20202489 (2021).

23 Baumgarth, N. The double life of a B-1 cell: self-reactivity selects for protective effector functions. *Nature reviews. Immunology* **11**, 34-46, doi:10.1038/nri2901 (2011).

24 Haas, K. M., Poe, J. C., Steeber, D. A. & Tedder, T. F. B-1a and B-1b cells exhibit distinct developmental requirements and have unique functional roles in innate and adaptive immunity to S. pneumoniae. *Immunity* **23**, 7-18, doi:10.1016/j.immuni.2005.04.011 (2005).

25 Alugupalli, K. R. *et al.* B1b lymphocytes confer T cell-independent long-lasting immunity. *Immunity* **21**, 379-390, doi:10.1016/j.immuni.2004.06.019 (2004).

26 Shahaf, G., Zisman-Rozen, S., Benhamou, D., Melamed, D. & Mehr, R. B Cell Development in the Bone Marrow Is Regulated by Homeostatic Feedback Exerted by Mature B Cells. *Frontiers in immunology* **7**, 77, doi:10.3389/fimmu.2016.00077 (2016).

27 Meffre, E., Casellas, R. & Nussenzweig, M. C. Antibody regulation of B cell development. *Nature immunology* **1**, 379-385, doi:10.1038/80816 (2000).

28 Cerutti, A., Cols, M. & Puga, I. Marginal zone B cells: virtues of innate-like antibody-producing lymphocytes. *Nature reviews. Immunology* **13**, 118-132, doi:10.1038/nri3383 (2013).

29 Dorner, T., Radbruch, A. & Burmester, G. R. B-cell-directed therapies for autoimmune disease. *Nature reviews. Rheumatology* **5**, 433-441, doi:10.1038/nrrheum.2009.141 (2009).

30 Stebegg, M. *et al.* Regulation of the Germinal Center Response. *Frontiers in immunology* **9**, 2469, doi:10.3389/fimmu.2018.02469 (2018).

31 Allen, C. D. *et al.* Germinal center dark and light zone organization is mediated by CXCR4 and CXCR5. *Nature immunology* **5**, 943-952, doi:10.1038/ni1100 (2004).

32 Banchereau, J. *et al.* The CD40 antigen and its ligand. *Annual review of immunology*

12, 881-922, doi:10.1146/annurev.iy.12.040194.004313 (1994).

33 Foy, T. M., Masters, S. R. & Noelle, R. J. Hyper IgM syndrome: two mutations distinguish HIM. *The Journal of clinical investigation* **94**, 1349-1350, doi:10.1172/JCI117467 (1994).

34 Linterman, M. A. *et al.* IL-21 acts directly on B cells to regulate Bcl-6 expression and germinal center responses. *The Journal of experimental medicine* **207**, 353-363, doi:10.1084/jem.20091738 (2010).

35 Koncz, G. & Hueber, A. O. The Fas/CD95 Receptor Regulates the Death of Autoreactive B Cells and the Selection of Antigen-Specific B Cells. *Frontiers in immunology* **3**, 207, doi:10.3389/fimmu.2012.00207 (2012).

36 Allen, C. D., Okada, T. & Cyster, J. G. Germinal-center organization and cellular dynamics. *Immunity* **27**, 190-202, doi:10.1016/j.immuni.2007.07.009 (2007).

37 Gudelj, I., Lauc, G. & Pezer, M. Immunoglobulin G glycosylation in aging and diseases. *Cell Immunol* **333**, 65-79, doi:10.1016/j.cellimm.2018.07.009 (2018).

38 Parhami-Seren, B. & Margolies, M. N. Contribution of heavy chain junctional amino acid diversity to antibody affinity among p-azophenylarsonate-specific antibodies. *J Immunol* **157**, 2066-2072 (1996).

39 Janeway, C., Murphy, K, Travers, P, and Walport, M. Immunobiology, 7th edition. *Garland Science,New York and London* (2008).

40 Alberts B, J. A., Lewis J, et al. Molecular Biology of the Cell. 4th edition. *New York: Garland Science* (2002).

41 Tonegawa, S. Somatic generation of antibody diversity. *Nature* **302**, 575-581, doi:10.1038/302575a0 (1983).

42 Oettinger, M. A., Schatz, D. G., Gorka, C. & Baltimore, D. RAG-1 and RAG-2, adjacent genes that synergistically activate V(D)J recombination. *Science* **248**, 1517-1523, doi:10.1126/science.2360047 (1990).

43 Janeway CA Jr, T. P., Walport M, et al. Immunobiology: The Immune System in Health and Disease. 5th edition. *New York: Garland Science* (2001).

44 Nemazee, D. Mechanisms of central tolerance for B cells. *Nature reviews.*

Immunology **17**, 281-294, doi:10.1038/nri.2017.19 (2017).

45 Shlomchik, M. J., Zharhary, D., Saunders, T., Camper, S. A. & Weigert, M. G. A rheumatoid factor transgenic mouse model of autoantibody regulation. *International immunology* **5**, 1329-1341, doi:10.1093/intimm/5.10.1329 (1993).

46 Souroujon, M., White-Scharf, M. E., Andreschwartz, J., Gefter, M. L. & Schwartz, R. S. Preferential autoantibody reactivity of the preimmune B cell repertoire in normal mice. *Journal of immunology* **140**, 4173-4179 (1988).

47 Rajewsky, K. Clonal selection and learning in the antibody system. *Nature* **381**, 751-758, doi:10.1038/381751a0 (1996).

48 Armengol MP, J. M., Lucas-Martín A, Fernández-Figueras MT, & Jaraquemada D, G. T., Pujol-Borrell R. . Thyroid autoimmune disease: demonstration of thyroid antigen-specific B cells and recombination-activating gene expression in chemokine-containing active intrathyroidal germinal centers. *Am J Pathol* (2001).

49 Sims, G. P., Shiono, H., Willcox, N. & Stott, D. I. Somatic hypermutation and selection of B cells in thymic germinal centers responding to acetylcholine receptor in myasthenia gravis. *Journal of immunology* **167**, 1935-1944, doi:10.4049/jimmunol.167.4.1935 (2001).

50 Hill, M. E., Shiono, H., Newsom-Davis, J. & Willcox, N. The myasthenia gravis thymus: a rare source of human autoantibody-secreting plasma cells for testing potential therapeutics. *J Neuroimmunol* **201-202**, 50-56, doi:10.1016/j.jneuroim.2008.06.027 (2008).

51 Rose, N. R. & Bona, C. Defining criteria for autoimmune diseases (Witebsky's postulates revisited). *Immunology today* **14**, 426-430, doi:10.1016/0167-5699(93)90244-F (1993).

52 Suurmond, J. & Diamond, B. Autoantibodies in systemic autoimmune diseases: specificity and pathogenicity. *J Clin Invest* **125**, 2194-2202, doi:10.1172/JCI78084 (2015).

53 Danke, N. A., Koelle, D. M., Yee, C., Beheray, S. & Kwok, W. W. Autoreactive T cells

in healthy individuals. *J Immunol* **172**, 5967-5972, doi:10.4049/jimmunol.172.10.5967 (2004).

54 Lee, S., Ko, Y. & Kim, T. J. Homeostasis and regulation of autoreactive B cells. *Cell Mol Immunol* **17**, 561-569, doi:10.1038/s41423-020-0445-4 (2020).

55 Azizi, G. *et al.* Autoimmunity in Primary Antibody Deficiencies. *International archives of allergy and immunology* **171**, 180-193, doi:10.1159/000453263 (2016).

56 Sayantan Ray*, N. S., Supratip Kundu and Satyabrata Ganguly. Autoimmune Disorders: An Overview of Molecular and Cellular Basis in Today's Perspective. *Journal of Clinical & Cellular Immunology* (2012).

57 Bolon, B. Cellular and molecular mechanisms of autoimmune disease. *Toxicol Pathol* **40**, 216-229, doi:10.1177/0192623311428481 (2012).

58 Rosenblum, M. D., Remedios, K. A. & Abbas, A. K. Mechanisms of human autoimmunity. *J Clin Invest* **125**, 2228-2233, doi:10.1172/JCI78088 (2015).

59 Chablani, A. T., Badakere, S. S. & Bhatia, H. M. Non-organ specific autoantibodies associated with auto-immune haematologic disorders & systemic autoimmune disease. *The Indian journal of medical research* **86**, 337-342 (1987).

60 Marrie, R. A. Environmental risk factors in multiple sclerosis aetiology. *Lancet Neurol* **3**, 709-718, doi:10.1016/S1474-4422(04)00933-0 (2004).

61 Davidson, A. & Diamond, B. Autoimmune diseases. *N Engl J Med* **345**, 340-350, doi:10.1056/NEJM200108023450506 (2001).

62 Goodnow, C. C. Multistep pathogenesis of autoimmune disease. *Cell* **130**, 25-35, doi:10.1016/j.cell.2007.06.033 (2007).

63 Ruff, W. E., Greiling, T. M. & Kriegel, M. A. Host-microbiota interactions in immune-mediated diseases. *Nat Rev Microbiol* **18**, 521-538, doi:10.1038/s41579-020-0367-2 (2020).

64 Chang, A. *et al.* In situ B cell-mediated immune responses and tubulointerstitial inflammation in human lupus nephritis. *J Immunol* **186**, 1849-1860, doi:10.4049/jimmunol.1001983 (2011).

65 Steinmetz, O. M. *et al.* Analysis and classification of B-cell infiltrates in lupus and

ANCA-associated nephritis. *Kidney international* **74**, 448-457, doi:10.1038/ki.2008.191 (2008).

66 Takemura, S. *et al.* Lymphoid neogenesis in rheumatoid synovitis. *Journal of immunology* **167**, 1072-1080, doi:10.4049/jimmunol.167.2.1072 (2001).

67 Lee, Y. *et al.* Recruitment and activation of naive T cells in the islets by lymphotoxin beta receptor-dependent tertiary lymphoid structure. *Immunity* **25**, 499-509, doi:10.1016/j.immuni.2006.06.016 (2006).

68 GeurtsvanKessel, C. H. *et al.* Dendritic cells are crucial for maintenance of tertiary lymphoid structures in the lung of influenza virus-infected mice. *J Exp Med* **206**, 2339-2349, doi:10.1084/jem.20090410 (2009).

69 Petitprez, F. *et al.* B cells are associated with survival and immunotherapy response in sarcoma. *Nature* **577**, 556-560, doi:10.1038/s41586-019-1906-8 (2020).

70 Helmink, B. A. *et al.* B cells and tertiary lymphoid structures promote immunotherapy response. *Nature* **577**, 549-555, doi:10.1038/s41586-019-1922-8 (2020).

71 Cabrita, R. *et al.* Tertiary lymphoid structures improve immunotherapy and survival in melanoma. *Nature* **577**, 561-565, doi:10.1038/s41586-019-1914-8 (2020).

72 Pikor, N. B., Prat, A., Bar-Or, A. & Gommerman, J. L. Meningeal Tertiary Lymphoid Tissues and Multiple Sclerosis: A Gathering Place for Diverse Types of Immune Cells during CNS Autoimmunity. *Frontiers in immunology* **6**, 657, doi:10.3389/fimmu.2015.00657 (2015).

73 Barone, F. *et al.* Stromal Fibroblasts in Tertiary Lymphoid Structures: A Novel Target in Chronic Inflammation. *Frontiers in immunology* **7**, 477, doi:10.3389/fimmu.2016.00477 (2016).

74 Buckley, C. D., Barone, F., Nayar, S., Benezech, C. & Caamano, J. Stromal cells in chronic inflammation and tertiary lymphoid organ formation. *Annual review of immunology* **33**, 715-745, doi:10.1146/annurev-immunol-032713-120252 (2015).

75 Corsiero, E., Nerviani, A., Bombardieri, M. & Pitzalis, C. Ectopic Lymphoid Structures: Powerhouse of Autoimmunity. *Frontiers in immunology* **7**, 430, doi:10.3389/fimmu.2016.00430 (2016).

76 Ruddle, N. H. High Endothelial Venules and Lymphatic Vessels in Tertiary Lymphoid Organs: Characteristics, Functions, and Regulation. *Frontiers in immunology* **7**, 491, doi:10.3389/fimmu.2016.00491 (2016).

77 Humby, F. *et al.* Ectopic lymphoid structures support ongoing production of class-switched autoantibodies in rheumatoid synovium. *PLoS medicine* **6**, e1, doi:10.1371/journal.pmed.0060001 (2009).

78 Wengner, A. M. *et al.* CXCR5- and CCR7-dependent lymphoid neogenesis in a murine model of chronic antigen-induced arthritis. *Arthritis and rheumatism* **56**, 3271-3283, doi:10.1002/art.22939 (2007).

79 Shi, K. *et al.* Lymphoid chemokine B cell-attracting chemokine-1 (CXCL13) is expressed in germinal center of ectopic lymphoid follicles within the synovium of chronic arthritis patients. *Journal of immunology* **166**, 650-655, doi:10.4049/jimmunol.166.1.650 (2001).

80 Fava, R. A. *et al.* Lymphotoxin-beta receptor blockade reduces CXCL13 in lacrimal glands and improves corneal integrity in the NOD model of Sjogren's syndrome. *Arthritis research & therapy* **13**, R182, doi:10.1186/ar3507 (2011).

81 Bombardieri, M. *et al.* Inducible tertiary lymphoid structures, autoimmunity, and exocrine dysfunction in a novel model of salivary gland inflammation in C57BL/6 mice. *Journal of immunology* **189**, 3767-3776, doi:10.4049/jimmunol.1201216 (2012).

82 Holdgate, N. & St Clair, E. W. Recent advances in primary Sjogren's syndrome. *F1000Research* **5**, doi:10.12688/f1000research.8352.1 (2016).

83 Buettner, M. & Lochner, M. Development and Function of Secondary and Tertiary Lymphoid Organs in the Small Intestine and the Colon. *Frontiers in immunology* **7**, 342, doi:10.3389/fimmu.2016.00342 (2016).

84 Olivier, B. J. *et al.* Vagal innervation is required for the formation of tertiary lymphoid tissue in colitis. *European journal of immunology* **46**, 2467-2480, doi:10.1002/eji.201646370 (2016).

85 Moyron-Quiroz, J. E. *et al.* Persistence and responsiveness of immunologic memory in the absence of secondary lymphoid organs. *Immunity* **25**, 643-654,

doi:10.1016/j.immuni.2006.08.022 (2006).

86 Carrega, P. *et al.* NCR(+)ILC3 concentrate in human lung cancer and associate with intratumoral lymphoid structures. *Nature communications* **6**, 8280, doi:10.1038/ncomms9280 (2015).

87 Meier, D. *et al.* Ectopic lymphoid-organ development occurs through interleukin 7-mediated enhanced survival of lymphoid-tissue-inducer cells. *Immunity* **26**, 643-654, doi:10.1016/j.immuni.2007.04.009 (2007).

88 Serafini, B., Rosicarelli, B., Magliozzi, R., Stigliano, E. & Aloisi, F. Detection of ectopic B-cell follicles with germinal centers in the meninges of patients with secondary progressive multiple sclerosis. *Brain Pathol* **14**, 164-174, doi:10.1111/j.1750-3639.2004.tb00049.x (2004).

89 Nistala, K. *et al.* Th17 plasticity in human autoimmune arthritis is driven by the inflammatory environment. *Proceedings of the National Academy of Sciences of the United States of America* **107**, 14751-14756, doi:10.1073/pnas.1003852107 (2010).

90 Harbour, S. N., Maynard, C. L., Zindl, C. L., Schoeb, T. R. & Weaver, C. T. Th17 cells give rise to Th1 cells that are required for the pathogenesis of colitis. *Proceedings of the National Academy of Sciences of the United States of America* **112**, 7061-7066, doi:10.1073/pnas.1415675112 (2015).

91 Chan, O. T., Madaio, M. P. & Shlomchik, M. J. B cells are required for lupus nephritis in the polygenic, Fas-intact MRL model of systemic autoimmunity. *Journal of immunology* **163**, 3592-3596 (1999).

92 Weyand, C. M., Goronzy, J. J., Takemura, S. & Kurtin, P. J. Cell-cell interactions in synovitis. Interactions between T cells and B cells in rheumatoid arthritis. *Arthritis research* **2**, 457-463, doi:10.1186/ar128 (2000).

93 Ross, R. Atherosclerosis--an inflammatory disease. *The New England journal of medicine* **340**, 115-126, doi:10.1056/NEJM199901143400207 (1999).

94 Glass, C. K. & Witztum, J. L. Atherosclerosis. the road ahead. *Cell* **104**, 503-516, doi:10.1016/s0092-8674(01)00238-0 (2001).

95 Breslow, J. L. Cardiovascular disease burden increases, NIH funding decreases.

Nature medicine **3**, 600-601, doi:10.1038/nm0697-600 (1997).

96 Kriszbacher, I., Koppan, M. & Bodis, J. Inflammation, atherosclerosis, and coronary artery disease. *The New England journal of medicine* **353**, 429-430; author reply 429-430 (2005).

97 Weissberg, P. L. & Bennett, M. R. Atherosclerosis--an inflammatory disease. *The New England journal of medicine* **340**, 1928-1929 (1999).

98 Teslovich, T. M. *et al.* Biological, clinical and population relevance of 95 loci for blood lipids. *Nature* **466**, 707-713, doi:10.1038/nature09270 (2010).

99 Mallika, V., Goswami, B. & Rajappa, M. Atherosclerosis pathophysiology and the role of novel risk factors: a clinicobiochemical perspective. *Angiology* **58**, 513-522, doi:10.1177/0003319707303443 (2007).

100 Rafieian-Kopaei, M., Setorki, M., Doudi, M., Baradaran, A. & Nasri, H. Atherosclerosis: process, indicators, risk factors and new hopes. *International journal of preventive medicine* **5**, 927-946 (2014).

101 Mayerl, C. *et al.* Atherosclerosis research from past to present--on the track of two pathologists with opposing views, Carl von Rokitansky and Rudolf Virchow. *Virchows Arch* **449**, 96-103, doi:10.1007/s00428-006-0176-7 (2006).

102 Geovanini, G. R. & Libby, P. Atherosclerosis and inflammation: overview and updates. *Clinical science* **132**, 1243-1252, doi:10.1042/CS20180306 (2018).

103 Tabas, I. & Lichtman, A. H. Monocyte-Macrophages and T Cells in Atherosclerosis. *Immunity* **47**, 621-634, doi:10.1016/j.immuni.2017.09.008 (2017).

104 Tsiantoulas, D., Diehl, C. J., Witztum, J. L. & Binder, C. J. B cells and humoral immunity in atherosclerosis. *Circ Res* **114**, 1743-1756, doi:10.1161/CIRCRESAHA.113.301145 (2014).

105 Hansson, G. K. & Hermansson, A. The immune system in atherosclerosis. *Nature immunology* **12**, 204-212, doi:10.1038/ni.2001 (2011).

106 Hansson, G. K. & Libby, P. The immune response in atherosclerosis: a double-edged sword. *Nature reviews. Immunology* **6**, 508-519, doi:10.1038/nri1882 (2006).

107 Weber, C. & Noels, H. Atherosclerosis: current pathogenesis and therapeutic options.

Nat Med **17**, 1410-1422, doi:10.1038/nm.2538 (2011).

108 Sherer, Y. & Shoenfeld, Y. Immunomodulation for treatment and prevention of atherosclerosis. *Autoimmunity reviews* **1**, 21-27, doi:10.1016/s1568-9972(01)00003-9 (2002).

109 Doran, A. C. *et al.* B-cell aortic homing and atheroprotection depend on Id3. *Circulation research* **110**, e1-12, doi:10.1161/CIRCRESAHA.111.256438 (2012).

110 Zhou, X. & Hansson, G. K. Detection of B cells and proinflammatory cytokines in atherosclerotic plaques of hypercholesterolaemic apolipoprotein E knockout mice. *Scandinavian journal of immunology* **50**, 25-30 (1999).

111 Aubry, M. C. *et al.* B-Lymphocytes in plaque and adventitia of coronary arteries in two patients with rheumatoid arthritis and coronary atherosclerosis: preliminary observations. *Cardiovascular pathology : the official journal of the Society for Cardiovascular Pathology* **13**, 233-236, doi:10.1016/j.carpath.2004.02.005 (2004).

112 Caligiuri, G., Nicoletti, A., Poirier, B. & Hansson, G. K. Protective immunity against atherosclerosis carried by B cells of hypercholesterolemic mice. *J Clin Invest* **109**, 745-753, doi:10.1172/JCI7272 (2002).

113 Ait-Oufella, H. *et al.* B cell depletion reduces the development of atherosclerosis in mice. *The Journal of experimental medicine* **207**, 1579-1587, doi:10.1084/jem.20100155 (2010).

114 Kyaw, T. *et al.* Conventional B2 B cell depletion ameliorates whereas its adoptive transfer aggravates atherosclerosis. *J Immunol* **185**, 4410-4419, doi:10.4049/jimmunol.1000033 (2010).

115 Centa, M. *et al.* Germinal Center-Derived Antibodies Promote Atherosclerosis Plaque Size and Stability. *Circulation* **139**, 2466-2482, doi:10.1161/CIRCULATIONAHA.118.038534 (2019).

116 Kyaw, T., Tipping, P., Bobik, A. & Toh, B. H. Protective role of natural IgM-producing B1a cells in atherosclerosis. *Trends in cardiovascular medicine* **22**, 48-53, doi:10.1016/j.tcm.2012.06.011 (2012).

117 Perry, H. M. & McNamara, C. A. Refining the role of B cells in atherosclerosis.

Arteriosclerosis, thrombosis, and vascular biology **32**, 1548-1549, doi:10.1161/ATVBAHA.112.249235 (2012).

118 Kyaw, T., Tipping, P., Toh, B. H. & Bobik, A. Current understanding of the role of B cell subsets and intimal and adventitial B cells in atherosclerosis. *Current opinion in lipidology* **22**, 373-379, doi:10.1097/MOL.0b013e32834adaf3 (2011).

119 Shoenfeld, Y. *et al.* Accelerated atherosclerosis in autoimmune rheumatic diseases. *Circulation* **112**, 3337-3347, doi:10.1161/CIRCULATIONAHA.104.507996 (2005).

120 Hollan, I. *et al.* Cardiovascular disease in autoimmune rheumatic diseases. *Autoimmunity reviews* **12**, 1004-1015, doi:10.1016/j.autrev.2013.03.013 (2013).

121 Nussinovitch, U. & Shoenfeld, Y. Atherosclerosis and macrovascular involvement in systemic sclerosis: myth or reality. *Autoimmunity reviews* **10**, 259-266, doi:10.1016/j.autrev.2010.09.014 (2011).

122 Xu, Q. Role of heat shock proteins in atherosclerosis. *Arteriosclerosis, thrombosis, and vascular biology* **22**, 1547-1559, doi:10.1161/01.atv.0000029720.59649.50 (2002).

123 Steinberg, D. & Witztum, J. L. Oxidized low-density lipoprotein and atherosclerosis. *Arteriosclerosis, thrombosis, and vascular biology* **30**, 2311-2316, doi:10.1161/ATVBAHA.108.179697 (2010).

124 Kobayashi, K. *et al.* A specific ligand for beta(2)-glycoprotein I mediates autoantibody-dependent uptake of oxidized low density lipoprotein by macrophages. *Journal of lipid research* **42**, 697-709 (2001).

125 Shoenfeld, Y., Sherer, Y., George, Y. & Harats, D. beta 2-glycoprotein I in human and murine atherosclerosis. *The Israel Medical Association journal : IMAJ* **3**, 85-87 (2001).

126 Libby, P., Ridker, P. M. & Hansson, G. K. Progress and challenges in translating the biology of atherosclerosis. *Nature* **473**, 317-325, doi:10.1038/nature10146 (2011).

127 Choi, J. H. *et al.* Flt3 signaling-dependent dendritic cells protect against atherosclerosis. *Immunity* **35**, 819-831, doi:10.1016/j.immuni.2011.09.014 (2011).

128 Wick, G., Knoflach, M. & Xu, Q. Autoimmune and inflammatory mechanisms in atherosclerosis. *Annual review of immunology* **22**, 361-403, doi:10.1146/annurev.immunol.22.012703.104644 (2004).

129 Hahn, B. H., Grossman, J., Chen, W. & McMahon, M. The pathogenesis of atherosclerosis in autoimmune rheumatic diseases: roles of inflammation and dyslipidemia. *Journal of autoimmunity* **28**, 69-75, doi:10.1016/j.jaut.2007.02.004 (2007).

130 Galkina, E. & Ley, K. Immune and inflammatory mechanisms of atherosclerosis (*). *Annual review of immunology* **27**, 165-197, doi:10.1146/annurev.immunol.021908.132620 (2009).

131 Rosenfeld, S. M. *et al.* B-1b Cells Secrete Atheroprotective IgM and Attenuate Atherosclerosis. *Circulation research* **117**, e28-39, doi:10.1161/CIRCRESAHA.117.306044 (2015).

132 Matsuura, E., Hughes, G. R. & Khamashta, M. A. Oxidation of LDL and its clinical implication. *Autoimmunity reviews* **7**, 558-566, doi:10.1016/j.autrev.2008.04.018 (2008).

133 Srikakulapu, P. *et al.* Artery Tertiary Lymphoid Organs Control Multilayered Territorialized Atherosclerosis B-Cell Responses in Aged ApoE-/- Mice. *Arteriosclerosis, thrombosis, and vascular biology* **36**, 1174-1185, doi:10.1161/ATVBAHA.115.306983 (2016).

134 Grabner, R. *et al.* Lymphotoxin beta receptor signaling promotes tertiary lymphoid organogenesis in the aorta adventitia of aged ApoE-/- mice. *The Journal of experimental medicine* **206**, 233-248, doi:10.1084/jem.20080752 (2009).

135 Houtkamp, M. A., de Boer, O. J., van der Loos, C. M., van der Wal, A. C. & Becker, A. E. Adventitial infiltrates associated with advanced atherosclerotic plaques: structural organization suggests generation of local humoral immune responses. *The Journal of pathology* **193**, 263-269, doi:10.1002/1096-9896(2000)9999:9999<::AID-PATH774>3.0.CO;2-N (2001).

136 Hu, D. *et al.* Artery Tertiary Lymphoid Organs Control Aorta Immunity and Protect against Atherosclerosis via Vascular Smooth Muscle Cell Lymphotoxin beta Receptors. *Immunity* **42**, 1100-1115, doi:10.1016/j.immuni.2015.05.015 (2015).

137 Lotzer, K. *et al.* Mouse aorta smooth muscle cells differentiate into lymphoid tissue

organizer-like cells on combined tumor necrosis factor receptor-1/lymphotoxin beta-receptor NF-kappaB signaling. *Arteriosclerosis, thrombosis, and vascular biology* **30**, 395-402, doi:10.1161/ATVBAHA.109.191395 (2010).

138 Emini Veseli, B. *et al.* Animal models of atherosclerosis. *European journal of pharmacology* **816**, 3-13, doi:10.1016/j.ejphar.2017.05.010 (2017).

139 Yin, C. *et al.* ApoE attenuates unresolvable inflammation by complex formation with activated C1q. *Nature medicine* **25**, 496-506, doi:10.1038/s41591-018-0336-8 (2019).

140 Knowles, J. W. & Maeda, N. Genetic modifiers of atherosclerosis in mice. *Arteriosclerosis, thrombosis, and vascular biology* **20**, 2336-2345 (2000).

141 Getz, G. S. & Reardon, C. A. Animal models of atherosclerosis. *Arterioscler Thromb Vasc Biol* **32**, 1104-1115, doi:10.1161/ATVBAHA.111.237693 (2012).

142 Lorenzo, C. *et al.* ALDH4A1 is an atherosclerosis auto-antigen targeted by protective antibodies. *Nature* **589**, 287-292, doi:10.1038/s41586-020-2993-2 (2021).

143 Shoenfeld, Y., Wu, R., Dearing, L. D. & Matsuura, E. Are anti-oxidized low-density lipoprotein antibodies pathogenic or protective? *Circulation* **110**, 2552-2558, doi:10.1161/01.CIR.0000143225.07377.EA (2004).

144 Yin, C., Mohanta, S. K., Srikakulapu, P., Weber, C. & Habenicht, A. J. Artery Tertiary Lymphoid Organs: Powerhouses of Atherosclerosis Immunity. *Frontiers in immunology* **7**, 387, doi:10.3389/fimmu.2016.00387 (2016).

145 Tiller, T. *et al.* Efficient generation of monoclonal antibodies from single human B cells by single cell RT-PCR and expression vector cloning. *Journal of immunological methods* **329**, 112-124, doi:10.1016/j.jim.2007.09.017 (2008).

146 Christian E. Busse, I. C., Peter Braun, Peter F. Arndt and Hedda Wardemann. Single-cell based high-throughput sequencing of full-length immunoglobulin heavy and light chain genes. *European journal of immunology*, doi:10.1002/eji201343917 (2014).

147 von Boehmer, L. *et al.* Sequencing and cloning of antigen-specific antibodies from mouse memory B cells. *Nature protocols* **11**, 1908-1923, doi:10.1038/nprot.2016.102 (2016).

148 Belkina, A. C. *et al.* Automated optimized parameters for T-distributed stochastic

neighbor embedding improve visualization and analysis of large datasets. *Nature communications* **10**, 5415, doi:10.1038/s41467-019-13055-y (2019).

149 Maaten, L. H., G. Visualizing data using t-SNE. *J MACH LEARN RES 9*, 2579-2605 (2008).

150 Tas, J. M. *et al.* Visualizing antibody affinity maturation in germinal centers. *Science* **351**, 1048-1054, doi:10.1126/science.aad3439 (2016).

151 Daugherty, A. & Rateri, D. L. Development of experimental designs for atherosclerosis studies in mice. *Methods* **36**, 129-138, doi:10.1016/j.ymeth.2004.11.008 (2005).

152 Naito, Y. *et al.* Germinal center marker GL7 probes activation-dependent repression of N-glycolylneuraminic acid, a sialic acid species involved in the negative modulation of B-cell activation. *Molecular and cellular biology* **27**, 3008-3022, doi:10.1128/MCB.02047-06 (2007).

153 Cervenak, L., Magyar, A., Boja, R. & Laszlo, G. Differential expression of GL7 activation antigen on bone marrow B cell subpopulations and peripheral B cells. *Immunology letters* **78**, 89-96, doi:10.1016/s0165-2478(01)00239-5 (2001).

154 Shinall, S. M., Gonzalez-Fernandez, M., Noelle, R. J. & Waldschmidt, T. J. Identification of murine germinal center B cell subsets defined by the expression of surface isotypes and differentiation antigens. *Journal of immunology* **164**, 5729-5738, doi:10.4049/jimmunol.164.11.5729 (2000).

155 Ichiyoshi, Y. & Casali, P. Analysis of the structural correlates for antibody polyreactivity by multiple reassortments of chimeric human immunoglobulin heavy and light chain V segments. *The Journal of experimental medicine* **180**, 885-895, doi:10.1084/jem.180.3.885 (1994).

156 Radic, M. Z. & Weigert, M. Genetic and structural evidence for antigen selection of anti-DNA antibodies. *Annual review of immunology* **12**, 487-520, doi:10.1146/annurev.iy.12.040194.002415 (1994).

157 Crouzier, R., Martin, T. & Pasquali, J. L. Heavy chain variable region, light chain variable region, and heavy chain CDR3 influences on the mono- and polyreactivity and on the affinity of human monoclonal rheumatoid factors. *Journal of immunology*

154, 4526-4535 (1995).

158 Barbas, S. M. *et al.* Human autoantibody recognition of DNA. *Proceedings of the National Academy of Sciences of the United States of America* **92**, 2529-2533, doi:10.1073/pnas.92.7.2529 (1995).

159 Wardemann, H. *et al.* Predominant autoantibody production by early human B cell precursors. *Science* **301**, 1374-1377, doi:10.1126/science.1086907 (2003).

160 Takahashi, Y., Dutta, P. R., Cerasoli, D. M. & Kelsoe, G. In situ studies of the primary immune response to (4-hydroxy-3-nitrophenyl)acetyl. V. Affinity maturation develops in two stages of clonal selection. *The Journal of experimental medicine* **187**, 885-895, doi:10.1084/jem.187.6.885 (1998).

161 Feuillard, J., Taylor, D., Casamayor-Palleja, M., Johnson, G. D. & MacLennan, I. C. Isolation and characteristics of tonsil centroblasts with reference to Ig class switching. *International immunology* **7**, 121-130, doi:10.1093/intimm/7.1.121 (1995).

162 Kuppers, R., Zhao, M., Hansmann, M. L. & Rajewsky, K. Tracing B cell development in human germinal centres by molecular analysis of single cells picked from histological sections. *The EMBO journal* **12**, 4955-4967 (1993).

163 Fairfax, K. A., Gantier, M. P., Mackay, F., Williams, B. R. & McCoy, C. E. IL-10 regulates Aicda expression through miR-155. *Journal of leukocyte biology* **97**, 71-78, doi:10.1189/jlb.2A0314-178R (2015).

164 Muramatsu, M. *et al.* Specific expression of activation-induced cytidine deaminase (AID), a novel member of the RNA-editing deaminase family in germinal center B cells. *The Journal of biological chemistry* **274**, 18470-18476, doi:10.1074/jbc.274.26.18470 (1999).

165 Victora, G. D. & Mesin, L. Clonal and cellular dynamics in germinal centers. *Current opinion in immunology* **28**, 90-96, doi:10.1016/j.coi.2014.02.010 (2014).

166 Soto, M. E. *et al.* Predictive value of antinuclear antibodies in autoimmune diseases classified by clinical criteria: Analytical study in a specialized health institute, one year follow-up. *Results Immunol* **5**, 13-22, doi:10.1016/j.rinim.2013.10.003 (2015).

167 Lodh, M., Pradhan, D. & Parida, A. Autoimmune hepatitis with anti centromere

antibodies. *Case Reports Immunol* **2013**, 742080, doi:10.1155/2013/742080 (2013).

168 Sun, X. Y., Shi, J., Han, L., Su, Y. & Li, Z. G. Anti-histones antibodies in systemic lupus erythematosus: prevalence and frequency in neuropsychiatric lupus. *J Clin Lab Anal* **22**, 271-277, doi:10.1002/jcla.20248 (2008).

169 Nosalski, R. & Guzik, T. J. Perivascular adipose tissue inflammation in vascular disease. *British journal of pharmacology* **174**, 3496-3513, doi:10.1111/bph.13705 (2017).

170 Bennett, M. R., Sinha, S. & Owens, G. K. Vascular Smooth Muscle Cells in Atherosclerosis. *Circ Res* **118**, 692-702, doi:10.1161/CIRCRESAHA.115.306361 (2016).

171 Bobryshev, Y. V., Ivanova, E. A., Chistiakov, D. A., Nikiforov, N. G. & Orekhov, A. N. Macrophages and Their Role in Atherosclerosis: Pathophysiology and Transcriptome Analysis. *BioMed research international* **2016**, 9582430, doi:10.1155/2016/9582430 (2016).

172 Moore, K. J. & Tabas, I. Macrophages in the pathogenesis of atherosclerosis. *Cell* **145**, 341-355, doi:10.1016/j.cell.2011.04.005 (2011).

173 Feil, S. *et al.* Transdifferentiation of vascular smooth muscle cells to macrophage-like cells during atherogenesis. *Circulation research* **115**, 662-667, doi:10.1161/CIRCRESAHA.115.304634 (2014).

174 Matsumoto, K. *et al.* Expression of macrophage (Mphi) scavenger receptor, CD36, in cultured human aortic smooth muscle cells in association with expression of peroxisome proliferator activated receptor-gamma, which regulates gain of Mphi-like phenotype in vitro, and its implication in atherogenesis. *Arteriosclerosis, thrombosis, and vascular biology* **20**, 1027-1032, doi:10.1161/01.atv.20.4.1027 (2000).

175 E., S. Reconstitution of Nucleosome Core Particles from Recombinant Histones and DNA. *E2003ReconstitutionON* (2003).

176 Geraldino-Pardilla, L. *et al.* Association of Anti-Citrullinated Peptide Antibodies With Coronary Artery Calcification in Rheumatoid Arthritis. *Arthritis care & research* **69**, 1276-1281, doi:10.1002/acr.23106 (2017).

177 Chua, A., Blankstein, R. & Ko, B. Coronary artery calcium in primary prevention. *Australian journal of general practice* **49**, 464-469, doi:10.31128/AJGP-03-20-5277 (2020).

178 Timaran, C. H., McKinsey, J. F., Schneider, P. A. & Littooy, F. Reporting standards for carotid interventions from the Society for Vascular Surgery. *Journal of vascular surgery* **53**, 1679-1695, doi:10.1016/j.jvs.2010.11.122 (2011).

179 Dubland, J. A. & Francis, G. A. So Much Cholesterol: the unrecognized importance of smooth muscle cells in atherosclerotic foam cell formation. *Current opinion in lipidology* **27**, 155-161, doi:10.1097/MOL.0000000000000279 (2016).

180 Lin, L., Hu, X., Zhang, H. & Hu, H. Tertiary Lymphoid Organs in Cancer Immunology: Mechanisms and the New Strategy for Immunotherapy. *Frontiers in immunology* **10**, 1398, doi:10.3389/fimmu.2019.01398 (2019).

181 Cheong, C. *et al.* Microbial stimulation fully differentiates monocytes to DC-SIGN/CD209(+) dendritic cells for immune T cell areas. *Cell* **143**, 416-429, doi:10.1016/j.cell.2010.09.039 (2010).

182 Lee, J. W. *et al.* Peripheral antigen display by lymph node stroma promotes T cell tolerance to intestinal self. *Nature immunology* **8**, 181-190, doi:10.1038/ni1427 (2007).

183 Kratz, A., Campos-Neto, A., Hanson, M. S. & Ruddle, N. H. Chronic inflammation caused by lymphotoxin is lymphoid neogenesis. *The Journal of experimental medicine* **183**, 1461-1472, doi:10.1084/jem.183.4.1461 (1996).

184 Stott, D. I., Hiepe, F., Hummel, M., Steinhauser, G. & Berek, C. Antigen-driven clonal proliferation of B cells within the target tissue of an autoimmune disease. The salivary glands of patients with Sjogren's syndrome. *The Journal of clinical investigation* **102**, 938-946, doi:10.1172/JCI3234 (1998).

185 Vinuesa, C. G., Sanz, I. & Cook, M. C. Dysregulation of germinal centres in autoimmune disease. *Nature reviews. Immunology* **9**, 845-857, doi:10.1038/nri2637 (2009).

186 Allen, C. D., Okada, T., Tang, H. L. & Cyster, J. G. Imaging of germinal center selection events during affinity maturation. *Science* **315**, 528-531, doi:10.1126/science.1136736

(2007).

187 Kosco-Vilbois, M. H. Are follicular dendritic cells really good for nothing? *Nature reviews. Immunology* **3**, 764-769, doi:10.1038/nri1179 (2003).

188 Sallusto, F., Geginat, J. & Lanzavecchia, A. Central memory and effector memory T cell subsets: function, generation, and maintenance. *Annual review of immunology* **22**, 745-763, doi:10.1146/annurev.immunol.22.012703.104702 (2004).

189 Sheridan, B. S. & Lefrancois, L. Regional and mucosal memory T cells. *Nature immunology* **12**, 485-491, doi:10.1038/ni.2029 (2011).

190 Phan, T. G. *et al.* High affinity germinal center B cells are actively selected into the plasma cell compartment. *The Journal of experimental medicine* **203**, 2419-2424, doi:10.1084/jem.20061254 (2006).

191 Scheid, J. F. *et al.* Differential regulation of self-reactivity discriminates between IgG+ human circulating memory B cells and bone marrow plasma cells. *Proceedings of the National Academy of Sciences of the United States of America* **108**, 18044-18048, doi:10.1073/pnas.1113395108 (2011).

192 Paus, D. *et al.* Antigen recognition strength regulates the choice between extrafollicular plasma cell and germinal center B cell differentiation. *The Journal of experimental medicine* **203**, 1081-1091, doi:10.1084/jem.20060087 (2006).

193 Goldstein, L. D. *et al.* Massively parallel single-cell B-cell receptor sequencing enables rapid discovery of diverse antigen-reactive antibodies. *Communications biology* **2**, 304, doi:10.1038/s42003-019-0551-y (2019).

194 Zhang, M. J., Ntranos, V. & Tse, D. Determining sequencing depth in a single-cell RNA-seq experiment. *Nature communications* **11**, 774, doi:10.1038/s41467-020-14482-y (2020).

195 Stern, J. N. *et al.* B cells populating the multiple sclerosis brain mature in the draining cervical lymph nodes. *Science translational medicine* **6**, 248ra107, doi:10.1126/scitranslmed.3008879 (2014).

196 Eggers, E. L. *et al.* Clonal relationships of CSF B cells in treatment-naive multiple sclerosis patients. *JCI insight* **2**, doi:10.1172/jci.insight.92724 (2017).

197 Griffiths, G. M., Berek, C., Kaartinen, M. & Milstein, C. Somatic mutation and the maturation of immune response to 2-phenyl oxazolone. *Nature* **312**, 271-275, doi:10.1038/312271a0 (1984).

198 Eisen, H. N. & Siskind, G. W. Variations in Affinities of Antibodies during the Immune Response. *Biochemistry* **3**, 996-1008, doi:10.1021/bi00895a027 (1964).

199 Yaari, G., Benichou, J. I., Vander Heiden, J. A., Kleinstein, S. H. & Louzoun, Y. The mutation patterns in B-cell immunoglobulin receptors reflect the influence of selection acting at multiple time-scales. *Philosophical transactions of the Royal Society of London. Series B, Biological sciences* **370**, doi:10.1098/rstb.2014.0242 (2015).

200 Parums, D. & Mitchinson, M. J. Demonstration of immunoglobulin in the neighbourhood of advanced atherosclerotic plaques. *Atherosclerosis* **38**, 211-216, doi:10.1016/0021-9150(81)90118-0 (1981).

201 Sage, A. P., Tsiantoulas, D., Binder, C. J. & Mallat, Z. The role of B cells in atherosclerosis. *Nature reviews. Cardiology* **16**, 180-196, doi:10.1038/s41569-018-0106-9 (2019).

202 Holman, H. R. & Kunkel, H. G. Affinity between the lupus erythematosus serum factor and cell nuclei and nucleoprotein. *Science* **126**, 162-163, doi:10.1126/science.126.3265.162 (1957).

203 Nilsson, J., Lichtman, A. & Tedgui, A. Atheroprotective immunity and cardiovascular disease: therapeutic opportunities and challenges. *Journal of internal medicine* **278**, 507-519, doi:10.1111/joim.12353 (2015).

204 Polack, F. P. *et al.* Safety and Efficacy of the BNT162b2 mRNA Covid-19 Vaccine. *The New England journal of medicine* **383**, 2603-2615, doi:10.1056/NEJMoa2034577 (2020).

205 Delany, I., Rappuoli, R. & De Gregorio, E. Vaccines for the 21st century. *EMBO molecular medicine* **6**, 708-720, doi:10.1002/emmm.201403876 (2014).

206 Melero, I. *et al.* Therapeutic vaccines for cancer: an overview of clinical trials. *Nature reviews. Clinical oncology* **11**, 509-524, doi:10.1038/nrclinonc.2014.111 (2014).

207 Lei, J. *et al.* HPV Vaccination and the Risk of Invasive Cervical Cancer. *The New*

England journal of medicine **383**, 1340-1348, doi:10.1056/NEJMoa1917338 (2020).

208 Nilsson, J. & Hansson, G. K. Vaccination Strategies and Immune Modulation of Atherosclerosis. *Circulation research* **126**, 1281-1296, doi:10.1161/CIRCRESAHA.120.315942 (2020).

209 Palinski, W., Miller, E. & Witztum, J. L. Immunization of low density lipoprotein (LDL) receptor-deficient rabbits with homologous malondialdehyde-modified LDL reduces atherogenesis. *Proceedings of the National Academy of Sciences of the United States of America* **92**, 821-825, doi:10.1073/pnas.92.3.821 (1995).

210 Ameli, S. *et al.* Effect of immunization with homologous LDL and oxidized LDL on early atherosclerosis in hypercholesterolemic rabbits. *Arteriosclerosis, thrombosis, and vascular biology* **16**, 1074-1079, doi:10.1161/01.atv.16.8.1074 (1996).

211 Benagiano, M. *et al.* Human 60-kDa heat shock protein is a target autoantigen of T cells derived from atherosclerotic plaques. *Journal of immunology* **174**, 6509-6517, doi:10.4049/jimmunol.174.10.6509 (2005).

212 Xu, Q. *et al.* Association of serum antibodies to heat-shock protein 65 with carotid atherosclerosis. *Lancet* **341**, 255-259, doi:10.1016/0140-6736(93)92613-x (1993).

213 Zhu, J. *et al.* Antibodies to human heat-shock protein 60 are associated with the presence and severity of coronary artery disease: evidence for an autoimmune component of atherogenesis. *Circulation* **103**, 1071-1075, doi:10.1161/01.cir.103.8.1071 (2001).

214 Huittinen, T. *et al.* Autoimmunity to human heat shock protein 60, Chlamydia pneumoniae infection, and inflammation in predicting coronary risk. *Arteriosclerosis, thrombosis, and vascular biology* **22**, 431-437, doi:10.1161/hq0302.104512 (2002).

215 Foteinos, G., Afzal, A. R., Mandal, K., Jahangiri, M. & Xu, Q. Anti-heat shock protein 60 autoantibodies induce atherosclerosis in apolipoprotein E-deficient mice via endothelial damage. *Circulation* **112**, 1206-1213, doi:10.1161/CIRCULATIONAHA.105.547414 (2005).

Supplementary materials

Histone proteins blast results.

```
P0C0S8 H2A1_HUMAN            1   MSGRGKQGGKARAKAKTRSSRAGLQFPVGRVHRLLRKGNYAERVGAGAPVYLAAVLEYLT   60
P0C0S9 H2A1_BOVIN            1   MSGRGKQGGKARAKAKTRSSRAGLQFPVGRVHRLLRKGNYAERVGAGAPVYLAAVLEYLT   60
C0HKE1 H2A1B_MOUSE           1   MSGRGKQGGKARAKAKTRSSRAGLQFPVGRVHRLLRKGNYSERVGAGAPVYLAAVLEYLT   60
                                 ****************************************:*********************

P0C0S8 H2A1_HUMAN           61   AEILELAGNAARDNKKTRIIPRHLQLAIRNDEELNKLLGKVTIAQGGVLPNIQAVLLPKK  120
P0C0S9 H2A1_BOVIN           61   AEILELAGNAARDNKKTRIIPRHLQLAIRNDEELNKLLGKVTIAQGGVLPNIQAVLLPKK  120
C0HKE1 H2A1B_MOUSE          61   AEILELAGNAARDNKKTRIIPRHLQLAIRNDEELNKLLGRVTIAQGGVLPNIQAVLLPKK  120
                                 ****************************************:*********************

P0C0S8 H2A1_HUMAN          121   TESHHKAKGK                                                    130
P0C0S9 H2A1_BOVIN          121   TESHHKAKGK                                                    130
C0HKE1 H2A1B_MOUSE         121   TESHHKAKGK                                                    130
                                 **********

P62807 H2B1C_HUMAN           1   MPEPAKSAPAPKKGSKKAVTKAQKKDGKKRKRSRKESYSVYVYKVLKQVHPDTGISSKAM   60
Q6ZWY9 H2B1C_MOUSE           1   MPEPAKSAPAPKKGSKKAVTKAQKKDGKKRKRSRKESYSVYVYKVLKQVHPDTGISSKAM   60
P62808 H2B1_BOVIN            1   MPEPAKSAPAPKKGSKKAVTKAQKKDGKKRKRSRKESYSVYVYKVLKQVHPDTGISSKAM   60
                                 ************************************************************

P62807 H2B1C_HUMAN          61   GIMNSFVNDIFERIAGEASRLAHYNKRSTITSREIQTAVRLLLPGELAKHAVSEGTKAVT  120
Q6ZWY9 H2B1C_MOUSE          61   GIMNSFVNDIFERIAGEASRLAHYNKRSTITSREIQTAVRLLLPGELAKHAVSEGTKAVT  120
P62808 H2B1_BOVIN           61   GIMNSFVNDIFERIAGEASRLAHYNKRSTITSREIQTAVRLLLPGELAKHAVSEGTKAVT  120
                                 ************************************************************

P62807 H2B1C_HUMAN         121   KYTSSK                                                        126
Q6ZWY9 H2B1C_MOUSE         121   KYTSSK                                                        126
P62808 H2B1_BOVIN          121   KYTSSK                                                        126
                                 ******

P68433 H31_MOUSE             1   MARTKQTARKSTGGKAPRKQLATKAARKSAPATGGVKKPHRYRPGTVALREIRRYQKSTE   60
P68431 H31_HUMAN             1   MARTKQTARKSTGGKAPRKQLATKAARKSAPATGGVKKPHRYRPGTVALREIRRYQKSTE   60
P68432 H31_BOVIN             1   MARTKQTARKSTGGKAPRKQLATKAARKSAPATGGVKKPHRYRPGTVALREIRRYQKSTE   60
                                 ************************************************************

P68433 H31_MOUSE            61   LLIRKLPFQRLVREIAQDFKTDLRFQSSAVMALQEACEAYLVGLFEDTNLCAIHAKRVTI  120
P68431 H31_HUMAN            61   LLIRKLPFQRLVREIAQDFKTDLRFQSSAVMALQEACEAYLVGLFEDTNLCAIHAKRVTI  120
P68432 H31_BOVIN            61   LLIRKLPFQRLVREIAQDFKTDLRFQSSAVMALQEACEAYLVGLFEDTNLCAIHAKRVTI  120
                                 ************************************************************

P68433 H31_MOUSE           121   MPKDIQLARRIRGERA                                              136
P68431 H31_HUMAN           121   MPKDIQLARRIRGERA                                              136
P68432 H31_BOVIN           121   MPKDIQLARRIRGERA                                              136
                                 ****************

P84228 H32_MOUSE             1   MARTKQTARKSTGGKAPRKQLATKAARKSAPATGGVKKPHRYRPGTVALREIRRYQKSTE   60
Q71DI3 H32_HUMAN             1   MARTKQTARKSTGGKAPRKQLATKAARKSAPATGGVKKPHRYRPGTVALREIRRYQKSTE   60
P84227 H32_BOVIN             1   MARTKQTARKSTGGKAPRKQLATKAARKSAPATGGVKKPHRYRPGTVALREIRRYQKSTE   60
                                 ************************************************************

P84228 H32_MOUSE            61   LLIRKLPFQRLVREIAQDFKTDLRFQSSAVMALQEASEAYLVGLFEDTNLCAIHAKRVTI  120
Q71DI3 H32_HUMAN            61   LLIRKLPFQRLVREIAQDFKTDLRFQSSAVMALQEASEAYLVGLFEDTNLCAIHAKRVTI  120
P84227 H32_BOVIN            61   LLIRKLPFQRLVREIAQDFKTDLRFQSSAVMALQEASEAYLVGLFEDTNLCAIHAKRVTI  120
                                 ************************************************************

P84228 H32_MOUSE           121   MPKDIQLARRIRGERA                                              136
Q71DI3 H32_HUMAN           121   MPKDIQLARRIRGERA                                              136
P84227 H32_BOVIN           121   MPKDIQLARRIRGERA                                              136
                                 ****************

P84243 H33_HUMAN             1   MARTKQTARKSTGGKAPRKQLATKAARKSAPSTGGVKKPHRYRPGTVALREIRRYQKSTE   60
P84244 H33_MOUSE             1   MARTKQTARKSTGGKAPRKQLATKAARKSAPSTGGVKKPHRYRPGTVALREIRRYQKSTE   60
Q5E9F8 H33_BOVIN             1   MARTKQTARKSTGGKAPRKQLATKAARKSAPSTGGVKKPHRYRPGTVALREIRRYQKSTE   60
                                 ************************************************************

P84243 H33_HUMAN            61   LLIRKLPFQRLVREIAQDFKTDLRFQSAAIGALQEASEAYLVGLFEDTNLCAIHAKRVTI  120
P84244 H33_MOUSE            61   LLIRKLPFQRLVREIAQDFKTDLRFQSAAIGALQEASEAYLVGLFEDTNLCAIHAKRVTI  120
Q5E9F8 H33_BOVIN            61   LLIRKLPFQRLVREIAQDFKTDLRFQSAAIGALQEASEAYLVGLFEDTNLCAIHAKRVTI  120
                                 ************************************************************

P84243 H33_HUMAN           121   MPKDIQLARRIRGERA                                              136
P84244 H33_MOUSE           121   MPKDIQLARRIRGERA                                              136
Q5E9F8 H33_BOVIN           121   MPKDIQLARRIRGERA                                              136
                                 ****************
```

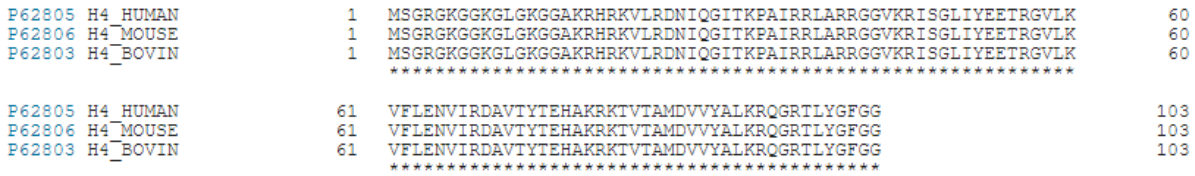

sFigure 1. Multiple sequence alignment of five major families of histone proteins from human, mouse, and bovine. The overall amino acid identity and homology is almost 100%. Histones are highly conserved proteins.

Table s1. Sequence data of Ig antibodies from ATLOs GC B cells of aged ApoE$^{-/-}$ mice.

ATLO 1

VH	D	JH	RF	V-Mut	CDR3(aa)	Length	κ/λ	Vκ/Vλ	Jκ/Jλ	V-Mut	CDR3
							κ	5-39*01	1*01 or1*02	8	QNGHSFPPT
1-67*01	/	2*01	/	17	GSPFFDY	7	κ	10-96*01	1*01 or1*02	10	QQGDTLPPT
1-81*01	1-1*01	4*01	3	3	ARRGYGSSSYAMDY	14	λ	1*01	1*01	2	ALWYSNHWV
							κ	3-5*01	2*01	17	QQTNEDPYT
1-81*01	3-2*02	4*01	2	8	AREGDSSGYGGVGY	14					
							κ	3-2*01	1*01	5	QQSKEVPWT
1-80*01	/	3*01	/	7	ARGAY	5					
							κ	3-5*01	2*01	12	QQTNEDPFT
							κ	1-135*01	2*01	13	WQGTRFPYT
							κ	3-2*01	2*01	0	QQSKEVPCT
1-82*01	3-1*01	2*01	2	14	AREGLGPFDS	10					

1-53*01	1-1*01	2*01	3	13	ARGSGYYPFDY	11	κ	3-2*01	1*01	7	QQSKEVPWT
1-82*01	2-12*01	3*01	1	3	ARFSPAWFAY	10					
14-4*01	2-10*02	2*01	1	10	TRIWN	5					
10-1*01	5-1*01	4*01	2	4	VRHTYGAMDY	10					
							κ	3-2*01	2*01	6	QQSKEVPYT
1-80*01	1-1*01	2*01	3	3	ALIRDGSSYVDYFDY	15					
1-50*01	3-2*02	3*01	2	11	ARSGSSGYFSWFAY	14					
14-2*01	2-1*01	4*01	3	4	ARQPIYYGNPYYAMDY	16					
1-53*01	2-3*01	2*01	3	13	ARGSGYYPFDY	11	κ	3-2*01	1*01	6	QQSKEVPWT
							κ	1-117*01	1*01	7	FQGSHVPFT
							κ	3-5*01	2*01	10	QQTNEDPYT
5-4*01	1-1*02	4*01	3	22	VRDGGERWSLCMDY	14	κ	5-39*01	5*01	8	QNGHSFPLT
							κ	4-57-1*01	5*01	6	QQYSGYPLT
1-36*01	2-2*01	4*01	3	3	AKGYYYAMDY	10	κ	3-2*01	1*01	0	QQSKEVPLT
							κ	3-2*01	4*01	2	QQSKEVPFT
1-81*01	1-2*01	1*03	2	3	AKGPLRLNFDV	11	κ	8-28*01	1*01 or 5*01	7	QNDHNPTCAHSVIT
1-72*01	2-13*01	4*01	3	22	TRGAYSGALDY	11	κ	3-5*01	2*01	15	QQTNEDPYT
							κ	3-5*01	2*01	17	QQTNEDPYT

1-42*01	1-3*01	1*03	1	4	ARKEGRYFDV	10	κ	3-2*01	2*01	6	QQSKEVPYT
							κ	8-19*01	4*01	3	QNDYSYPLT
							κ	5-43*01	5*01	1	QQSNSWPFT
1-55*01	3-1*01	4*01	2	10	ARSLRGGGDY	10	κ	3-10*01	2*01	4	QQNNEDPYT
1-5*01	2-10*01	3*01	3	3	TRRTYYGNWFAY	12					
							κ	4-74*01	2*01	6	HQYHRSPP
							κ	14-111*01	2*01	9	LQYDEFPPT
							κ	1-122	2*01	7	LQFTHVPPT
1-82*01	3-2*02	4*01	3	3	ARGGTAQATKSMDY	14	κ	3-5*01	2*01	10	HQSNEDPPT
							κ	14-100*01	2*01	5	VQYAQFPHT
							κ	1-110*01	1*01 or 2*01	8	SQTTHVPRT
1-19*01	2-3*01	2*01	3	3	ARGYYAFDY	9	κ	8-24*01	2*01	0	QQHYSTPLT
							κ	3-10*01	1*01	1	QQNNEDPWT
1-81*01	1-1*02	4*01	3	3	ANGYYAMDY	9					
2-9-1*01	1-1*01	2*01	2	9	ASPLLLRSLYYFDY	14					
							κ	1-135*01	1*01	9	WQGTHFLRS
1-9*01	1-1*01	3*01	3	23	ARDYYGSSYGGFTY	14	κ	3-5*01	1*01	17	QQSYEAPWT
							κ	3-5*01	1*01	17	QQTNEVPFT
1-81*01	3-3*01	2*01	3	6	ASPWDEKVDY	10	κ	1-133*01	1*01	3	VQGTHFPHT

1-72*01	3-3*01	4*01	3	21	TRGAYSGALDY	11	κ	3-5*01	1*01	15	QQGNEDPHT
							κ	3-2*01	1*01	4	QQSKEVPLT
							κ	3-4*01	1*01	6	QQSDEDPFT
							κ	3-5*01	2*01	14	QQTNEVLYT
1-42*01	1-1*01	1*03	2	3	ARSLLLRYLDV	11	κ	3-2*01	2*01	2	QQSKEVPRT
							κ	3-2*01	1*01or 2*01	4	QQSKEVPWT
1-80*01	2-4*01	3*01	3	21	ATYDFGFIF	9	κ	14-111*01	2*01	15	LQYDEFPLT
							κ	8-24*01	2*01	1	QPHYSTLST
1-31*01	1-1*01	2*01	1	16	ARYTTSVVADY	11					
1-55*01	6-3*01	4*01	3	8	ARSHAMDY	8					
							κ	3-2*01	1*01or 2*01	6	QQSKEVPWT
1-71*01	1-1*01	1*03	3	3	ARHEDAYYYGSSWYFDV	17					
1-42*01	1-3*01	1*03	1	2	ARKEGRYFDV	10	κ	3-2*01	2*01	5	QQSKEVPPT
1-80*01	3-1*01	2*01	1	9	ARGAY	5	κ	8-24*01	5*01	3	QQHYSTPLT

ATLO2

VH	D	JH	RF	V-Mut	CDR3(aa)	Length	κ/λ	Vκ/Vλ	Jκ/Jλ	V-Mut	CDR3
							κ	4-59*01	4*01	12	QQWSSNPFT
							κ	10-96*01	5*01	14	QQGNTLPLT
							κ	3-2*01	1*01	2	QQSKEVPWT

							κ	1-110*01	1*01	19	SQSTHFPWT
							κ	3-2*01	1*01	4	QQSKEVPWT
5-6*01	1-1*01	1*03	3	4	GRQGYYGSSGYFDV	14					
							κ	4-53*01	5*01	4	QQWSSYPLT
							κ	1-110*01	2*01	7	SQSTHVPYT
							κ	8-30*01	2*01	10	QQYYSYPYT
10-3*01	1-1*01	2*01	3	1	VREPYYGSSYDY	12					
							κ	3-10*01	2*01	9	QQNNEGPYT
1-75*01	2-4*01	3*01	3	9	ARDEDDYDPWFAY	13	κ	4-53*01	2*01	10	QQWSSYPL
1-36*01	1-1*01	3*01	3	15	ARGNYYGGSDWGFDV	13	κ	1-110*01	5*01	3	SQNTHVPLT
2-9-1*01	2-12*01	4*01	3	7	ARSYDDAMDY	10	κ	3-2*01	1*01	0	QQSKEVPWT
							κ	4-74*01	1*01	8	HQYYRSPRT
							κ	3-10*01	1*01	2	QQNNEDPRT
							κ	3-2*01	2*01	4	QQSKEVPYT
							κ	14-110*01	4*01	10	LQYGDFPPT
							κ	3-2*01	2*01	0	QQSKEVPYT
							κ	6-15*01	2*01	3	QQYNSYPHT
							κ	3-5*01	4*01	8	QQSNEDPFT
							κ	4-59*01	5*01	2	QQWSSNPLT
							κ	9-124*01	5*01	6	LQYASYPPA
							κ	1-110*01	1*01	14	SQSTHVPWT
1-42*01	1-1*01	4*01	3	13	ARKGSFSGAMDY	12	κ	3-10*01	1*01	5	QQNNEDPRT
							κ	8-19*01	4*01	7	QNDYSYPFT
1-67*01	2-3*01	3*01	1	7	ARAGVMVTTGGFAY	14	κ	3-5*01	1*01	6	QQNNEDPWT
1-42*01	4-1*01	4*01	1	8	ARRELTGSWDY	11					
							κ	1-110*01	1*01	16	SQSTHFPWT

							κ	4-53*01	5*01	0	QQWSSYPLT
							κ	4-58*01	2*01	1	QQWSGYPYT
							κ	1-117*01	2*01	13	FQGSHVPYA
3-8*01	4-1*01	1*03	3	0	ARYMDWVHYFDV	12					
1-62*01	1-1*01	3*01	3	3	ARHEERFYYYGSSYGAWFAY	20	κ	8-30*01	2*01	2	QQYYSYPYT
							κ	4-53*01	5*01	2	QQWSSYPLT
1-81*01	1-1*01	1*03	3	3	ARNPPYYGSSYRRYFDV	17	κ	4-55*01	5*01	1	QQWSSYPPT
							κ	9-124*01	5*01	8	LQYATYPPT
							κ	4-63*01	5*01	21	SQGSGYPLT
							κ	9-120*01	4*01 or 4*02	7	LQYASSFT
							κ	9-124*01	5*01	6	LQYASYPPT
							κ	4-72*01	1*01	9	QQWSSNPWT
							κ	3-2*01	2*01	3	QQNKEVPYT
1-42*01	4-1*01	4*01	1	7	ARRELTGSWDY	11					
							κ	1-110*01	1*01	12	SQSTHVPWT
1-70*01	2-5*01	3*01	1	10	TREG**LREWFP	12	κ	14-111*01	4*01	15	LQYGDFPPT
1-82*01	2-4*01	3*01	1	20	SRWTKMITTRASWFAY	16	κ	3-10*01	2*01	10	QQNNEGPYT
							κ	3-10*01	1*01	6	QQNNEDPRT
							κ	4-53*01	5*01	2	QQWTSYPLT
							κ	1-117*01	1*01	6	FQGSHVPWT
							κ	16-104*01	5*01	8	QQHNEYPLT
1-42*01	1-1*01	2*01	3	21	SRRGGFSLDY	10	κ	3-2*01	1*01	12	QQSKEVPWT
1-20*01	3-1*01	4*01	3	10	ARSGGFYAMDY	11	κ	4-70*01	1*01	6	HQRSSYPWT
							κ	3-10*01	2*01	10	QQNNEGPYT
							κ	4-63*01	5*01	15	FQGSGYPLT

ATLO3

VH	D	JH	RF	V-Mut	CDR3(aa)	Length	κ/λ	Vκ/Vλ	Jκ/Jλ	V-Mut	CDR3
							κ	6-15*01	2*01	3	QQYNSYPYT
1-55*01	6-3*01	1*03	2	15	ARKILRRGGWYFDV	14	κ	3-4*01	1*01	3	QQSNEDPWT
							κ	3-4*01	1*01	4	QQSNEDPWT
5-1*01	1-1*01	4*01	2	3	LRILPPYMDY	10					
1-55*01	1-1*01	2*01	1	7	ARTGIATDLFDY	12					
1-81*01	2-3*01	4*01	3	3	ASPSYDGYYVRAMDY	15	λ	1*01	1*01	1	ALWYSNHWV
5-17*01	2-10*02	3*01	1	2	AKGR * * APGLLT		κ	5-48*01	2*01	5	QQSNSWPYT
10-1*01	3-3*01	4*01	3	4	VRGDGTMDY	9					
10-1*01	3-3*01	4*01	3	4	VRGDGTMDY	9					
5-6*01	1-1*01	2*01	1	15	AITTVVSYEGYFDY	14	κ	8-19*01	5*01	15	QNDYIYPLT
1-80*01	/	2*01	/	9	ARGYY	5	κ	17-127*01	5*01	8	LQSDNMPLT
10-1*01	1-1*01	3*01	3	4	VSEGSWFAY	9					
							κ	1-135*01	1*01	6	WQGTHFPRT
1-75*01	1-1*02	4*01	3	6	ARGYGGHAMDY	11	κ	17-127*01	2*01	10	LQSDNMPYT
1-55*01	1-1*01	2*01	1	9	ARTGVATDLFDY	12					
1-80*01	/	2*01	/	7	ARGPY	5	κ	4-55*01	2*01	12	QQWSNYPYT
							κ	1-110*01	5*01	6	SQSTHVPPLT
							κ	4-59*01	5*01	9	QQWSSNPLT
1-26*01	2-2*01	4*01	3	6	AGYYYAMDY	9	κ	1-117*01	2*01	7	FQGSHVPYT
							κ	4-59*01	5*01	9	QQWSSNPLT
1-80*01	1-1*01	1*03	1	12	ASSPITTVVASDV	13	κ	4-55*01	2*01	10	QQWSSYPPT
1-80*01	1-1*01	2*01	1	6	APIATIVENYFDY	13	κ	5-39*01	4*01	2	QNGHSFPPT
1-26*01	2-4*01	3*01	3	4	ARDYAY	6	κ	1-110*01	5*01	5	SQSTHVPLT

1-9*01	1-1*01	2*01	3	7	ARRDYYGSFDY	11	κ	8-27*01	4*01	6	HQYLSSFT
1-55*01	1-1*01	2*01	1	5	ARTGIATDLFDY	12					
1-81*01	4-1*02	4*01	3	4	ARSTGKAMDY	10	κ	10-94*01	1*01	3	QQYSKLPWT
2-9*01	2-1*01	1*03	3	3	ARGGGYGNYWYFDV	14	κ	5-39*01	5*01	2	QNGHSFPLT
							κ	5-48*01	2*01	7	QQSNTWPTT
14-2*01	1-1*02	4*01	3	11	SRDYDDGYYGMDY	13					
14-2*01	2-1*01	4*01	3	13	ARGGYYGNYGDMDY	14					
1-52*01	2-3*01	3*01	3	5	ASDDGYFAY	9	κ	3-5*01	2*01	2	QQSNEDPYT
							κ	3.-4*01	4*01	7	QQSNEDPPT
1-50*01	3-2*02	3*01	2	14	ASGGYLAY	8	κ	4-70*01	2*01	15	HQRSSYT
1-63*01	3-2*02	3*01	2	3	ARSLDSSGYPFAY	13	κ	1-117*01	1*01	11	FQGSHVPRT
11-2*01	2-5*01	1*03	3	5	MRYSNYWYFDV	11					
1-22*01	1-1*01	1*03	1	4	ARTPLTTVVGDWYFDV	16					
							κ	5-39*01	5*01	3	QNGHSFPLT
							κ	12-44*01	4*01	12	QHHYGTPFT
							κ	12-44*01	4*01	5	QHHYGTPFT
1-71*01	1-1*01	3*01	3	5	ARHEDYYGNGYPAGFAY	17	κ	8-28*01	5*01	5	QNDHSYPLT
1-85*01	1-1*01	1*03	1	9	ARRRRPIITVVVSRWYFDV	19					
							κ	5-39*01	5*01	3	QNGHSFPLT
1-53*01	2-3*01	1*03	3	5	ARRGGDDGYYWYFDV	15	κ	5-39*01	5*01	3	QNGHSFPLT
2-9-1*01	1-1*01	1*03	3	4	ASNYYGSGWYFDV	13	κ	1-110*01	1*01	7	SQSTHVPWT
							κ	4-55*01	5*01	19	QVWSSYPPT
1-80*01	/	3*01	/	3	ARGAY	5					
14-2*01	1-1*02	4*01	3	11	ARDYDDGYYGMDY	13					
1-9*01	4-1*01	2*01	1	10	ARGTGTKIFDS	11	κ	9-120*01	2*01	8	LQYASSPYT
							κ	9-120*01	5*01	6	LQYASSPLT

1-19*01	2-3*01	2*01	3	3	ARTEDDYQGGFDY	13					
							κ	5-39*01	5*01	14	QNGHSFPLT
1-84*01	2-3*01	1*03	3	7	ANSHPYDGDYEDWYFDV	17	κ	8-19*01	5*01	6	QNDYSYPLT
1-67*01	2-2*01	2*01	2	8	ARERLQHNFDY	11					
							κ	4-70*01	2*01	4	HQRSSFT
14-2*01	1-1*02	4*01	3	11	ARDYDDGYYGMDY	13	κ	5-39*01	5*01	5	QNGHSFPPT
1-81*01	4-1*01	4*01	1	3	ARTGTEAMDY	10	κ	4-91*01	4*01	6	QQGSSIPFT
5-17*01	2-12*01	4*01	2	29	ARGK**RVYAMDY		κ	4-59*01	5*01	9	QQWSSNPLT
1-80*01	/	3*01	/	6	ARGAY	5	κ	9-120*01	2*01	5	LQYASSPYT
							κ	3-5*01	1*01	4	QQSNEDPWT
1-53*01	2-3*01	4*01	3	16	ARGGYDGYYGAMDS	14	κ	4-55*01	5*01	14	QQWNSYPPT
1-80*01	/	3*01	/	12	ARGAY	5	κ	4-55*01	4*01	9	QQWSSDPFT
1-69*01	1-1*01	2*01	3	5	ARDYYGSSWGY	11	κ	8-27*01	1*01	4	HQYLSSRT
1-81*01	2-2*01	3*01	3	3	ARVHYGYDEAY	11	κ	14-100*01	2*01	5	VQYAQFPYT
							κ	12-44*01	4*01	6	QHHYGTPFT
14-1*01	1-1*01	1*03	3	3	ATTPLYYGSSHWYFDV	16	κ	8-27*01	1*01	5	HQYLSSWT
14-4*01	3-1*01	3*01	2	2	TLDVH	5					
							κ	3-4*01	1*01	5	QQSNEDPWT
							κ	4-57*01	4*01	7	QQRSSYPPFT
5-4*01	1-1*01	1*03	3	3	ARGGIDYYGSSYWYFDV	17	κ	5-39*01	4*01	8	QNGHSFPFT
							κ	5-39*01	2*01	2	QNGHSFPPT
1-26*01	1-1*01	1*03	3	12	ARDYYGSSWYFDV	13	κ	6-15*01	1*01	11	QQYNSYPRT
1-7*01	1-1*01	2*01	1	5	AAITTVVAIDY	11					
							κ	4-59*01	5*01	9	QQWSSNPLT
5-6*01	1-2*01	2*01	1	23	TKTLITAVDY	10	κ	1-135*01	1*01	13	WQGTHFPRT
1-9*01	4-1*01	2*01	2	19	ARLLGDY	7					

1-39*01	1-1*01	1*03	1	6	ARRGPLITTVVATGYFDV	18	κ	6-17*01	2*01	4	QQHYSAPYT
1-63*01	2-1*01	4*01	3	3	ARIRTYYGNSYYYAMDY	17	κ	19-93*01	1*01	3	LQYDNLWT
1-5*01	1-1*01	2*01	1	10	SKGTVDY	7	κ	3-2*01	1*01	8	QQSKEVPWT
1-80*01	/	2*01	/	7	ARGPY	5	κ	4-55*01	2*01	12	QQWSNYPYT

VH: variable heavy chain family. D: Diversity region. JH: Join region. V-Mut: Somatic mutation. CDR3: Complementarity Determining Region. aa: amino acid.

Table s2. Sequence data of Ig antibodies from spleen GC B cells of aged ApoE$^{-/-}$ mice.

Spleen 1

VH	D	JH	RF	V-Mut	CDR3(aa)	Length	κ/λ	Vκ/Vλ	Jκ/Jλ	V-Mut	CDR3
							κ	5-39*01	1*01 or1*02	8	QNGHSFPPT
1-67*01	/	2*01	/	17	GSPFFDY	7	κ	10-96*01	1*01 or1*02	10	QQGDTLPPT
1-81*01	1-1*01	4*01	3	3	ARRGYGSSSYAMDY	14	λ	1*01	1*01	2	ALWYSNHWV
							κ	3-5*01	2*01	17	QQTNEDPYT
1-81*01	3-2*02	4*01	2	8	AREGDSSGYGGVGY	14					
							κ	3-2*01	1*01	5	QQSKEVPWT
1-80*01	/	3*01	/	7	ARGAY	5					
							κ	3-5*01	2*01	12	QQTNEDPFT
							κ	1-135*01	2*01	13	WQGTRFPYT
							κ	3-2*01	2*01	0	QQSKEVPCT
1-82*01	3-1*01	2*01	2	14	AREGLGPFDS	10					
1-53*01	1-1*01	2*01	3	13	ARGSGYYPFDY	11	κ	3-2*01	1*01	7	QQSKEVPWT
1-82*01	2-12*01	3*01	1	3	ARFSPAWFAY	10					
14-4*01	2-10*02	2*01	1	10	TRIWN	5					

10-1*01	5-1*01	4*01	2	4	VRHTYGAMDY	10					
							κ	3-2*01	2*01	6	QQSKEVPYT
1-80*01	1-1*01	2*01	3	3	ALIRDGSSYVDYFDY	15					
1-50*01	3-2*02	3*01	2	11	ARSGSSGYFSWFAY	14					
14-2*01	2-1*01	4*01	3	4	ARQPIYYGNPYYAMDY	16					
1-53*01	2-3*01	2*01	3	13	ARGSGYYPFDY	11	κ	3-2*01	1*01	6	QQSKEVPWT
							κ	1-117*01	1*01	7	FQGSHVPFT
							κ	3-5*01	2*01	10	QQTNEDPYT
5-4*01	1-1*02	4*01	3	22	VRDGGERWSLCMDY	14	κ	5-39*01	5*01	8	QNGHSFPLT
							κ	4-57-1*01	5*01	6	QQYSGYPLT
1-36*01	2-2*01	4*01	3	3	AKGYYYAMDY	10	κ	3-2*01	1*01	0	QQSKEVPLT
							κ	3-2*01	4*01	2	QQSKEVPFT
1-81*01	1-2*01	1*03	2	3	AKGPLRLNFDV	11	κ	8-28*01	1*01 or 5*01	7	QNDHNPTCAHSVIT
1-72*01	2-13*01	4*01	3	22	TRGAYSGALDY	11	κ	3-5*01	2*01	15	QQTNEDPYT
							κ	3-5*01	2*01	17	QQTNEDPYT
1-42*01	1-3*01	1*03	1	4	ARKEGRYFDV	10	κ	3-2*01	2*01	6	QQSKEVPYT
							κ	8-19*01	4*01	3	QNDYSYPLT
							κ	5-43*01	5*01	1	QQSNSWPFT
1-55*01	3-1*01	4*01	2	10	ARSLRGGGDY	10	κ	3-10*01	2*01	4	QQNNEDPYT
1-5*01	2-10*01	3*01	3	3	TRRTYYGNWFAY	12					
							κ	4-74*01	2*01	6	HQYHRSPP
							κ	14-111*01	2*01	9	LQYDEFPPT
							κ	1-122	2*01	7	LQFTHVPPT
1-82*01	3-2*02	4*01	3	3	ARGGTAQATKSMDY	14	κ	3-5*01	2*01	10	HQSNEDPPT

							κ	14-100*01	2*01	5	VQYAQFPHT
							κ	1-110*01	1*01 or 2*01	8	SQTTHVPRT
1-19*01	2-3*01	2*01	3	3	ARGYYAFDY	9	κ	8-24*01	2*01	0	QQHYSTPLT
							κ	3-10*01	1*01	1	QQNNEDPWT
1-81*01	1-1*02	4*01	3	3	ANGYYAMDY	9					
2-9-1*01	1-1*01	2*01	2	9	ASPLLLRSLYYFDY	14					
							κ	1-135*01	1*01	9	WQGTHFLRS
1-9*01	1-1*01	3*01	3	23	ARDYYGSSYGGFTY	14	κ	3-5*01	1*01	17	QQSYEAPWT
							κ	3-5*01	1*01	17	QQTNEVPFT
1-81*01	3-3*01	2*01	3	6	ASPWDEKVDY	10	κ	1-133*01	1*01	3	VQGTHFPHT
1-72*01	3-3*01	4*01	3	21	TRGAYSGALDY	11	κ	3-5*01	1*01	15	QQGNEDPHT
							κ	3-2*01	1*01	4	QQSKEVPLT
							κ	3-4*01	1*01	6	QQSDEDPFT
							κ	3-5*01	2*01	14	QQTNEVLYT
1-42*01	1-1*01	1*03	2	3	ARSLLLRYLDV	11	κ	3-2*01	2*01	2	QQSKEVPRT
							κ	3-2*01	1*01or2*01	4	QQSKEVPWT
1-80*01	2-4*01	3*01	3	21	ATYDFGFIF	9	κ	14-111*01	2*01	15	LQYDEFPLT
							κ	8-24*01	2*01	1	QPHYSTLST
1-31*01	1-1*01	2*01	1	16	ARYTTSVVADY	11					
1-55*01	6-3*01	4*01	3	8	ARSHAMDY	8					
							κ	3-2*01	1*01or2*01	6	QQSKEVPWT
1-71*01	1-1*01	1*03	3	3	ARHEDAYYYGSSWYFDV	17					
1-42*01	1-3*01	1*03	1	2	ARKEGRYFDV	10	κ	3-2*01	2*01	5	QQSKEVPPT
1-80*01	3-1*01	2*01	1	9	ARGAY	5	κ	8-24*01	5*01	3	QQHYSTPLT

Spleen 2

VH	D	JH	RF	V-Mut	CDR3(aa)	Length	κ/λ	Vκ/Vλ	Jκ/Jλ	V-Mut	CDR3
							κ	4-59*01	4*01	12	QQWSSNPFT
							κ	10-96*01	5*01	14	QQGNTLPLT
							κ	3-2*01	1*01	2	QQSKEVPWT
							κ	1-110*01	1*01	19	SQSTHFPWT
							κ	3-2*01	1*01	4	QQSKEVPWT
5-6*01	1-1*01	1*03	3	4	GRQGYYGSSGYFDV	14					
							κ	4-53*01	5*01	4	QQWSSYPLT
							κ	1-110*01	2*01	7	SQSTHVPYT
							κ	8-30*01	2*01	10	QQYYSYPYT
10-3*01	1-1*01	2*01	3	1	VREPYYGSSYDY	12					
							κ	3-10*01	2*01	9	QQNNEGPYT
1-75*01	2-4*01	3*01	3	9	ARDEDDYDPWFAY	13	κ	4-53*01	2*01	10	QQWSSYPL
1-36*01	1-1*01	3*01	3	15	ARGNYYGGSDWGFDV	13	κ	1-110*01	5*01	3	SQNTHVPLT
2-9-1*01	2-12*01	4*01	3	7	ARSYDDAMDY	10	κ	3-2*01	1*01	0	QQSKEVPWT
							κ	4-74*01	1*01	8	HQYYRSPRT
							κ	3-10*01	1*01	2	QQNNEDPRT
							κ	3-2*01	2*01	4	QQSKEVPYT
							κ	14-110*01	4*01	10	LQYGDFPPT
							κ	3-2*01	2*01	0	QQSKEVPYT
							κ	6-15*01	2*01	3	QQYNSYPHT
							κ	3-5*01	4*01	8	QQSNEDPFT
							κ	4-59*01	5*01	2	QQWSSNPLT
							κ	9-124*01	5*01	6	LQYASYPPA

							κ	1-110*01	1*01	14	SQSTHVPWT
1-42*01	1-1*01	4*01	3	13	ARKGSFSGAMDY	12	κ	3-10*01	1*01	5	QQNNEDPRT
							κ	8-19*01	4*01	7	QNDYSYPFT
1-67*01	2-3*01	3*01	1	7	ARAGVMVTTGGFAY	14	κ	3-5*01	1*01	6	QQNNEDPWT
1-42*01	4-1*01	4*01	1	8	ARRELTGSWDY	11					
							κ	1-110*01	1*01	16	SQSTHFPWT
							κ	4-53*01	5*01	0	QQWSSYPLT
							κ	4-58*01	2*01	1	QQWSGYPYT
							κ	1-117*01	2*01	13	FQGSHVPYA
3-8*01	4-1*01	1*03	3	0	ARYMDWVHYFDV	12					
1-62*01	1-1*01	3*01	3	3	ARHEERFYYYGSSYGAW FAY	20	κ	8-30*01	2*01	2	QQYYSYPYT
							κ	4-53*01	5*01	2	QQWSSYPLT
1-81*01	1-1*01	1*03	3	3	ARNPPYYGSSYRRYFDV	17	κ	4-55*01	5*01	1	QQWSSYPPT
							κ	9-124*01	5*01	8	LQYATYPPT
							κ	4-63*01	5*01	21	SQGSGYPLT
							κ	9-120*01	4*01 or 4*02	7	LQYASSFT
							κ	9-124*01	5*01	6	LQYASYPPT
							κ	4-72*01	1*01	9	QQWSSNPW T
							κ	3-2*01	2*01	3	QQNKEVPYT
1-42*01	4-1*01	4*01	1	7	ARRELTGSWDY	11					
							κ	1-110*01	1*01	12	SQSTHVPWT
1-70*01	2-5*01	3*01	1	10	TREG**LREWFP	12	κ	14-111*01	4*01	15	LQYGDFPPT
1-82*01	2-4*01	3*01	1	20	SRWTKMITTRASWFAY	16	κ	3-10*01	2*01	10	QQNNEGPYT
							κ	3-10*01	1*01	6	QQNNEDPRT

							κ	4-53*01	5*01	2	QQWTSYPLT
							κ	1-117*01	1*01	6	FQGSHVPWT
							κ	16-104*01	5*01	8	QQHNEYPLT
1-42*01	1-1*01	2*01	3	21	SRRGGFSLDY	10	κ	3-2*01	1*01	12	QQSKEVPWT
1-20*01	3-1*01	4*01	3	10	ARSGGFYAMDY	11	κ	4-70*01	1*01	6	HQRSSYPWT
							κ	3-10*01	2*01	10	QQNNEGPYT
							κ	4-63*01	5*01	15	FQGSGYPLT

VH: variable heavy chain family. D: Diversity region. JH: Join region. V-Mut: Somatic mutation. CDR3: Complementarity Determining Region. aa: amino acid.

Acknowledgments

First, I would like to express my warmest thanks to my supervisor, Prof. Dr. rer. nat. Sabine Steffens, Prof. Dr. med. Andreas JR Habenicht, and Dr. Changjun Yin. This thesis would not have been possible without their generous intellectual, emotional support, insistent patience, and encouragement.

Special thanks to Prof. Andreas JR Habenicht and Dr. Changjun Yin's help, so, I did not miss the birth of my son, which is the most memorable moment in my life.

I would like to thank Dr. Xavier Blanchet for his excellent kinetics/affinity analyses results. Thanks to Dr. Shibojyoti.Lahiri for sharing his protocol on preparing Co-Immunoprecipitation (Co-IP) samples for Mass Spectrometry (MS) and help me to perform MS.

Furthermore, I would like to thanks all the members of the Habenicht labs. Thanks to Dr. Sarajo Mohanta for his advice and aid. Thanks to Xi Zhang for the great help in single-cell analysis. Thanks to all students in our lab, Zhe Ma, Shu Lu, Ting Sun, Zhihua Wang, YuanFang Li, and Yutao Li, for their excellent suggestions.

Most importantly, without my wife, parents, and friends' constant support, encouragement, and understanding, none of this would have been possible. I would like to give special thanks to my wife ShiShi Jiang and my lovely son ZhiRui Zhang, who enriches our lives every day.

Affidavit

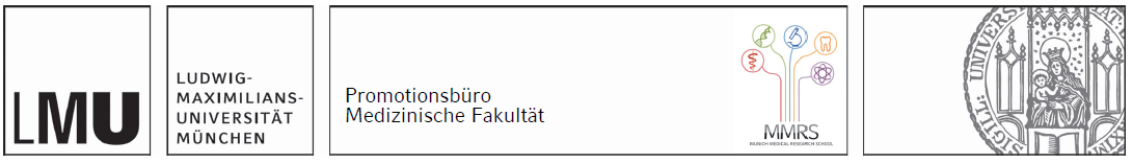

Affidavit

Zhang Chuankai

_____

Surname, first name

_____

Street

_____

Zip code, town, country

I hereby declare, that the submitted thesis entitled:

Searching for autoimmune B cells in atherosclerosis

is my own work. I have only used the sources indicated and have not made unauthorized use of services of a third party. Where the work of others has been quoted or reproduced, the source is always given.

I further declare that the submitted thesis or parts thereof have not been presented as part of an examination degree to any other university.

Munchen, 16.05.2022 Chuankai Zhang

_____ _____

Place, data Signature doctoral candidate